TOWARDS A DISTRIBUTED CONTROL REGIME FOR ROBUST SYNCHRONIZATION AND POWER SHARING OF INVERTER-BASED AC POWER NETWORKS

A Thesis
Presented to
The Academic Faculty

by

Nathan Ainsworth

In Partial Fulfillment
of the Requirements for the Degree
Doctor of Philosophy in the
School of Electrical and Computer Engineering

Georgia Institute of Technology
August 2014

TOWARDS A DISTRIBUTED CONTROL REGIME FOR ROBUST SYNCHRONIZATION AND POWER SHARING OF INVERTER-BASED AC POWER NETWORKS

Approved by:

Professor Ronald Harley,
Committee Chair
Professor, School of ECE
Georgia Institute of Technology

Professor Santiago Grijalva, Advisor
Associate Professor, School of ECE
Georgia Institute of Technology

Professor Magnus Egerstedt
Professor, School of ECE
Georgia Institute of Technology

Professor Maryam Saeedifard
Assistant Professor, School of ECE
Georgia Institute of Technology

Professor Arkadi Nemirovski
Professor, School of ISYE
Georgia Institute of Technology

Date Approved: June 13, 2014

To my parents, Mark and Rosemary Ainsworth, for their unending encouragement, support, and love. I have learned far more from them than any formal education could ever teach me.

To my wife Keela, who believes in me and my work even when I don't.

ACKNOWLEDGEMENTS

TABLE OF CONTENTS

LIST OF TABLES

LIST OF FIGURES

SUMMARY

The contributions of this dissertation are 1) a general dynamic condition suffi-
cient to ensure frequency synchronization of inverter-based AC power networks, and
2) a distributed control regime that is capable of guaranteeing that the above condi-
tion holds for all expected operating conditions of such networks. These methods are
applicable to networks of arbitrary structure and scale. First, we develop a structure-
preserving model of the frequency and voltage-angle dynamics of an arbitrary network
whose sources are all inverters operating frequency-droop control. By applying graph-
theoretic methods to the model, we will show that there exists a "safe region" of the
state space such that if the network voltage-angle trajectory stays in this region, then
synchronization and power sharing are shown by Lyapunov-like methods. By analogy
to similar problems solved in other applications, we will develop a new distributed
control regime to constrain an all-active-bus, acyclic inverter-based network to the
safe operating region, thus guaranteeing synchronization and a new form of power
sharing that enforces line power flow constraints. We then extend these methods to
a much more general class of inverter-based networks by introducing the concept of
power flow rigidity and developing a control method (which does not require com-
munication or centralized control) to enforce the power flow rigidity of a network for
all network operating conditions within an explicitly defined range. These techniques
will form the basis for future development of ultra-reliable inverter-based networks.

CHAPTER I

INTRODUCTION AND MOTIVATION

1.1 Introduction

Frequency synchronization and sharing of real power demand between power sources
is a necessary fundamental requirement of AC power networks, which almost all other
features of the power system take as an assumption. Emerging smart grid technolo-
gies, such as the Prosumer-based Power System Architecture being developed by the
Advanced Computational Electricity Systems (ACES) laboratory at Georgia Tech, re-
quire that synchronization and power sharing of networks be assured for all expected
network operating conditions without requiring communication or centralized con-
trol. At the same time, increasing penetrations of inverter-interfaced power devices
violate long-standing assumptions about synchronization. Therefore, new methods
of understanding frequency synchronization in networks with high penetration of
inverter-interfaced sources are needed, along with new distributed control regimes to
provide robust synchronization and power sharing behavior for such networks. Since
inverters are the least understood component of this new system, this dissertation
contributes new methods of analysis and control for networks whose sources are all
inverters, and makes significant steps towards providing truely robust, distiributed
sychronization and power sharing behavior.

The contributions of this dissertation are 1) a general dynamic condition sufficient
to ensure frequency synchronization of inverter-based AC power networks, and 2) a
distributed control regime that is capable of guaranteeing that the above condition
holds for all expected operating conditions of such networks. These methods are

applicable to networks of arbitrary structure and scale. First, we develop a structure-preserving model of the frequency and voltage-angle dynamics of an arbitrary network whose sources are all inverters operating frequency-droop control. By applying graph-theoretic methods to the model, we will show that there exists a "safe region" of the state space such that if the network voltage-angle trajectory stays in this region, then synchronization and power sharing are shown by Lyapunov-like methods. By analogy to similar problems solved in other applications, we will develop a new distributed control regime to constrain an all-active-bus, acyclic inverter-based network to the safe operating region, thus guaranteeing synchronization and a new form of power sharing that enforces line power flow constraints. We then extend these methods to a much more general class of inverter-based networks by introducing the concept of power flow rigidity and developing a control method (which does not require communication or centralized control) to enforce the power flow rigidity of a network for all network operating conditions within an explicitly defined range. These techniques will form the basis for future development of ultra-reliable inverter-based networks.

1.2 Motivation

The traditional architecture and control regime of the North American electric power system is based on the technologies available and consumer needs at the time of the grid's inception. As a result, the grid depends on a system of assumptions based around these technologies and needs, which include inertial sources that are (relatively) small in number and large in scale, lack of energy storage capability, and static network structure. However, in the past few decades, new power devices and power-management technologies have emerged (e.g., inertialess sources that are small in scale and large in number and the possibility of energy storage), which defy the assumptions that underly the traditional control regime. At the same time, new use-cases and needs arise as the amount of electric power used increases and the way that

it is used becomes more complex (e.g., controllable loads, need for dynamic networks, and electric vehicles). As a result, the traditional control regime is unable to effectively integrate key new technologies or meet the needs of a 21-century society. A new control regime is needed, one that continues to provide traditional services, but also allows technology independance, more flexible structure, greater reliability, and more consumer participation.

The most basic capabilities required of a power network are synchronization of power devices to a shared system frequency (frequency synchronization), sharing of the network load power between sources according to some defined relationship (power sharing), and enuring that the physical constraints of the network are met (physical security), even in the face of unexpected disturbances and changes in the network. Traditionally, these capabilities have been provided by the inertia and governor response of the large synchronous machine sources, combined with centralized supervisory control. The mathematical tools available for analyzing synchronization of the network have been largely based on numeric simulation, in which it was assumed that the network is static in structure and strongly dominated by inertial sources. However, emerging power technologies are often interfaced to the power network by power electronic inverters, which are not inertial, but are capable of much greater controllability than machines. In addition, full consumer participation in the market requires that the method of control be capable of integrating a large number of new devices with ownership by many entities, which motivates a distributed control regime. As a result, existing tools for analysis and control are inadequate to the needs of the emerging grid.

In response to the above described needs, the Advanced Computational Electricity Systems (ACES) lab at the Georgia Institute of Technology is in the process of developing a new control regime to meet the needs of the emerging power network.

Titled the "Prosumer-based Power System Architecture," this system provides a vision for an "Energy Internet" allowing distributed, plug-and-play integration of new technologies and full participation of consumers in the electricity market [32, 34]. The scope of this architecture is the operation of an internet-like power network from sub-microsecond device controls to large-scale market transactions.

The Prosumer-based Power System Architecture works in layers, where each layer performs significant functions of the power network and abstracts those functions away from the layers above it. The Local Control Layer, which consists of controllers operating locally on power devices without explicit communication, is response for ensuring frequency synchronization and power sharing of the network. The integration of these capabilities into the Local Control Layer provides a basis for higher layers that ensures physical operation of the network, even in the event of a failure of communication or higher control layers. Therefore, it is necessary for the operation of the Prosumer-based Power System Architecture to develop a distributed control regime for a power network of arbitrary size and structure that provides frequency synchronization and power sharing for all expected operating conditions of the network.

The full specification of a control regime to meet all the requirements of the Local Control Layer of the Prosumer-based Power System Architecture is beyond the scope of this dissertation. However, since inverter-interfaced devices are the most novel component of the emerging power system, and the creation of a stable network of such devices is not well understood, this work will advance the understanding of frequency synchronization, power sharing, and line-power-flow security of networks containing high penetration of inverters by considering a network of *ALL* inverter sources, particularly focusing on how a control regime can ensure synchronization and power sharing in a way that is robust to changes in the generation references and

loads. In addition, the outcome of this work will be applicable to isolated inverter-based networks, such as military forward operating base networks [10] or inverter-based microgrids (such as CERTS microgrids [46]).

1.3   Outline

This dissertation begins with a survey of the existing state of methods for modeling and control of synchronization and power sharing in AC networks (both synchronous generator and inverter-based networks), as well as survey of existing methods for analysis of network convergence and synchronization in multi-agent system theory (Chapter 2). We then propose a new *structure-preserving dynamic model of the frequency/voltage-angle/real-power dynamics* of an inverter-based network whose sources operate frequency-droop control. By applying multi-agent system methods to this model, we show that synchronization and power sharing of such a network can be guaranteed by satisfaction of a specified set of line power flow constraints on each line in the network (Chapter 3). Based on the above condition, we then propose a modified form of the frequency-droop control law (which we term the *Constraint-Enforcing Droop (CED) Control Law*), and show that if each inverter in an all-active-bus, acyclic network implements the CED control law, then robust synchronization and a constrained form of power sharing behavior are guaranteed (Chapter 4). In order to allow application to a more general class of networks, we then introduce the concept of *power flow rigidity* (and *power flow rigid key line sets*), and show that they permit relaxation of the sufficient condition for stability to the enforcement of the line power flow conditions on only a subset of the network lines when the network operates within a specified range of generation and load values (Chapter 5). Based on the concept of power flow rigidity, we introduce *rigidity-enforcing sparse CED*, a control approach applicable to very general inverter-based networks that provides significantly improved synchronization and power sharing with only sparse application of

CED-controlled inverters (Chapter 6). While our results fall short of formally control-theoretic robustness, they provide significant improved performance as compared to existing methods, and we argue that the non-robust assumptions they require are mild in practice. Finally, we discuss the applications, capabilities, and limitations of our proposed modeling and control methods (Chapter 7).

CHAPTER II

LITERATURE REVIEW

2.1   Synchronization and Stability in Power Networks

This dissertation will combine results from two fields which have traditionally had little interaction with each other: power system analysis and graph-theoretic methods for multi-agent system analysis. These fields often use different terminology to describe similar concepts, or in some cases, they use the same term to mean different things. In particular, the definitions of the concepts of frequency synchronization and angle stability of an inverter-based power system bear discussion.

Frequency synchronization (sometimes simply called "synchronization") is a topic of significant discussion in power system analysis. A paper by the IEEE/CIGRE Joint Task Force on Stability Terms and Definitions [44] seems to be the accepted source for the definitions of terms relating to power system stability. This paper uses the term "synchronization" undefined, but there seems to be general acceptance that this term refers to the convergence of power system bus voltage angles and frequencies to a state in which all bus frequencies are equal (e.g., [38]). Because of the physical relationship between bus voltage angles and power-flow values in AC power networks, frequency synchronization is also understood to imply the convergence of line power flows (and thereby source generation values) to a known relationship. Frequency, therefore, acts as a shared system variable by which power sources may coordinate their output, and thus frequency synchronization is critical to almost all other functions of the power system.

In control theory, many different definitions of stability may be adopted. Most definitions are based on the concept of Lyapunov stability of an unforced system

(see [43, Chapter 4]), which is the property of a system and an equilibrium such that for initial conditions sufficiently near the equilibrium, the state dynamics will stay near the equilibrium for all time, or in the case of asymptotic stability, will converge to the equilibrium. LaSalle's theorem allows expansion of this definition to limit sets and compact sets of initial conditions. Further generalizations of this definition include input-to-state stability, which ensures robustness to time-varying forcing inputs, and local input-to-state stability [68, 69], which limits the region of input-to-state stability to a compact set of inputs and initial conditions. Many of the above definitions can be modified by the concept of partial stability, which considers the stability of only a subset of the variables of the system [74, 73]. Multi-agent system theory often considers stability of network state to "agreement", which is the state in which all nodes in the network share a common local state (see [54, Chapter 3]). While different in several significant ways, all of these definitions share a common goal: the state trajectory of concern should stay within a bounded region (or converge to a target equilibrium) for all expected initial conditions and inputs.

While in many ways similar, the understanding of stability in power systems is much more specific. In [44], power system stability is defined as "the ability of an electric power system, for a given initial operating condition, to regain a state of operating equilibrium after being subjected to a physical disturbance, with most system variables bounded so that practically the entire system remains intact." Notice that this definition is specific to a given operating point and a given set of physical disturbances (rather than ALL expected operating points and disturbances). In practice, this concept is usually divided into several different partial stability concepts related to the particular system variables of interest, such as rotor angle stability, voltage stability, frequency stability, etc. It is generally assumed that it is not possible to ensure stability of a power system to any disturbance or from all operating points [44].

The concept of "angle stability" in a power system deals with the conditions under which frequency synchronization can be expected to occur. In [44], "rotor angle stability" is defined as "the ability of the synchronous machines in a system to maintain synchronization after being subjected to a disturbance." Obviously this definition is specific to synchronous machines, but it can be easily generalized to voltage angles (rather than rotor angles) since in synchronous machines the two are directly related. The term "transient stability" deals with angle stability of a network in response to large disturbances. It is generally assumed that the system is initially in an equilibrium condition, a physical disturbance is applied, and then it is determined whether the system is able to return to a (possibly changed) post-disturbance equilibrium [44, 64]. Transient stability of a power system has traditionally been assessed by time-domain simulation of a dynamic model of the power system under a given set of disturbance contingencies [44, 75], which is generally known as "contingency analysis." Because of the large computational complexity of this type of analysis, only a limited number of possible operating points or contingencies can be considered [48, 5].

Another major category of methods for analysis of transient stability of machine-based networks are *energy function methods*, which involve the creation of a function of network parameters and state, whose values gives some information about transient stability of the network, such as a margin to instability. Excellent summaries of the field are provided by [72, 64]. Many energy function methods (e.g. [7, 70, 71]) are based on reduced-order models of the power network, in which load buses are algebraically eliminated so that only active (generator) buses need to be considered. In 1981, Bergen and Hill proposed their famous *structure preserving model* [9], in which no load bus elimination is made, allowing a much more physical interpretation of the results. Based upon the structure-preserving model, numerous methods have been developed to provide greater physical insight into transient stability in machine-based networks (e.g. [16, 37, 11, 29, 18]). However, a closed form method for determination

9

of the boundaries of transient stability of a power network as a function of network structure and parameters has not yet been developed [38].

2.2 *Inverter Frequency-Droop Control*

To enable high penetrations of inverter-interfaced sources, it is necessary to ensure that such sources participate in the stabilization of the network. Much recent literature has discussed the *frequency-droop controller* for inverter-interfaced sources, which was first proposed in [12]. This method is based on the physical intuition that inverter real power tends to increase with increasing voltage angle. Therefore, the inverter is operated as a voltage source and implements a linear droop of frequency with respect to output power. This controller therefore creates a similar relationship between frequency and source output power seen in traditional machine networks, and so has been claimed to allow a network with high to complete penetration of inverter sources to maintain frequency synchronization and share power between sources. Based on the inverter droop controller, many methods for stabilization and power sharing in inverter-based and mixed inverter/machine microgrids have been proposed [62, 47, 61, 17, 35, 42, 51, 8], including the well known CERTS Microgrid Concept [46, 24, 58].

Several related methods for the analysis of angle stability in droop inverter-based networks have been proposed in the literature [15, 40, 52], which rely on detailed modeling of the inverter device and controller, but with a simplified network model. Small-signal stability is assessed numerically at a particular operating point by linearization of the dynamics. These methods allow assessment of the local stability of a particular network for a particular operating point, but they do not allow for assessment of boundaries of stability or provide physical insight into how such stability characteristics can be improved. In addition, little attempt is made at connection with traditional system-level theory, and simplified network models do not allow complex

or dynamic network structure to be considered.

2.3 Graph-theoretic Methods and Multi-agent Systems

Recent contributions to the field of algebraic graph theory (see [30]) have provided powerful new mathematical tools with which to understand networks of interconnected dynamic systems. This has resulted in the development of graph-theoretic methods for multi-agent system analysis (for a summary, see [63, 54]), which study convergence in dynamic networks through the underlying graph. In particular, [80] considers a network of coupled dynamic systems through the edge states, that is, the differences of state across each edge in the underlying graph. Some research has also considered the possibility of non-linear coupling dynamics [63, 76, 81] for example the Kuramoto Oscillator model [45], in which the agents represent coupled oscillators with sinusoidal coupling functions. Using graph-theoretic methods, [1, 13, 22, 28, 27] have explored conditions for synchronization of the Kuramoto Oscillator model (and generalizations thereof). Some literature has observed the connection between Kuramoto oscillator model and power networks [50, 26]. Source [38] constrasts network-focused modeling approaches with the dynamics-focused modeling approach traditional in power system theory, and calls for application of network focused methods to power system analysis.

One problem considered by multi-agent system control is that of achieving distributed agreement among mobile robots with limited sensor range. Mathematically, this problem is formulated as an edge preservation problem in Δ-disk interaction graphs (see [54, Chapter 7], [79]). A discrete-time method to achieve agreement under limited sensor range was proposed in [6]. In [53] Meng and Egerstedt propose an agreement controller to preserve edges in a network of agents with single-integrator dynamics, based on application of unbounded non-linear gains to network coupling terms. Other methods have been proposed to solve the single-integrator problem with

11

bounded control terms [19, 4]. Finally, [59] has proposed a discrete-time method to preserve connectivity among second-order agents with limited sensor range.

A significant concept often used in grapth-theoretic or multi-agent control is that of graph rigidity or persistence (for an explanation, see [36]). Each vertex in a graph is assigned a position in $\mathbb{R}^2$. An undirected graph is rigid if every such assignment of positions such that the distance across each edge is a specified value is sufficient to ensure that all pairwise distances between edges are maintained. Persistence is a similar concept for directed graphs, in which any movement of vertices that maintains the distances on the outgoing edges of each will also maintain the distance between each other pair of vertices. In [41], a combinatoric method (the "pebble game") was introduced which allows analysis of rigidity. The concepts of rigidity and persistence were extended to three and higher dimensions in [78]. Finally, in [67], methods were proposed allowing for automatic generation of peristent formation for mobile robots under sensing and communication range constraints.

2.4   Application of Graph-Theoretic Methods to Angle Stability of Power Networks

Recently, Dörfler and Bullo developed a reduced network model [23] for a machine-based AC power network based on the Kuramoto model. They showed that in some cases angle stability of the power system models can be approximated by the first order *non-uniform Kuramoto model*. Using this model, they provide a system-level condition on edge coupling weights that ensure angle stability of the network. In [21], they showed that the structure-preserving model of a machine-based network can in some cases also be approximated by non-uniform Kuramoto model. Very recently, Simpson-Porco, Dörfler, and Bullo observed in [66] that radial, lossless networks of droop controlled inverter sources may be modeled *exactly* as non-uniform Kuramoto oscillators, and provided a system-level necessary and sufficient condition for angle stability of such a network.

In summary, a strong need exists for new mathematical tools for analysis and control design in frequency synchronization of inverter-based network. In addition, recent developments in graph-theoretic methods may provide many such tools, and preliminary work has shown the potential for application of such tools to the problems of frequency synchronization in inverter-based networks. The field is ripe for further development and application of these methods to enable new functionality and improved reliability for inverter-based power networks.

CHAPTER III

A STRUCTURE-PRESERVING MODEL AND SUFFICIENT CONDITION FOR FREQUENCY SYNCHRONIZATION OF LOSSLESS DROOP INVERTER-BASED AC NETWORKS

In order to determine methods by which synchronization and power sharing can be guaranteed for an inverter-based power network, it is first necessary to develop methods allowing analysis of such a network, and determination of conditions under which synchronization occurs (or fails to occur). Because frequency-droop control has been shown to provide the desired synchronization and power sharing characteristics under many (though not all) network conditions, and because it has the advantages of modularity and locality, we will choose to focus on networks of inverters operating frequency-droop control.

As was discussed in the previous chapter, existing models of inverter-based networks operating frequency-droop control are based on linearization about a specified operating point, which is sufficient to show local stability to a synchronization equilibrium under many conditions [15, 40, 52]. However, because AC power network dynamics are highly non-linear, and because an inverter-based network may need to operate under a wide range of conditions, local stability to a pre-specified equilibrium is not sufficient to establish the desired guaranteed synchronization property across the entire expected network operation range. Therefore, new dynamics models of such a network, which include the full non-linear power-flow equations, must be developed. Further, based on those models, conditions must be derived which are sufficient to ensure synchronization and power sharing of the network, ideally conditions which

14

can be determined based on local measurements.

In [66], the connection was made between network of frequency-droop inverters and Kuramoto Oscillators [45], allowing development of system-level synchronization conditions for a specific structure of network. However, in order to allow development of distributed control methods to guarantee synchronization for arbitrary networks, it is necessary to develop more a general dynamic model for any network structure, and synchronization conditions which can be determined from local measurements.

In this chapter, we develop such a model of an inverter-based power nework and sufficient conditions for its synchronization, which will be used as the basis for our control methods to guarantee such synchronization using distributed control in the following chapters. The results in this chapter were published in the paper *A Structure-Preserving Model and Sufficient Condition for Frequency Synchronization of Inverter-Based Networks* [3] in the IEEE Transactions on Power Systems. We build on [66] by constructing a structure-preserving model which allows extention of many of their results to an arbitrary (radial or meshed) network. Rather than focusing on calculating the maximum stable droop constants, we use a simplified model of the inverters to allow us to develop greater physical insight into how the interaction between the inverters creates (or fails to create) the network frequency synchronization (as suggested by [38]). Our primary contributions are the connection of our model to traditional structure-preserving power system models, a new condition for existence of equilibria, and a sufficient criterion for frequency synchronization. Our results are applicable to either radial (acyclic) or meshed (cyclic) networks. We emphasize that our sufficient criterion for frequency synchronization consists of a set of local criteria, each of which can be determined from local measurements.

3.1 Class of Networks Under Consideration

An electric power system consists of sources, loads, and the network connecting them together. The network consists of buses (electrical locations, to which loads and possibly a source are attached) and lines (which each create an electrical connection between a pair of buses). The voltage on each bus in an AC network is sinusoidal, and is specified by a voltage magnitude, phase, and frequency. An AC network also has a specified nominal frequency, which in North America is 60 Hz. Power flows in an AC network consist of both real and reactive power. Real power sources energy to loads (and losses), while reactive power supports voltage across reactances.

In this chapter, we develop a dynamic model for the voltage angle, frequency, and real power dynamics of a 3-phase AC power network whose sources are voltage-source inverters operating the frequency-droop control law developed in [12]. Such an inverter regulates the AC voltage magnitude on its terminals to a specified value, and controls the frequency based on its measured real power output. In contrast to the methods of analysis used by [15, 40, 52] for network of such inverters, we approach this modeling by focusing on the interaction of the inverter droop controllers and the power network structure, rather than on detail power electronic models of the individual components. To support this focus, we will address the following simplified class of networks:

Definition 3.1. *A* lossless droop inverter-based power network with ideal voltage regulation *(abbreviated as* droop inverter-based network*) is a 3-phase AC power network with the following characteristics:*

3.1.A All lines are lossless and inductive.

3.1.B All sources are voltage-source inverters implementing frequency-droop control as described in [12] with no controller delays.

3.1.C Each network bus has attached load with positive frequency dependence coefficient.

3.1.D Each bus has a constant (not necessarily homogeneous) voltage magnitude.

3.1.E Graph representing the network is connected.

A lossless droop inverter-based power network with ideal voltage regulation is an idealized form of many inverter-based networks such as an isolated inverter-based microgrid, though our results should apply to a network of any scale. The set of assumptions in Definition 3.1 is similar to that made by Bergen and Hill's famous structure-preserving model [9], except that Bergen and Hill's model considers a network whose sources are all synchronous machines (hence referred to as a *machine-based power network*). While in some ways restrictive, these assumptions result in a model which is generally sufficient to study sychronization and real power sharing between inverter sources. In particular, the assumption of constant bus voltage magnitudes (Definition 3.1.D) decouples the problem of synchronization from that of voltage stability (which is outside of the scope of this dissertation, see [44] for general definitions of these terms).

3.2 Scalar Dynamic System-of-Equations Model

Consider a droop inverter-based network (per Definition 3.1) with $M > 0$ voltage source inverters. Each electrical bus in such a network is either an inverter bus (whose voltage is regulated by an attached inverter) or a network bus (to which no inverter is attached). In our model, each inverter may be modeled as either an ideal voltage source or an ideal voltage source behind a reactance. If the latter is used, an additional bus is added to the model to represent the internal voltage of the inverter with a line modeling its output reactance. Once these supplementary buses and lines are added, the system has N total buses and L total lines.

Each electrical bus in the network is assigned an index $k \in \{1 \ldots N\}$, and the network state consists of the positive-sequence voltage on all buses, each of which is represented by the phasor $V_k \angle \delta_k$, where $V_k > 0$ is the voltage magnitude, $\delta_k \in \mathbb{T}$ is the voltage synchronous phase relative to an (arbitrary) system reference rotating at the nominal network frequency, and $\mathbb{T}$ is the torus $[-pi \quad pi)$. If an offset $\Delta\omega_k \in \mathbb{R}$ is applied to the frequency of the voltage sinusoid at a bus k, then $\dot{\delta}_k = \Delta\omega_k$. Recall that we have assumed that voltage magnitude V_k at each bus k can be treated as constant (Definition 3.1.D), since our focus in this dynamic model is the voltage-angle and frequency dynamics.

3.2.1 Network Power-Flow Laws

Consider an arbitrary bus $k \in \{1 \ldots N\}$ in the network. Kirkoff's law (in power form) states that the sum of the (real) power flows into bus k equals zero at any instant in time:

$$P_{G,k} = P_{L,k} + \sum_{m \in \mathcal{N}(k)} P_{Line,k,m}(\delta_k - \delta_m) \tag{1}$$

where $P_{G,k}$ is the power generation of the source at bus k (zero if no source), $P_{L,k}$ is the total load at bus k, $P_{Line,k,m}$ is the line power flow from bus k to bus m (measured at bus k), and $\mathcal{N}(k)$ is the set of neighbors of bus k (that is, the set of buses to which k is directly connected by a line).

The line power-flow value $P_{Line,k,m}$ on the line from bus k to bus m is a function of the difference between the voltage angles at its incident buses $(\delta_k - \delta_m)$. Since (by assumption) all lines are lossless and inductive (Definition 3.1.A), we can find line power flow $P_{Line,k,m}$ as:

$$P_{Line,k,m} = -P_{Line,m,k} = Y_{k,m}V_kV_m\sin(\delta_k - \delta_m), \tag{2}$$

where $Y_{k,m} = Y_{m,k} > 0$ is the series line admittance magnitude parameter of line (k, m). Substituting (2) for each line into (1) for each bus $k \in \{1 \ldots N\}$ yields the

associated bus real power-flow equation. Since we have assumed constant voltage magnitudes, the bus reactive power-flow equations are not necessary for our analysis, and so are not considered in this dissertation.

We adopt Bergen and Hill's model of a frequency-dependent load [9], which is:

$$P_{L,k} = P_{L,k}^0 + D_k' \Delta\omega_k = P_{L,k}^0 + D_k' \dot{\delta}_k \qquad (3)$$

where $P_{L,k}^0$ is the nominal-frequency load at bus k and $D_k' \geq 0$ is the frequency dependence coefficient of the load at bus k. By Definition 3.1.C, we require that $D_k > 0$ if k is a network bus.

3.2.2 Inverter Dynamic Model

Now consider an arbitrary inverter in the network, which we will address by the bus index of its attached bus. Each such inverter $k \in \{1 \dots N\}$ implements the frequency-droop control law, which operates by applying a frequency offset $\Delta\omega_k \in \mathbb{R}$ to the sinusoidal voltage waveform it creates at its attached bus k. The frequency-droop control law (described in [12]) is as follows:

$$\Delta\omega_k = \dot{\delta}_k = R_k \left[P_{Ref,k} - P_{G,k} \right] \qquad (4)$$

where $R_k > 0$ is the frequency-droop constant for the inverter at bus k and $P_{Ref,k}$ is its assigned internal power reference, which we will treat as an input. By substituting (1) and (3) into (4) and solving for $\dot{\delta}_k$, we find the local dynamic equation governing inverter bus k:

$$\dot{\delta}_k = (R_k^{-1} + D_k')^{-1} \left[P_{Ref,k} - P_{L,k}^0 - \sum_{m \in \mathcal{N}(k)} P_{Line,k,m}(\delta_k - \delta_m) \right] \qquad (5)$$

The dynamic equation (5) represents the voltage-angle dynamics at an arbitrary inverter bus k. It reveals that the effect of the frequency-droop controller is to adjust the first-derivative of the bus synchronous voltage angle δ_k based on the difference between the inverter reference and local nominal-frequency load ($P_{Ref,k} - P_{L,k^0}$), and

to create a coupling between its voltage angle δ_k and the voltage angle δ_m of each of its neighbors m. It is this coupling (and its characteristics) that create the desired frequency synchronization behavior. In addition, the coupling between frequency and real power offset $P_{Ref,k} - P_{G,k}$ in the frequency-droop control law (4) ensures that if the inverter frequencies synchronize, then their real power output values must also converge so that power is shared between the inverters according to their specified reference and droop constant values. In this chapter, we will explore both of these behaviors to determine their characteristics and the conditions under which they occur (or fail to occur).

3.2.3 Network Dynamic System of Equations Model

At a network bus, since no inverter is present the inverter control law (4) does not apply, and instead $P_{G,k} = 0$. Therefore, we may obtain the dynamic equation at a network bus k by substituting (3) and $P_{G,k} = 0$ into (1) and solving for $\dot{\delta}_k$:

$$\dot{\delta}_k = D_k'^{-1} \left[-P_{L,k}^0 - \sum_{m \in \mathcal{N}(k)} P_{Line,k,m}(\delta_k - \delta_m) \right] \tag{6}$$

We can combine equations (5) and (6) for each bus in the network to form a dynamic system of equations representing the entire droop inverter-based network as follows:

$$\dot{\delta}_k = D_k^{-1} \left[P_{Ref,k} - P_{L,k}^0 - \sum_{m \in \mathcal{N}(k)} P_{Line,k,m}(\delta_k - \delta_m) \right] \ \forall\, k \in \{1 \dots N\}, \tag{7}$$

where D_k is the total frequency dependence coefficient at bus k and $P_{Ref,k} = 0$ if k is a network bus.

If k is an inverter bus, then $D_k = R_k^{-1} + D_k'$, while if k is a network bus then $D_k = D_k'$. In either case, we assume that $D_k > 0$ (see Definition 3.1.C). This is almost always true, since in practice network load almost always increases with frequency. In general, the droop constant inverse R_k^{-1} will generally be much larger

than the load frequency dependence constant D_k for a bus, and therefore the total frequency dependence term D_k at an inverter bus will be much larger than that at a network bus. While this fact does not have significant influence on our stability criterion (which will apply even if D'_k approaches zero), it means that inverter buses will generally have longer time constants than network buses, and that the inverter time constant is primarily determined by the selection of the control constant R_k.

The dynamic system of equations (7) represents the voltage-angle state dynamics of the entire droop inverter-based network. It reveals that both inverter and network bus dynamics include a local forcing term ($P_{Ref,k} - P_{L,k}^0$, which is always non-positive for a network bus) as well as line power-flow terms $P_{Line,k,m}$ to each neighbor m. As we will see, the effect of these line power-flow terms is to couple the voltage angle (and frequency) at each bus to those of its neighbors. By studying these couplings and their characteristics using graph-theoretic methods, we will determine the synchronization and power sharing characteristics of the network and their relationships to the network structure and parameters.

3.2.4   Comparison to Existing Models

We observe that Bergen and Hill's model of a network of machine sources [9, Equation (2)] reduces to our model (7) with the following substitutions:

1. No inertial term ($M_k = 0$).

2. Machine damping term D_k replaced with bus total frequency dependence coefficient.

3. Machine mechanical power $P_{M,k}$ replaced with inverter power reference $P_{Ref,k}$.

This confirms several intuitive relationships between inverter and machine power networks, namely that the dynamics of frequency-droop inverters closely resemble those

of strongly overdamped machines, and that inverter power reference takes on an analogous role to machine mechanical power. In this dissertation, we make use of this lack of interia to show results that may not hold for networks with significant inertia (e.g. machine-based networks).

In comparison to small-signal stability models of inverter-based networks, such as that presented in [15], our model explicitly integrates the non-linear real power-flow equations of the full network and (as we will show below) makes explicit connection to graph-theoretic dynamic methods. However, we do not model an inverter voltage-droop characteristic, and we do not consider a controller delay in the inverter droop controller.

3.3   Graph-theoretic Model

A coupled dynamic system of the form of (7) with coupling functions (2) can be viewed as a forced form of the "non-linear consensus equation" discussed in [63]. Based on this observation, we will represent (7) and (2) in a form which is convenient for analysis by graph-theoretic methods.

3.3.1   Power-flow Structure Graph and Network Vector Quantities

We can explicitly represent the structure of the power network by defining the undirected power-flow structure graph $\mathfrak{G} = (\mathcal{V}, \mathcal{E})$. The vertex set $\mathcal{V} = \{1 \ldots N\}$ represents the buses of the droop inverter-based network, and the edge set $\mathcal{E} \subset \mathcal{V} \times \mathcal{V}$ representing its lines. Since $\mathfrak{G}$ is undirected, then if buses k and m are connected by a line, then both (k, m) and (m, k) are in $\mathcal{E}$. If there exists (k, m) or (m, k) in $\mathcal{E}$, then we say that buses k and $m \in \mathcal{V}$ are *adjacent*, while we say that the line $(k, m) \in \mathcal{E}$ and bus $k \in \mathcal{V}$ are *incident* (as are (k, m) and m). We also assign each bus $k \in \mathcal{V}$ to one of two distinct sets: $\mathcal{V}_{Droop}$ (indicating the droop inverters buses) or $\mathcal{V}_{Net}$ (indicating the network buses).

Some quantities of interest in a droop inverter-based power network are bus-oriented (such as bus voltage angles, power references, loads, etc.) while others are line-oriented (such as power flows, admittances, etc). Since both kinds of quantities are significant for our analysis, it is valuable to be able to quickly and easily reference both and relate them to each other. For each bus-oriented quantity x_k associated with the bus $k \in \mathcal{V}$, we assign the vector $\boldsymbol{x} = \begin{bmatrix} x_1 \ldots x_N \end{bmatrix}^T$ (see Table 3.1 for a list).

Since the graph $\mathfrak{G} = (\mathcal{V}, \mathcal{E})$ is undirected, then for each line (k,m) in the edge set $\mathcal{E}$, its reverse (m,k) is also in $\mathcal{E}$. Line-oriented quantities (such as the line power flow $P_{Line,k,m}$) have one of the following three properties:

1. Line-Even: A line-even quantity $z_{k,m}$ has the property $z_{k,m} = z_{m,k}$.

2. Line-Odd: A line-odd quantity $z_{k,m}$ has the property $z_{k,m} = -z_{m,k}$.

3. Line-Asymmetric: A line-asymmetric quantity $z_{k,m}$ is neither line-even nor line-odd.

For example, the line power flow $P_{Line,k,m}$ is line-odd, since by (2) $P_{Line,k,m} = -P_{Line,m,k}$. In contrast, the line series admittance $Y_{k,m}$ is line-even, since $Y_{k,m} = Y_{m,k}$. Throughout this work we will introduce other line-oriented quantities, and for each note whether it is line-even, line-odd, or line-asymmetric.

In order to simplify our notation, we will define a vector of length L for each line-even or line-odd quantity, which contains exactly one of $z_{k,m}$ or $z_{m,k}$ for each physical line in the network. It is therefore valuable to associate with each physical line a direction indicating positive power flow, as well as an index $i \in \{1 \ldots L\}$. The directed edges indicating the direction of positive power flow for each line are assigned to a directed-edge set $\overrightarrow{\mathcal{E}}$. Therefore, if (k,m) and (m,k) are in $\mathcal{E}$, then there exists exactly one of (k,m) or (m,k) in $\overrightarrow{\mathcal{E}}$. We will then define the vector $\boldsymbol{z} = \begin{bmatrix} z_1 \ldots z_L \end{bmatrix}^T$ to represent the network line-oriented quanties (see Table 3.1 for a list), where $z_i = z_{k,m}$ for each line $(k,m) \in \overrightarrow{\mathcal{E}}$, where i is the index assigned to (k,m). If $(k,m) \in \mathcal{E}$, then

Table 3.1: Vector Quantities for Structure-Preserving Model

Name	Symbol	Definition	Type
Bus voltage-angle vector	$\boldsymbol{\delta}$	$\begin{bmatrix} \delta_1 \ldots \delta_N \end{bmatrix}^T$	$\mathbb{T}^N$
Bus frequency offset vector	$\boldsymbol{\Delta\omega}$	$\begin{bmatrix} \Delta\omega_1 \ldots \Delta\omega_N \end{bmatrix}^T$	$\mathbb{R}^N$
Bus power generation vector	$\boldsymbol{P_G}$	$\begin{bmatrix} P_{G,1} \ldots P_{G,N} \end{bmatrix}^T$	$\mathbb{R}^N$
Bus power reference vector	$\boldsymbol{P_{Ref}}$	$\begin{bmatrix} P_{Ref,1} \ldots P_{Ref,N} \end{bmatrix}^T$	$\mathbb{R}^N$
Bus load vector	$\boldsymbol{P_L}$	$\begin{bmatrix} P_{L,1} \ldots P_{L,N} \end{bmatrix}^T$	$\mathbb{R}^N$
Bus nominal-frequency load vector	$\boldsymbol{P_L}^0$	$\begin{bmatrix} P_{L,1}^0 \ldots P_{L,N}^0 \end{bmatrix}^T$	$\mathbb{R}^N$
Line power-flow vector	$\boldsymbol{P_{Line}}$	$\begin{bmatrix} P_{Line,1} \ldots P_{Line,L} \end{bmatrix}^T$	$\mathbb{R}^L$ (Line-Odd)
Line voltage-angle vector	$\boldsymbol{\theta}$	$\begin{bmatrix} \theta_1 \ldots \theta_L \end{bmatrix}^T$	$\mathbb{T}^L$ (Line-Odd)

for line-even quantities $z_{m,k} = z_{k,m}$ and for line-odd quantities $z_{m,k} = -z_{k,m}$. We do not assign line-asymmetric quantities to vectors.

From (2), the line power flow $P_{Line,k,m}$ (line-odd) for each line $(k,m) \in \overrightarrow{\mathcal{E}}$ is a function of the difference between the voltage-angle states at its terminals $(\delta_k - \delta_m)$. It is therefore valuable to assign the line-oriented quantity $\theta_{k,m} = -\theta_{m,k} = \delta_k - \delta_m$ (line-odd), which can be viewed as the *line voltage-angle* state associated with the physical line $(k,m) \in \overrightarrow{\mathcal{E}}$ with index i. These line voltage-angle states may be formed into a vector $\boldsymbol{\theta} = \begin{bmatrix} \theta_1 \ldots \theta_L \end{bmatrix} \in \mathbb{T}^L$, which may be viewed as a *line-oriented network state*, an alternative perspective to the bus-oriented network state $\boldsymbol{\delta}$.

The incidence matrix $\mathfrak{D}$ (as defined in [54, Chapter 2]) of the power-flow structure graph $\mathfrak{G}$ conveniently encodes the relationship between buses and lines, as well as the assigned orientation of each line. The incidence matrix is defined in terms of an arbitrary orientation of the lines, for which we will choose the positive power-flow directions in $\overrightarrow{\mathcal{E}}$. Rows in the incidence matrix $\mathfrak{D}$ correspond to lines in $\mathfrak{G}$, while columns in $\mathfrak{G}$ correspond to its vertices. The element at row i and column k of $\mathfrak{D}$ has the value 1 if $(k,m) \in \overrightarrow{\mathcal{E}}$, -1 if $(m,k) \in \overrightarrow{\mathcal{E}}$, and 0 otherwise. Therefore, $\mathfrak{D}$ explicitly encodes the structure of the power network, and allows easy conversion between bus-oriented quantities and line-oriented quantities, and in particular $\boldsymbol{\theta} = \mathfrak{D}^T \boldsymbol{\delta}$.

Notice that the sum of the line voltage angles around a cycle equals some integer

multiple of 2π. Therefore, if the network contains cycles, then the line voltage angles are *not* linearly independent, and so there exist values of $\boldsymbol{\theta} \in \mathbb{T}^L$ which are not feasible, that is, there does not exist $\boldsymbol{\delta}$ such that $\boldsymbol{\theta} = \mathfrak{D}^T\boldsymbol{\delta}$.

3.3.2 Bus and Line-oriented Forms of the Structure-Preserving Model

The vector of line power flows $\mathbf{P_{Line}} \in \mathbb{R}^L$ may be viewed as a function either of $\boldsymbol{\delta}$ or of $\boldsymbol{\theta}$ as follows:

$$\mathbf{P_{Line}}(\mathfrak{D}^T\boldsymbol{\delta}) = \mathbf{P_{Line}}(\boldsymbol{\theta}) = \mathbf{Y_{Line}}\mathbf{V_{In}}\mathbf{V_{Out}}\sin(\boldsymbol{\theta}), \tag{8}$$

where

- $\mathbf{Y_{Line}} \in \mathbb{R}^{L \times L} = diag(\begin{bmatrix} Y_1 & \ldots & Y_L \end{bmatrix}^T)$ is the constant diagonal matrix of line admittance magnitude values.

- $\mathbf{V_{In}} \in \mathbb{R}^{L \times L}$ is the constant diagonal matrix of "in" (per the power-flow direction) bus voltage magnitudes.

- $\mathbf{V_{Out}} \in \mathbb{R}^{L \times L}$ is the constant diagonal matrix of "out" (per the power-flow direction) bus voltage magnitudes.

- $\sin(\boldsymbol{\theta}) = \begin{bmatrix} \sin(\theta_1) & \ldots & \sin(\theta_L) \end{bmatrix}^T$

It can be easily verified that each row i of (8) (associated with line $(k, m) \in \overrightarrow{\mathcal{E}}$ which was assigned index i) reduces to (2). Since $P_{Line,m,k} = -P_{Line,k,m}$, then the line power flow associated with each line in $\mathcal{E}$ can be directly derived from an element of $\mathbf{P_{Line}}$.

Using the definition of $\mathbf{P_{Line}}$ in (8), we can then write the bus voltage-angle ($\boldsymbol{\delta}$) dynamics in a convenient vector form as follows:

$$\boldsymbol{\Delta\omega} = \dot{\boldsymbol{\delta}} = \mathbf{D}^{-1}\big[\mathbf{P_{Ref}} - \mathbf{P_L^0} - \mathfrak{D}\mathbf{P_{Line}}(\mathfrak{D}^T\boldsymbol{\delta})\big], \tag{9}$$

where $\mathbf{D} \in \mathbb{R}^{N \times N} = diag(\begin{bmatrix} D_1 & \ldots & D_N \end{bmatrix}^T)$ is the diagonal matrix of the bus frequency dependence coefficients. Since (by assumption) the network is lossless, $P_{Line,m,k} = -P_{Line,k,m}$ so each row k of (9) reduces to (7).

25

The line voltage-angle state vector $\boldsymbol{\theta} = \mathfrak{D}^T\boldsymbol{\delta}$ provide an alternative perspective on the voltage-angle and frequency dynamics, since they may be viewed as a *line-oriented state* in contrast to the *bus-oriented state* $\boldsymbol{\delta}$. We may obtain the $\boldsymbol{\theta}$-space dynamics by transforming (9) as follows:

$$\dot{\boldsymbol{\theta}} = \mathfrak{D}^T\dot{\boldsymbol{\delta}} = \mathfrak{D}^T\mathbf{D}^{-1}\big[\mathbf{P_{Ref}} - \mathbf{P_L^0}\big] - \mathfrak{L}_E\mathbf{P_{Line}}(\theta), \tag{10}$$

where $\mathfrak{L}_E = \mathfrak{D}^T\mathbf{D}^{-1}\mathfrak{D} \in \mathbb{R}^{L \times L}$ is the edge Laplacian matrix of the graph $\mathfrak{G}$ (as defined in [80]) weighted by $\mathbf{D}^{-1}$. Each element i of the vector $\dot{\boldsymbol{\theta}}$ corresponds to $\dot{\theta}_i = \dot{\theta}_{k,m} = \dot{\delta}_k - \dot{\delta}_m = \Delta\omega_k - \Delta\omega_m$, that is, the frequency difference across the line $(k,m) \in \overrightarrow{\mathcal{E}}$ which was assigned index i and direction k to m.

The vector dynamic equations (9) and (10) represent the voltage-angle and frequency dynamics of a droop inverter-based power network (respectively in bus-oriented and line-oriented forms). These two models provide alternative perspectives on the dynamics, which will allow for easy analysis of bus or line quantities respectively. In addition, both forms explicitly integrate the power-flow structure of the network (through the incidence matrix $\mathfrak{D}$), the control law of each inverter (through the inverter model), the load frequency dependence (through the frequency-dependence term D'_k for load bus k), and the non-linear bus coupling (through the line power-flow function represented in (8)). By analyzing the equilibria and convergence behavior of (9) and (10) in the following sections, we will determine the frequency synchronization and power sharing characteristics of a droop inverter-based network of arbitrary size and structure.

3.4   Steady-State Equilibria (Frequency Agreement)

In [23], a dynamic model in the form of (9) with coupling functions (8) was designated as the *non-uniform Kuramoto oscillator model*, and based on it [66] derived conditions for frequency synchronization applicable to radial (acyclic) inverter-based power networks. We will now extend these results by considering how our models can

be used to analyze frequency synchronization for connected networks of arbitrary size and structure.

In power system analysis, *steady state* is the state in which all bus frequencies are equal, that is:

$$\Delta\boldsymbol{\omega} = \dot{\boldsymbol{\delta}} \in span\{\mathbf{1}_N\} \tag{11}$$

where $\mathbf{1}_N$ is the vector of length N where each element equals one and $span\{\mathbf{1}_N\}$ indicates the set of all $\Delta\boldsymbol{\omega}$ such that $\Delta\boldsymbol{\omega} = \mathbf{1}_N\Delta\omega_{Sys}$ for some $\Delta\omega_{Sys} \in \mathbb{R}$.

Now consider the line voltage-angle state $\boldsymbol{\theta} = \mathfrak{D}^T\boldsymbol{\delta}$. It has been shown that the incidence matrix transpose $\mathfrak{D}^T$ of a graph $\mathfrak{G}$ has null space $span\{\mathbf{1}_N\}$ if and only $\mathfrak{G}$ is connected (see [54, Theorem 2.8]). Since the power-flow structure graph $\mathfrak{G}$ is connected (by assumption, see Definition 3.1.E), then the network is at steady state ($\boldsymbol{\delta} \in span\{\mathbf{1}_N\}$) if and only if:

$$\dot{\boldsymbol{\theta}} = \mathfrak{D}^T span\{\mathbf{1}_N\} = \mathbf{0}_L \tag{12}$$

where $\mathbf{0}_L$ is the vector of length L where each element equals zero.

We observe that the condition of all equal bus frequencies ($\dot{\boldsymbol{\delta}} \in span\{\mathbf{1}_N\}$ or $\dot{\boldsymbol{\theta}} = \mathbf{0}_L$) can be viewed as a form of network agreement, and therefore, we will use the term *frequency agreement* to describe it. Similarly, we will adopt the term *frequency synchronization* to describe convergence to the above state, that is, $\lim_{t\to\infty} \inf_{\Delta\omega_{sys}} ||\dot{\boldsymbol{\delta}}(t) - \mathbf{1}_N\Delta\omega_{Sys}|| = 0$ (or $\lim_{t\to\infty} ||\dot{\boldsymbol{\theta}}|| = 0$). Throughout this paper, we will use the shorthand notation $\boldsymbol{x}(t) \to \bar{\boldsymbol{x}}$ to indicate convergence of $\boldsymbol{x}(t)$ to a point $\bar{\boldsymbol{x}}$ ($\lim_{t\to\infty} ||\boldsymbol{x}(t) - \bar{\boldsymbol{x}}|| = 0$) and $\boldsymbol{x}(t) \to \bar{\boldsymbol{X}}$ to indicate convergence of $\boldsymbol{x}(t)$ to a set $\bar{\boldsymbol{X}}$ ($\lim_{t\to\infty} \inf_{\bar{\boldsymbol{x}}\in\bar{X}} ||\boldsymbol{x}(t) - \bar{\boldsymbol{x}}|| = 0$) using the standard Euclidian norm $|| \bullet ||$. Therefore, frequency synchronization is indicated by the shorthand $\boldsymbol{\delta} \to span\{\mathbf{1}_N\}$ or $\dot{\boldsymbol{\theta}} \to \mathbf{0}_L$.

3.4.1 Center-of-Mass Frequency

To calculate the shared system frequency to which the network may converge, we will create the concept of a *center-of-mass frequency* $\Delta\omega_{COM}$, defined as follows:

Definition 3.2 (Center-of-Mass Frequency).

$$\Delta\omega_{COM}(t) = \frac{\sum_{k\in\mathcal{V}} D_k \Delta\omega_k(t)}{\sum_{k\in\mathcal{V}} D_k} = \frac{\mathbf{1}_N^T \mathbf{D}}{\mathbf{1}_N^T \mathbf{D} \mathbf{1}_N} \boldsymbol{\Delta\omega}(t) \tag{13}$$

The center-of-mass frequency $\Delta\omega_{COM}$ of a network represents the weighted average of the bus frequency offsets $\Delta\omega_k$ (each weighted by the corresponding total frequency dependence coefficient D_k) for each bus in network. We show in Lemma 3.1 that frequency synchronization corresponds to convergence of all bus frequencies to $\Delta\omega_{COM}$, and further that $\Delta\omega_{COM}$ is independent of state and can be calculated purely from system inputs and parameters:

Lemma 3.1 (Static Center-of-Mass Frequency of Droop Inverter-Based Networks).
Consider the dynamic equation (9) representing the voltage-angle dynamics of a lossless droop inverter-based power network with ideal voltage regulation (Definition 3.1), and define center of mass frequency $\Delta\omega_{COM}$ as in Definition 3.2. Then $\dot{\boldsymbol{\delta}} \to span\{\mathbf{1}_N\}$ (Frequency Synchronization) corresponds to $\dot{\boldsymbol{\delta}} \to \mathbf{1}_N \Delta\omega_{COM}$, and furthermore

$$\Delta\omega_{COM} = \frac{\sum_{k\in\mathcal{V}} P_{Ref,k} - \sum_{k\in\mathcal{V}} P_{L,k}^0}{\sum_{k\in\mathcal{V}} D_k} \tag{14}$$

Proof. If the network is in frequency agreement at a time t ($\dot{\boldsymbol{\delta}}(t) \in span\{\mathbf{1}_N\}$), then there exists $\Delta\omega_{Sys}(t) \in \mathbb{R}$ such that $\dot{\boldsymbol{\delta}}(t) = \boldsymbol{\Delta\omega}(t) = \mathbf{1}_N \Delta\omega_{Sys}(t)$. Therefore:

$$\Delta\omega_{COM}(t) = \frac{\mathbf{1}_N^T \mathbf{D}}{\mathbf{1}_N^T \mathbf{D} \mathbf{1}_N} \mathbf{1}_N \omega_{Sys}(t) = \Delta\omega_{Sys}(t) \tag{15}$$

Therefore, frequency synchronization of the network ($\dot{\boldsymbol{\delta}} \to span\{\mathbf{1}_N\}$) corresponds to convergence of all frequencies to the center-of-mass frequency ($\dot{\boldsymbol{\delta}} \to \mathbf{1}_N \Delta\omega_{COM}(t)$).

By substituting the state dynamic model (9) into the center-of-mass frequency definition (13), we find:

$$\Delta\omega_{COM} = \frac{\sum_{k\in\mathcal{V}} (P_{Ref,k} - P_{L,k}^0)}{\sum_{k\in\mathcal{V}} D_k} + \frac{\sum_{k\in\mathcal{V}} \sum_{m\in\mathcal{N}(k)} P_{Line,k,m}}{\sum_{k\in\mathcal{V}} D_k} \tag{16}$$

Each line $(k, m) \in \mathcal{E}$ appears twice in the sum in the second term of (16), first for k and then for m. Since $P_{Line,k,m} = -P_{Line,m,k}$, then the second term of (16) cancels, yielding (14). $\square$

Lemma 3.1 above shows that, while the bus frequencies change with state, the center-of-mass frequency is a function only of power injections and bus frequency dependence values, and can be viewed as a generalization of the *scaled power imbalance* ω_{avg} derived in [66, Theorem 3.3]. This concept also bears similarity to the *static centroid property* used in linear consensus networks (see [60, 54]), and we therefore refer to it as the *static center-of-mass frequency property* of a droop inverter-based network.

The center-of-mass frequency of a network could be directly calculated (using (14)) in real-time if complete input and parameter information for the network (not necessarily state) were available. However, even if no device in the network has the complete parameter and input information, $\Delta\omega_{COM}$ can be used to show the steady-state power sharing characteristics of the network, and to determine conditions under which such a steady-state equilibrium will exist.

3.4.2 Power Sharing at Frequency Agreement

In addition to frequency synchronization, one of the major purposes of the inverter frequency-droop control law is that it is claimed to result in power sharing between inverters. We will investigate this claim below.

We define the following concepts related to inverter power sharing:

- *Network total reference error* $\Delta\mathcal{P}_{Ref}$ is

$$\Delta\mathcal{P}_{Ref} = \sum_{k\in\mathcal{V}} P_{Ref,k} - \sum_{k\in\mathcal{V}} P_{L,k}^0 = \mathbf{1}_N^T \mathbf{P_{Ref}} - \mathbf{1}_N^T \mathbf{P_L^0} \tag{17}$$

- *Network total frequency dependence*:

$$\mathcal{D} = \sum_{k\in\mathcal{V}} D_k = trace\{\mathbf{D}\} \tag{18}$$

Observe that we can rewrite (14) as

$$\Delta\omega_{COM} = \frac{\Delta\mathcal{P}_{Ref}}{\mathcal{D}} \tag{19}$$

29

Therefore, network total frequency dependence $\mathcal{D}$ represents the dependence of center-of-mass frequency $\Delta\omega_{COM}$ on network total reference error $\Delta\mathcal{P}_{Ref}$.

The frequency-droop control law (4) creates an explicit connection between inverter output power error (the difference between its reference and measured output power) and frequency. Therefore, if the network synchronizes in frequency (and so all inverters converge to the same frequency), then the inverters must share the total network load according to their reference and droop constant values. We formalize this result below:

Lemma 3.2 (Simple Power Sharing Property of a Droop Inverter-Based Network).
Consider the lossless droop inverter-based power network with ideal voltage regulation (Definition 3.1) whose bus voltage-angle ($\boldsymbol{\delta}$) dynamics are described by (9). Frequency synchronization ($\dot{\boldsymbol{\delta}} \to span\{\mathbf{1}_N\}$) implies convergence of all inverter output power values to inverter final power value $P_{F,k}$ ($P_{G,k} \to P_{F,k} \ \forall \ k \in \mathcal{V}_{Droop}$), where

$$P_{F,k} = P_{Ref,k} - R_k^{-1}\frac{\Delta\mathcal{P}_{Ref}}{\mathcal{D}} \ \forall \ k \in \mathcal{V}_{Droop} \tag{20}$$

Proof. Since frequency synchronization implies convergence of all inverter frequencies to the center of mass frequency $\Delta\omega_{COM}$ (see Lemma 3.1), by solving the droop control law (4) for $P_{G,k}$ and subsitituting $\Delta\omega_k = \Delta\omega_{COM} \ \forall \ k \in \{1\ldots M\}$ and (19), we get:

$$\begin{aligned}P_{G,k} &= P_{Ref,k} - R_k^{-1}\Delta\omega_{COM} \\ &= P_{Ref,k} - R_k^{-1}\frac{\Delta\mathcal{P}_{Ref}}{\mathcal{D}}\end{aligned} \tag{21}$$

$\square$

Lemma 3.2 shows that frequency synchronization of a droop inverter-based network implies convergence of each inverter's output power $P_{G,k}$ to a value $P_{F,k}$ defined by (20). This means that at frequency agreement, each inverter will source its reference power value $P_{Ref,k}$, with an offset such that the inverters share the total network

reference error $\Delta\mathcal{P}_{Ref}$ inverse-proportionally to their droop constants. We refer to this property as the *simple power sharing property* of a droop inverter-based network.

The simple power sharing property is a desirable behavior for a droop inverter-based network, since it means that, if frequency synchronization occurs, then the steady-state power values of the inverters can be determined by the selection of the reference and droop constants. However, it is not clear that a frequency agreement equilibrium must always exist, or that such equilibria will be stable. These properties of frequency agreement equilibria will be assessed in the following sections.

3.4.3 Equilibrium Equation

From Lemma 3.1, the points of frequency agreement are the points in which $\dot{\boldsymbol{\delta}} = \mathbf{1}_N \Delta\omega_{COM}$. We define the set of all such $\boldsymbol{\delta}$ as:

Definition 3.3 ($\boldsymbol{\delta}$ Equilibrium Set).

$$\Delta_{Eq}(\mathbf{P_{Ref}} - \mathbf{P_L^0}) = \{\boldsymbol{\delta} \text{ such that } \dot{\boldsymbol{\delta}} = \mathbf{1}_N \Delta\omega_{COM}\} \tag{22}$$

From (9), the members of Δ_{Eq} are the solutions of:

$$\mathbf{1}_N \Delta\omega_{COM} = \mathbf{D}^{-1}\big[\mathbf{P_{Ref}} - \mathbf{P_L^0} - \mathfrak{D}\mathbf{P_{Line}}(\mathfrak{D}^T\boldsymbol{\delta})\big] \tag{23}$$

Observe that (since $null\{\mathfrak{D}^T\} = span\{\mathbf{1}_N\}$) if $\boldsymbol{\delta}_{Eq} \in \Delta_{Eq}$, then $[\boldsymbol{\delta}_{Eq} + \mathbf{1}_N\alpha] \in \Delta_{Eq}$ for all $\alpha \in \mathbb{R}$, that is, each $\boldsymbol{\delta}_{Eq} \in \Delta_{Eq}$ defines an affine space $[\boldsymbol{\delta}_{Eq} + span\{\mathbf{1}_N\}] \in \Delta_{Eq}$. While not technically equilibria, with some abuse of terminology we will use the term *equilibrium affine space* to describe these spaces.

Similarly we define the set of all points in the line-oriented structure-preserving model ($\boldsymbol{\theta}$) corresponding to frequency agreement ($\dot{\boldsymbol{\theta}} = \mathbf{0}_L$) as:

Definition 3.4 ($\boldsymbol{\theta}$ Equilibrium Set).

$$\Theta_{Eq}(\mathbf{P_{Ref}} - \mathbf{P_L^0}) = \{\boldsymbol{\theta} \text{ such that } \dot{\boldsymbol{\theta}} = \mathbf{0}_L \text{ and } \exists \boldsymbol{\delta} \text{ such that } \boldsymbol{\theta} = \mathfrak{D}^T\boldsymbol{\delta}\} \tag{24}$$

From (10), the members of Θ_{Eq} are the *feasible* solutions of:

$$0_L = \mathfrak{D}^T \mathbf{D}^{-1} \left[\mathbf{P_{Ref}} - \mathbf{P_L^0} \right] - \mathfrak{L}_E \mathbf{P_{Line}}(\boldsymbol{\theta}) \tag{25}$$

Each equilibrium affine space $[\boldsymbol{\delta}_{Eq} + span\{\mathbf{1}_N\}] \in \Delta_{Eq}$ maps to a single point $\boldsymbol{\theta}_{Eq} = \mathfrak{D}^T \boldsymbol{\delta}_{Eq} \in \Theta_{Eq}$.

The equilibria of both the $\boldsymbol{\delta}$ and $\boldsymbol{\theta}$ dynamics are functions of $\mathbf{P_{Ref}} - \mathbf{P_L^0}$, which we will designate as the *reference power injection vector* and treat as a system disturbance. Most power system transient analysis considers power injection input constant during pre-fault and post-fault condition, and so in this chapter we will treat this analogous input as a (piecewise) constant.

3.4.4 Existence of Frequency-Agreement Equilibria

Since network convergence to frequency agreement corresponds to convergence of $\boldsymbol{\delta}$ to an equilibrium affine space in Δ_{Eq} (or equivalently convergence of $\boldsymbol{\theta}$ to a point in Θ_{Eq}), it is clear that non-emptiness of Δ_{Eq} (or equilvalently Θ_{Eq}) is a necessary condition for frequency synchronization. We will therefore consider conditions under which such an equilibrium exists.

In [66, Theorem 3.3], a necessary and sufficient condition for existance of an equilibrium of a *radial* (acyclic) lossless inverter-based power network was presented. This condition is based on maximum power transfer capability of each system line to the radial center bus; however it is not applicable to meshed networks since no such center bus exists. Below, we will generalize this condition to the meshed case, and show that it generalizes as a necessary, but not sufficient, condition.

In order to assess the existence of a frequency agreement equilibrium for a droop inverter-based network, we will introduce the concept of the *frequency agreement power imbalance* for cuts in the network. The frequency agreement power imbalance represents the power that must flow across each cut of the droop inverter-based

network at frequency agreement. Since the power generation of each inverter at frequency agreement can be calculated a-priori based on network references, loads, and total frequency dependence coefficients (see Lemma 3.2), then the required power flow across each network cut can also be calculated.

Consider any set of buses $\mathcal{V}_C \subset \mathcal{V}$ on the power-flow structure graph $\mathfrak{G} = (\mathcal{V}, \mathcal{E})$. Each such bus set defines a directional cut $\overrightarrow{\mathcal{E}_C} \subset \overrightarrow{\mathcal{E}}$, where the removal of $\overrightarrow{\mathcal{E}_C}$ from $\mathfrak{G}$ seperates $\mathcal{V}_C$ from $(\mathcal{V} \setminus \mathcal{V}_C)$. If $\mathcal{V}_C$ and $(\mathcal{V} \setminus \mathcal{V}_C)$ are considered as supernodes of the power network, then Kirchoff's law (in power form) states that any power imbalance in $\mathcal{V}_C$ must flow across the lines in $\overrightarrow{\mathcal{E}_C}$ to $(\mathcal{V} \setminus \mathcal{V}_C)$.

More formally, let $\mathbf{x_C} \in \mathbb{R}^N$ be the characteristic vector of $\mathcal{V}_C$, that is:

$$\mathbf{x_C} = \begin{bmatrix} x_{C,1} & \dots & x_{C,N} \end{bmatrix}^T \text{ where } x_{C,k} = \begin{cases} 1 & \text{Bus } k \in \mathcal{V}_C \\ 0 & \text{Bus } k \notin \mathcal{V}_C \end{cases} \tag{26}$$

At frequency agreement, the equilibrium equation (23) must be satisfied. Left-multiplying (23) by $\mathbf{x_C}^T \mathbf{D}$ (which is equivalent to taking a D_k-weighted sum of the rows associated with buses in $\mathcal{V}_C$) and re-arranging:

$$0 = \mathbf{x_C}^T (\mathbf{P_{Ref}} - \mathbf{P_L^0} - D\mathbf{1}_N \Delta\omega_{COM}) - \mathbf{x_C}^T \mathfrak{D} \mathbf{P_{Line}}(\mathfrak{D}^T \boldsymbol{\delta}_{Eq}) \tag{27}$$

The quantity $\mathbf{x_C}^T \mathfrak{D}$ is the sum of rows of $\mathfrak{D}$ corresponding to buses in $\mathcal{V}_C$, that is, the transpose of the signed cut vector associated with the cut $(\mathcal{V}_C, V \setminus \mathcal{V}_C)$ (see [30, Chapter 14]). Therefore, we can rewrite (27) as:

$$\sum_{k \in \mathcal{V}_C} (P_{Ref,k} - P_{L,k}^0 - D_k \Delta\omega_{COM}) = \sum_{(k,m) \in \overrightarrow{\mathcal{E}_C}} \pm P_{Line,k,m}(\delta_{Eq,k} - \delta_{Eq,m}), \tag{28}$$

where the sign of $P_{Line,k,m}$ in the sum on the right hand side is determined by the direction of the directed line $(k,m) \in \overrightarrow{\mathcal{E}_C}$ relative to the the bus set $\mathcal{V}_C$. The left-hand side of (29) is a constant for constant inputs $P_{Ref,k}$ and $P_{L,k}^0$, and we designate this constant as the frequency agreement power imbalance associated with the the bus set $\mathcal{V}_C$:

Definition 3.5 (Frequency Agreement Power Imbalance). *The frequency agreement power imbalance $\Delta P_{Eq,C}$ associated with the bus set $\mathcal{V}_C$ of the graph power-flow structure graph $\mathfrak{G}$ is defined as:*

$$\Delta P_{Eq,C} = \sum_{k \in \mathcal{V}_C} (P_{Ref,k} - P_{L,k}^0 - D_k \Delta\omega_{COM}) \tag{29}$$

where the center-of-mass frequency $\Delta\omega_{COM}$ is calculated as in (14).

The constant $\Delta P_{Eq,C}$ is the total power injection to the bus set $\mathcal{V}_C$ at frequency agreement, and therefore (by (28)) it represents the total power that must flow across the associated cut $\overrightarrow{\mathcal{E}_C}$ at frequency agreement.

Since total power transfer capacity of a cut is limited, if there exists a cut of the network that is not capable of carrying its required steady-state power imbalance, then no frequency-agreement equilibrium can exist, and the network cannot achieve frequency synchronization. We formalize this result in Theorem 3.1 below:

Theorem 3.1 (Necessary Condition for Existence of Equilibria in Droop Inverter-Based Network). *Consider a lossless droop inverter-based power network with ideal voltage regulation (Definition 3.1) whose bus voltage-angle dynamics are described by (9) and whose power-flow structure graph is $\mathfrak{G} = (\mathcal{V}, \mathcal{E})$. Assume that there exists a non-empty bus set $\mathcal{V}_C \subset \mathcal{V}$ and line set $\overrightarrow{\mathcal{E}_C} \subset \overrightarrow{\mathcal{E}}$ associated with the cut $(\mathcal{V}_C, \mathcal{V} \setminus \mathcal{V}_C)$ of the graph $\mathfrak{G}$ such that*

$$|\Delta P_{Eq,C}| > \sum_{(k,m) \in \overrightarrow{\mathcal{E}_C}} Y_{k,m} V_k V_m \tag{30}$$

Then $\Delta_{Eq} = \Theta_{Eq} = \emptyset$, and the network will NOT *converge to frequency agreement.*

Proof. Contradiction Hypothesis: There exists a bus set $\mathcal{V}_C \subset \mathcal{V}$ and associated cut $\overrightarrow{\mathcal{E}_C}$ such that (30) holds but Δ_{Eq} is non-empty. Then there exists $\boldsymbol{\delta}_{Eq} \in \Delta_{Eq}$, that is, $\boldsymbol{\delta} = \boldsymbol{\delta}_{Eq}$ solves (23).

We have already shown that if $\boldsymbol{\delta}_{Eq}$ solves (23), then:

$$\sum_{(k,m)\in\overrightarrow{\mathcal{E}_C}} \pm P_{Line,k,m}(\delta_{Eq,k} - \delta_{Eq,m}) = \Delta P_{Eq,C}, \tag{31}$$

for each cut $\overrightarrow{\mathcal{E}_C}$ of the graph $\mathfrak{G}$.

Now consider the maximum absolute value of power-flow capacity of lines in the cut $\mathcal{E}_C$ from $\mathcal{V}_C$ to $(\mathcal{V} \setminus \mathcal{V}_C)$. From (2), we can bound the absolute value of the left-hand side of (31) by:

$$\left| \sum_{(k,m)\in\overrightarrow{\mathcal{E}_C}} \pm P_{Line,k,m}(\delta_{Eq,k} - \delta_{Eq,m}) \right| \leq \sum_{(k,m)\in\overrightarrow{\mathcal{E}_C}} Y_{k,m} V_k V_m \tag{32}$$

Taking the absolute value of (31) and substituting into (32), we find

$$|\Delta P_{Eq,C}| \leq \sum_{(k,m)\in\overrightarrow{\mathcal{E}_C}} Y_{k,m} V_k V_m \tag{33}$$

which contradicts the assumption that (30) holds for $\mathcal{V}_C$. Therefore, if (30) holds for some $\mathcal{V}_C \subset V$, then no solution to (23) exists ($\Delta_{Eq} = \emptyset$), and the network cannot converge to frequency agreement.

By Definition 3.4, $\boldsymbol{\theta}_{Eq} = \mathfrak{D}^T \boldsymbol{\delta}_{Eq} \in \Theta_{Eq}$ implies that $\dot{\boldsymbol{\theta}} = \mathbf{0}_L$ when $\boldsymbol{\theta} = \boldsymbol{\theta}_{Eq}$. Notice that $\dot{\boldsymbol{\theta}} = \mathbf{0}_L = \mathfrak{D}^T \dot{\boldsymbol{\delta}}$ implies that $\dot{\boldsymbol{\delta}} \in null\{\mathfrak{D}^T\} = span\{\mathbf{1}_N\}$, that is, $\boldsymbol{\delta} = \boldsymbol{\delta}_{Eq}$ is a solution (23). Therefore $\Delta_{Eq} = \emptyset$ implies $\Theta_{Eq} = \emptyset$ and the proof is complete. $\square$

Theorem 3.1 states that an equilibrium cannot exist if there exists a cut whose total power transfer capacity is less than the frequency agreement power imbalance of its shore subnetworks. If this is the case, then sufficient power to balance the network cannot flow across the cut, and therefore no equilibrium can exist.

If the power-flow structure graph $\mathfrak{G}$ is radial (acyclic), then the condition of Theorem 3.1 reduces to the necessary and sufficient parametric condition 3.5 in [66, Theorem 3.3] since each cut of a radial graph is a linear combination of cuts of single lines incident to the center bus.

However, if the network is meshed, then the non-existence of a bus set $\mathcal{V}_C$ such that the condition of (30) holds is *not* sufficient to ensure existence of an equilibrium. If (30) does not hold for any $\mathcal{V}_C \subset V$, then there exists $\boldsymbol{\theta}_{Eq}$ such that

$$\sum_{k \in \mathcal{V}_C} (P_{Ref,k} - P_{L,k} - D_k \Delta\omega_{COM}) = \sum_{(k,m) \in \mathcal{E}_C} \pm P_{Line,k,m}(\theta_{Eq,i}) \tag{34}$$

However, if graph $\mathfrak{G}$ contains cycles (network is meshed), then there may not exist $\boldsymbol{\delta}_{Eq}$ such that $\boldsymbol{\theta}_{Eq} = \mathfrak{D}^T \boldsymbol{\delta}_{Eq}$, that is, $\boldsymbol{\theta}_{Eq}$ may not be feasible. Therefore, the condition defined in Theorem 3.1 is only a necessary condition (not necessary and sufficient) for existence of an equilibrium in meshed networks.

3.5   Local Stability of Equilibria

Now that the power sharing properties of frequency agreement equilbria have been determined, and a conditions for their existence found, we turn to considering their local stability properties. In [15, 40, 52], linearized models of droop inverter-based networks were developed, and it was suggested that local stability of equilibria could be determined by eigenvalue analysis. In this section, we will generalize on their results by using a linearized form of the structure-preserving models developed earlier in this chapter, allowing general eigenvalue analysis to determine local stability properties of frequency agreement equilibria based on their location in the voltage-angle state space.

In [70], Tavora defines the concept of the *principal region* of the voltage-angle state space, defined as the region in which all line voltage angles $\theta_{k,m} = \delta_k - \delta_m$ for each $(k,m) \in \mathcal{E}$ have magnitude less than $\pi/2$. Following Tavora, we define the following:

Definition 3.6 (Principal Region)**.** *The* principal region *of the voltage-angle state space is defined (respectively in bus voltage angle $\boldsymbol{\delta}$ and line voltage angle $\boldsymbol{\theta}$ spaces) as:*

$$\Delta_{Principal} = \{\boldsymbol{\delta} \text{ such that } ||\mathfrak{D}^T \boldsymbol{\delta}||_\infty < \frac{\pi}{2}\}$$

$$\Theta_{Principal} = \{\boldsymbol{\theta} \ such \ that \ ||\boldsymbol{\theta}||_\infty < \frac{\pi}{2}\}$$

Since $\boldsymbol{\theta} = \mathfrak{D}^T \boldsymbol{\delta}$, then $\boldsymbol{\theta} \in \Theta_{Principal}$ if and only if $\boldsymbol{\delta} \in \Delta_{Principal}$, that is, the two regions simply represent transformed versions of each other. The principal region is more simply defined in $\boldsymbol{\theta}$-space than in $\boldsymbol{\delta}$-space, since in $\boldsymbol{\theta}$-space it is a (bounded) symmetric hypercube, while in $\boldsymbol{\delta}$-space it is dependant on the power-flow structure graph $\mathfrak{G}$ (and not necessarily bounded).

In [1], it was shown that for the classical Kuramoto oscillator model with homogeneous coupling weights, all stable equilibria exist inside the principal region. The bus-oriented structure-preserving model (9) with coupling functions (8) is similar to the classical Kuramoto model analyzed in [1], except that is forced (by the reference power injection terms $\mathbf{P_{Ref}} - \mathbf{P_L^0}$) and has non-homogeneous coupling weights (the peak line power terms $\mathbf{Y_{Line} V_{In} V_{Out}}$). However, as we will show below, the result of [1] (local stability of equilibria on the principal region) also extends to our structure-preserving models of inverter-based networks.

We determine the local stability properties of an equilibrium affine space $[\boldsymbol{\delta}_{Eq} + span\{\mathbf{1}_N\}] \in \Delta_{Eq}$ by small signal analysis. Linearization of the dynamics of $\boldsymbol{\delta}$ near this affine space will require the partial-derivative matrix $\partial \dot{\boldsymbol{\delta}}/\partial \boldsymbol{\delta}$, which may be found by differentiating (9) with respect to $\boldsymbol{\delta}$:

$$\frac{\partial \dot{\boldsymbol{\delta}}}{\partial \boldsymbol{\delta}} = -\mathbf{D}^{-1} \mathfrak{D} \frac{\partial \mathbf{P_{Line}}(\mathfrak{D}^T \boldsymbol{\delta})}{\partial(\mathfrak{D}^T \boldsymbol{\delta})} \mathfrak{D}^T = -L^W(\mathfrak{D}^T \boldsymbol{\delta}), \tag{35}$$

where $L^W(\mathfrak{D}^T \boldsymbol{\delta})$ is the *vertex and edge weighted Laplacian* of graph $\mathfrak{G}$ with constant vertex weight matrix $\mathbf{D}^{-1}$ and state-dependant diagonal edge weight matrix $W(\mathfrak{D}^T \boldsymbol{\delta})$ where

$$W(\mathfrak{D}^T \boldsymbol{\delta}) = W(\boldsymbol{\theta}) := \frac{\partial \mathbf{P_{Line}}(\mathfrak{D}^T \boldsymbol{\delta})}{\partial(\mathfrak{D}^T \boldsymbol{\delta})} = \frac{\partial \mathbf{P_{Line}}(\boldsymbol{\theta})}{\partial \boldsymbol{\theta}} \tag{36}$$

We designate the matrix $W(\mathfrak{D}^T \boldsymbol{\delta})$ as the *line power-flow/voltage-angle Jacobian*. Since each line power flow $P_{Line,k,m}$ associated with line $(k,m) \in \vec{\mathcal{E}}$ is a function only of its own line voltage angle $\theta_{k,m} = \delta_k - \delta_m$, $W(\mathfrak{D}^T \boldsymbol{\delta})$ is in fact a diagonal matrix.

Lemma 3.3 below shows that the line power-flow/voltage-angle Jacobian $W(\mathfrak{D}^T\boldsymbol{\delta})$ is positive definite if and only if $\boldsymbol{\delta}$ is in the principal region:

Lemma 3.3 (Line Power-Flow/Voltage-Angle Jacobian Positive Definite on Principal Region). *Consider the line power-flow/voltage-angle Jacobian* $W(\mathfrak{D}^T\boldsymbol{\delta}) := \dfrac{\partial \mathbf{P_{Line}}(\mathfrak{D}^T\boldsymbol{\delta})}{\partial(\mathfrak{D}^T\boldsymbol{\delta})}$ *where* $\mathbf{P_{Line}}(\mathfrak{D}^T\boldsymbol{\delta})$ *is defined as in (8). Then* $W(\mathfrak{D}^T\boldsymbol{\delta})$ *is positive definite for some* $\boldsymbol{\delta} \in \mathbb{T}^N$ *if and only if* $\boldsymbol{\delta} \in \Delta_{Principal}$. *Equivalently,* $W(\boldsymbol{\theta})$ *is positive definite for some* $\boldsymbol{\theta} \in \mathbb{T}^L$ *if and only if* $\boldsymbol{\theta} \in \Theta_{Principal}$.

Proof. From (8), the partial derivative of $\mathbf{P_{Line}}(\mathfrak{D}^T\boldsymbol{\delta})$ with respect to $\mathfrak{D}^T\boldsymbol{\delta}$ is

$$W(\mathfrak{D}^T\boldsymbol{\delta}) = \mathbf{Y_{Line}}\mathbf{V_{In}}\mathbf{V_{Out}}diag\big[\cos(\mathfrak{D}^T\boldsymbol{\delta})\big], \tag{37}$$

where $\cos(\boldsymbol{\theta}) = \begin{bmatrix} \cos(\theta_1) & \dots & \cos(\theta_L) \end{bmatrix}^T$.

The matrices $\mathbf{Y_{Line}}$, $\mathbf{V_{In}}$, and $\mathbf{V_{Out}}$ are all (by assumption) constant, diagonal, and positive definite. Therefore $W(\mathfrak{D}^T\boldsymbol{\delta})$ is positive definite if and only if $diag[\cos(\mathfrak{D}^T\boldsymbol{\delta})]$ is positive definite, which holds if and only if $||\mathfrak{D}^T\boldsymbol{\delta}||_\infty < \pi/2$ (recall that $\boldsymbol{\delta}$ is defined on the N-torus $[-\pi \quad \pi)^N$), that is, if and only if $\boldsymbol{\delta} \in \Delta_{Principal}$. Finally, $\boldsymbol{\theta} = \mathfrak{D}^T\boldsymbol{\delta} \in \Theta_{Principal}$ if and only if $\boldsymbol{\delta} \in \Delta_{Principal}$, and therefore $W(\boldsymbol{\theta})$ positive definite if and only if $\boldsymbol{\theta} \in \Theta_{Principal}$. $\qquad\square$

From Lemma 3.3 we can determine the following significant properties of the state-dependent weighted Laplacian $L^W(\mathfrak{D}^T\boldsymbol{\delta})$:

Corollary 3.1 (Bus Laplacian Non-Negative on Principal Region). *Consider the state-dependant weighted Laplacian*

$$L^W(\mathfrak{D}^T\boldsymbol{\delta}) := \mathbf{D}^{-1}\mathfrak{D}\,W(\mathfrak{D}^T\boldsymbol{\delta})\,\mathfrak{D}^T \tag{38}$$

This matrix has no negative eigenvalues if and only if $\mathfrak{G}$ is connected and $\boldsymbol{\delta} \in \Delta_{Principal}$. Further, if $\mathfrak{G}$ is connected and $\boldsymbol{\delta} \in \Delta_{Principal}$ then $null\{L^W(\mathfrak{D}^T\boldsymbol{\delta})\} = span\{\mathbf{1}_N\}$.

Proof. It has been shown that a graph Laplacian with vertex and edge weights has no negative eigenvalues if all vertex weights are positive [14] and if and only if all edge weights are positive (for example, see [54, Chapter 7]). By assumption we have $\mathbf{D}^{-1}$ diagonal and positive definite (all positive vertex weights), and we showed in Lemma 3.3 that the edge weights (represented by the line power-flow/voltage-angle Jacobian) evaluated at $\boldsymbol{\delta}_{Eq}$ are all positive if and only if $\boldsymbol{\delta}_{Eq} \in \Delta_{Principal}$. Further since $\mathfrak{G}$ connected implies $null\{\mathfrak{D}^T\} = span\{\mathbf{1}_N\}$ (see [54, Theorem 2.8]) and both $\mathbf{D}^{-1}$ and $W(\mathfrak{D}^T\boldsymbol{\delta})$ are full rank for $\boldsymbol{\delta} \in \Delta_{Principal}$, it is then easily shown from (38) that $null\{L^W(\mathfrak{D}^T\boldsymbol{\delta})\} = span\{\mathbf{1}_N\}$. $\qquad\square$

We are now ready to perform small-signal analysis of the $\boldsymbol{\delta}$ dynamics and state our equilibrium local stability result:

Theorem 3.2 (Local Stability of Frequency Agreement Equilibria). *Consider the lossless droop inverter-based power network with ideal voltage regulation (Definition 3.1) whose bus voltage-angle ($\boldsymbol{\delta}$) dynamics are described by (9). Define static equilibrium set $\Delta_{Eq}(\mathbf{P_{Ref}} - \mathbf{P_L^0})$ as in Definition 3.3 and Principal Region $\Delta_{Principal}$ as in Definition 3.6, and assume that there exists static equilibrium $\boldsymbol{\delta}_{Eq} \in \Delta_{Eq}$. Then the equilibirum affine space $[\boldsymbol{\delta}_{Eq} + span\{\mathbf{1}_N\}]$ is locally asymptotically stable if and only if $\boldsymbol{\delta}_{Eq} \in \Delta_{Principal}$.*

Proof. We define $\boldsymbol{\xi} = \boldsymbol{\delta} - \boldsymbol{\delta}_{Eq}$, the deviation of $\boldsymbol{\delta}$ from equilibrium $\boldsymbol{\delta}_{Eq}$. The dynamics of $\boldsymbol{\xi}$ are $\dot{\boldsymbol{\xi}} = \dot{\boldsymbol{\delta}}$. If the affine space $[\boldsymbol{\delta}_{Eq} + span\{\mathbf{1}_N\}]$ is locally asymptotically stable, then $\boldsymbol{\xi} \to span\{\mathbf{1}_N\}$ for values of $\boldsymbol{\xi}$ near $span\{\mathbf{1}_N\}$. Therefore, we begin by linearizing for $\boldsymbol{\xi}$ near $span\{\mathbf{1}_N\}$:

$$\dot{\boldsymbol{\xi}} \approx \dot{\boldsymbol{\xi}}\big|_{\boldsymbol{\xi}\in span\{\mathbf{1}_N\}} + \frac{\partial \dot{\boldsymbol{\xi}}}{\partial \boldsymbol{\xi}}\big|_{\boldsymbol{\xi}\in span\{\mathbf{1}_N\}}\boldsymbol{\xi}$$

$$= \dot{\boldsymbol{\delta}}\big|_{\boldsymbol{\delta}\in[\boldsymbol{\delta}_{Eq}+span\{\mathbf{1}_N\}]} + \frac{\partial \dot{\boldsymbol{\delta}}}{\partial \boldsymbol{\delta}}\big|_{\boldsymbol{\delta}\in[\boldsymbol{\delta}_{Eq}+span\{\mathbf{1}_N\}]}\boldsymbol{\xi} \qquad (39)$$

Substituting (35) and $\dot{\boldsymbol{\delta}}\big|_{\boldsymbol{\delta}\in[\boldsymbol{\delta}_{Eq}+span\{\mathbf{1}_N\}]} = \mathbf{1}_N\Delta\omega_{COM}$ (since $[\boldsymbol{\delta}_{Eq}+span\{\mathbf{1}_N\}] \in \Delta_{Eq}$) into (39) we find:

$$\dot{\boldsymbol{\xi}} \approx \mathbf{1}_N\Delta\omega_{COM} - L^W(\mathfrak{D}^T\boldsymbol{\delta}_{Eq})\boldsymbol{\xi} \tag{40}$$

We showed in Corollary 3.1 that $L^W(\mathfrak{D}^T\boldsymbol{\delta}_{Eq})$ has no negative eigenvalues if and only if $\boldsymbol{\delta}_{Eq} \in \Delta_{Principal}$. Since a linear system with all non-negative eigenvalues is asymptotically stable to the null space and $null\{L^W(\mathfrak{D}^T\boldsymbol{\delta}_{Eq})\} = span\{\mathbf{1}_N\}$, the forced linearized dynamic in (40) are locally asymptotically stable to the agreement subspace (and $\boldsymbol{\delta}$ locally asymptotically stable to the affine space $[\boldsymbol{\delta}_{Eq} + span\{\mathbf{1}_N\}]$) if and only if $\boldsymbol{\delta}_{Eq} \in \Delta_{Principal}$.

□

Theorem 3.2 shows the powerful result that while points of frequency agreement may exist elsewhere in the $\boldsymbol{\delta}$ space, *all equilibria in the principal region $\Delta_{Principal}$ are locally asymptotically stable, and all equilibria outside $\Delta_{Principal}$ are not locally asymptotically stable.*

From Theorem 3.2 we may define the set of all *stable* equilibria of the $\boldsymbol{\delta}$ (or $\boldsymbol{\theta}$) dynamics as:

Definition 3.7 (Stable Frequency Agreement Equilibrium Sets).

$$\Delta_{Eq,Stable}(\mathbf{P_{Ref}} - \mathbf{P_L^0}) = \Delta_{Eq}(\mathbf{P_{Ref}} - \mathbf{P_L^0}) \cap \Delta_{Principal}$$

$$\Theta_{Eq,Stable}(\mathbf{P_{Ref}} - \mathbf{P_L^0}) = \Theta_{Eq}(\mathbf{P_{Ref}} - \mathbf{P_L^0}) \cap \Theta_{Principal}$$

Theorem 3.2 describes the stability properties of static equilibria in a small region around each equilibrium, but it does not describe the convergence properties elsewhere on the state space or provide a global condition for convergence to frequency agreement. Therefore, we must seek a more general result (based on the full non-linear model) describing convergence properties elsewhere in the $\boldsymbol{\delta}$ (or $\boldsymbol{\theta}$) state space.

3.6 Frequency Synchronization of the Inverter-Based Power Network

We now extend the logic of Theorem 3.2 to determine a condition on bus voltage-angle trajectory $\boldsymbol{\delta}(t)$ (or line voltage-angle trajectory $\boldsymbol{\theta}(t)$) that ensures convergence of the network to frequency agreement.

In [23, Lemma 3.1], it was shown that a network whose dynamics can be described by non-uniform Kuramoto oscillator model (similar to (9)) will reach agreement if the entire state trajectory remains in the principal region. Rather than apply [23, Lemma 3.1] to our model, we will re-derive this principal in terms of the line power-flow/voltage-angle Jacobian, and show that positive definiteness of this matrix is sufficient to ensure frequency synchronization.

We propose the following energy function for $\boldsymbol{\delta}$:

$$U(\boldsymbol{\delta}) = \frac{1}{2}||D^{\frac{1}{2}}\dot{\boldsymbol{\delta}}(t)||^2 = \frac{1}{2}\dot{\boldsymbol{\delta}}^T \mathbf{D} \dot{\boldsymbol{\delta}} \tag{41}$$

This function is non-negative and finite for all $\boldsymbol{\delta} \in \mathbb{T}^N$. The time-derivative of $V(\boldsymbol{\delta})$ may be found as follows:

$$\dot{U}(\boldsymbol{\delta}) = \dot{\boldsymbol{\delta}}^T \mathbf{D} \frac{\partial \dot{\boldsymbol{\delta}}}{\partial \boldsymbol{\delta}} \dot{\boldsymbol{\delta}} \tag{42}$$

By substitituting (35) into (42) we find:

$$\dot{U}(\boldsymbol{\delta}) = -\dot{\boldsymbol{\delta}}^T \mathbf{D} L^W(\mathfrak{D}^T \boldsymbol{\delta}) \dot{\boldsymbol{\delta}}$$
$$= -\dot{\boldsymbol{\delta}}^T \mathfrak{D} \, W(\mathfrak{D}^T \boldsymbol{\delta}) \, \mathfrak{D}^T \dot{\boldsymbol{\delta}} \tag{43}$$

We showed in Lemma 3.3 that the line power-flow/voltage-angle Jacobian $W(\mathfrak{D}^T \boldsymbol{\delta})$ is positive definite for $\boldsymbol{\delta} \in \Delta_{Principal}$; therefore $\dot{U}(\boldsymbol{\delta}) \leq 0$ for $\boldsymbol{\delta} \in \Delta_{Principal}$. Further since $null\{\mathfrak{D}^T\} = span\{\mathbf{1}_N\}$, $\dot{U}(\boldsymbol{\delta}) = 0$ only when $\dot{\boldsymbol{\delta}} \in span\{\mathbf{1}_N\}$, that is, only when the network is in frequency agreement. Therefore, given a trajectory $\boldsymbol{\delta}(t)$ for $t \geq 0$, if $\boldsymbol{\delta}(t) \in \Delta_{Principal}$ for all $t \geq 0$, then $\dot{\boldsymbol{\delta}}$ must converge to the agreement space, that is, *a network whose state trajectory does not leave the principal region MUST converge to frequency agreement.* We state this result more formally below:

Theorem 3.3 (Sufficient Condition for Frequency Agreement Based on Bus Voltage Angles). *Consider the lossless droop inverter-based power network with ideal voltage regulation (Definition 3.1) whose bus voltage-angle ($\boldsymbol{\delta}$) dynamics are described by (9). Define stable equilibrium set $\Delta_{Eq,Stable}(\mathbf{P_{Ref}} - \mathbf{P_L^0})$ as in Definition 3.7 and Principal Region $\Delta_{Principal}$ as in Definition 3.6. Assume that input $\mathbf{P_{Ref}} - \mathbf{P_L^0}$ is constant and that $\Delta_{Eq,Stable}(\mathbf{P_{Ref}} - \mathbf{P_L^0}) \neq \emptyset$. Consider the trajectory $\boldsymbol{\delta}(t)$ defined on $t \geq 0$, and assume $\boldsymbol{\delta}(t) \in \Delta_{Principal} \; \forall \, t \geq 0$. Then*

3.3.A Frequency Synchronization: $\boldsymbol{\Delta\omega} \to \Delta\omega_{COM}\mathbf{1}_N$.

3.3.B Simple Power Sharing: $P_{G,k} \to P_{F,k} = P_{Ref,k} - R_k^{-1}\Delta\omega_{COM} \; \forall \, k \in \mathcal{V}_{Droop}$.

Proof. Contradiction Hypothesis: There exists trajectory $\boldsymbol{\delta}(t)$ such that $\boldsymbol{\delta}(t) \in \Delta_{Principal} \; \forall \, t \geq 0$ but $\dot{\boldsymbol{\delta}}$ does not converge to $span\{\mathbf{1}_N\}$.

We have shown that $U(\boldsymbol{\delta})$ is non-negative and finite for all $\boldsymbol{\delta} \in \mathbb{T}^N$ and $\dot{U}(\boldsymbol{\delta})$ is non-positive for all $\boldsymbol{\delta} \in \Delta_{Principal}$. Since (by assumption) $\boldsymbol{\delta}(t) \in \Delta_{Principal} \; \forall \, t \geq 0$, we know that $\dot{U}(\boldsymbol{\delta}) \leq 0 \; \forall \, t \geq 0$. Further, since $\dot{U}(\boldsymbol{\delta}) = 0$ only when $\dot{\boldsymbol{\delta}} \in span\{\mathbf{1}_N\}$ and (by the contradiction hypothesis) $\dot{\boldsymbol{\delta}}$ does not converge to $span\{\mathbf{1}_N\}$, then $\dot{U}(\boldsymbol{\delta})$ does not converge to 0.

Consider the quantity

$$U(\boldsymbol{\delta}(t)) = \int_0^t \dot{U}(\boldsymbol{\delta}(\tau))d\tau + U(\boldsymbol{\delta}(0)), \tag{44}$$

along trajectory $\boldsymbol{\delta}(t)$. Since $U(\boldsymbol{\delta}(0))$ finite and $\dot{U}(\boldsymbol{\delta}(t)) \leq 0$ does not converge to 0 along trajectory $\boldsymbol{\delta}(t)$, then there exists time $T > 0$ such that $U(\boldsymbol{\delta}(t)) < 0 \; \forall \, t > T$. However, this contradicts the observation that $U(\boldsymbol{\delta}) \geq 0 \; \forall \, t \geq 0$. Therefore, the contradiction hypothesis is shown false, and instead $\boldsymbol{\delta}(t) \in \Delta_{Principal} \; \forall \, t \geq 0 \implies \dot{\boldsymbol{\delta}} \to span\{\mathbf{1}_N\}$.

In Lemma 3.1 we have shown that convergence of $\dot{\boldsymbol{\delta}}$ to the agreement space corresponds to convergence to the center-of-mass frequency ($\dot{\boldsymbol{\delta}} = \boldsymbol{\Delta\omega} \to \mathbf{1}_N\Delta\omega_{COM}$).

Finally, in Lemma 3.2 we have shown that network convergence to the center-of-mass frequency implies convergence of all inverter output power values to the final power value $P_{G,k} \to P_{F,k}$ where $P_{F,k}$ is defined by (20), and the proof is complete. □

Theorem 3.3 may also be reformulated in $\boldsymbol{\theta}$ space as follows:

Theorem 3.4 (Sufficient Condition for Frequency Synchronization Based on Line Voltage Angles)**.** *Consider the lossless droop inverter-based power network with ideal voltage regulation (Definition 3.1) whose line voltage-angle ($\boldsymbol{\theta}$) dynamics are described by (10). Define stable equilibrium set $\Theta_{Eq,Stable}(\mathbf{P_{Ref}} - \mathbf{P_L^0})$ as in Definition 3.7 and Principal Region $\Theta_{Principal}$ as in Definition 3.6. We assume that input $\mathbf{P_{Ref}} - \mathbf{P_L^0}$ is constant and that $\Theta_{Eq,Stable}(\mathbf{P_{Ref}} - \mathbf{P_L^0}) \neq \emptyset$. Consider the trajectory $\boldsymbol{\theta}(t)$ defined on $t \geq 0$, and assume $\boldsymbol{\theta}(t) \in \Theta_{Principal} \; \forall \, t \geq 0$. Then*

3.4.A Frequency Synchronization: $\dot{\boldsymbol{\theta}}(t) \to \mathbf{0}_L$.

3.4.B Simple Power Sharing: $P_{G,k} \to P_{F,k} = P_{Ref,k} - R_k^{-1}\Delta\omega_{COM} \; \forall \, k \in \mathcal{V}_{Droop}$.

Proof. We have shown that $\boldsymbol{\theta} = \mathfrak{D}^T\boldsymbol{\delta} \in \Theta_{Principal}$ implies $\boldsymbol{\delta} \in \Delta_{Principal}$, and so $\boldsymbol{\theta}(t) \in \Theta_{Principal}$ implies $\boldsymbol{\delta}(t) \in \Delta_{Principal}$. Also, notice that $\dot{\boldsymbol{\theta}} = \mathbf{0}_L = \mathfrak{D}^T\dot{\boldsymbol{\delta}}$ implies that $\dot{\boldsymbol{\delta}} \in null\{\mathfrak{D}^T\} = span\{\mathbf{1}_N\}$, and by Lemma 3.1 $\dot{\boldsymbol{\delta}} \in span\{\mathbf{1}_N\}$ implies $\dot{\boldsymbol{\delta}} = \mathbf{1}_N\Delta\omega_{COM}$. Therefore, if $\Theta_{Eq,Stable}(\mathbf{P_{Ref}} - \mathbf{P_L^0}) \neq \emptyset$ then $\Delta_{Eq,Stable}(\mathbf{P_{Ref}} - \mathbf{P_L^0}) \neq \emptyset$. Therefore, if the criteria in Theorem 3.4 hold then Theorem 3.3 also holds, and the proof follows. □

Theorems 3.3 and 3.4 provide sufficient conditions (in each of $\boldsymbol{\delta}$ and $\boldsymbol{\theta}$ spaces) for frequency agreement based on bus/line voltage-angle trajectory. Conceptually, we may think of Theorems 3.3 and 3.4 as defining a *safe region* (the principal region and all subsets thereof) of the voltage-angle state space of a droop inverter-based network. This means that as long as the network operates only within the safe region, then frequency synchronization and simple power sharing are guaranteed.

3.7 A Sufficient Condition for Frequency Synchronization Based on Line Power Flows

Theorems 3.3 and 3.4 provide a state-space condition on the trajectories of $\boldsymbol{\delta}(t)$ or $\boldsymbol{\theta}(t)$ respectively sufficient to guarantee frequency synchronization and simple power sharing of droop inverter-based networks. Since $\boldsymbol{\theta} = \mathfrak{D}^T \boldsymbol{\delta}$ is the vector of line voltage angles, we stress that the conditions in Theorems 3.3 and 3.4 are *local* in the sense that they consist of a condition on each line voltage angle. However, these conditions may not (in general) be determined directly from only local measurements (since line voltage angles may not be measured locally at a bus). Therefore, we seek another form of Theorems 3.3 or 3.4 which may be determined from local measurements.

3.7.1 Equivalence of Line Voltage-Angle and Line Power-Flow Constraints on Principal Region

While the line voltage-angle values needed by the conditions of Theorems 3.3 and 3.4 cannot be measured locally, line power flows can be. Consider the relationship between line voltage angle $\theta_{k,m}$ and line power flow $P_{Line,km}$ for an arbitrary line $(k,m) \in \mathcal{E}$. On the principal region (where $|\theta_{k,m}| \in (\pi/2 \quad \pi/2)$), this relationship is invertible and non-decreasing, which means that line power-flow bounds can be used in place of line voltage-angle bounds on $\Theta_{Principal}$ (assuming constant voltage magnitudes). We state this result formally in Lemma 3.4.

Lemma 3.4 (Equivalence of Line Voltage-Angle and Power-Flow Constraints). *Consider the quantity $P_{Line,k,m}(\theta_{k,m})$ for line $(k,m) \in \mathcal{E}$ as defined in (2). Then for each $P_{Max,k,m}$ such that $|P_{Max,k,m}| < Y_{k,m}V_kV_m$ there exists $\theta_{Max,k,m}$ such that $|\theta_{Max,k,m}| < \pi/2$ and $P_{Max,k,m} = P_{Line,k,m}(\theta_{Max,k,m})$, where $\theta_{Max,k,m}$ is found by:*

$$\theta_{Max,k,m} = \arcsin(Y_{k,m}^{-1}V_k^{-1}V_m^{-1}P_{Max,k,m}) \tag{45}$$

Further, if $\boldsymbol{\theta} \in \Theta_{Principal}$ then $|\theta_{k,m}| \leq \theta_{Max,k,m} \iff |P_{Line,k,m}(\theta_{k,m})| \leq P_{Max,k,m}$ for all $(k,m) \in \mathcal{E}$.
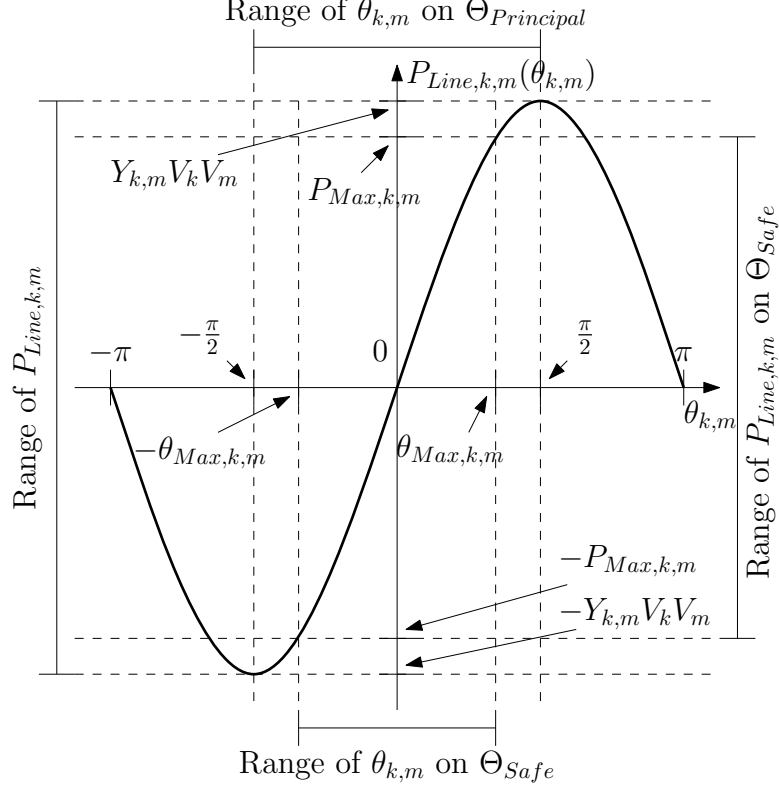
Figure 3.1: Example $P_{Line,k,m}$ vs. $\theta_{k,m}$ for arbitrary line $(k,m) \in \mathcal{E}$.

Proof. From (2), we have $P_{Line,k,m}(\theta_{Max,k,m}) = Y_{k,m}V_kV_m \sin(\theta_{Max,k,m}) = P_{Max,k,m}$ for line (k,m). Since the quantities $Y_{k,m}$, V_k, and V_m are all strictly positive, we may then write:

$$Y_{k,m}^{-1}V_k^{-1}V_m^{-1}P_{Max,k,m} = \sin(\theta_{Max,k,m}) \tag{46}$$

The left hand side of (46) is by assumption is within $(-1 \quad 1)$. On this domain, the sin function is invertible and its inverse is arcsin, whose range is $(-\pi/2 \quad \pi/2)$. Therefore, there exists unique $\theta_{Max,k,m} \in \mathbb{T}$ such that $|\theta_{Max,k,m}| < \pi/2$ and (45) is found by solving (46) for $\theta_{Max,k,m}$. Finally:

$$\frac{\partial |P_{Line,k,m}|}{\partial |\theta_{k,m}|} = Y_{k,m}V_kV_m cos(|\theta_{k,m}|) \geq 0 \,\forall\, \theta_{k,m} \in (-\frac{\pi}{2} \quad \frac{\pi}{2}) \tag{47}$$

Therefore, since $|P_{Line,k,m}|$ is non-decreasing in $|\theta_{k,m}|$ for $\theta_{k,m} \in (-\pi/2 \quad \pi/2)$, then if $\boldsymbol{\theta} \in \Theta_{Principal}$ then $|\theta_{k,m}| \leq \theta_{Max,k,m} \iff |P_{Line,k,m}(\theta_{k,m})| \leq P_{Max,k,m}$. $\qquad\square$

Lemma 3.4 shows that $P_{Line,k,m}(\theta_{k,m})$ is invertible on the principal region, and so

for each line power flow bound $P_{Max,k,m} < Y_{k,m}V_kV_m$ associated with line $(k,m) \in \mathcal{E}$, there exists unique line voltage-angle value $\theta_{Max,k,m}$ such that $|\theta_{Max,k,m}| < \pi/2$ and $|P_{Line,k,m}(\theta_{k,m})| \leq P_{Max,k,m}$ if an only if $|\theta_{k,m}| \leq \theta_{Max,k,m}$ on the principal region, that is, each line voltage-angle constraint within the principal region has an equivalent line power flow constraint.

3.7.2   Safe Region of Line Voltage-Angle Space

Effectively, the sufficient conditions for synchronization presented by Theorems 3.3 and 3.4 are based on a set of line voltage-angle constraints $|\theta_{k,m}| < \pi/2$ for all lines $(k,m) \in \mathcal{E}$ (which define the principal region). This also implies that a subset of the principal region (defined by the line voltage-angle constraints $|\theta_{k,m}| \leq \theta_{Max,k,m}$ where $0 < \theta_{Max,k,m} < Y_{k,m}V_kV_m$ for each line $(k,m) \in \mathcal{E}$) is also a safe region. Further, Lemma 3.4 allows us to replace the line voltage-angle constraints $|\theta_{k,m}| \leq \theta_{Max,k,m}$ with the corresponding line power-flow constraints $|P_{Line,k,m}| \leq P_{Max,k,m}$ (where $P_{Max,k,m}$ and $\theta_{Max,k,m}$ are related by (45)). Since line power flows can be measured locally and in real-time, this condition can be tested by inverters locally. We assume that the line-oriented quantities $\theta_{Max,k,m}$ and $P_{Max,k,m}$ are both line-even, that is $\theta_{Max,k,m} = \theta_{Max,m,k}$ and $P_{Max,k,m} = P_{Max,m,k}$ for all $(k,m) \in \mathcal{E}$. Like other line-even quantities, we define the vector $\mathbf{P_{Max}} = [P_{Max,1} \ldots P_{Max,L}]^T \in \mathbb{R}^L$ where $P_{Max,i} = P_{Max,k,m}$ for each line $(k,m) \in \overrightarrow{\mathcal{E}}$ where i is the index assigned to line (k,m).

More formally, we will define the sets of safe line voltage-angle values Θ_{Safe} as follows:

Definition 3.8 (Safe Region of the Voltage-Angle State Space). *Assume that each line $(k,m) \in \mathcal{E}$ is assigned a line-even maximum power-flow magnitude bound $P_{Max,k,m} = P_{Max,m,k}$ such that $0 < P_{Max,k,m} < Y_{k,m}V_kV_m$. Then we define the* safe region Θ_{Safe}

of the line voltage-angle state space $\boldsymbol{\theta}$ as:

$$\Theta_{Safe} = \{\boldsymbol{\theta} \subset \Theta_{Principal} \text{ such that } |P_{Line,k,m}(\theta_{k,m})| \leq P_{Max,k,m} \ \forall \ (k,m) \in \mathcal{E}\} \quad (48)$$

It follows from Lemma 3.4 that $\boldsymbol{\theta}$ is a member of Θ_{Safe} if and only if $|\theta_{k,m}| \leq$ $\theta_{Max,k,m}$ for all $(k,m) \in \mathcal{E}$ where $\theta_{Max,k,m}$ is found by (45):

Corollary 3.2. *Consider the safe region Θ_{Safe} as defined in Definition 3.8. Then Θ_{Safe} is equivalent to*

$$\Theta_{Safe} = \{\boldsymbol{\theta} \in \mathbb{T}^L \text{ such that } |\theta_{k,m}| \leq \theta_{Max,k,m} \ \forall \ (k,m) \in \mathcal{E}\}, \quad (49)$$

and therefore Θ_{Safe} is compact and is a strict subset of $\Theta_{Principal}$.

Proof. Proof of (49) follows from Definition 3.8 and Lemma 3.4. It follows from (49) that Θ_{Safe} is closed and bounded (and therefore compact). Finally, since $\theta_{Max,k,m} <$ $\pi/2$ (Lemma 3.4), the membership criterion of (49) is always stricter than that of $\Theta_{Principal}$ (Definition 3.6), and therefore Θ_{Safe} is a strict subset of $\Theta_{Principal}$. □

The fact that the two definitions of Θ_{Safe} ((48) and (49)) are equivalent is very useful, because it means that Θ_{Safe} is compact, that it is a strict subset of $\Theta_{Principal}$, and that its boundaries can be detected locally by line power-flow measurements. We will use this fact below to develop a sufficient condition for droop inverter-based network synchronization that be determined from local measurements.

3.7.3 Development of Sufficient Condition for Synchronization Based on Line Power Flows

Now assume that there exists a trajectory $\boldsymbol{\theta}(t)$ such that $\boldsymbol{\theta}(0) \in \Theta_{Safe}$. If $\boldsymbol{\theta}(t)$ leaves Θ_{Safe}, then it must cross the boundary of Θ_{Safe}, that is, at least one line voltage angle $\theta_{k,m}$ must cross its corresponding boundary ($\theta_{Max,k,m}$ or $-\theta_{Max,k,m}$). This means that $P_{Line,k,m}(\theta_{k,m})$ must cross its corresponding $P_{Max,k,m}$ or $-P_{Max,k,m}$. Since Θ_{Safe} is a subset of $\Theta_{Principal}$, then if $\boldsymbol{\theta}(t)$ stays in Θ_{Safe} for all $t \geq 0$ (and if there exists

an equilibrium in Θ_{Safe}) then Theorem 3.4 holds and frequency synchronziation and power sharing are guaranteed. Therefore, we have a condition on $\mathbf{P_{Line}}$ that ensures convergence to frequency agreement: No line power flow magnitude $|P_{Line,k,m}|$ may cross its corresponding $P_{Max,k,m}$ (assuming that $\boldsymbol{\theta}(0) \in \Theta_{Safe}$ and that there exists an equilibrium in Θ_{Safe}).

We state this result more formally below:

Theorem 3.5 (Sufficient Condition for Frequency Synchronization Based on Line Power Flows)**.** *Consider the lossless droop inverter-based power network with ideal voltage regulation whose line voltage-angle ($\boldsymbol{\theta}$) dynamics are described by (10). Select a constant $\mathbf{P_{Max}} \in \mathbb{R}^L = \begin{bmatrix} P_{Max,1} & \ldots & P_{Max,L} \end{bmatrix}^T$ such that $0 < P_{Max,k,m} < Y_{km}V_kV_m$ for each $(k,m) \in \mathcal{E}$, and define Θ_{Safe} as in Definition 3.8. Define $\Theta_{Eq,Stable}(\mathbf{P_{Ref}} - \mathbf{P_L^0})$ as in Definition 3.7 and assume that $\mathbf{P_{Ref}} - \mathbf{P_L^0}$ constant such that $[\Theta_{Safe} \cap \Theta_{Eq,Stable}(\mathbf{P_{Ref}} - \mathbf{P_L^0})] \neq \emptyset$. Consider the trajectory $\boldsymbol{\theta}(t)$ defined on $t \geq 0$ where $\boldsymbol{\theta}(0) \in \Theta_{Safe}$. Then if $|P_{Line,k,m}(\theta_{k,m}(t))| \leq P_{Max,k,m}$ for all $(k,m) \in \mathcal{E}$ and for all $t \geq 0$ then*

3.5.A Frequency Synchronization: $\dot{\boldsymbol{\theta}}(t) \to \mathbf{0}_L$.

3.5.B Simple Power Sharing: $P_{G,k} \to P_{F,k} = P_{Ref,k} - R_k^{-1}\Delta\omega_{COM} \; \forall \, k \in \mathcal{V}_{Droop}$.

Proof. We have shown in Corollary 3.2 that the definitions of Θ_{Safe} (48) and (49) are equivalent and that Θ_{Safe} is a strict subset of $\Theta_{Principal}$. Therefore, we need only to show that satisfaction of the line power-flow constraints $|P_{Line,k,m}(\theta_{k,m}(t))| \leq P_{Max,k,m}$ is sufficient to ensure that $\boldsymbol{\theta}(t)$ stays in $\Theta_{Principal}$ (and therefore also in Θ_{Safe}), since if this result holds then Theorem 3.4 applies.

Contradiction Hypothesis: There exists trajectory $\boldsymbol{\theta}(t)$ for $t \geq 0$ such that $\boldsymbol{\theta}(0) \in \Theta_{Safe}$ and $|P_{Line,k,m}(\theta_{k,m}(t))| \leq P_{Max,k,m}$ for all $(k,m) \in \mathcal{E}$ and for all $t \geq 0$, but that $\boldsymbol{\theta}(t) \notin \Theta_{Principal}$ for all $t \geq 0$.

Therefore, there must exist some line $(k, m) \in \mathcal{E}$ such that $|\theta_{k,m}|(0)| \leq \theta_{Max,k,m} < \pi/2$ and some time $T > 0$ such that $|\theta_{k,m}(T)| > \pi/2$. Since trajectory $\boldsymbol{\theta}(t)$ is continuous, then there also exits a time T_1 such that $0 < T_1 < T$ and $\theta_{Max,k,m} < |\theta_{k,m}(T_1)| < \pi/2$, which implies that $|P_{Line,k,m}(\theta_{k,m}(T_1))| > P_{Max,k,m}$ (this case is illustrated in Figure 3.2). However, this contradicts the assumption that $|P_{Line,k,m}(\theta_{k,m}(t))| \leq P_{Max,k,m}$ for all $(k, m) \in \mathcal{E}$ and all $t \geq 0$. Therefore, the contradiction hypothesis is shown false, and $\theta(0) \in \Theta_{Safe}$ and $|P_{Line,k,m}(\theta_{k,m}(t))| \leq P_{Max,k,m}$ for all $(k, m) \in \mathcal{E}$ and all $t \geq 0$ implies that $\boldsymbol{\theta}(t) \in \Theta_{Principal}$ for all $t \geq 0$.
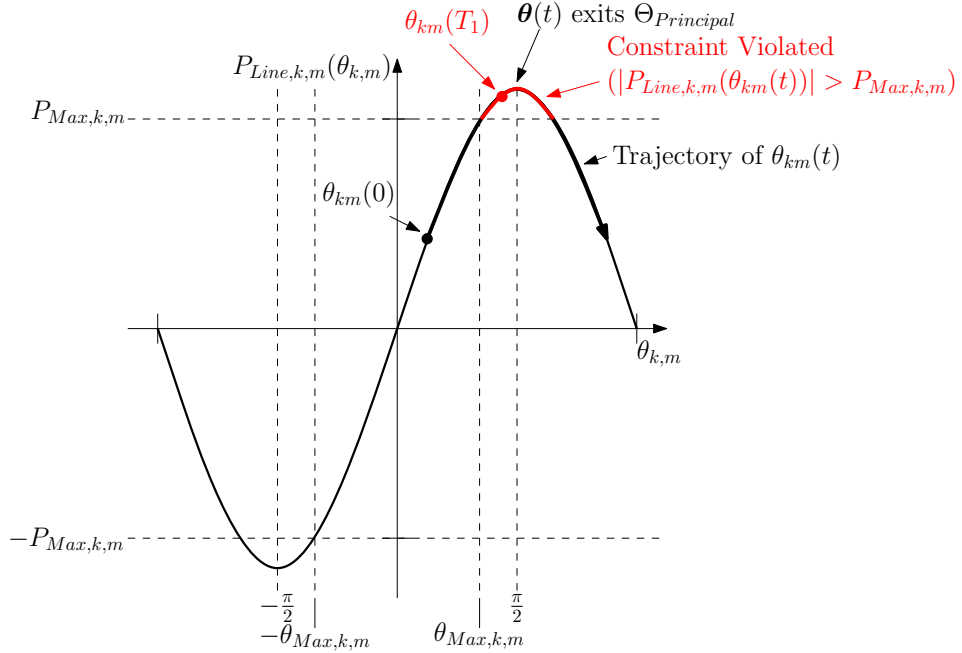
Figure 3.2: Trajectory of a line $(k, m) \in \mathcal{E}$ exiting the principal region

Since all line power-flow constraints $|P_{Line,k,m}| \leq P_{Max,k,m}$ are (by assumption) met for all $t \geq 0$, then $\boldsymbol{\theta}(t)$ is also in Θ_{Safe} for all $t \geq 0$. Finally, the assumption that $[\Theta_{Safe} \cap \Theta_{Eq,Stable}(\mathbf{P_{Ref}} - \mathbf{P_L^0})] \neq \emptyset$ implies that $\Theta_{Eq,Stable}(\mathbf{P_{Ref}} - \mathbf{P_L^0}) \neq \emptyset$, and that $\boldsymbol{\theta}(t) \to \boldsymbol{\theta}_{Eq} \in \Theta_{Eq,Stable}$ is consistent with $\boldsymbol{\theta}(t) \in \Theta_{Safe}$ for all $t \geq 0$. The above satisfies all the conditions of Theorem 3.4, and the proof is complete. $\square$

We state Theorem 3.5 conceptually as follows: "If no line power flow exceeds its assigned maximum value (and if there exists an equilbrium in the safe region), then

the network must converge to frequency agreement and simple power sharing." We emphasize that the condition of Theorem 3.5 consists of a set of local line-power-flow constraints, each of which can be determined from only local measurements at each incident bus.

A note on the selection of $\mathbf{P_{Max}}$: Since our only requirement is that $0 < P_{Max,k,m} < Y_{km}V_kV_m$ for each line $(k, m) \in \mathcal{E}$, there is a great deal of freedom in the selection of $P_{Max,k,m}$. The smaller the value of $P_{Max,k,m}$ chosen, the smaller the associated $\theta_{Max,k,m}$ will be. Since $\theta_{Max,k,m}$ will always be smaller than $\pi/2$, the condition in Theorem 3.5 is a stricter condition than that of Theorems 3.3 and 3.4, and choosing a smaller $P_{Max,k,m}$ will make it stricter still. Considerations for optimal selection of $\mathbf{P_{Max}}$ for a given network are very application specific, and are beyond the scope of this dissertation.

3.7.4 Discussion on Significance of Sufficient Condition for Synchronization Based on Line Power Flows

At first glace, Theorem 3.5 doesn't seem to carry much value for design of control for inverter-based networks. It consists of a set of line power-flow constraints such that the satisfaction of those constraints (along with several parametric conditions, including both an initial condition in the safe region and the existence of an equilibrium in the safe region) is sufficient to guarantee frequency synchronization and (by implication) simple power sharing between inverters. However, the condition requires a test of *every* line power flow in the network at *every* time, and it is not clear how the condition advances the ability to guarantee synchronization in inverter-based power networks.

The value of Theorem 3.5 is in the approach that is suggests for control design, namely that if the line power-flow constraints could be enforced in real-time, then guaranteed frequency synchronization and (possibly) simple power sharing would follow. Stated another way, Theorem 3.5 shows that there exists operating a safe region

of the network line voltage-angle state space such that bounding of the network trajectory within that region would guarantee synchronization. Further, the boundaries of the safe region can be detected locally, meaning that potentially an inverter performing local measurement could respond so as to direct the network back into the safe region. In the following chapters, we will use this concept to develop a modified form of frequency-droop control which is capable of enforcing the specified set of line power-flow constraints in real-time using only local measurements, thereby bounding the network into the safe region and providing the desired frequency synchronization and power sharing properties without requiring communication.

3.8 Example System Simulation

To clarify the results of this chapter, we present several simulations on an example system. Our example system is a lossless six-bus inverter-based network, a single-line diagram of which is shown in Figure 3.3. Notice that this network is meshed, and structurally asymmetric. All voltage magnitudes are assumed to be unity, and the input configuration for all four simulation cases are shown in Table 3.2. Each simulation and the significance of its results is described below.
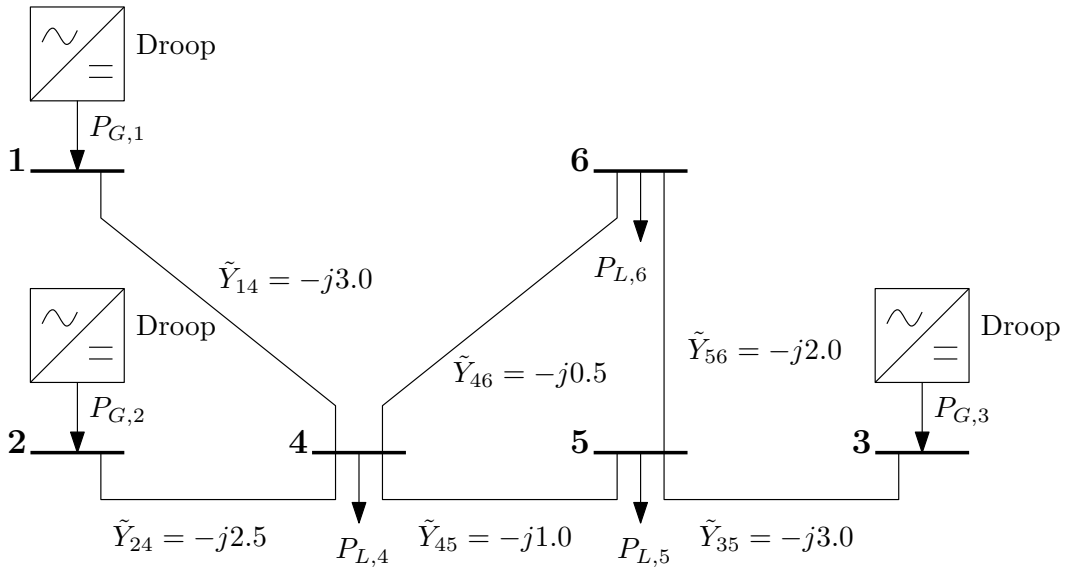
Figure 3.3: Example Six-Bus Meshed Network

Table 3.2: Input Conditions for Simulation Cases

	Simulation 3.1		Simulation 3.2		Simulation 3.3	Simulation 3.4
	$t < 0$	$t \geq 0$	$t < 0$	$t \geq 0$	$t \geq 0$	$t \geq 0$
$P_{Ref,1}$	1.0	1.0	1.0	1.0	1/3	0.0
$P_{Ref,2}$	1.0	1.0	1.0	1.0	1/3	1.5
$P_{Ref,3}$	1.0	1.0	1.0	1.0	1/3	1.5
$P_{L,4}$	1.0	1.0	0.0	0.0	0.0	1.25
$P_{L,5}$	0.0	0.0	1.0	1.0	0.5	$2 - \sqrt{3}$
$P_{L,6}$	1.0	2.0	1.0	2.0	0.5	$\sqrt{3} - 0.25$

3.8.1 Simulation 3.1: Stable Load Step

Our first simulation case demonstrates a simple load step to a stable configuration. At $t = 0^-$, the network is in steady state (at a stable equilibrium). At $t = 0$, the load on bus 6 steps from 1.0p.u. to 2.0p.u., disturbing the equilibrium. The post-step input conditions still reside in the range of $\mathfrak{D}\mathbf{P_{Line}}(\boldsymbol{\theta})$ (and therefore there exists a stable equilibrium). Response of the line voltage angles $\boldsymbol{\theta}$, line power flows $\mathbf{P_{Line}}$, inverter output power $\mathbf{P_G}$, and bus frequency offsets $\boldsymbol{\Delta\omega}$ for Simulation 3.1 is shown in Figure 3.4. Notice that after the step, the $\boldsymbol{\theta}$ trajectory stays inside the principal region, and therefore Theorem 3.4 holds and the system stabilizes to the new equilibrium and frequency agreement is achieved.

3.8.2 Simulation 3.2: Unstable Load Step

Our second simulation case demonstrates a load step similar to Case 1, but with a slight alteration: a load of 1.0p.u. is moved from bus 4 to bus 6, resulting in a post-step condition such that the condition of Theorem 3.1 is met across the cut consisting of lines $(4, 5)$ and $(4, 6)$, and therefore there exist no post-step equilibria. Response of the line voltage angles $\boldsymbol{\theta}$, line power flows $\mathbf{P_{Line}}$, inverter output power $\mathbf{P_G}$, and bus frequency offsets $\boldsymbol{\Delta\omega}$ for Simulation 3.2 is shown in Figure 3.5. Observe that the line voltage angles $\theta_{4,5}$ and $\theta_{4,6}$ begin to cycle around the torus, indicating that
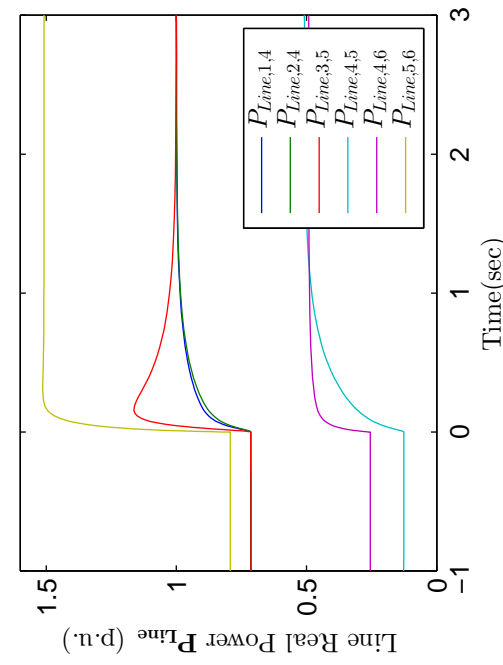
(a) Bus Frequency Error $\boldsymbol{\Delta\omega}$
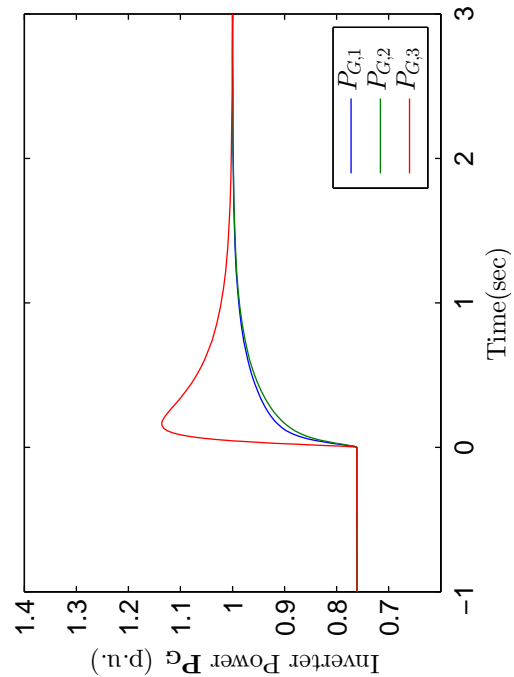
(b) Line Power Flows $\mathbf{P_{Line}}$
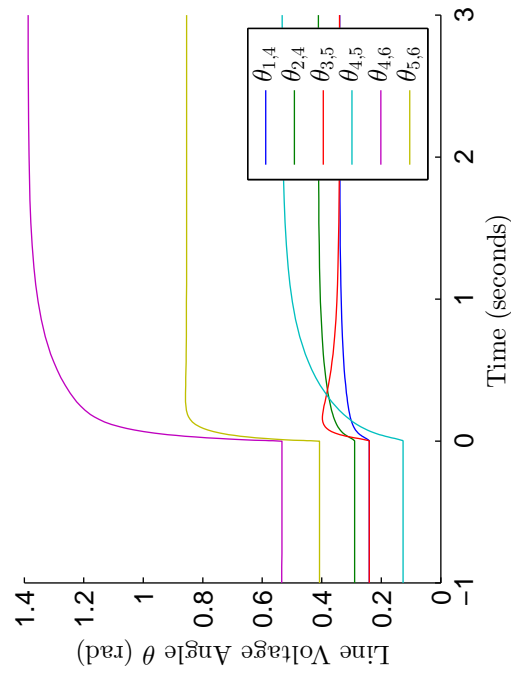
(c) Inverter Generated Power $\mathbf{P_G}$

(d) Line Voltage Angles $\boldsymbol{\theta}$

Figure 3.4: Simulation 3.1: Stable Load Step on Six-Bus Meshed Network

the subnetwork of buses 1, 2, and 4 has lost synchronization with the subnetwork of buses 3, 5, and 6 (across the cut of lines $(4, 5)$ and $(4, 6)$).

3.8.3 Simulation 3.3: Seperation and Resynchronization

Our third simulation case is a pathological condition designed to show an interesting special case. In this case, a stable equilibrium exists, and the network is initialized at $t = 0$ in a non-equilibrium state. This initial state is within the principal region and there exists a stable equilibrium, but the state trajectory exits the principal region, and so the sufficient condition of Theorem 3.4 does not hold. Response of the line voltage angles $\boldsymbol{\theta}$, line power flows $\mathbf{P_{Line}}$, inverter output powers $\mathbf{P_G}$, and bus frequency offsets $\boldsymbol{\Delta\omega}$ for Simulation 3.3 is shown in Figure 3.6.

What we observe is that the line voltage angles $\theta_{4,5}$ and $\theta_{4,6}$ both diverge from the principal region, indicating the seperation of the subnetwork of buses 1, 2, and 4 from the subnetwork of buses 3, 5, and 6. However, after cycling around the torus, the two subnetworks then *resynchronize*, with one subnetwork one complete cycle ahead of the other. The network reaches stability, but by a highly undesirable trajectory: several line power flows crossed their maximum power transfer point, which in practice might result in hardware damage or result in unsafe conditions. This case bears further consideration and study.

3.8.4 Simulation 3.4: Behavior Near Unstable Equilibrium

Our final simulation case in this chapter demonstrates behavior of a droop inverter network near an unstable equilibrium. The unstable equilibrium is one in which the voltage-angle magnitudes around the cycle ($\theta_{4,5}$, $\theta_{5,6}$, and $-\theta_{4,6}$) sum to 2π, resulting in a non-trivial cyclical power flow. This equilibrium is unstable because it lies outside of the principal region (see Theorem 3.2). There also exists a stable equilibrium inside the principal region. Response of the line voltage angles $\boldsymbol{\theta}$, line power flows $\mathbf{P_{Line}}$, inverter output power $\mathbf{P_G}$, and bus frequency offsets $\boldsymbol{\Delta\omega}$ for Simulation 3.4 is shown

(a) Bus Frequency Error $\mathbf{\Delta\omega}$

(b) Line Power Flows $\mathbf{P_{Line}}$

(c) Inverter Generated Power $\mathbf{P_G}$

(d) Line Voltage Angles $\boldsymbol{\theta}$
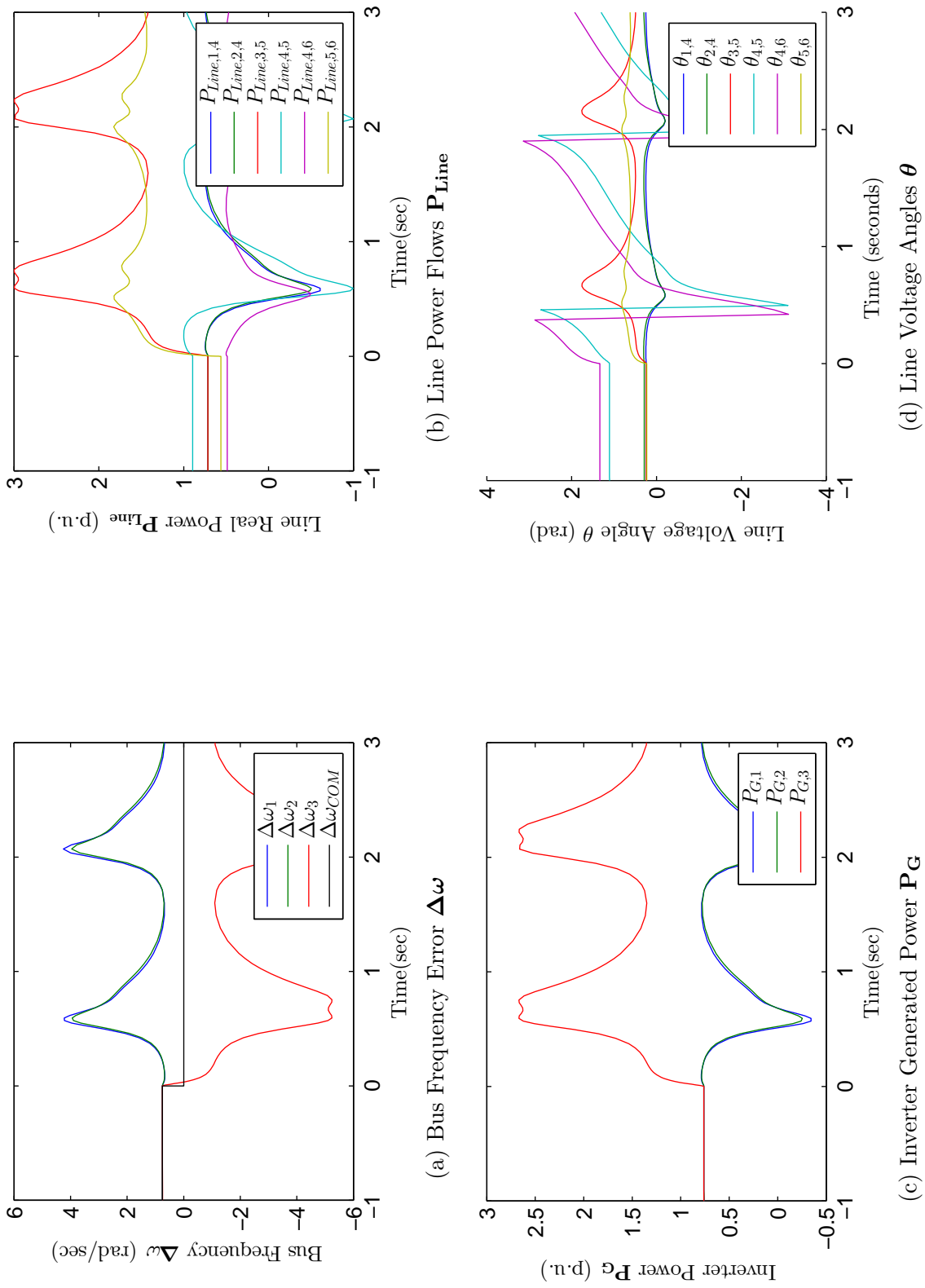
Figure 3.5: Simulation 3.2: Unstable Load Step on Six-Bus Radial Network

(a) Bus Frequency Error $\boldsymbol{\Delta\omega}$

(b) Line Power Flows $\mathbf{P_{Line}}$

(c) Inverter Generated Power $\mathbf{P_G}$

(d) Line Voltage Angles $\boldsymbol{\theta}$
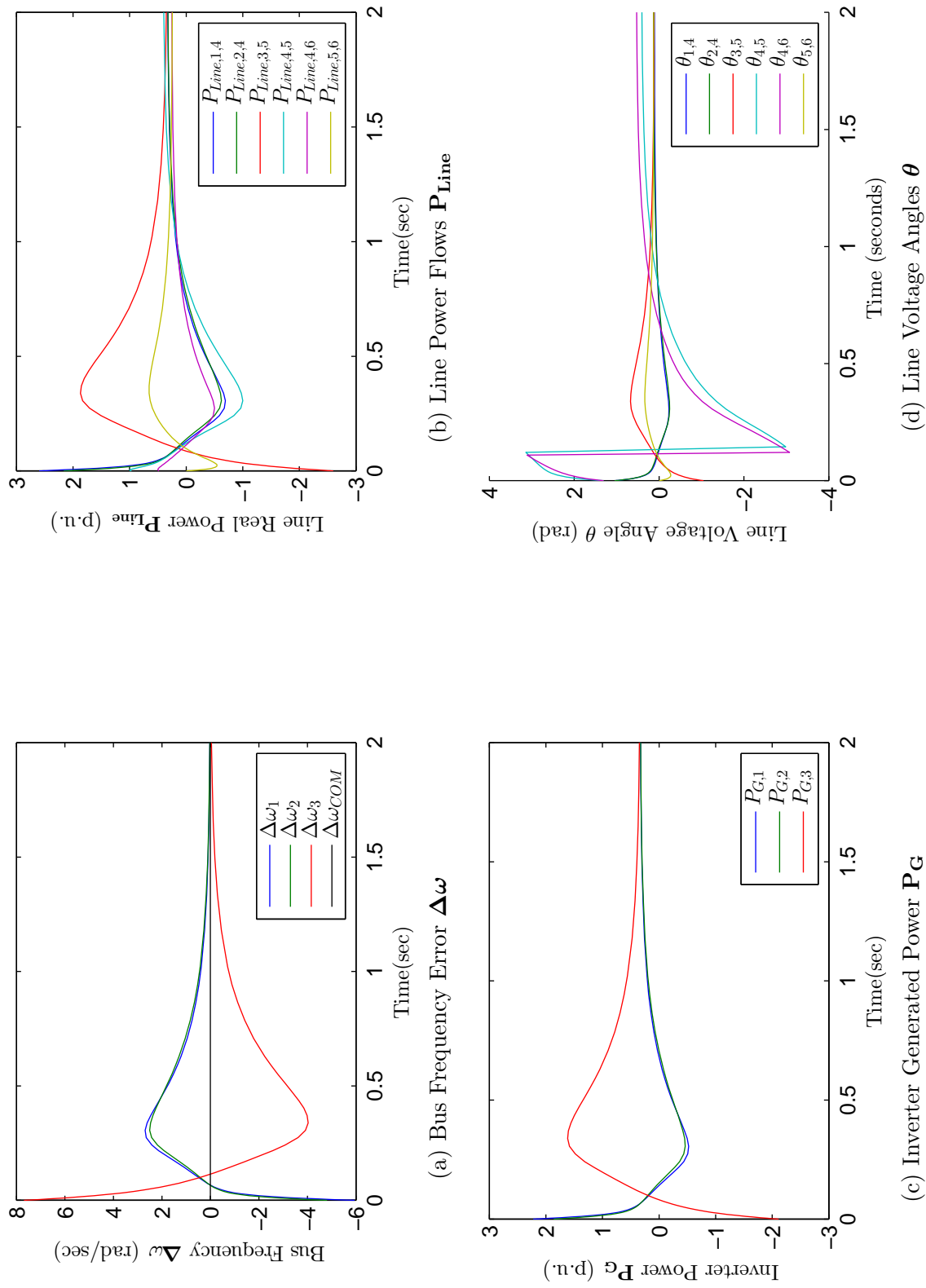
Figure 3.6: Simulation 3.3: Seperation and Resynchronization on Six-Bus Radial Network

in Figure 3.7.

The initial condition of the network is placed a small distance from the unstable equilibrium. The network state accelerates away from the unstable equilibrium, enters the principal region and eventually settles to the stable equilibrium, thus demonstrating both the instability of the equilibrium outside the principal region and the stability of the equilibrium inside the principal region as claimed by Theorem 3.2.

3.9 Conclusions

In this chapter, we have developed a structure-preserving model for the voltage-angle, frequency, and real-power dynamics of a droop inverter-based network. This model may be stated in two forms (one bus-oriented and the other line-oriented). We showed that frequency synchronization corresponds to convergence to an equilibrium of the model, and determined a necessary condition for existence of such equilibria (Theorem 3.1). We showed that convergence to frequency agreement necessarily corresponds to convergence of the network to a state where network load is shared between the inverters based on assigned references and droop constants (Lemma 3.2), a property which we designate the *simple power sharing property* of droop inverter-based networks. We showed that equilibria are locally asymptotically stable if and only if they lie in the principal region (Theorem 3.2). We presented sufficient criteria for frequency synchronization based on bus voltage angles (Theorem 3.3) or line voltage angles (Theorem 3.4). Finally, we used the concept of invertibility of the line power flows to create a distributed sufficient criterion for frequency synchronization based on line power flows (Theorem 3.5), which consists of a set of local criteria each of which can be determined using only local measurements.

In the development of our model, we made a number of idealizing assumptions to simplify the network to be considered (see Section 3.2), but these assumptions may not always be realistic. In particular, the assumption of constant voltage magnitude does
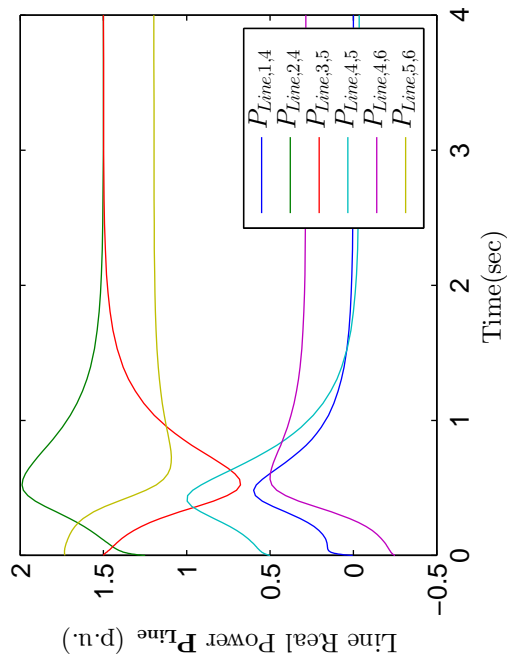
(a) Bus Frequency Error $\boldsymbol{\Delta\omega}$
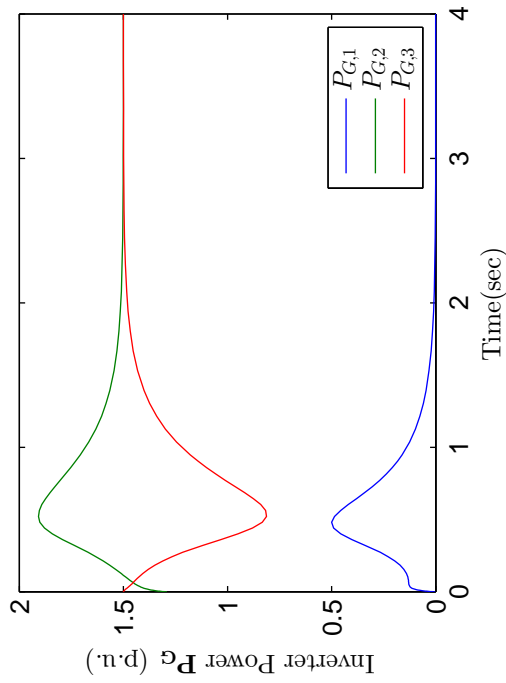
(b) Line Power Flows $\mathbf{P_{Line}}$

(c) Inverter Generated Power $\mathbf{P_G}$
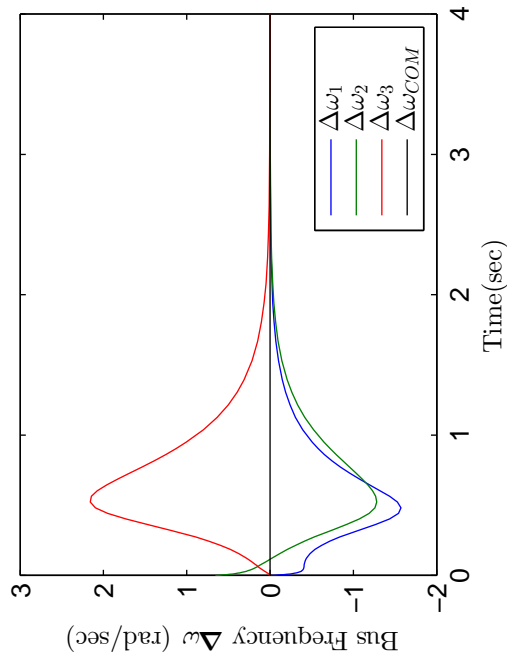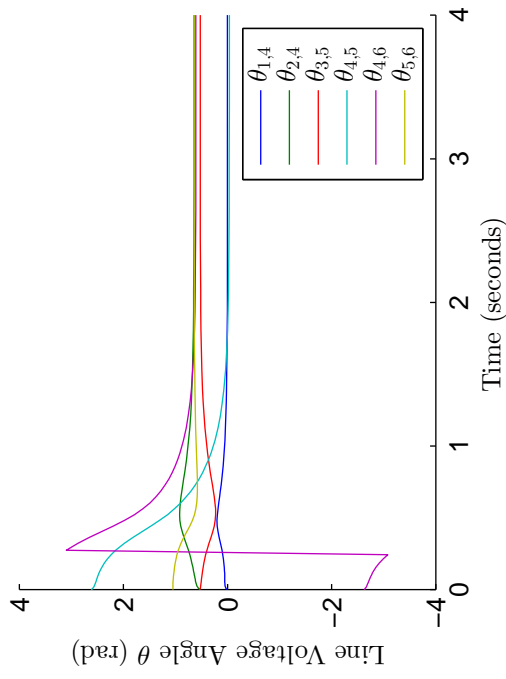
(d) Line Voltage Angles $\boldsymbol{\theta}$

Figure 3.7: Simulation 3.4: Behavior Near Unstable Equilibrium on Six-Bus Meshed Network

not consider the possibility of voltage collapse, and our results only apply to frequency synchronization, not voltage stability. In addition, the omission of controller delays in our model may not accurately reflect the real limitations of hardware frequency-droop inverters, and does not allow for calculation of maximum stable droop constants. Despite these limitations, our model captures the most significant dynamics effecting synchronization and power sharing in droop inverter-based networks, and as such can be used to develop new understand of synchronization and methods for improving synchronzation properties of inverter-based networks.

The results in this chapter provide a new method of modeled the frequency and voltage-angle dynamics of a droop inverter-based network, and they confirm that such a network has several desirable properties, notably simple power sharing, local convergence to frequency agreement, and no need for explicit communication between inverters. However, due to the lack of a method to enforce line power flow constraints in the network, it may fail to synchronize, resulting in power oscillations. Therefore, a new method of control must be developed which is capable of enforcing these line power flow constraints in real-time without sacrificing the desirable properties of droop control. In the following chapters, we develop such a control method to improve the synchronization properties of inverter-based networks by integrating constraint-enforcement into the droop control law.

CHAPTER IV

A CONSTRAINT-ENFORCING DROOP CONTROLLER FOR ROBUST SYNCHRONIZATION OF ALL-ACTIVE-BUS RADIAL INVERTER-BASED AC NETWORKS

4.1   Introduction

In the previous chapter, we introduced a *structure-preserving model* of an inverter-based AC network operating frequency-droop control, which includes the full non-linear network equations. Using this model, we showed that frequency synchronization of the network (that is, convergence of the bus frequencies to a common value) ensures that all inverters share power according to their assigned reference values and offsets (Lemma 3.2), which we termed the simple power sharing property. Further, frequency synchronization can be guaranteed by enforcement of a specified set of line power flow constraints (Theorem 3.5), which bound the network state trajectory within a safe region of the voltage-angle state space. However, the traditional frequency-droop control law (4) is *not* sufficient to ensure that these constraints are met, and as a result the network may lost frequency synchronization, resulting in power oscillations and potentially network failure. Therefore, the traditional frequency-droop controller is not sufficient to provide guaranteed frequency synchronization and power sharing for inverter-based networks across the entire expected operating range of the network.

Traditional frequency-droop control fails to provide the desired behavior because it fails to integrate the non-linearities and constraints of the network power flows. If droop control were able to enforce a specified line power flow constraint on each line in

the network, then by Theorem 3.5 frequency synchronization would be guarananteed. Further, if relationship between frequency and real power generation created by the droop control law (4) were maintained, then guaranteed power sharing would follow.

Our approach in this work is based on an appliation of multi-agent system theorem to AC inverter-based networks, in which we view the frequency synchronization of inverters as a form of network consensus (see [63, 54]). In other applications of multi-agent system theory, network constraints have been enforced in a distributed way by explicit integration of those constraints into the consensus control law [79, 6, 53, 4, 19]. In particular, [53] enforces distance constraints between robots in a mobile robotic network by application of unbounded adaptive gains to the edge tensions between robots. We will show in this chapter that the problem of enforcement of line power flow constraints in a droop inverter-based network is strongly analagous to that of distance constraints in mobile robotic networks, and introduce a new method inspired by [53] to enforce such line power flow constraints using only local data.

In this chapter, we introduce a modified form of the frequency-droop controller, which is capable of enforcing specified line power flow constraints on its incident lines. We term this new control law the *constraint-enforcing droop (CED) controller*, and like the traditional frequency-droop controller it does not require explicit communication or non-local data (though it does require measurements beyond those required by traditional droop). We consider in this chapter the most direct application of the CED controller, in which an inverter implementing the proposed CED control law is placed at each bus in a acyclic network, which we refer to as an *all-active-bus, acyclic CED network*. While this case is limited in practice, it is valuable as a proof-of-concept of distributed constraint enforcement in inverter-based networks. We show that in such a network, the CED-controlled inverters are capable of enforcing the line power flow constraints derived in Theorem 3.5, thereby bounding the network state trajectory to the safe region of the voltage-angle state space. Further, we show that

frequency synchronization is then guaranteed as long as the network initial condition is in the safe region. Finally, we show that such a network has a modified form of the simple power sharing property, which we term the *constrained power sharing property*. These properties hold for all bounded, constant reference and load conditions (in the absence of generation constraints), thus providing robust synchronization and power sharing properties for this limited class of networks.

In Section 4.2, we reintroduce the all-active-bus CED control law and discuss its requirements. In Section 4.3, we introduce the class of network under consideration and state our main synchronization and power sharing result for networks of this class. In Section 4.4, we consider the steady state behavior of an all-active-bus, acyclic CED network, and derive the constrained power sharing property of such an network. In Section 4.5, we prove our main result by showing that for such a network, there exists a compact subset of the safe region which is invariant to he network dynamics, thereby bouding network operation within the safe region and guaranteeing frequency synchronization and constrained power sharing. Finally, in Section 4.7 we draw conclusions.

4.2   Constraint-Enforcing Droop (CED) Controller

The frequency-droop control law (4) (introduced in [12]) creates an explicit connection between an inverter's frequency offset $\Delta\omega_k$ and its output power $P_{G,k}$, providing the simple power sharing property (Lemma 3.2) and ensuring convergence of frequencies between inverters as long as the network state trajectory stays within a safe region Θ_{Safe} (Theorem 3.5), which is defined by a set of line power flow constraints, one on each line in the network (Definition 3.8). However, since it does not enforce any such constraints, the frequency-droop control law is not sufficient to ensure that the network remains bounded within the safe region, and therefore the network

may lose frequency synchronization, resulting in power oscillations and possibly network failure. To correct this shortcoming, we will introduce a modified form of the frequency-droop control law that explicitly integrates the line power flow constraints defining the boudaries of the safe region, enforcing them locally and thereby guaranteeing frequency synchronization and power sharing for all reference and load input conditions.

4.2.1 Constraint Enforcement in Inverter-Based AC Networks

Consider again the view of the traditional frequency-droop dynamics (7) as a forced, nonlinear form of the consensus equation from multi-agent system theory (for example, see [63]). Under this interpretation, the line power flow values $P_{Line,k,m}$ can be viewed as a non-linear dynamic "tensions" in the dynamics of δ_k. Since $-P_{Line,k,m}(\theta_{k,m})$ always has the opposite sign of $\theta_{k,m}$ on the principal region, then the dynamic tension associated with line $(k, m) \in \mathcal{E}$ tends to "pull" the state $\theta_{k,m}$ towards zero. However, since $|P_{Line,k,m}|$ is bounded, this tension may not be sufficient to overcome the other dynamic tensions pulling the state $\theta_{k,m}$, and so the constraint $|P_{Line,k,m}(\theta_{k,m})| < P_{Max,k,m}$ may be violated (and the network may lose synchronization). Notice that we now consider the strict form of the line power flow constraint ($|P_{Line,k,m}(\theta_{k,m})| < P_{Max,k,m}$ vs. $|P_{Line,k,m}(\theta_{k,m})| \leq P_{Max,k,m}$).

A similar problem occurs in mobile robotic networks with range-limited sensing (see [53]). Each robot operates a consensus controller (similar in form to (7)), which causes each robot to converge towards the centroid of the neighbors it can sense. It can be shown that as long as the mobile robot network operates within a safe region defined by distance constraints, then the robots will always converge (similar to Theorem 3.4). However, if the robots leave each other's sensing range, then they lose contact and may not converge. In [53], this problem is solved by introduction of state-dependent weights to the edge tension values, which increase unbounded as

any edge approaches its assigned distance constraint. As a result, when any edge approaches its constraint, the associated edge tension increases to "pull" the network back into the safe region, enforcing the constraint. Since the gain approaches infinity as the state approaches its constraint, the associated tension will always be "large enough" to overcome any opposing tension and strictly enforce the constraint.

The problem of line power flow constraint enforcement in inverter-based power networks has several significant differences from the problem considered by [53]. First, [53] considers agents with unforced linear dynamics, while the inverter network dynamics in (7) are forced and non-linear. Second, it assumes that the state difference across an edge can be measured directly, while in the inverter network case voltage angle difference $\theta_{k,m} = \delta_k - \delta_m$ cannot be measured locally at bus k (without application of emerging PMU technology). However, while it is not possible to measure $\theta_{k,m}$ at a bus k, it is possible to measure line power flow $P_{Line,km}$ at bus k, and it follows from Lemma 3.4 that $|\theta_{k,m}| < \theta_{Max,k,m}$ corresponds to $|P_{Line,km}| < P_{Max,k,m}$. Using these characteristics, we can implement a controller analagous to that proposed in [53] to enforce line power flow constraints as shown in the next section.

4.2.2 All-Incident-Line CED Control Law

We now introduce a modified form of the frequency-droop control law for voltage-source inverters, which explicitly integrates the line power flow constraints from Theorem 3.5. We term this new control law the *All-Incident-Line Constraint-Enforcing Droop (CED) Control Law*, since it enforces the specified line power flow constraint on each line incident to the inverter. Similar to the method of constraint enforcing proposed by [53] for mobile robotic networks, the CED control law (50) applies adaptive gain $\gamma_{k,m}(|P_{Line,k,m}|)$ to each line "tension" value, resulting in the "adaptive line tension" $\gamma_{k,m}(|P_{Line,k,m}|)P_{Line,k,m}$ (which for simplicity of notation we will indicate as $\gamma_{k,m}P_{Line,k,m}$). By increasing the gain $\gamma_{k,m}$ unbounded as $|P_{Line,k,m}|$ approaches

$P_{Max,k,m}$, we can ensure that the adaptive line tension is always large enough to overcome the tension opposing it as it nears its constraint, thus guaranteeing that the constraint will be enforced.

The new *All-Incident-Line Constraint-Enforcing Droop (CED) Control Law* is defined as follows:

Definition 4.1 (All-Incident-Line Constraint-Enforcing Droop Control Law)**.** *The All-Incident-Line Constraint-Enforcing Droop (CED) Controller obeys the following control law:*

$$\Delta\omega_k = R_k \left[P_{Ref,k} - P_{L,k} - \sum_{m \in \mathcal{N}(k)} \gamma_{k,m}(|P_{Line,k,m}|)\, P_{Line,k,m} \right] \tag{50}$$

where $\gamma_{k,m}(|P_{Line,k,m}|) = \gamma_{m,k}(|P_{Line,m,k}|)$ is a line-even, positive weight function associated with line $(k,m) \in \mathcal{E}$ whose purpose is to enforce the line flow constraint $|P_{Line,k,m}| < P_{Max,k,m}$.

The control law introduced in Definition 4.1 is called the '"all-incident-line" CED control law because it applies an adaptive gain $\gamma_{k,m}$ to each line incident to the bus k. Observe that when $\gamma_{k,m} = 1.0$ for all incident lines to bus k, the CED control law (50) reduces to the traditional droop dynamics (7).

4.2.3 Selection of Adaptive Gain Function $\gamma_{k,m}$

The adaptive gain function $\gamma_{k,m}(|P_{Line,k,m}|)$ for each line $(k,m) \in \mathcal{E}$ is selected during control design so that it has a set of characteristics needed to enforce the (strict) line power flow constraint $|P_{Line,k,m}| < P_{Max,k,m}$, and so that when no incident constraints are active a CED-controlled inverter behaves identically to a traditional-droop-controlled inverter. In particular, we require that $\gamma_{k,m}$ be selected from the following class of functions:

Definition 4.2 (Feasible Set $\boldsymbol{\Gamma}_{Unbounded}$ for $\gamma_{k,m}$). *A function* $\gamma_{k,m} : [0 \quad P_{Max,k,m}) \rightarrow [1 \quad \infty)$ *is a member of the set* $\boldsymbol{\Gamma}_{Unbounded}$ *for a given constant* $P_{Max,k,m} > 0$ *if it has the following characteristics:*

4.2.A $\gamma_{k,m}$ *is Lipschitz continuous with respect to* $|P_{Line,k,m}|$ *for all* $|P_{Line,k,m}| < (1 - \mu)P_{Max,k,m}$ *and for all* $\mu \in (0 \quad 1)$.

4.2.B $\gamma_{k,m}$ *equals unity for small* $|P_{Line,k,m}|$:

$\exists \; \epsilon_{k,m} \in (0 \quad 1)$ *such that* $\gamma_{k,m}(|P_{Line,k,m}|) = 1$ *for all* $|P_{Line,k,m}| \leq (1 - \epsilon_{k,m})P_{Max,k,m}$.

4.2.C $\gamma_{k,m}$ *goes to* ∞ *as* $|P_{Line,k,m}|$ *approaches* $P_{Max,k,m}$ *(from below):*

$$\lim_{|P_{Line,k,m}| \rightarrow P_{Max,k,m}} \gamma_{k,m}(|P_{Line,k,m}|) = \infty.$$

4.2.D $\gamma_{k,m}$ *is line-even:*

$$\gamma_{k,m}(|P_{Line,k,m}|) = \gamma_{m,k}(|P_{Line,m,k}|)$$

4.2.E $\gamma_{k,m}$ *is non-decreasing in* $|P_{Line,k,m}|$:

$$\frac{\partial \gamma_{k,m}}{\partial |P_{Line,k,m}|} \geq 0 \; \forall \; |P_{Line,k,m}| < P_{Max,k,m}.$$

4.2.F $\gamma_{k,m}$ *is bounded for all* $|P_{Line,k,m}| < P_{Max,k,m}$:

For each $\mu \in (0 \quad 1)$ *there exists finite* $\gamma_{k,m,\mu} > 1$ *such that* $1 \leq \gamma_{k,m}(|P_{Line,k,m}|) \leq \gamma_{k,m,\mu}$ *for all* $|P_{Line,k,m}| \leq (1 - \mu)P_{Max,k,m}$.

Any function which is a member of $\boldsymbol{\Gamma}_{Unbounded}$ may be selected for each $\gamma_{k,m}$ in the CED control law. Later in this chapter, we will show that the characteristics required by Definition 4.2 are sufficient to ensure enforcement of line power flow constraints, convergence to frequency synchronization, and constrained power sharing between inverters.

The quantity $\epsilon_{k,m}$ in Definition 4.2.B is a constant chosen to determine when a constraint is considered to be active. If $|P_{Line,k,m}| < P_{Max,k,m}$, we say that the line constraint at line $(k, m) \in \mathcal{E}$ is met, and if $|P_{Line,k,m}| \geq P_{Max,k,m}$ we say that the

constraint is violated. Finally, if $(1 - \epsilon_{k,m})P_{Max,k,m} < |P_{Line,k,m}| < P_{Max,k,m}$, we say that the constraint is ϵ-active.
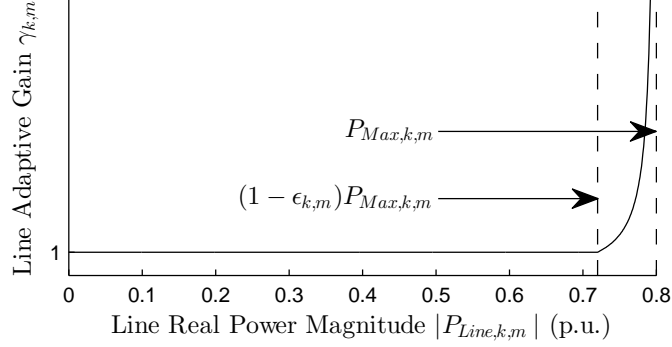
Figure 4.1: Example selection of line weight $\gamma_{k,m}$ vs. $P_{Line,k,m}$ (as in (51)) for line $(k,m) \in \mathcal{E}$ with $P_{Max,k,m} = 0.8$ p.u., $\epsilon_{k,m} = 0.1$, and $C_{k,m} = 0.1$

For example, consider the function $\gamma_{k,m}$ defined as in (51). This selection of $\gamma_{k,m}$ for given constants $C_{k,m} > 0$ and $\epsilon_{k,m} \in (0 \quad 1)$ can be shown to meet the requirements of Definition 4.2, and is therefore a member of $\mathbf{\Gamma}_{Unbounded}$ and a valid selection for $\gamma_{k,m}$. Figure 4.1 shows a plot of $\gamma_{k,m}$ vs. $|P_{Line,k,m}|$ for the example selection (51) for $\gamma_{k,m}$.

4.3 Synchronization and Power Sharing in All-Active-Bus, Acyclic CED Networks

4.3.1 All-Active Bus, Acyclic CED Networks

In this chapter, we consider a simplified class of inverter-based AC networks for the purpose of enforcement of the set of line power flow constraints in Theorem 3.5. We

Example selection of $\gamma_{k,m} \in \Gamma_{Unbounded}$ for given constants $C_{k,m} > 0$, $P_{Max,k,m} > 0$, and $\epsilon_{k,m} > 0$:

$$\gamma_{k,m}(|P_{Line,k,m}|) := \begin{cases} 1.0 & |P_{Line,k,m}| \leq (1 - \epsilon_{k,m})P_{Max,k,m} \\ 1.0 - \dfrac{C_{k,m}}{\epsilon_{k,m}P_{Max,k,m}} \\ \quad + \dfrac{C_{k,m}}{P_{Max,k,m} - |P_{Line,k,m}|} & (1 - \epsilon_{k,m})P_{Max,k,m} < |P_{Line,k,m}| < P_{Max,k,m} \end{cases}$$

(51)

refer to this class of networks as *all-active-bus, acyclic CED networks*:

Definition 4.3 (All-Active-Bus, Acyclic CED Networks). *An all-active-bus, acyclic CED network is a 3-phase AC power network, which is identical to a lossless droop inverter-based power network with ideal voltage regulation (Definition 3.1) with the following differences:*

4.3.A Each line $(k, m) \in \mathcal{E}$ is assigned a line-even, constant maximum power flow value $P_{Max,k,m} = P_{Max,m,k}$, where $0 < P_{Max,k,m} < Y_{k,m}V_kV_m$.

4.3.B Each line $(k, m) \in \mathcal{E}$ is assigned a line-even, positive gain function $\gamma_{k,m} \in \Gamma_{Unbounded}$ meeting the requirements of Definition 4.2.

4.3.C Each bus $k \in \mathcal{V}$ is an inverter bus, and implements the all-incident-lines constraint-enforcing droop control law (Definition 4.1) using the assigned $P_{Max,k,m}$ and $\gamma_{k,m}$ for each of its incident line.

4.3.D The network is acyclic (contains no cycles).

In an all-active-bus, acyclic CED network, each line $(k, m) \in \mathcal{E}$ is incident to two CED inverters, one at each of its incident buses. This is the simplest case to consider for constraint-enforcment in inverter-based networks, since each line constraint is explicitly measured and enforced by both of its incident CED inverters. We will show that for this class of networks, each (strict) line power flow constraint $|P_{Line,k,m}| < P_{Max,k,m}$ will be enforced, thus bounding the network state trajectory within the safe region and resulting in guaranteed frequency synchronization and (constrained) power sharing.

4.3.2 Structure-Preserving Model for All-Active Bus, Acyclic CED Networks

Since all-active-bus, acyclic CED network have most of the same characteristics as the droop inverter-based network considered in Chapter 3, it is possible to modify our

structure-preserving model to represent their dynamics. Substituting the frequency-dependent load model (3) into the all-incident-line CED control law (50) at each bus $k \in \mathcal{V}$ and solving for $\Delta\omega_k = \dot{\delta}_k$, we obtain the bus-oriented dynamic system-of-equations model for an all-active-bus, acyclic CED network:

$$\dot{\delta}_k = D_k^{-1} \left[P_{Ref,k} - P_{L,k}^0 - \sum_{m \in \mathcal{N}(k)} \gamma_{k,m}(|P_{Line,k,m}|) \, P_{Line,k,m} \right] \quad \forall \, k \in \mathcal{V} \qquad (52)$$

where $D_k = R_k^{-1} + D_k'$ is the total bus frequency-dependence coefficient at bus k.

As in Chapter 3, in order to form vectors of each line-oriented quantity we associated a direction and an index $i \in \{1 \ldots L\}$ with each physical line, and assign these directed edges to a set $\overrightarrow{\mathcal{E}}$. We may then form vectors $\boldsymbol{\theta} = \begin{bmatrix} \theta_1 \ldots \theta_L \end{bmatrix}^T \in \mathbb{R}^L$ and $\mathbf{P_{Line}} = \begin{bmatrix} P_{Line,1} \ldots P_{Line,L} \end{bmatrix}^T \in \mathbb{R}^L$, where $\theta_i = \theta_{k,m} = -\theta_{m,k}$ and $P_{Line,i} = P_{Line,k,m} = -P_{Line,m,k}$ for each line $(k,m) \in \overrightarrow{\mathcal{E}}$ which was assigned index i. In addition, we assign the vectors $\mathbf{P_{Max}} = \begin{bmatrix} P_{Max,1} \ldots P_{Max,L} \end{bmatrix}^T \in \mathbb{R}^L$ and $\boldsymbol{\gamma} = \begin{bmatrix} \gamma_1 \ldots \gamma_L \end{bmatrix}^T \in \mathbb{R}^L$, where $P_{Max,i} = P_{Max,k,m} = P_{Max,m,k}$ and $\gamma_i = \gamma_{k,m} = \gamma_{m,k}$ for each $(k,m) \in \overrightarrow{\mathcal{E}}$ (recall that $P_{Max,k,m}$ and $\gamma_{k,m}$ are line-even).

Using the above line-oriented vectors and the incidence matrix $\mathfrak{D}$ of the graph $\mathfrak{G}$ (using the line direction in $\overrightarrow{\mathcal{E}}$), we can represent the state dynamics of the line voltage angle state $\boldsymbol{\theta}$ as follows:

$$\dot{\boldsymbol{\theta}} = \mathfrak{D}^T \mathbf{D}^{-1} \big[\mathbf{P_{Ref}} - \mathbf{P_L^0} - \mathfrak{D} \, diag\{\boldsymbol{\gamma}(\mathbf{P_{Line}}(\boldsymbol{\theta}))\} \, \mathbf{P_{Line}}(\boldsymbol{\theta}) \big]$$

$$= \mathfrak{D}^T \mathbf{D}^{-1} \big[\mathbf{P_{Ref}} - \mathbf{P_L^0} - \mathfrak{D} \, \boldsymbol{\gamma}\mathbf{P_{Line}}(\boldsymbol{\theta}) \big] \qquad (53)$$

where $\mathbf{D} = diag\left\{ \begin{bmatrix} D_1 \ldots D_N \end{bmatrix}^T \right\}$ is the diagonal matrix of bus total frequency-dependence coefficients, and we again use the shorthand notation

$$\boldsymbol{\gamma}\mathbf{P_{Line}}(\boldsymbol{\theta}) := diag\{\boldsymbol{\gamma}(\mathbf{P_{Line}}(\boldsymbol{\theta}))\} \, \mathbf{P_{Line}}(\boldsymbol{\theta}) \qquad (54)$$

Each line $i \in \{1 \ldots L\}$ of the vector equation (53) (associated with the line $(k,m) \in \overrightarrow{\mathcal{E}}$ that was assigned index i) reduces to $\dot{\theta}_i = \dot{\theta}_{k,m} = \Delta\omega_k - \Delta\omega_m$, the difference between the bus dynamic equation (52) at bus k and bus m.

4.3.3 Main Synchronization and Power Sharing Result

The main result is this chapter is that an all-active-bus acyclic CED network has three very desirable properties:

1. *Constraint Enforcement*: An all-active-bus acyclic CED network enforces the (strict) line power flow constraints $|P_{Line,k,m}| < P_{Max,k,m}$ for all $(k,m) \in \mathcal{E}$ using only local measurement and actuation. This capability is not provided by traditional frequency-droop control.

2. *Robust Frequency Synchronization*: An all-active-bus acyclic CED network provides guaranteed convergence to a shared network frequency for *all* bounded, constant network inputs ($\mathbf{P_{Ref}}$ and $\mathbf{P_L^0}$) as long as the network begins within the principal region with all constraints initially strictly met. This capability is also not provided by traditional frequency-droop control, though traditional frequency-droop does provide local convergence to a shared frequency for many operating conditions (see [15, 40, 52]).

3. *Constrained Power Sharing*: An all-active-bus acyclic CED network provides similar power sharing behavior to that of the equivalent traditional droop network at each inverter that is not adjacent to an ϵ-active constraint. Inverters adjacent to active constraints must adjust their power output away from the reference in order to enforce the active constraint. This is in contrast to the *simple power sharing* property of a traditional droop network, in which synchronization and power sharing may not be reached if a constraint is violated.

These properties make an all-active-bus, acyclic CED network much more robust than traditional droop network, and means that CED-controlled inverters can provide functionality to the network beyond what traditional droop can provide.

We state these results more formally below:

Theorem 4.1 (Robust Synchronization and Power Sharing of All-Active-Bus Acyclic CED Network). *Consider an all-active-bus, acyclic CED network (Definition 4.3) whose structure is described by the acyclic graph $\mathfrak{G} = (\mathcal{V}, \mathcal{E})$ and whose line voltage angle ($\boldsymbol{\theta}$) dynamics are described by (53). Assume that the network inputs $\mathbf{P_{Ref}}$ and $\mathbf{P_L^0}$ are bounded and constant. Then if $\boldsymbol{\theta}(t_0) \in \Theta_{Principal}$ and there exists $\mu \in (0 \quad 1)$ such that $|P_{Line,k,m}(\boldsymbol{\theta}(t_0))| < (1 - \mu)P_{Max,k,m}$ for all $(k, m) \in \mathcal{E}$ then:*

4.1.A Strict Constraint Enforcement: $|P_{Line,k,m}(\boldsymbol{\theta}(t))| < P_{Max,k,m}$ for all $(k, m) \in \mathcal{E}$ and for all $t \geq t_0$.

4.1.B Frequency Synchronization: $\Delta\omega_k \to \Delta\omega_{COM}$ for all buses $k \in \mathcal{V}$ where

$$\Delta\omega_{COM} = \frac{\sum_{k \in \mathcal{V}} P_{Ref,k} - \sum_{k \in \mathcal{V}} P_{L,k}^0}{\sum_{k \in \mathcal{V}} D_k} = \frac{\Delta\mathcal{P}_{Ref}}{\mathcal{D}} \tag{55}$$

4.1.C Constrained Power Sharing: $P_{G,k} \to P_{F,k}$ where

$$P_{F,k} = P_{Ref,k} - R_k^{-1}\frac{\Delta\mathcal{P}_{Ref}}{\mathcal{D}} \tag{56}$$

for each bus $k \in \mathcal{V}$ such that $|\Delta P_{Eq,k,m}(\mathbf{P_{Ref}} - \mathbf{P_L^0})| \leq (1 - \epsilon_{k,m})P_{Max,k,m}$ for all $m \in \mathcal{N}(k)$ where:

$$\Delta P_{Eq,k,m}(\mathbf{P_{Ref}} - \mathbf{P_L^0}) = \sum_{l \in \mathcal{V}_{C,k,m}} \left| P_{Ref,l} - P_{L,l}^0 - R_l^{-1}\Delta\omega_{COM} \right| \tag{57}$$

where $\mathcal{V}_{C,k,m} \subset \mathcal{V}$ is the cut of the graph $\mathfrak{G}$ associated with the edge $(k, m) \in \mathcal{E}$.

Theorem 4.1 considers the convergence and steady-state behavior of an all-active-bus acyclic CED network under constant reference and load inputs. The network is assumed to start (at $t = t_0$) in the principal region with all constraints initially met.

Theorem 4.1.A states that the line power flow constraints will be enforced for *all $t \geq t_0$*. Notice that this result applies both during transient and steady-state conditions. We prove this result in Lemma 4.5 later in this chapter.

Theorem 4.1.B states that the CED network under the above conditions must always synchronize to a shared system frequency $\Delta\omega_{COM}$. The quantity $\Delta\omega_{COM}$ is

the *center-of-mass frequency* of the network, and is defined in the same way as for a tradition droop network (Definition 3.2). We will show in Lemma 4.2 an all-active-bus acyclic CED network, like a traditional droop network, has the *static center-of-mass frequency property* (see Lemma 3.1).

Theorem 4.1.C states that the inverter output power $P_{G,k}$ for each inverter $k \in \mathcal{V}$ must converge to its final power value $P_{F,k}$ (the same value to which inverter k's output power must converge if synchronization is reached by a traditional droop network, see Lemma 3.2) *if and only if it is not adjacent to a line which will be ϵ-active at steady-state.* However, if an inverter k is adjacent to a constrained line, then its final power will diverge from $P_{F,k}$, since it must adjust its output to enforce the constraint. The quantity $\Delta P_{Eq,k,m}(\mathbf{P_{Ref}} - \mathbf{P_L^0})$ is the *Frequency-Agreement Power Imbalance* (Definition 3.5) for the cut associated with the line $(k,m) \in \mathcal{E}$ for the network inputs $\mathbf{P_{Ref}}$ and $\mathbf{P_L^0}$. As we will show in Section 4.4 below, $\Delta P_{Eq,k,m}(\mathbf{P_{Ref}} - \mathbf{P_L^0})$ is the value of the line adaptive tension $\gamma_{k,m} P_{Line,k,m}$ at frequency agreement.

In the following sections, we will prove Theorem 4.1 in several steps. Our approach to the proof is similar to LaSalle's Theorem (see [43, Thm. 4.4]). We will first investigate the steady-state (frequency agreement) characteristics of the all-active-bus acyclic CED network and show the existence and uniqueness of its frequency-agreement equilibrium, as well as its power sharing characteristics. We will then show that an all-active-bus acyclic CED network is capable of constraining the network state trajectory $\boldsymbol{\theta}(t)$ to a compact subset of the safe region such that the line power flow constraints $|P_{Line,k,m}| < P_{Max,k,m}$ are met for all lines $(k,m) \in \mathcal{E}$. Finally, we will show that on this compact subset, the state trajectory must necessarily converge to the unique frequency-agreement equilibrium.

4.4 Steady-State Behavior of an All-Active-Bus Acyclic CED Network

We will first consider the steady-state characteristics of an all-active-bus acyclic CED network, that is, the behavior of the network when $\boldsymbol{\Delta\omega} = \mathbf{1}_N \Delta\omega_{Sys}$ for some $\Delta\omega_{Sys} \in \mathbb{R}$, which is equivalent to $\dot{\boldsymbol{\theta}} = \mathbf{0}_L$ (see Section 3.4). We will show that a network of the above described class has a unique steady-state equilibrium such that all constraints are enforced, and at that equilibrium, each inverter must source power identical to that at steady-state under traditional droop *as long as it is not adjacent to an ϵ-active constraint.*

4.4.1 Existence and Uniqueness of Frequency Synchronization Equilibrium

By (53), an equilibrium solution $\boldsymbol{\theta}_{Eq,CED}$ to the CED network dynamics (53) is a solution to the following vector algebraic equation:

$$\mathbf{0}_L = \mathfrak{D}^T \mathbf{D}^{-1} \big[\mathbf{P_{Ref}} - \mathbf{P_L} - \mathfrak{D}\,\boldsymbol{\gamma} \mathbf{P_{Line}}(\boldsymbol{\theta}) \big] \tag{58}$$

We will now show that, on the principal region, there exists a unique equilibrium solution $\boldsymbol{\theta}_{Eq,CED}$ such that all line power flow constraints are met:

Lemma 4.1 (Existence and Uniqueness of Equilibrium of All-Active-Bus Acyclic CED Network)**.** *Consider an all-active-bus, acyclic CED network (Definition 4.3) whose structure is described by the acyclic graph $\mathfrak{G} = (\mathcal{V}, \mathcal{E})$ and whose line voltage angle ($\boldsymbol{\theta}$) dynamics are described by (53). Then for each bounded input $\mathbf{P_{Ref}} - \mathbf{P_L^0}$ there exists a unique equilibrium solution $\boldsymbol{\theta}_{Eq,CED} \in \Theta_{Principal}$ to the CED network dynamics (53) such that $|P_{Line,k,m}(\theta_{Eq,CED,k,m})| < P_{Max,k,m}$ for all $(k,m) \in \mathcal{E}$.*

Proof. Rearranging (58):

$$\mathfrak{D}^T \mathbf{D} \mathfrak{D}\,\boldsymbol{\gamma} \mathbf{P_{Line}}(\boldsymbol{\theta}) = \mathfrak{D}^T \mathbf{D} \big[\mathbf{P_{Ref}} - \mathbf{P_L^0} \big] \tag{59}$$

Since the graph $\mathfrak{G}$ contains no cycles, then $\mathfrak{D}$ has full column rank (see [54, Thm. 2.7]), and so the matrix $\mathfrak{D}^T \mathbf{D}^{-1} \mathfrak{D}$ is invertible. Therefore, there exists a unique line tension vector $\boldsymbol{\gamma} \mathbf{P_{Line}}(\boldsymbol{\theta})$ that solves

$$\boldsymbol{\gamma} \mathbf{P_{Line}}(\boldsymbol{\theta}) = diag\{\boldsymbol{\gamma}(|\mathbf{P_{Line}}(\boldsymbol{\theta})|)\} \, \mathbf{P_{Line}}(\boldsymbol{\theta})$$
$$= (\mathfrak{D}^T \mathbf{D}^{-1} \mathfrak{D})^{-1} \mathfrak{D}^T \mathbf{D}^{-1} [\mathbf{P_{Ref}} - \mathbf{P_L^0}] \qquad (60)$$

The adaptive gain matrix $diag\{\boldsymbol{\gamma}(\mathbf{P_{Line}}(\boldsymbol{\theta}))\}$ is diagonal and (by Definition 4.2.E) non-decreasing in $|\mathbf{P_{Line}}|$, and therefore $\boldsymbol{\gamma} \mathbf{P_{Line}}(\boldsymbol{\theta})$ is strictly increasing in $\mathbf{P_{Line}}$. Also, we have shown in [3, Lemma 4] that $\mathbf{P_{Line}}(\boldsymbol{\theta})$ is invertible in $\boldsymbol{\theta}$ on $\Theta_{Principal}$, and therefore $\boldsymbol{\gamma} \mathbf{P_{Line}}(\boldsymbol{\theta})$ is invertible in $\boldsymbol{\theta}$ on $\Theta_{Principal}$. Further, by Definition 4.2.C $\gamma_{k,m}$ has a range $[1.0 \quad \infty)$ for $|P_{Line,k,m}| < P_{Max,k,m}$ on $\Theta_{Principal}$, and therefore $\gamma_{k,m} P_{Line,k,m}$ has range $(-\infty \quad \infty)$ on the same domain. Therefore, for each bounded value of the right-hand side of (60) there exists a unique solution $\boldsymbol{\theta}_{Eq,CED} \in \Theta_{Principal}$ to (60) such that $|P_{Line,k,m}(\theta_{Eq,CED,k,m})| < P_{Max,k,m}$ for all $(k,m) \in \mathcal{E}$. $\qquad \square$

Lemma 4.1 shows that there always exists a unique synchronization equilibrium for the all-active-bus acyclic CED network on the principal region such that the line power flow constraints are met for any bounded inputs $\mathbf{P_{Ref}} - \mathbf{P_L^0}$ (in the absence of inverter generation constraints). Notice that this result is in contrast with Lemma 3.1, which shows that for a traditional droop network, there may not exist an equilibrium solution for many values of the inputs $\mathbf{P_{Ref}} - \mathbf{P_L^0}$. Conceptually, this is because $P_{Line,k,m}$ (the line tension in the traditional droop network) is bounded, and therefore may not have sufficient range to compensate the network forcing inputs $\mathbf{P_{Ref}} - \mathbf{P_L^0}$.

4.4.2 Center-of-Mass Frequency

In Chapter 3, we introduced the concept of the *center-of-mass frequency* $\Delta\omega_{COM}$ of an inverter-based network (Definition 3.2). In Lemma 3.1, it was shown that for a traditional droop network, the center-of-mass frequency is the frequency to which the

network will converge if it achieves frequency synchronization and that it is static for static inputs, which we termed the *static center-of-mass frequency property*. We will now show that the same results holds for the all-active-bus acyclic CED network:

Lemma 4.2 (Static Center-of-Mass Frequency of All-Active-Bus, Acyclic CED Network). *Consider an all-active-bus, acyclic CED network (Definition 4.3) whose structure is described by the acyclic graph $\mathfrak{G} = (\mathcal{V}, \mathcal{E})$ and whose line voltage angle ($\boldsymbol{\theta}$) dynamics are described by (53). Assume that the network inputs $\mathbf{P_{Ref}}$ and $\mathbf{P_L^0}$ are bounded and constant. Consider the center-of-mass frequency $\Delta\omega_{COM}$ as defined in (13). Then $\dot{\boldsymbol{\theta}} \to \mathbf{0}_L \iff \Delta\omega_k \to \Delta\omega_{COM}$ for all $k \in \mathcal{V}$. Further, the quantity $\Delta\omega_{COM}$ for the CED network is equal to that of the equivalent traditional droop network, that is, (55) holds for the all-active-bus, acyclic network.*

Proof. Since $\dot{\theta}_{k,m} = \Delta\omega_k - \Delta\omega_m$ and the graph $\mathfrak{G}$ is assumed to be connected, then $\dot{\theta}_{k,m} \to 0$ for all $(k,m) \in \mathcal{E}$ if and only if $\Delta\omega_k$ and $\Delta\omega_m$ converge for each pair of buses $k, m \in \mathcal{N}$, that is, $\dot{\boldsymbol{\theta}} \to \mathbf{0}_L$ if and only if there exists $\Delta\omega_{Sys} \in \mathbb{R}$ such that $\Delta\omega_k \to \Delta\omega_{Sys}$ for all $k \in \mathcal{V}$. It can then be shown that $\Delta\omega_{Sys} = \Delta\omega_{COM}$ by substituting $\Delta\omega_k = \Delta\omega_{Sys} \; \forall \; k \in \mathcal{V}$ into (13):

$$\Delta\omega_{COM} = \frac{\sum_{k \in \mathcal{V}} D_k \Delta\omega_{Sys}}{\sum_{k \in \mathcal{V}} D_k} = \Delta\omega_{Sys} \tag{61}$$

In addition, substituting the CED control law (50) into (13) and rearranging:

$$\Delta\omega_{COM} = \frac{\sum_{k \in \mathcal{V}} (P_{Ref,k} - P_{L,k})}{\sum_{k \in \mathcal{V}} D_k}$$
$$- \frac{\sum_{(k,m) \in \mathcal{E}} (\gamma_{k,m}(|P_{Line,k,m}|) P_{Line,k,m} + \gamma_{k,m}(|P_{Line,m,k}|) P_{Line,m,k})}{\sum_{k \in \mathcal{V}} D_k} \tag{62}$$

Since $P_{Line,k,m}$ is line-odd (see (2)) and $\gamma_{k,m}$ is line-even (Definition 4.2.D) for all $(k, m) \in \mathcal{E}$, then

$$\gamma_{k,m}(|P_{Line,k,m}|) P_{Line,k,m} + \gamma_{k,m}(|P_{Line,m,k}|) P_{Line,m,k} = 0, \tag{63}$$

(that is, the line tension $\gamma_{k,m} P_{Line,k,m}$ is line-odd), and therefore (62) simplifies to (55). $\qquad\square$

Lemma 4.2 shows that an all-active-bus, acyclic CED network also possesses the *static center-of-mass frequency property*, similar to that shown for traditional droop inverter-based network shown in Lemma 3.1. This is because while the line adaptive tension values $\gamma_{k,m}P_{Line,k,m}$ for each line $(k,m) \in \mathcal{E}$ may differ from those in the traditional droop network ($P_{Line,k,m}$), they are still line-odd, and therefore still cancel in the center-of-mass frequency weighted average.

4.4.3 Line Frequency-Agreement Power Imbalances

In Chapter 3, we developed the concept of *frequency-agreement power imbalance* (Definition 3.5) associated with cuts of the network. In a traditional droop network, the frequency-agreement power imbalance $\Delta P_{Eq,C}$ associated with a cut V_C is the total power that must flow across the cut at frequency agreement (see (28)). As we will show below, in an all-active-bus, acyclic CED network, each line defines a cut, and the associated frequency-agreement power imbalance is the value of the line adaptive tension (*not* necessarily the line power flow) at frequency-agreement.

Consider an arbitrary line $(k,m) \in \mathcal{E}$. In an acyclic graph, each such line defines a cut $\mathcal{V}_{C,k,m} \subset \mathcal{N}$, where the removal of line (k,m) from $\mathfrak{G}$ seperates $\mathcal{V}_{C,k,m}$ (containing k) from $\mathcal{V} \setminus \mathcal{V}_{C,k,m}$ (containing m). Now consider the all-active-bus acyclic CED network bus dynamic equation (52) at an arbitrary bus $l \in \mathcal{V}$ when the network is at steady state ($\boldsymbol{\theta} = \boldsymbol{\theta}_{Eq,CED}$ and (by Lemma 4.2) $\Delta\omega_l = \Delta\omega_{COM} \; \forall \, l \in \mathcal{V}$), which may be rewritten as:

$$\sum_{p \in \mathcal{N}(l)} \gamma_{l,p} P_{Line,l,p}(\theta_{Eq,CED,l,p}) = \sum_{l \in \mathcal{V}_{C,k,m}} P_{Ref,l} - P_{L,l}^0 - R_l^{-1}\Delta\omega_{COM} \qquad (64)$$

Taking the sum of (64) for all $l \in \mathcal{V}_{C,k,m}$:

$$\sum_{l \in \mathcal{V}_{C,k,m}} P_{Ref,l} - P_{L,l}^0 - R_l^{-1}\Delta\omega_{COM} = \sum_{l \in \mathcal{V}_{C,k,m}} \sum_{p \in \mathcal{N}(l)} \gamma_{l,p} P_{Line,l,p}(\theta_{Eq,CED,l,p}) \qquad (65)$$

Since the bus set $\mathcal{V}_{C,k,m}$ is a cut defined by the edge $(k,m) \in \mathcal{E}$, each line $(l,p) \in \mathcal{E}$ incident to a bus $l \in \mathcal{V}_{C,k,m}$ is either internal to $\mathcal{V}_{C,k,m}$ (in which case $p \in \mathcal{V}_{C,k,m}$),

or the cut line (k, m) itself. Therefore, we can rearrange the summation in (65) as follows:

$$\sum_{l \in \mathcal{V}_{C,k,m}} P_{Ref,l} - P_{L,l}^0 - R_l^{-1} \Delta\omega_{COM} = P_{Line,k,m}(\theta_{Eq,CED,k,m})$$

$$+ \sum_{(l,p) \in \mathcal{E} \text{ s.t. } l,p \in \mathcal{V}_{C,k,m}} \left[\gamma_{l,p} P_{Line,l,p}(\theta_{Eq,CED,l,p}) + \gamma_{l,p} P_{Line,p,l}(\theta_{Eq,CED,p,l}) \right]$$

$$(66)$$

We have already shown (in the proof to Lemma 4.2) that $\gamma_{l,p} P_{Line,l,p}$ is line-odd, and therefore $\gamma_{l,p} P_{Line,l,p} + \gamma_{p,l} P_{Line,p,l} = 0$. Therefore, (66) simplies to:

$$\gamma_{k,m} P_{Line,k,m}(\theta_{Eq,CED,k,m}) = \sum_{l \in \mathcal{V}_{C,k,m}} \left[P_{Ref,l} - P_{L,l}^0 - R_l^{-1} \Delta\omega_{COM} \right]$$

$$= \Delta P_{Eq,k,m}(\mathbf{P_{Ref}} - \mathbf{P_L^0}) \qquad (67)$$

The (constant) right-hand side of (67) is the *frequency-agreement power imbalance* $\Delta P_{Eq,k,m}(\mathbf{P_{Ref}} - \mathbf{P_L^0})$ (Definition 3.5) for the cut defined by $\mathcal{E}_C = (k, m)$. Observe that since $\gamma_{k,m} P_{Line,k,m}$ is line-odd, then so is $\Delta P_{Eq,k,m}$ (that is, $\Delta P_{Eq,k,m}(\mathbf{P_{Ref}} - \mathbf{P_L^0}) = -\Delta P_{Eq,m,k}(\mathbf{P_{Ref}} - \mathbf{P_L^0})$).

In the traditional droop network, $\Delta P_{Eq,k,m}$ represents the power that must flow across line $(k, m) \in \mathcal{E}$ at frequency agreement (see Section 3.4.4). In the CED network, it represents the value of the line tension $\gamma_{k,m} P_{Line,k,m}$ at frequency agreement. If $|\Delta P_{Eq,k,m}| > (1 - \epsilon_{k,m}) P_{Max,k,m}$, then the line power flow constraint on line $(k, m) \in \mathcal{E}$ will be ϵ-active (or violated) at frequency agreement.

4.4.4 Constrained Power Sharing of All-Active-Bus, Acyclic CED Network

The traditional frequency-droop control law (4) creates an explicit link between the output power of an inverter and its AC frequency. In Chapter 3, we showed that as a result of this connection, frequency synchronization between inverters in a droop inverter-based network implies a convergence of their output power values such that

they share the network load according to their assigned reference and droop constants (Lemma 3.2), which we termed the simple power sharing property of a droop inverter-based network.

The all-incident-line CED control law (50) at an arbitrary bus $k \in \mathcal{V}$ also creates such a connection between inverter output power and frequency, but less directly: rather than operating directly on the output power $P_{G,k}$, the CED control law instead operates on a weighted sum of the load and incident line power flows. We have already observed that when $\gamma_{k,m} = 1$ for all $m \in \mathcal{N}(k)$, then the all-incident-line CED control law reduces to the droop dynamics (7), that is, the CED control law *implicitly* creates the same output power/frequency connection as traditional droop. By Definition 4.2.B, this condition occurs when no line incident to bus k is ϵ-active. The line steady-state tension values determine when a line constraint will be ϵ-active at steady-state.

Therefore, we would expect that if frequency synchronization occurs in an all-active-bus CED network such that no line incident to k is ϵ-active at steady state, then the CED inverter at bus k should converge to the same output power value that it would under traditional droop. However, if any line incident to bus k is ϵ-active, then $\gamma_{k,m}$ does not equal unity for some $m \in \mathcal{N}(k)$, and therefore we would *not* expect the CED inverter at bus k to converge to the same output power as in a traditional droop network. We state this result formally in Lemma 4.3 below:

Lemma 4.3 (Constrained Power Sharing of All-Active-Bus Acyclic CED Networks)**.**
Consider an all-active-bus, acyclic CED network (Definition 4.3) whose structure is described by the acyclic graph $\mathfrak{G} = (\mathcal{V}, \mathcal{E})$ and whose line voltage angle ($\boldsymbol{\theta}$) dynamics are described by (53). Assume that the network inputs $\mathbf{P_{Ref}}$ and $\mathbf{P_L^0}$ are bounded and constant. Consider an arbitrary bus $k \in \mathcal{V}$ and assume that the following holds for

all $m \in \mathcal{N}(k)$:

$$|\Delta P_{Eq,k,m}(\mathbf{P_{Ref}} - \mathbf{P_L^0})| \leq (1 - \epsilon_{k,m})P_{Max,k,m} \tag{68}$$

Then at frequency agreement ($\dot{\boldsymbol{\theta}} = \mathbf{0}_L$) where $|P_{Line,k,m}| < P_{Max,k,m}$ for all $(k,m) \in \mathcal{E}$, each inverter power $P_{G,k} = P_{F,k} = P_{Ref,k} - R_k^{-1}\Delta\omega_{COM}$ where $P_{F,k}$ is the same final power as results from the traditional frequency-droop dynamics (10) *(Lemma 3.2).*

Proof. We have shown in Lemma 4.1 that there exists a unique equilibrium $\boldsymbol{\theta}_{Eq,CED} \in \Theta_{Principal}$ such that $\dot{\boldsymbol{\theta}} = \mathbf{0}_L$ and $|P_{Line,k,m}| < P_{Max,k,m}$ for all $(k,m) \in \mathcal{E}$. By assumption, the magnitude of the right-hand side of (67) is bounded by $(1 - \epsilon_{k,m})P_{Max,k,m}$ for all $m \in \mathcal{N}(k)$. Since (by Definition 4.2) $\gamma_{k,m} \geq 1.0$ for all $P_{Line,k,m}$, then $|P_{Line,k,m}(\theta_{Eq,CED,k,m})| \leq (1 - \epsilon_{k,m})P_{Max,k,m}$ for all $m \in \mathcal{N}(k)$, and so (by Definition 4.2.B) $\gamma_{k,m} = 1.0$ for all $m \in \mathcal{N}(k)$ at $\boldsymbol{\theta}_{Eq,CED}$.

We have shown in Lemma 4.2 that $\dot{\boldsymbol{\theta}} = \mathbf{0}_L \iff \Delta\omega_k = \Delta\omega_{COM}$ for all $k \in \mathcal{V}$. Substituting $\Delta\omega_k = \Delta\omega_{COM}$ and $\gamma_{k,m} = 1.0$ for all $m \in \mathcal{N}(k)$ into (50) at $\boldsymbol{\theta}_{Eq,CED}$:

$$\Delta\omega_{COM} = R_k\left[P_{Ref,k} - P_{L,k} - \sum_{m \in \mathcal{N}(k)} P_{Line,k,m}(\theta_{Eq,CED,k,m})\right] \tag{69}$$

Substituting Kirchoff's Law into (69) and rearranging, we find that $P_{G,k} = P_{Ref,k} - R_k^{-1}\Delta\omega_{COM} = P_{F,k}$ at $\boldsymbol{\theta}_{Eq,CED}$ where $P_{F,k}$ is the final power value determined for the traditional frequency-droop network in Lemma 3.2. Therefore, if (68) holds for all $m \in \mathcal{N}(k)$ then $\dot{\boldsymbol{\theta}} = \mathbf{0}_L \implies P_{G,k} = P_{F,k}$. $\qquad\square$

Lemma 4.3 shows that an all-active-bus, acyclic CED network provides similar (but not identical) power sharing behavior to that provided by traditional frequency-droop networks. At steady-state (frequency agreement), inverters not incident to a constrained line share the total network load according to their assigned reference and droop values. However, inverters incident to active constraints must adjust their output power in order to enforce the constraints on incident lines. We designate this result as the *constrained power sharing property* of an all-active-bus, acyclic CED

network (in contrast to the simple power sharing property of droop inverter-based networks).

However, the primary strength of an all-active-bus, acyclic CED network is its ability to enforce the line power constraints and guarantee frequency synchronization (and therefore constrained power sharing) much more robustly than similar droop inverter-based networks. We prove this result in the following section.

4.5 Convergence Behavior of an All-Active-Bus Acyclic CED Network

In this section, we will show that an all-active-bus acyclic CED network will enforce the line power flow constraints and converge to an equilibrium of the type described by Lemma 4.3 if it begins in the principal region with all constraints initially met, thus proving Theorem 4.1. Our approach to this proof is similar to LaSalle's Theorem. We first consider a family of compact, strict subsets of the safe region Θ_{Safe}, where the network dynamics (53) are locally Lipschitz continuous. We show as long as the intial network condition is contained within any one of these subsets, then there exists a (possibly larger) such subset that contains the entire state trajectory $\boldsymbol{\theta}(t)$. This means that the network state trajectory is bounded within the interior of the safe region Θ_{Safe}, that is, all line power flow constraints are strictly enforced. We then show that convergence to a frequency agreement equilibrium necessarily follows, thus guaranteeing the frequency synchronization and constrained power sharing of the all-active-bus, acyclic CED network.

4.5.1 Compact Subsets Θ_{μ} of the Safe Region

Consider the following family of subsets of $\Theta_{Principal}$:

Definition 4.4 (μ-Safe Regions).

$$\Theta_{\mu} = \{\boldsymbol{\theta} \in \Theta_{Principal} \ s.t. \ |P_{Line,k,m}(\theta_{k,m})| \leq (1 - \mu)P_{Max,k,m} \ \forall \ (k,m) \in \mathcal{E}\} \quad (70)$$

for $\mu \in (0 \quad 1)$.

The sets Θ_μ for all $\mu \in (0 \quad 1)$ are strict subsets of Θ_{Safe} (Definition 3.8) where each line power flow magnitude $|P_{Line,k,m}|$ is bounded by $(1 - \mu)P_{Max,k,m}$. Following the same logic as in Corollary 3.2, we can show that the sets Θ_μ for all $\mu \in (0 \quad 1)$ have the following characteristics:

Lemma 4.4 (Characteristics of Θ_μ)**.** *Consider the μ-safe region Θ_μ as defined in Definition 4.4. Then:*

4.4.A For each $\mu \in (0 \quad 1)$, there exists $\theta_{\mu,k,m}$ such that $0 < \theta_{\mu,k,m} < \pi/2$ and Θ_μ is equivalent to

$$\Theta_\mu = \{\boldsymbol{\theta} \in \mathbb{R}^L \text{ such that } |\theta_{k,m}| \leq \theta_{\mu,k,m} \ \forall \ (k,m) \in \mathcal{E}\}, \tag{71}$$

4.4.B The set Θ_μ is compact for all $\mu \in (0 \quad 1)$.

4.4.C The dynamics of $\boldsymbol{\theta}$ in (53) are locally Lipschitz continuous on Θ_μ for all $\mu \in (0 \quad 1)$.

Proof.

Lemma 4.4.A:

Proof follows from Definition 4.4 and Lemma 3.4.

Lemma 4.4.B:

Since (by Lemma 4.4.A) Θ_μ is equivalent to (71), then Θ_μ is closed and bounded for each $\mu \in (0 \quad 1)$, which implies that it is compact.

Lemma 4.4.C:

In order to show that the network dynamic equation (53) is locally Lipschitz on Θ_μ for each $\mu \in (0 \quad 1)$, we must show that for each such μ there exists a constant

scalar $G_\mu > 0$ such that

$$||\dot{\boldsymbol{\theta}}|_{\boldsymbol{\theta}=\boldsymbol{\theta}_1} - \dot{\boldsymbol{\theta}}|_{\boldsymbol{\theta}=\boldsymbol{\theta}_2}|| \leq G_\mu ||\boldsymbol{\theta}_1 - \boldsymbol{\theta}_2|| \tag{72}$$

for every $\boldsymbol{\theta}_1, \boldsymbol{\theta}_2 \in \Theta_\mu$, where $|| \bullet ||$ indicates the standard $\mathfrak{L}2$-matrix norm.

Substituting (53) into the left-hand side of (72):

$$\begin{aligned}
||\dot{\boldsymbol{\theta}}|_{\boldsymbol{\theta}=\boldsymbol{\theta}_1} - \dot{\boldsymbol{\theta}}|_{\boldsymbol{\theta}=\boldsymbol{\theta}_2}|| &= ||\mathfrak{D}^T\mathbf{D}^{-1}\big[\mathbf{P_{Ref}} - \mathbf{P_L^0}\big] - \mathfrak{D}^T\mathbf{D}^{-1}\mathfrak{D}\,\boldsymbol{\gamma}\mathbf{P_{Line}}(\boldsymbol{\theta}_1) \\
&\quad - \mathfrak{D}^T\mathbf{D}^{-1}\big[\mathbf{P_{Ref}} - \mathbf{P_L^0}\big] + \mathfrak{D}^T\mathbf{D}^{-1}\mathfrak{D}\,\boldsymbol{\gamma}\mathbf{P_{Line}}(\boldsymbol{\theta}_2)|| \\
&= ||\mathfrak{D}^T\mathbf{D}^{-1}\mathfrak{D}\,\boldsymbol{\gamma}\mathbf{P_{Line}}(\boldsymbol{\theta}_1) - \mathfrak{D}^T\mathbf{D}^{-1}\mathfrak{D}\,\boldsymbol{\gamma}\mathbf{P_{Line}}(\boldsymbol{\theta}_2)|| \tag{73}
\end{aligned}$$

Applying the scalability property of the $\mathfrak{L}2$-norm:

$$\begin{aligned}
||\dot{\boldsymbol{\theta}}|_{\boldsymbol{\theta}=\boldsymbol{\theta}_1} - \dot{\boldsymbol{\theta}}|_{\boldsymbol{\theta}=\boldsymbol{\theta}_2}|| &\leq ||\mathfrak{D}^T\mathbf{D}^{-1}\mathfrak{D}||\,||\boldsymbol{\gamma}\mathbf{P_{Line}}(\boldsymbol{\theta}_1) - \boldsymbol{\gamma}\mathbf{P_{Line}}(\boldsymbol{\theta}_2)|| \\
&= ||\mathfrak{D}^T\mathbf{D}^{-1}\mathfrak{D}||\,||diag\{\boldsymbol{\gamma}(|\mathbf{P_{Line}}(\boldsymbol{\theta}_1)|)\}\mathbf{P_{Line}}(\boldsymbol{\theta}_1) \\
&\quad - diag\{\boldsymbol{\gamma}(|\mathbf{P_{Line}}(\boldsymbol{\theta}_2)|)\}\mathbf{P_{Line}}(\boldsymbol{\theta}_2)|| \tag{74}
\end{aligned}$$

By Definition 4.2.F, there exists a constant $\gamma_{\mu,k,m}$ for each $(k,m) \in \mathcal{E}$ such that $\gamma_{k,m}(|P_{Line,k,m}|) \leq \gamma_{\mu,k,m}$ when $\boldsymbol{\theta} \in \Theta_\mu$. Therefore, we can bound

$$||diag\{\boldsymbol{\gamma}(|\mathbf{P_{Line}}(\boldsymbol{\theta})|)\}|| \leq \gamma_{Max,\mu} \tag{75}$$

where

$$\gamma_{Max,\mu} = \left|\left|\begin{bmatrix} \gamma_{\mu,1} \ldots \gamma_{\mu,L} \end{bmatrix}\right|\right| \tag{76}$$

for all $\boldsymbol{\theta} \in \Theta_\mu$.

Substituting (75) into (74):

$$||\dot{\boldsymbol{\theta}}|_{\boldsymbol{\theta}=\boldsymbol{\theta}_1} - \dot{\boldsymbol{\theta}}|_{\boldsymbol{\theta}=\boldsymbol{\theta}_2}|| \leq \gamma_{Max,\mu}||\mathfrak{D}^T\mathbf{D}^{-1}\mathfrak{D}||\,||\mathbf{P_{Line}}(\boldsymbol{\theta}_1) - \mathbf{P_{Line}}(\boldsymbol{\theta}_2)|| \tag{77}$$

Substituting (8) into (77) and again applying the scalability property:

$$||\dot{\boldsymbol{\theta}}|_{\boldsymbol{\theta}=\boldsymbol{\theta}_1} - \dot{\boldsymbol{\theta}}|_{\boldsymbol{\theta}=\boldsymbol{\theta}_2}|| \leq \gamma_{Max,\mu}||\mathfrak{D}^T\mathbf{D}^{-1}\mathfrak{D}||\,||\mathbf{Y_{Line}}\mathbf{V_{In}}\mathbf{V_{Out}}||\,||\sin(\boldsymbol{\theta}_1) - \sin(\boldsymbol{\theta}_2)|| \tag{78}$$

Substituting the trigonometric identity $\sin(\boldsymbol{\theta}_1) - \sin(\boldsymbol{\theta}_2) = 1/2 \sin(\boldsymbol{\theta}_1 - \boldsymbol{\theta}_2) \cos(\boldsymbol{\theta}_1 + \boldsymbol{\theta}_2)$:

$$||\dot{\boldsymbol{\theta}}|_{\boldsymbol{\theta}=\boldsymbol{\theta}_1} - \dot{\boldsymbol{\theta}}|_{\boldsymbol{\theta}=\boldsymbol{\theta}_2}|| \leq \frac{1}{2}\gamma_{Max,\mu} ||\mathfrak{D}^T \mathbf{D}^{-1} \mathfrak{D}|| \, ||\mathbf{Y_{Line} V_{In} V_{Out}}|| \, ||\sin(\boldsymbol{\theta}_1 - \boldsymbol{\theta}_2)\cos(\boldsymbol{\theta}_1 + \boldsymbol{\theta}_2)||$$

$$(79)$$

Since $\cos(\theta) \leq 1$ for all θ:

$$||\dot{\boldsymbol{\theta}}|_{\boldsymbol{\theta}=\boldsymbol{\theta}_1} - \dot{\boldsymbol{\theta}}|_{\boldsymbol{\theta}=\boldsymbol{\theta}_2}|| \leq \frac{1}{2}\gamma_{Max,\mu} ||\mathfrak{D}^T \mathbf{D}^{-1} \mathfrak{D}|| \, ||\mathbf{Y_{Line} V_{In} V_{Out}}|| \, ||\sin(\boldsymbol{\theta}_1 - \boldsymbol{\theta}_2)|| \qquad (80)$$

Finally, since $\sin(\theta) \leq \theta$ for all θ:

$$||\dot{\boldsymbol{\theta}}|_{\boldsymbol{\theta}=\boldsymbol{\theta}_1} - \dot{\boldsymbol{\theta}}|_{\boldsymbol{\theta}=\boldsymbol{\theta}_2}|| \leq \frac{1}{2}\gamma_{Max,\mu} ||\mathfrak{D}^T \mathbf{D}^{-1} \mathfrak{D}|| \, ||\mathbf{Y_{Line} V_{In} V_{Out}}|| \, ||\boldsymbol{\theta}_1 - \boldsymbol{\theta}_2||$$

$$= G_\mu ||\boldsymbol{\theta}_1 - \boldsymbol{\theta}_2|| \tag{81}$$

for

$$G_\mu = \frac{1}{2}\gamma_{Max,\mu} ||\mathfrak{D}^T \mathbf{D}^{-1} \mathfrak{D}|| \, ||\mathbf{Y_{Line} V_{In} V_{Out}}|| \tag{82}$$

$\square$

Lemma 4.4 shows that the set Θ_μ for each $\mu \in (0 \quad 1)$ is a compact, strict subset of Θ_{Safe} where the the dynamics of the network state $\boldsymbol{\theta}$ are locally Lipschitz. Further, it follows from Definition 4.2.F that for each Θ_μ there exists a bounded maximum value $\gamma_{\mu,k,m}$ for each line adapative gain $\gamma_{k,m}$.

4.5.2 Enforcement of Line Power Flow Constraints

In Theorem 3.5, we showed that if the state trajectory $\boldsymbol{\theta}(t)$ of a traditional droop inverter-based network stays bounded within the safe region Θ_{Safe} (of which all Θ_μ are strict subsets), then it will necessarily achieve frequency synchronization (from which follows simple power sharing). The boundaries of Θ_{Safe} are defined by the line power flow constraints $|P_{Line,k,m}| \leq P_{Max,k,m}$ for all lines $(k,m) \in \mathcal{E}$. However, since the traditional frequendy-droop does not enforce any such constraints, then

the network may lose such synchronization, and with it convergence to simple power sharing.

In an all-active-bus CED network, each inverter $k \in \mathcal{V}$ measures the line power flow $P_{Line,k,m}$ on each line incident to it, and applies the adaptive gain $\gamma_{k,m}$ (meeting the requirements in Definition 4.2) to "pull" the network state trajectory back from its constraint. As we will show below, this bounds the network state trajectory within a strict subset of Θ_{Safe}, enforcing all such constraints in the network.

Lemma 4.5 (Existence of an Invariant Subset of Safe Region on All-Active-Bus Acyclic CED Network). *Consider an all-active-bus, acyclic CED network (Definition 4.3) whose structure is described by the acyclic graph $\mathfrak{G} = (\mathcal{V}, \mathcal{E})$ and whose line voltage angle $(\boldsymbol{\theta})$ dynamics are described by (53). Assume that the network inputs* $\mathbf{P_{Ref}}$ *and* $\mathbf{P_L^0}$ *are bounded and constant. Then for each $\mu \in (0 \quad 1)$ there exists $\beta(\mu) \in (0 \quad \mu)$ such that $\boldsymbol{\theta}(t_0) \in \Theta_\mu \implies \boldsymbol{\theta}(t) \in \Theta_{\beta(\mu)} \, \forall \, t \geq t_0$ where Θ_μ is defined in Definition 4.4.*

Proof. By assumption, $\boldsymbol{\theta}(t_0)$ is in some Θ_μ (interior of Θ_{Safe}). Since the network dynamics (53) are Lipschitz continuous on Θ_μ for all $\mu \in (0 \quad 1)$ (Lemma 4.4.C), then in order for $\boldsymbol{\theta}(t)$ to exit all Θ_μ it must approach the set where $|P_{Line,k,m}(\theta_{k,m})| = P_{Max,k,m}$ for at least one $(k, m) \in \mathcal{E}$ (the boundary of Θ_{Safe}) from the interior of Θ_{Safe}.

Contradiction Hypothesis: There exists state trajectory $\boldsymbol{\theta}(t)$ for $t \geq t_0$, time $T > t_0$, and line $(k, m) \in \mathcal{E}$ such that:

1. $\boldsymbol{\theta}(t_0)$ is in the interior of Θ_{Safe} prior to T ($\boldsymbol{\theta}(t_0) \in \Theta_\mu$ and $\boldsymbol{\theta}(t) \in \Theta_{Safe}$ for all $t_0 < t < T$).

2. $\boldsymbol{\theta}(t)$ approaches the (k, m) boundary of Θ_{Safe} as $t \to T$ ($\lim_{t \to T} |P_{Line,k,m}(\theta_{k,m}(t))| = P_{Max,k,m}$)

Consider the network energy function $U(\boldsymbol{\theta})$ introduced in (41), reprinted below:

$$U(\boldsymbol{\theta}) = \frac{1}{2}\dot{\boldsymbol{\delta}}^T \mathbf{D} \dot{\boldsymbol{\delta}} = \frac{1}{2}f(\boldsymbol{\theta})^T \mathbf{D} f(\boldsymbol{\theta})$$

Applying the same approach as in Section 3.3, the bus-oriented dynamic system-of-equations for an all-active-bus, acyclic CED network (52) can be written in vector form as:

$$f(\boldsymbol{\theta}) = \dot{\boldsymbol{\delta}} = \mathbf{D}^{-1}\left[\mathbf{P_{Ref}} - \mathbf{P_L^0} - \mathfrak{D}\,\boldsymbol{\gamma}\mathbf{P_{Line}}(\boldsymbol{\theta})\right] \tag{83}$$

We will now show that $U(\boldsymbol{\theta}(t_0))$ is bounded, and that $\dot{U}(\boldsymbol{\theta}(t)) \leq 0$ for all $t_0 \leq t < T$.

By Definition 4.2.F there exists $\gamma_{\mu,k,m}$ such that $\gamma_{k,m} \leq \gamma_{\mu,k,m}$ for all $\boldsymbol{\theta}(t_0) \in \Theta_\mu$. In addition, by (2) we can always bound $|P_{Line,k,m}| \leq Y_{k,m}V_kV_m$ and (by assumption) $\mathbf{P_{Ref}} - \mathbf{P_L^0}$ is bounded. Therefore, each of the terms in the linear sum (83) are bounded, and so there exists $f_{t_0,\mu} > 0$ such that $||f(\boldsymbol{\theta}(t_0))|| \leq f_{t_0,\mu}$, and so there exists $U_{t_0,\mu} > 0$ such that $U(\boldsymbol{\theta}(t_0)) \leq U_{t_0,\mu}$.

Taking the time-derivative of the energy function (41) and substituting $\dot{\boldsymbol{\theta}} = \mathfrak{D}^T f(\boldsymbol{\theta})$:

$$\begin{aligned}
\dot{U}(\boldsymbol{\theta}) &= f(\boldsymbol{\theta})^T \mathbf{D}^{-1} f(\dot{\boldsymbol{\theta}}) \\
&= -f(\boldsymbol{\theta})^T \mathfrak{D}\left[diag\{\boldsymbol{\gamma}(\mathbf{P_{Line}}(\boldsymbol{\theta}))\}\frac{\partial \mathbf{P_{Line}}}{\partial \boldsymbol{\theta}} + \frac{\partial \boldsymbol{\gamma}}{\partial \boldsymbol{\theta}}\,diag\{\mathbf{P_{Line}}(\boldsymbol{\theta})\}\right]\dot{\boldsymbol{\theta}} \\
&= -\dot{\boldsymbol{\theta}}^T \mathbf{D}^{-1}\left[diag\{\boldsymbol{\gamma}(\mathbf{P_{Line}}(\boldsymbol{\theta}))\}\frac{\partial \mathbf{P_{Line}}}{\partial \boldsymbol{\theta}} + \frac{\partial \boldsymbol{\gamma}}{\partial \boldsymbol{\theta}}\,diag\{\mathbf{P_{Line}}(\boldsymbol{\theta})\}\right]\dot{\boldsymbol{\theta}} \tag{84}
\end{aligned}$$

We have already shown in Lemma 3.3 that the partial-derivative matrix $\partial\mathbf{P_{Line}}\,/\,\partial\boldsymbol{\theta}$ is diagonal with all positive diagonal elements on $\Theta_\mu \subset \Theta_{Principal}$. By Definition 4.2, $\boldsymbol{\gamma}(\mathbf{P_{Line}}(\boldsymbol{\theta}))$ is similarly diagonal with all positive elements, and so the first term of the weight matrix of (84) is as well. Finally, the term $\partial\boldsymbol{\gamma}\,/\,\partial\boldsymbol{\theta}\,diag\{\mathbf{P_{Line}}\}$ is also diagonal with all non-negative diagonal elements:

$$\frac{\partial \gamma_{k,m}}{\partial \theta_{k,m}}P_{Line,k,m} = \frac{\partial \gamma_{k,m}}{\partial |P_{Line,k,m}|}\frac{\partial P_{Line,k,m}}{\partial \theta_{k,m}}|P_{Line,k,m}| \tag{85}$$

85

By Definition 4.2.E, $\partial \gamma_{k,m} \,/\, \partial |P_{Line,k,m}| \geq 0$ for $|P_{Line,k,m}| < P_{Max,k,m}$, and so (85) is non-negative on Θ_μ for all $\mu \in (0 \quad 1)$. Therefore, the weight matrix on the far right-hand side of (84) is diagonal with all positive diagonal elements, and so $\dot{U}(\boldsymbol{\theta}) \leq 0$ for all $\boldsymbol{\theta}$ in the interior of Θ_{Safe}.

By the contradiction hypothesis, $\boldsymbol{\theta}(t)$ is in the interior of Θ_{Safe} for all $t_0 \leq t < T$, and therefore $\dot{U}(\boldsymbol{\theta}(t)) \leq 0 \; \forall \; t_0 \leq t < T$. Since there exists $U_{t_0,\mu} > 0$ such that $U(\boldsymbol{\theta}(t_0)) \leq U_{t_0,\mu}$, then $U(\boldsymbol{\theta}(t)) \leq U_{t_0,\mu}$ for all $t_0 \leq t < T$.

Also by the contradiction hypothesis, $\lim_{t \to T} |P_{Line,k,m}(\theta_{k,m}(t))| = P_{Max,k,m} > 0$ for some $(k,m) \in \mathcal{E}$. Therefore, by Definition 4.2.C the associated

$$\lim_{t \to T} \gamma_{k,m}(|P_{Line,k,m}(\theta_{k,m}(t))|) = \infty \implies \lim_{t \to T} \gamma_{k,m} P_{Line,k,m}(\theta_{k,m}(t)) = \pm\infty. \qquad (86)$$

Since the network is acyclic, the incidence matrix $\mathfrak{D}$ has full column rank (see [54, Thm. 2.7]), and so it follows from (83) and (41) that

$$\lim_{t \to T} \gamma_{k,m} P_{Line,k,m}(\theta_{k,m}(t)) = \pm\infty \implies \lim_{t \to T} ||f(\boldsymbol{\theta}(t))|| = \infty$$
$$\implies \lim_{t \to T} U(\boldsymbol{\theta}(t)) = \infty \qquad (87)$$

However, this contradicts with the observation that $U(\boldsymbol{\theta}(t)) \leq U_{t_0,\mu}$ for all $t_0 \leq t < T$. Therefore, the contradiction hypothesis is proven false, and so $\boldsymbol{\theta}(t_0) \in \Theta_\mu$ for some $\mu \in (0 \quad 1)$ implies that there does not exist line $(k,m) \in \mathcal{E}$ such that $|P_{Line,k,m}|$ approaches $P_{Max,k,m}$ as t approaches T for any $T > t_0$ (that is, all line power flow constraints are strictly enforced).

Since we have shown that no line converges to its maximum power flow $P_{Max,k,m}$, then for each $(k,m) \in \mathcal{E}$ there exists $\mu_{k,m} \in (0 \quad \mu)$ such that $|P_{Line,k,m}| \leq (1 - \mu_{k,m}) P_{Max,k,m}$ for all $t > t_0$. Therefore, there exists

$$\beta(\mu) := \min_{(k,m) \in \mathcal{E}} \{\mu_{k,m}\} \in (0 \quad \mu) \qquad (88)$$

such that $|P_{Line,k,m}| \leq (1 - \beta(\mu)) P_{Max,k,m} \; \forall \; (k,m) \in \mathcal{E}$ and for all $t \geq t_0$, that is $\boldsymbol{\theta}(t) \in \Theta_{\beta(\mu)}$ for all $t \geq t_0$. $\qquad \square$

It follows from Lemma 4.5 that, as long as $\boldsymbol{\theta}$ starts (at $t = t_0$) in $\Theta_{Principal}$ and each $|P_{Line,k,m}|$ starts at least $\mu > 0$ less than $P_{Max,k,m}$, then all of the line power flow constraints $|P_{Line,k,m}| < P_{Max,k,m}$ will be enforced for all $t \geq t_0$, and the network will necessarily remain in the interior of safe region Θ_{Safe}.

4.5.3 Proof of Main Synchronization and Power Sharing Result

Lemma 4.5 has confirmed that state trajectories of an all-active-bus, acyclic CED network are invariant to a compact subset of the safe region (that is, state trajectories beginning in the interior of the safe region can't leave it). Theorem 3.5 stated that for a droop inverter-based network, this condition is sufficient to ensure network frequency synchronization, which suggests that it should be for an all-active-bus, acyclic network as well. In addition, we have already shown that convergence to frequency synchronization implies convergence to the static center-of-mass frequency (Lemma 4.2) and constrained power sharing (Lemma 4.3). Therefore, our main synchronization and power sharing result for all-active-bus, acyclic CED networks (Theorem 4.1) can be proven by a method very similar to that used for Theorem 3.5:

Proof of Theorem 4.1. Contradiction Hypothesis: There exists $\boldsymbol{\theta}(t)$ for $t \geq 0$ and $\mu \in (0 \quad 1)$ such that $\boldsymbol{\theta}(t_0) \in \Theta_\mu$ but $\dot{\boldsymbol{\theta}}$ does not converge to $\mathbf{0}_L$.

First, observe that (by assumption) $\boldsymbol{\theta}(t_0) \in \Theta_\mu$. Therefore, by Lemma 4.5, there exists $\beta(\mu) \in (0 \quad \mu)$ such that $\boldsymbol{\theta}(t) \in \Theta_{\beta(\mu)}$ for all $t \geq t_0$. Since (by Definition 4.4) $|P_{Line,k,m}| < P_{Max,k,m}$ for all $\boldsymbol{\theta} \in \Theta_{\beta(\mu)}$, this proves Theorem 4.1.A.

Consider the energy function $U(\boldsymbol{\theta}(t)) \geq 0$ introduced in (41). We showed in the proof to Lemma 4.5 that there exists finite $U_{t_0,\mu} > 0$ such that $U(\boldsymbol{\theta}(t)) \leq U_{t_0,\mu}$ and $\dot{U}(\boldsymbol{\theta}(t)) \leq 0$ for all $t \geq t_0$. By the contradiction hypothesis, $\dot{\boldsymbol{\theta}}(t)$ does not converge to $\mathbf{0}_L$, and so (by (84)) $\dot{U}(\boldsymbol{\theta}(t)) \leq 0$ does not converge to 0 along trajectory $\boldsymbol{\theta}(t)$.

Consider the quantity

$$U(\boldsymbol{\theta}(t)) = \int_{t_0}^{t} \dot{U}(\boldsymbol{\theta}(\tau)) d\tau + U(\boldsymbol{\theta}(t_0)) \tag{89}$$

87

along trajectory $\boldsymbol{\theta}(t)$. Since $U(\boldsymbol{\theta}(t_0)) \leq U_{t_0,\mu}$ and $\dot{U}(\boldsymbol{\theta}(t)) \leq 0$ does not converge to 0 along trajectory $\boldsymbol{\theta}(t)$, then there exists time $T > t_0$ such that $U(\boldsymbol{\theta}(t)) < 0 \; \forall \; t > T$. However, this contradicts the observation that $U(\boldsymbol{\theta}) \geq 0 \; \forall \; t \geq 0$. Therefore, the contradiction hypothesis is shown false, and instead $\boldsymbol{\theta}(t_0) \in \Theta_\mu \implies \dot{\boldsymbol{\theta}}(t) \to \mathbf{0}_L$.

We have shown in Lemma 4.2 that $\dot{\boldsymbol{\theta}} \to \mathbf{0}_L$ implies that $\Delta\omega_k \to \Delta\omega_{COM}$ for all $k \in \mathcal{V}$, thus proving Theorem 4.1.B. Finally, we have shown in Lemma 4.3 that $\dot{\boldsymbol{\theta}} \to \mathbf{0}_L$ implies that $P_{G,k} \to P_{F,k}$ for each bus k such that no incident line (k,m) for any $m \in \mathcal{N}(k)$ is ϵ-active at steady-state (inequality (68)), thus proving Theorem 4.1.C, and the proof is complete. $\qquad\square$

The above proof verifies that bounding of the network state trajectory within the safe region Θ_{Safe} (which follows from Lemma 4.5) is sufficient to ensure frequency synchronization and constrained power sharing of an all-active-bus, acyclic CED network (just as it was for a droop inverter-based network, see Theorem 3.5) for any bounded, constant reference and load inputs.

4.6   Simulation Results

In order to demonstrate the claims in this chapter, we will provide simulation results for an example all-active-bus, acyclic CED network showing both constained and unconstrained cases. Our example system is a six-bus, radial, inverter-based microgrid, a single-line diagram of which is shown in Figure 4.2. The six network buses, each with a voltage-source inverter, are located in two local subnetworks (subnetwork $\{1, 2, 3\}$ and subnetwork $\{4, 5, 6\}$), which are connected by a line $((3, 4))$ with a relatively low maximum power rating ($P_{Max,3,4} = 1.0$ p.u.). We will simulate the response of this network if all inverters use the all-incident-line constraint-enforcing droop control (Definition 4.1), and compare to traditional droop control (4) under three load step conditions:

1. Simulations 4.1 and 4.2: The post-step condition is such that no constraints will

be ϵ-active or violated at frequency agreement under traditional droop control (that is, $|\Delta P_{Eq,k,m}| \leq (1 - \epsilon)P_{Max,k,m}$ for all $(k, m) \in \mathcal{E}$).

2. Simulations 4.3 and 4.4: The post-step condition is such that the constraint line on line $(3, 4)$ will be violated at steady state under traditional droop, but there still exists a steady-state equilibrium $(P_{Max,3,4} < |\Delta P_{Eq,3,4}| \leq Y_{3,4}V_3V_4)$.

3. Simulations 4.5 and 4.6: The post-step condition is such that an instability exists due to the constraint on line $(3, 4)$ $(|\Delta P_{Eq,3,4}| \geq Y_{3,4}V_3V_4)$.
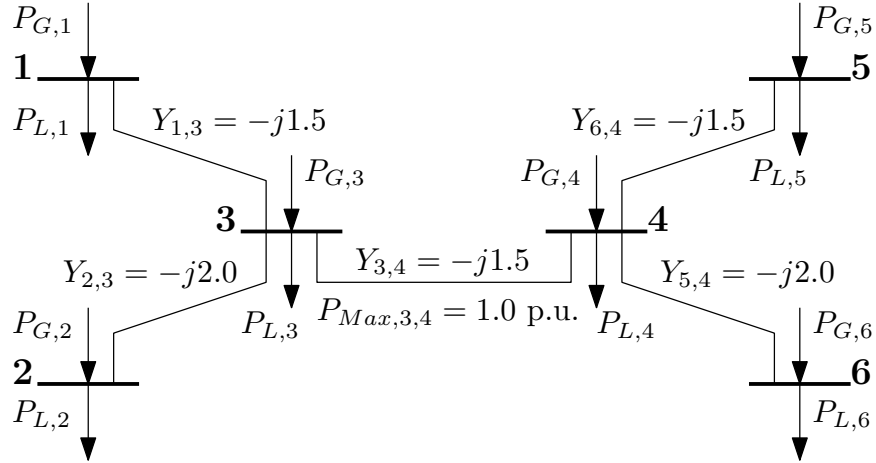
Figure 4.2: Example Six-Bus Radial Microgrid

The post-step input values of $\mathbf{P_{Ref}}$ and $\mathbf{P_L^0}$ for the example network under each of the simulation cases are listed in Table 4.1 below, along with the value of $P_{F,k}$ (the final power under traditional droop) calculated from (56) for each inverter. Table 4.2 lists the line parameters, along with the post-step frequency-agreement power imbalance value $\Delta P_{Eq,k,m}$ calculated from (57) for each line. All bus voltage magnitudes are assumed to be unity. We assign to each line $(k, m) \in \mathcal{E}$ an adaptive gain function $\gamma_{k,m}$ as in the example gain function (51), and we select $\epsilon_{k,m} = \epsilon = 0.1$ and $C_{k,m} = C = 0.1$ for each $(k, m) \in \mathcal{E}$.

Observe from Table 4.1 that for each simulation case, inverters 1, 2, 5, and 6 are are assigned a 1.0 p.u. power reference, while inverters 3 and 4 are assigned zero

reference. In addition, the final power values $P_{F,k}$ for all buses do not change between cases. The difference between the three cases is that load is shifted from bus 3 to bus 4, creating a frequency-agreement power imbalance across line $(3,4)$. This can be observed in the value of $\Delta P_{Eq,3,4}$ shown in Table 4.2, which increases from 0.75 p.u. (less than $(1-\epsilon)P_{Max,3,4}$) to 1.75 p.u. (greater than $Y_{3,4}V_3V_4$), thus creating different constraint conditions.

Table 4.1: Post-Step Bus Configuration for Six-Bus Radial Microgrid Simulation Cases

| Bus Index (k) | Simulation Cases: | | | | | | | | |
| | 4.1 and 4.2 | | | 4.3 and 4.4 | | | 4.5 and 4.6 | | |
	$\mathbf{P_{Ref}}$ (p.u.)	$\mathbf{P_L^0}$ (p.u.)	$\mathbf{P_F}$ (p.u.)	$\mathbf{P_{Ref}}$ (p.u.)	$\mathbf{P_L^0}$ (p.u.)	$\mathbf{P_F}$ (p.u.)	$\mathbf{P_{Ref}}$ (p.u.)	$\mathbf{P_L^0}$ (p.u.)	$\mathbf{P_F}$ (p.u.)
1	1.00	0.00	1.00	1.00	0.00	1.00	1.00	0.00	1.00
2	1.00	0.00	1.00	1.00	0.00	1.00	1.00	0.00	1.00
3	0.00	1.25	0.00	0.00	0.75	0.00	0.00	0.25	0.00
4	0.00	1.75	0.00	0.00	2.25	0.00	0.00	2.75	0.00
5	1.00	0.50	1.00	0.50	1.00	1.00	1.00	0.50	1.00
6	1.00	0.50	1.00	0.50	1.00	1.00	1.00	0.50	1.00

Table 4.2: Post-Step sLine Configuration for Six-Bus Radial Microgrid Simulation Cases

| i | k | m | $\mathbf{Y_{Line}}$ (p.u) | $(1-\epsilon)\mathbf{P_{Max}}$ (p.u) | $\mathbf{P_{Max}}$ (p.u) | Simulation Cases: | | |
| | | | | | | 4.1 and 4.2 | 4.3 and 4.4 | 4.5 and 4.6 |
						ΔP_{Eq} (p.u)		
1	1	3	2.00	1.35	1.50	1.00	1.00	1.00
2	2	3	2.00	1.35	1.50	1.00	1.00	1.00
3	3	4	1.50	0.9	1.00	0.75	1.25	1.75
4	5	4	2.00	1.35	1.50	0.00	0.00	1.00
5	6	4	2.00	1.35	1.50	0.00	0.00	1.00

4.6.1 Six-Bus Radial Network with No ϵ-Active Constraints

Simulations 4.1 and 4.2 consider the response of the example six-bus radial microgrid to a load step at bus 4 when all inverters operate the traditional frequency-droop control law (4) or the all-incident-line CED control law (Definition 4.1) respectively.

The conditions are such that under traditional droop control, no constraints are ϵ-active or violated (see Table 4.2), since $|\Delta P_{Eq,k,m}| \leq (1 - \epsilon)P_{Max,k,m}$ for all lines $(k, m) \in \mathcal{E}$. Figures 4.3 and 4.4 show the response of the network bus frequencies $\boldsymbol{\Delta\omega}(t)$, inverter output power values $\mathbf{P_G}(t)$, line power flows $\mathbf{P_{Line}}(t)$, and (in Figure 4.4) line adaptive gain values $\boldsymbol{\gamma}(t)$ to the step at $t = 0$ for Simulation 4.1 (Droop) and 4.2 (CED) respectively.

Observe in Figure 4.3 that under traditional droop, since no constraints are violated, then after the step the bus frequency values all converge to the center-of-mass frequency $\Delta\omega_{COM} = 0$, the power flow values $P_{Line,k,m}$ converge to their respective frequency-agreement power imbalance values $\Delta P_{Eq,k,m}$, and the inverter output power values $P_{G,k}$ converge to their respective final power values $P_{F,k}$. In addition, since $\Delta P_{Eq,3,4} \leq P_{Max,3,4}$, then the constraint on line $(3, 4)$ is neither ϵ-active or violated. This is the expected behavior of a traditional droop inverter-based network (from Theorem 3.5) for an unconstrained network.

From Theorem 4.1, since $|\Delta P_{Eq,k,m}| \leq (1 - \epsilon)P_{Max,k,m}$ for all lines $(k, m) \in \mathcal{E}$, then we expect the all-active-bus, radial CED network considered in Simulation 4.2 to have nearly identical behavior to that of the equivalent droop network. Indeed, Figure 4.4 shows that since no line becomes ϵ-active, then the line adaptive gain values $\gamma_{k,m}(t)$ for all lines $(k, m) \in \mathcal{E}$ equal unity for all $t \geq 0$, and therefore the all-active-bus CED network in Simulation 4.2 has nearly identical response to that of the equivalent droop network considered in Simulation 4.1. In particular, its bus frequencies also converge to the center-of-mass frequency (Theorem 4.1.B) and *all* of the inverters converge to their respective final power values $P_{F,k}$ (Theorem 4.1.C).

Therefore, Simulations 4.1 and 4.2 confirm that when no constraints are active, an all-active-bus, radial CED network has nearly identical behavior to that of a traditional droop inverter-based network, in particular that it provides the same frequency synchronization and power sharing behavior.
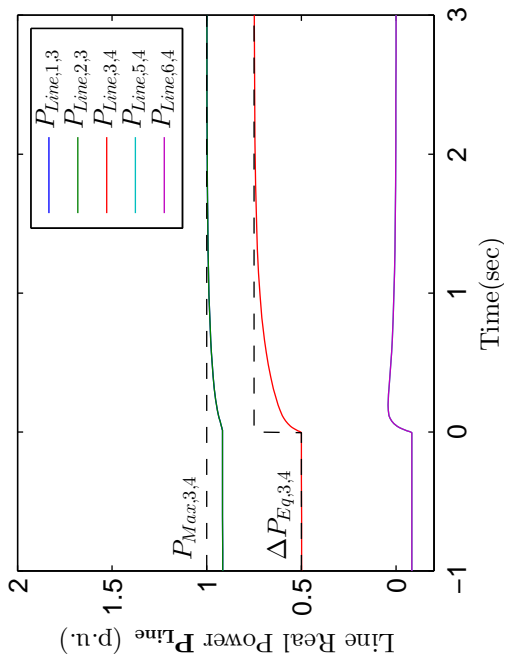
(a) Bus Frequency Error $\Delta\omega$
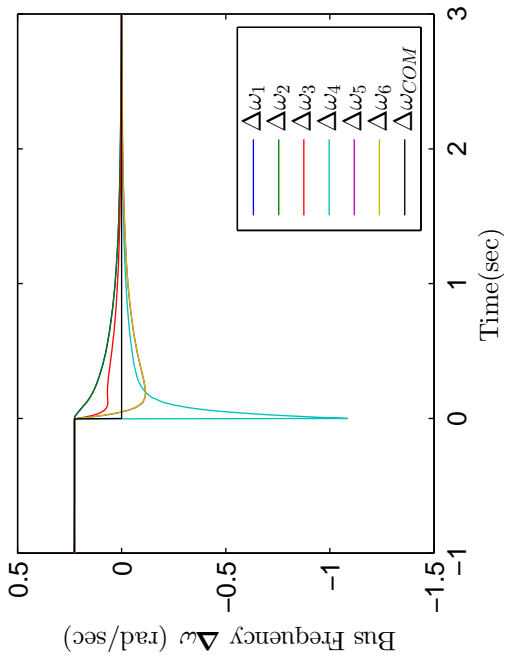
(b) Line Power Flows $\mathbf{P_{Line}}$
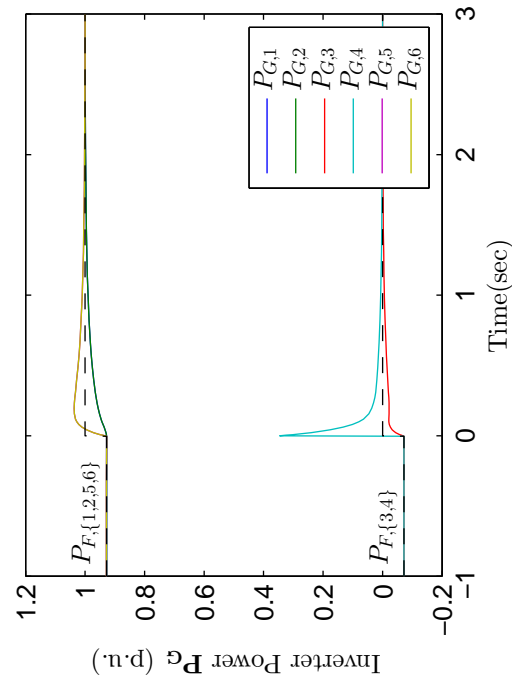
(c) Inverter Generated Power $\mathbf{P_G}$

Figure 4.3: Simulation 4.1: Six-Bus Radial Microgrid with no ϵ-active constraints: Droop
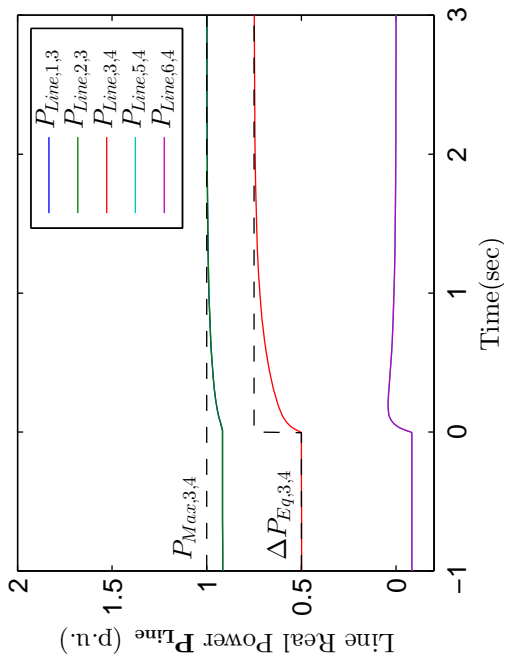
(a) Bus Frequency Error $\boldsymbol{\Delta\omega}$
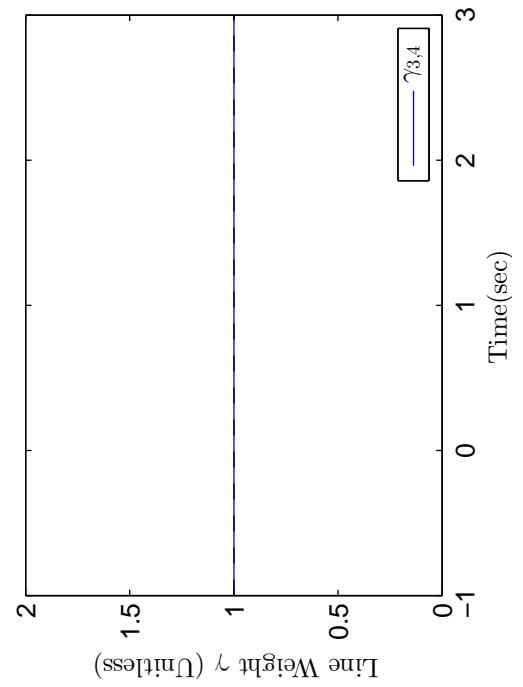
(b) Line Power Flows $\mathbf{P_{Line}}$
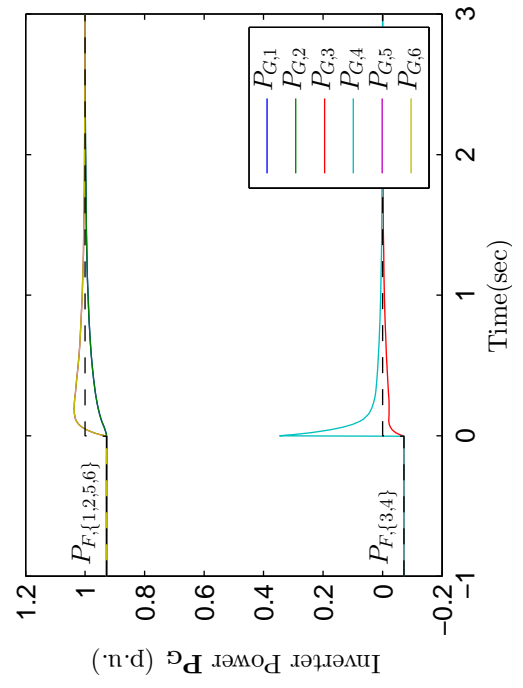
(c) Inverter Generated Power $\mathbf{P_G}$

(d) Line Weight $\boldsymbol{\gamma}$

Figure 4.4: Simulation 4.2: Six-Bus Radial Microgrid with no ϵ-active constraints: All-Incident-Line CED

4.6.2 Six-Bus Radial Network with Single ϵ-Active Constraint

Simulations 4.3 and 4.4 consider the same network, but under a different set of condi-
tions. Some of the post-step load at bus 3 is shifted to bus 4 (see Table 4.1), thereby
increasing the frequency-agreement power imbalance across line $(3,4)$ (see Table 4.1).
In this case, the post-step value of $|\Delta P_{Eq,3,4}|$ is greater than $P_{Max,3,4}$, and therefore
we would expect the line power flow constraints across line $(3,4)$ to be violated un-
der traditional droop at steady state. However, $|\Delta P_{Eq,3,4}|$ is less than $Y_{3,4}V_3V_4$, and
therefore Theorem 3.1, does *not* hold for this network, meaning that there still ex-
ists a frequency agreement equilibrium under traditional droop control (recall that
Theorem 3.1 is a necessary and sufficient condition for ayclic networks).

Figure 4.5 shows the response of the example network under traditional droop
control to the load step. Notice that under traditional droop, the bus frequencies still
converge to the center-of-mass frequency $\Delta \omega_{COM} = 0$, and each inverter converges to
its final power value $P_{F,k}$. However, since the frequency-agreement power imbalance
$|\Delta P_{Eq,3,4}|$ for line $(3,4)$ is greater than $P_{Max,3,4}$, then the constraint is violated under
traditional droop.

Figure 4.6 shows the response of the same network to the same step if each inverter
instead operates the all-incident-line CED control law. Notice that int his case, the
CED network response differs from the traditional droop network response. Inverters
3 and 4 respond to the approach of $|P_{Line,3,4}|$ to its constraint $P_{Max,3,4}$ by increas-
ing the value of the adaptive gain $\gamma_{3,4}$ above unity, thereby increasing its tension,
"pulling" the network back into the safe region, and enforcing the line power flow
constraint $|P_{Line,3,4}| \leq P_{Max,3,4}$. The bus frequencies still converge to the center-of-
mass frequency, which has the same value $(\Delta \omega_{COM} = 0)$ as under traditional droop.
Therefore, the network stabilizes to a different equilibrium than under traditional
droop: inverters 3 and 4 (which are incident to the active constraint) provide compli-
mentary power injections to enforce the constraint, while the other inverters (which

do not have any measurements indicating that a constraint is active) converge to their respective final power values.

Therefore, Simulations 4.3 and 4.4 demonstrate the following:

1. An all-active-bus, acyclic CED network is capable of enforcing line power flow constraints and thereby bounding the network within the safe region (Theorem 4.1.A).

2. An all-active-bus, acyclic CED network maintains the static center-of-mass frequency and frequency synchronization properties of a traditional droop inverter-based network (Theorem 4.1.B).

3. Each inverter k in an all-active-bus, acyclic CED network will converge to the same final power value $P_{F,k}$ as under traditional droop *if and only if it is not incident to an active constraint* (Theorem 4.1.C). When a constraint is active, the inverters incident to the active constraint provide complimentary power injections to enforce it.

4.6.3 Six-Bus Radial Microgrid with Instability

Finally, Simulations 4.5 and 4.6 consider the same six-bus radial microgrid under conditions such that no frequency agreement equilibrium exists under traditional droop control. Even more post-step load is moved from bus 3 to bus 4 (see Table 4.1), increasing the frequency-agreement power imbalance on line $(3, 4)$ to a value greater than $Y_{3,4}V_3V_4$ (see Table 4.2). Therefore, Theorem 3.1 holds for the cut consisting of line $(3, 4)$, and so there does not exist a post-step frequency-agreement equilibrium for this condition under traditional frequency droop, and therefore we should expect the subnetworks defined by the cut across line $(3, 4)$ to lost synchronization.

Figure 4.7 shows the response of the network to this step under traditional frequency-droop control. Observe that after the step, $P_{Line,3,4}$ exceeds its bound $P_{Max,3,4}$, and
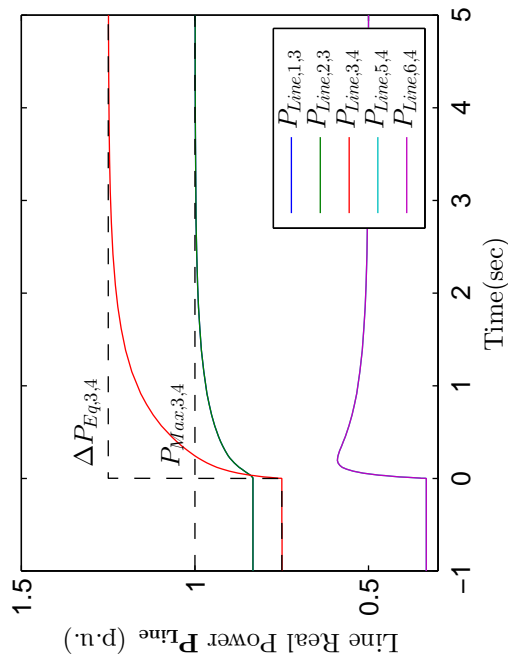
(a) Bus Frequency Error $\boldsymbol{\Delta\omega}$
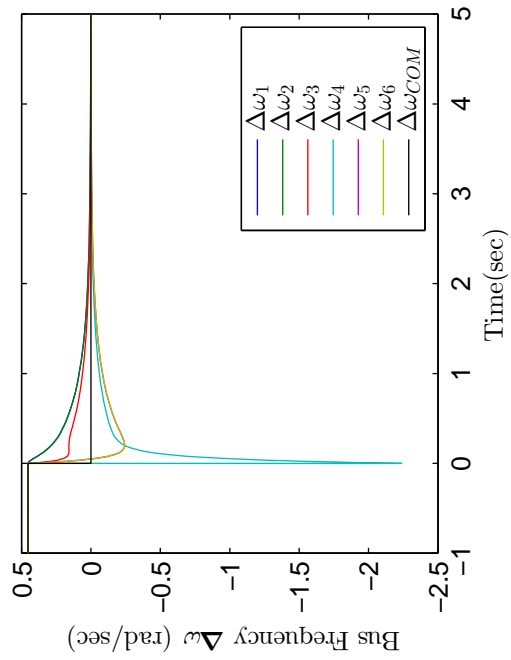
(b) Line Power Flows $\mathbf{P_{Line}}$
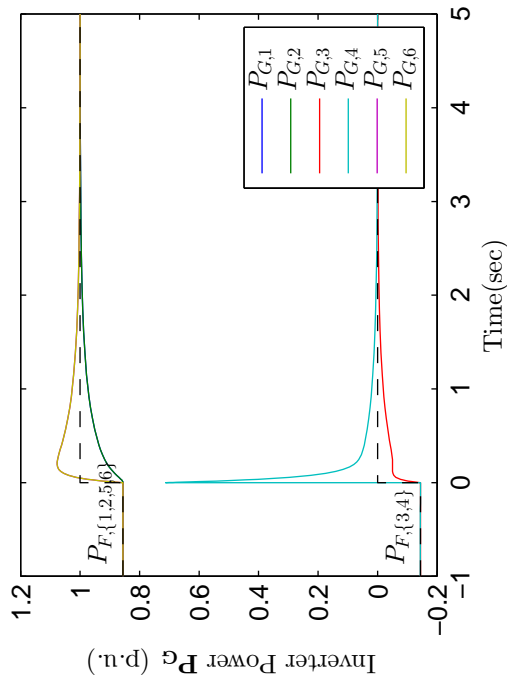
(c) Inverter Generated Power $\mathbf{P_G}$

Figure 4.5: Simulation 4.3: Six-Bus Radial Microgrid with single ϵ-active constraints: Droop
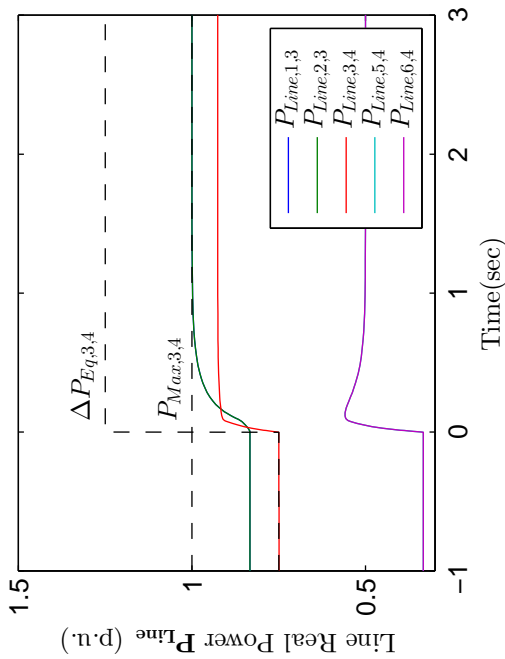
(a) Bus Frequency Error $\Delta\omega$
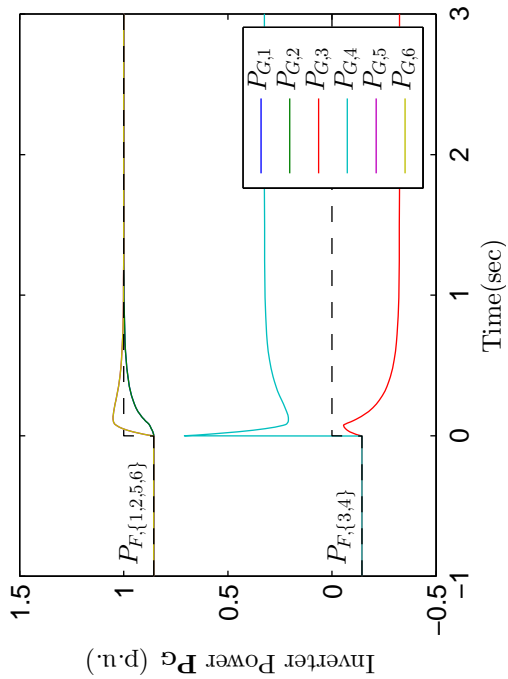
(b) Line Power Flows $\mathbf{P_{Line}}$

(c) Inverter Generated Power $\mathbf{P_G}$
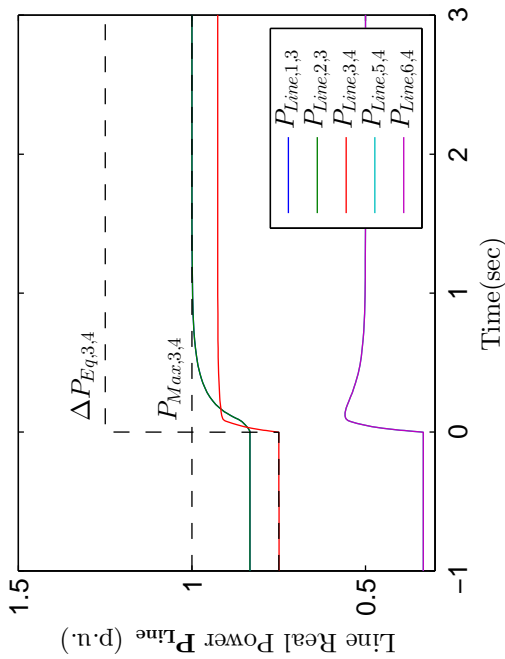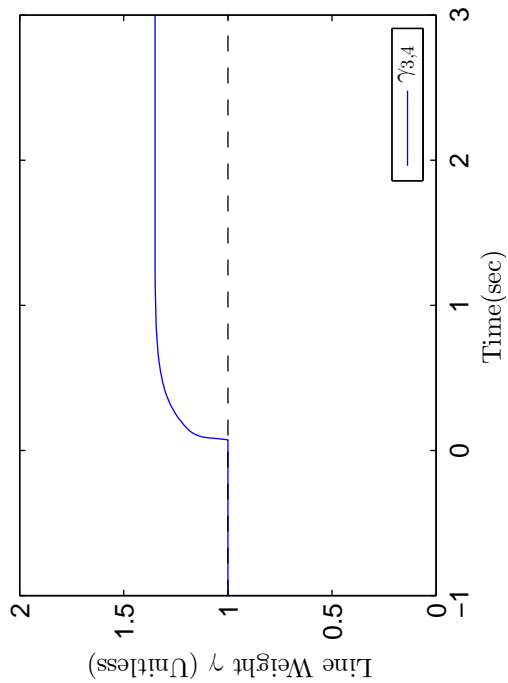
(d) Line Weight $\boldsymbol{\gamma}$

Figure 4.6: Simulation 4.4: Six-Bus Radial Microgrid with single ϵ-active constraints: All-Incident-Line CED

is also unable to reach its frequency-agreement power imbalance value $\Delta P_{Eq,3,4}$. This is because $|\Delta P_{Eq,3,4}|$ is greater than the peak power transfer $Y_{k,m}V_kV_m$ on line $(3,4)$. As a result, the inverters in subnetwork $\{1,2,3\}$ are unable to reach synchronization with the inverters of subnetwork $\{4,5,6\}$, resulting in a continuous oscillation of frequencies, line power flows, and inverter output powers. While no network protection is modeled in Simulation 4.7, in practice such a condition would almost certainly result in the operation of circuit breakers to prevent equipment damage or unsafe conditions.

However, the response of the same network to this step when each inverter implements the all-incident-line CED control law (Figure 4.8) is very different. After the step is applied, inverters 3 and 4 detect the approach of $|P_{Line,3,4}|$ to its bound $P_{Max,3,4}$ and increase the value of the adaptive gain $\gamma_{3,4}$ to enforce the constraint. As a result, the network trajectory is again pulled back into the safe region, enforcing the constraint. In addition, the bus frequencies now converge to the center-of-mass freqency (again the same as under traditional droop), and all inverters not incident to the constrained line converge to their respective final power values $P_{F,k}$. Inverter 3 and 4 again provide complimentary power injections to enforce the constraint, and as a result do not converge to their final power values.

Therefore, Simulations 4.5 and 4.6 demonstrate the following:

1. An all-incident-line, acyclic CED network enforces all line power flow constraints (Theorem 4.1.A).

2. The network frequencies in an all-incident-line, acyclic CED network synchronize to the center-of-mass frequency *even when no frequency agreement equilibrium exists under traditional droop* (Theorem 4.1.B).

3. In an all-incident-line acyclic CED network, all inverters not incident to active constraints converge to the final power value *even under conditions in which*
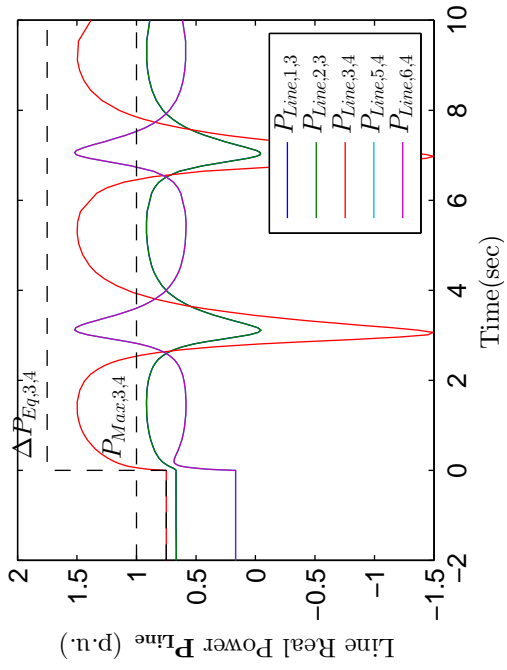
98

(a) Bus Frequency Error $\mathbf{\Delta\omega}$
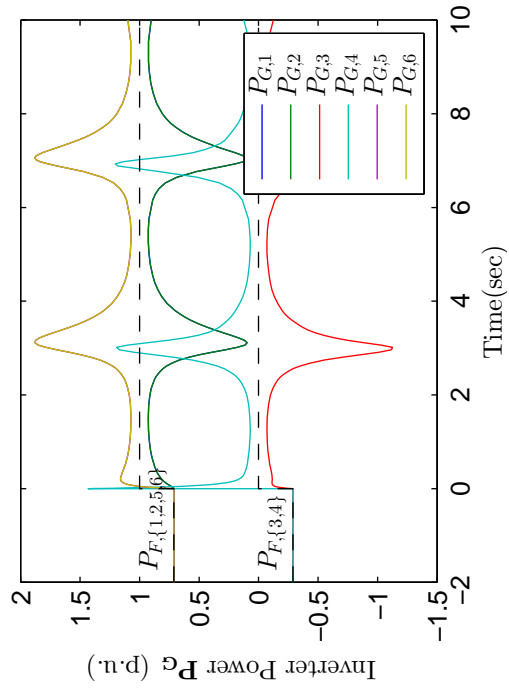
(b) Line Power Flows $\mathbf{P_{Line}}$
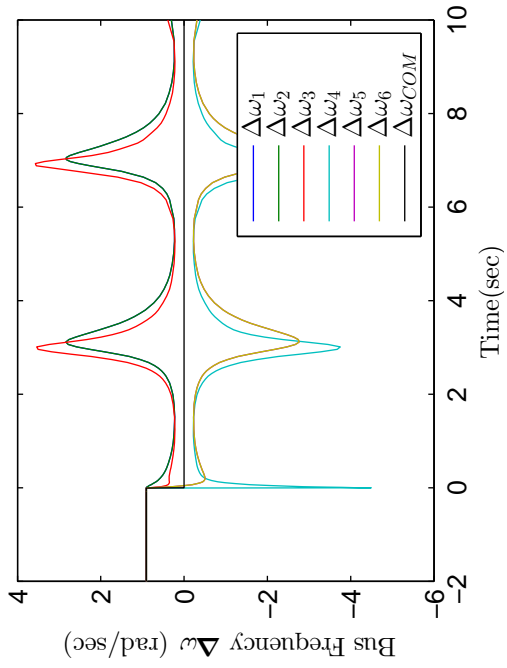
(c) Inverter Generated Power $\mathbf{P_G}$

Figure 4.7: Simulation 4.5: Six-Bus Radial Microgrid with single ϵ-active constraints: Droop
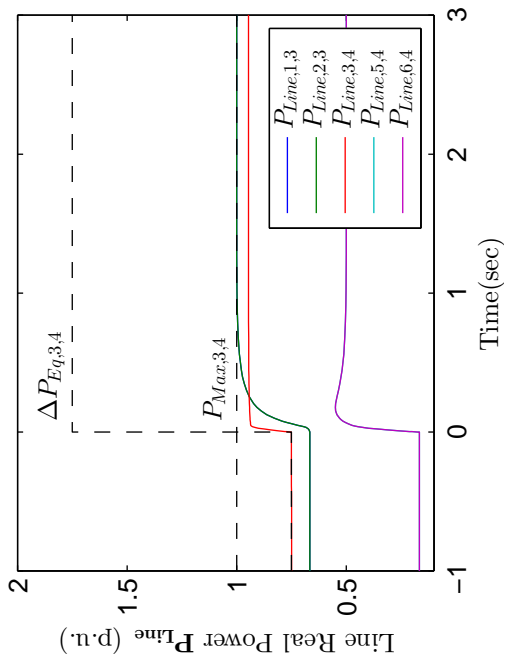
(a) Bus Frequency Error $\Delta\omega$
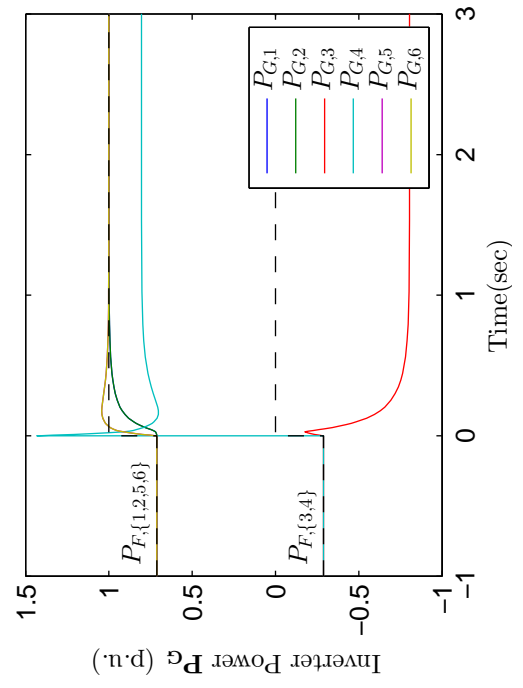
(b) Line Power Flows $\mathbf{P_{Line}}$

(c) Inverter Generated Power $\mathbf{P_G}$
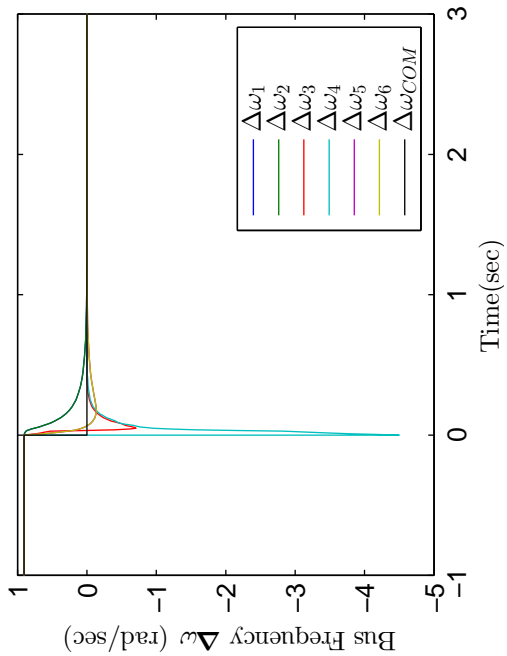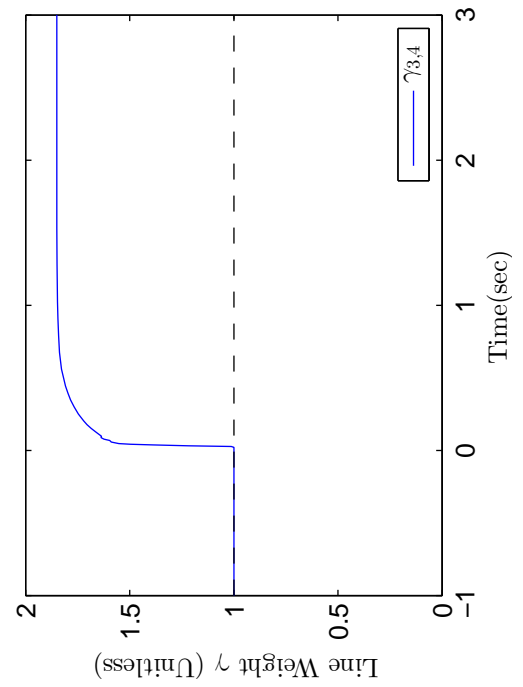
(d) Line Weight γ

Figure 4.8: Simulation 4.6: Six-Bus Radial Microgrid with Instability: All-Incident-Line CED

traditional droop fails to provide this behavior. Inverters incident to active constraints must inject power to enforce the constraint, and so do not converge to the final power value (Theorem 4.1.C).

4.6.4   Discussion on Simulation Results

The above simulation cases demonstrate both the capabilities of all-incident-line CED control and its limitations. When applied at each bus in an acyclic network, the all-incident-line CED control law is capable of enforcing all of the network line flow constraints, and in addition provides a signal (the line weights $\gamma_{k,m}$) that indicate which constraints are active. It maintains the frequency synchronization and static center-of-mass frequency properties of traditional frequency droop, and in fact when no constraints are active behaves identically to traditional droop. Most significantly, it is capable of providing robust frequency synchronization and constrained power sharing for all bounded, constant reference and load conditions (in the absence of generation constraints), including conditions in which traditional droop fails to provides these capabilities.

However, in order to enforce the line flow constraints, it is necessary that some inverters adjust their output such that they do not converge to the final power value $P_{F,k}$, and so the goal of achieving power sharing between the inverters is partially sacrificed in order to enforce the constraints. In addition, only the inverters directly incident to active constraints participate in their enforcement. This is due to the lack of communication in the network: the active constraint was recognized by the inverters incident to it, but that information is not passed to any other inverters in the network. Finally, the inverters adjacent to a constraint must have available capacity to source or sink sufficient power to enforce the constraint.

4.7   Chapter Conclusions

In recognition of the need to enforce line power flow constraints to ensure synchronization of an inverter-based network, we have proposed the All-Incident-Line Constraint-Enforcing Droop (CED) control law, a modified form of frequency-droop control that integrates specified line power flow constraints for each line in the network. We have proven that an acyclic network in which each bus has an inverter implementing the all-incident-line CED control law is capable of enforcing all the specified network line power flow constraints and guaranteeing synchronization for any network forcing inputs (in the absence of actuation constraints) and any initial condition in the interior of the safe region. Such synchronization ensures the convergence of inverter output power to the same value as under traditional frequency droop (subject to constraints). As a result, the CED controller provides significantly improved robustness of synchronization as compared to existing control methods and is also capable of contributing to network security by enforcement of constraints.

However, the proposed control method has several limitations. First, it requires additional measurements beyond those necessary for traditional droop, increasing cost. Second, when a constraint is active, the incident inverters must inject power to enforce the constraint, and the other network inverters do not contribute to this power injection, requiring the incident inverters to have sufficient available capacity. It requires the application of an unbounded gain to line power measurements. While we have shown that (in theory) the gains will never increase beyond a bounded maximum, in practice such large gains may interact with unmodeled control delays to cause oscillations or instability.

The most significant limitation of this chapter's results, however, are its very limited range of applicability. While it is possible to construct a network in which each bus has attached an inverter operating the proposed control law, in practice very few power networks are of this type. Most inverter-based networks contain a mix of active

(inverter) and passive (network) buses. In addition, it is desirable that some inverters may enforce contraints, while other simply implement traditional droop or constant-power controls. Therefore, in order for it to be applicable in practice, we must generalize the class of network that we consider for application of constraint-enforcement while maintaining the goals of robust frequency synchronization and power sharing within the expected network operating range. In the following chapters, we propose methods to achieve these goals with only sparse application of constraint-enforcing inverters to a network, thereby significantly increasing our methods applicability.

CHAPTER V

A TOOL FOR REDUCED-ORDER ENFORCEMENT OF LINE POWER-FLOW CONSTRAINTS IN AC NETWORKS

In the previous chapter, a novel frequency-droop controller was introduced, and a method shown for its application to ensure robust frequency synchronization and power sharing in an all-active-bus, acyclic inverter-based power network for all bounded, constant reference and load inputs. This control method is based on the observation (from Chapter 3) that synchronization of an inverter-based network operating frequency-droop control can be ensured by enforcement of a specified line power-flow constraint on each line in the system. However, while it is possible to construct a network of the type discussed in Chapter 4, in most cases it is not feasible to place an inverter at each bus in a network, and therefore the method in the preceeding chapter is not directly applicable to most power networks in practice. In this chapter, we develop the concept of *constraint-satisficing key line sets*, which will allow the replacement of the set of line flow constraints in Theorem 3.5 with a reduced-order set of constraints on only a few key lines in the network. We develop this concept, explain its significance, develop a sufficient (but not necessary) condition test for constraint-satisficing key line sets for a given AC network and expected operating range, and finally develop a search algorithm to find constraint-satisficing key line sets. In the final technical chapter, we will show that this concept can be used to allow enforcement of the synchronization and power-sharing conditions using only a few constraint-enforcing inverters, thereby allowing application of to a much broader class of AC networks.

5.1 Reduced-Order Power-Flow Constraint-Enforcement

In the preceeding chapters, we dealt with frequency synchronization in AC networks and showed that it can be modeled as a forced, non-linear network consensus problem. In Theorem 3.4, we showed that there exists a safe region of the voltage-angle state space such that bounding of the network state trajectory within that safe region guarantees frequency synchronization, from which followed simple power sharing (Lemma 3.2). We observed in Chapter 4 that the problem of bounding the voltage-angle state trajectory of an AC network in the safe region is strongly analagous to that of enforcement of distance constaints in a mobile multi-robot system (as in [53]), and our method of such enforcement in an all-active-bus network is inspired by that observation.

However, the method presented in Chapter 4 is very limited because it requires explicit enforcement of a line power-flow constraint (which we showed in Lemma 3.4 is equivalent to enforcement of a line voltage-angle constraint) on *every* line in the power network. This required placement of an inverter operating the proposed constraint-enforcing control law at *every* bus in the network, which is not feasible in practice. Therefore, in order to make our method of enforcement practical for deployment in real AC networks, we must reduce this requirement so that robust frequency synchronization and power sharing can be achieved by enforcement of line power-flow constraints on a only a subset of the network lines (rather than all of them).

In this chapter, we develop the concept of *constraint-satisficing key line sets*, which are subsets of the lines in a power network such that enforcement of the line power-flow constraints associated with only those lines (along with network operation within a specified expected operating range) is sufficient to ensure that *all* of the line power flow constraints are satisfied. The word "satisficing" is a portmanteau of "sufficient" and "satisfying" [65]. In this dissertation, it indicates that satisfaction of a smaller

set of constraints (the line power flow constraints associated with only the lines in the key line set, plus those defining the expected operating range) is sufficient to satisfy a larger set of constraints (the line power flow constraints on *all* lines in the network and the expected operating range constraints). Therefore, if a constraint-satisficing key line set of acceptable size is found for a given network and expected operating range, then it is not necessary to enforce the line power-flow constraint on every line in the network (as in Chapter 4), only on the lines in the satisficing key line set.

Section 5.2 below explicitly defines the concepts of expected operating range and constraint-satisficing key line sets for a given AC power network. Section 5.3 develops a sufficient condition test to determine whether a given candidate key line set is constraint-satisficing for a given AC network and expected operating range. Section 5.4 then develops a search algorithm for generation of constraint-satisficing key line sets for a given AC network and expected operating range. In Section 5.5, we present example applications of the test and search methods to several selected networks. Finally, in Section 5.6 we discuss the applications, capabilities, and limitations of the methods proposed in this chapter.

5.2   Expected Operating Range and Constraint-Satisficing Key Line Sets

Line power flows in an AC network are related to each other and to the generation and load power values by Kirchoff's Law applied to each bus in the network. Therefore, bounds on the generation and load, combined with bounds on some line power flows, imply bounds on the remaining line power flows. Assume that we select a subset of the lines $\mathcal{E}_{Key} \subset \mathcal{E}$, where the lines in $\mathcal{E}_{Key}$ are the "key" lines whose constraints will be explicitly enforced. Because the power-flow structure graph $\mathfrak{G} = (\mathcal{V}, \mathcal{E})$ specifies the structure of the power flows, by combining $\mathfrak{G}$ with a specification of possible values of generation and load (defining the expected operating range), it is possible to determine if enforcement of line power-flow cosntraints on lines in $\mathcal{E}_{Key}$ is sufficient

to ensure that all line power-flow constraints are met. If so, then enforement of the line power-flow constrants on only the lines in $\mathcal{E}_{Key}$ is sufficient to ensure satisfaction of the line power-flow constraints for *all* lines in the network for the entire expected operating range. In this section, we will formally define the expected operating range for an AC network, as well as the concept of constraint-satisficing key line sets.

5.2.1 Expected Operating Range of an AC Network

In Chapter 1, we stated the goal of this work as a framework for guaranteeing frequency synchronization and power sharing for an inverter-based AC network under *all expected operating conditions.* In order to define the concept of constraint-satisficing key line sets, we must first more clearly define "all expected operating conditions".

The purpose of an AC network is to deliver power from generation to load, and so for practical purposes the values and locations of generation and load define its operating point. Because of limitations of its physical capacity, an AC network has finite range of generation and load that it can support at each bus in the network. For generators, this limit is generally due to the minimum and maximum capacity of the generation hardware and power source. For loads, it is generally due to the maximum value of power that can be delivered to a given bus in the network. In practice, there are often time-dependent constraints as well (such as due to generation ramp rates), but in this dissertation we assume static bounds for generation and load at each bus. More formally, we define expected operating range of a network as follows:

Definition 5.1 (Expected Operating Range)**.** *Consider an AC power network whose power-flow structure is represented by the graph $\mathfrak{G} = (\mathcal{V}, \mathcal{E})$ where $\mathbf{P_G} = \begin{bmatrix} P_{G,1} & \dots & P_{G,N} \end{bmatrix}^T$ and $\mathbf{P_L} = \begin{bmatrix} P_{L,1} & \dots & P_{L,N} \end{bmatrix}^T$, where $P_{G,k}$ represents the generation and $P_{L,k}$ represents the load at bus $k \in \mathcal{V}$. The* expected operating range $\mathbb{P} \subset \mathbb{R}^N \times \mathbb{R}^N$ *of the AC network is defined by the constant vectors $\mathbf{P_{G,Max}} = \begin{bmatrix} P_{G,Max,1} & \dots P_{G,Max,N} \end{bmatrix}^T$,*

$$\mathbf{P_{G,Min}} = \begin{bmatrix} P_{G,Min,1} & \ldots P_{G,Min,N} \end{bmatrix}^T, \text{ and } \mathbf{P_{L,Max}} = \begin{bmatrix} P_{L,Max,1} & \ldots P_{L,Max,N} \end{bmatrix}^T \in \mathbb{R}^N$$

where $(\mathbf{P_G}, \mathbf{P_L}) \in \mathbb{P}$ if and only if

$$P_{G,k} \leq P_{G,Max,k} \; \forall \, k \in \mathcal{V} \tag{90}$$

$$P_{G,k} \geq P_{G,Min,k} \; \forall \, k \in \mathcal{V} \tag{91}$$

$$P_{L,k} \leq P_{L,Max,k} \; \forall \, k \in \mathcal{V} \tag{92}$$

$$P_{L,k} \geq 0 \; \forall \, k \in \mathcal{V} \tag{93}$$

The expected operating range as in Definition 5.1 defines a static range of values for the network inputs (generation $P_{G,k}$ and load $P_{L,k}$ at each bus in the network). This approach to definition of expected operating range is very general, and can encompass network buses, droop inverter buses interfacing generation or energy storage, and even constant-power inverter buses as follows:

- A network bus is characterized by $P_{G,k} = 0$. This can be represented by selecting $P_{G,Min,k} = P_{G,Max,k} = 0$.

- A droop inverter bus is characterized by its rated ("nameplate") power value $P_{Rated} > 0$, which can be represented by selecting $P_{G,Max,k} = P_{Rated}$ and $P_{G,Min,k} = -P_{Rated}$. In addition, if the inverter's power source has a minimum sustainable power, then this can assigned to $P_{G,Min,k}$ (e.g. $P_{G,Min,k} = 0$ if the source is not capable of sinking power).

- A constant-power inverter is characterized by an assigned generation value P_{Const}, which can be represented by selecting $P_{G,Min,k} = P_{G,Max,k} = P_{Const}$.

5.2.2 Constraint-Satisficing Key Line Sets

The expected operating range of an AC network defines a set of constraints on its bus generation and load values. Combined with the line power-flow constraints, they

define an expected range of all of the power-flow values in the network. Because the generation, load, and line power-flow values are all related by Kirchoff's laws, their constraints are similarly related, and combinations of constraints on some quantities imply constraints on others. Therefore, many of the constraints may be rendered unnecessary by others. Therefore, it is possible to select a subset of the constraints such that the satisfaction of the subset is sufficient to ensure satisfaction of the original (larger) constraint set.

In this chapter, we are concerned with reducing the size of the line power-flow constraint set that must be enforced to ensure synchronization and power sharing. Therefore, we will develop methods that allow some of the line power-flow constraints to be eliminated, resulting in a smaller set of line constraints that must be enforced. The set of lines associated with this reduced set of line power-flow constraints is called a *constraint-satisficing key line set*, since the enforcement of the line power-flow constraints associated with only the key lines (along with network generation and loads within the expected operating range) is sufficient to ensure satisfaction of the line power-flow constraints on *all* lines in the network. More formally, we define constraint-satisficing key line sets for a AC network and a given expected operating range as follows:

Definition 5.2 (Constraint-Satisficing Key Line Sets). *Consider an AC power network whose power-flow structure is represented by the graph $\mathfrak{G} = (\mathcal{V}, \mathcal{E})$. Assume that there exist generation and load bounding vectors $\mathbf{P_{G,Max}}$, $\mathbf{P_{G,Min}}$, and $\mathbf{P_{L,Max}} \in \mathbb{R}^N$ defining expected operating range $\mathbb{P}$ as in Definition 5.1. Assume that each line $(k,m) \in \mathcal{E}$ is assigned a maximum line power-flow constant $P_{Max,k,m} > 0$.*

Consider the line subset $\mathcal{E}_{Key} \subset \mathcal{E}$. Then:

5.2.A The line set $\mathcal{E}_{Key}$ is a Constraint-Satisficing Key Line Set *for the triple $(\mathfrak{G}, \mathbb{P}, \mathbf{P_{Max}})$ if and only if $|P_{Line,k,m}| \leq P_{Max,k,m} \; \forall \, (k,m) \in \mathcal{E}_{Key}$ implies that $|P_{Line,k,m}| \leq P_{Max,k,m} \; \forall \, (k,m) \in \mathcal{E}$ for all $(\mathbf{P_G}, \mathbf{P_L}) \in \mathbb{P}$.*

5.2.B The line set $\mathcal{E}_{Key}$ is an Irreducable Constraint-Satisficing Key Line Set *for the triple* $(\mathfrak{G}, \mathbb{P}, \mathbf{P_{Max}})$ *if it is constraint-satisficing and there do not exist any constraint-satisficing subsets of $\mathcal{E}_{Key}$.*

5.2.C The line set $\mathcal{E}_{Key}$ is a Minimal Constraint-Satisficing Key Line Set *for the triple* $(\mathfrak{G}, \mathbb{P}, \mathbf{P_{Max}})$ *if it is constraint-satisficing and there do not exist any constraint-satisficing subsets of $\mathcal{E}$ with fewer lines than $\mathcal{E}_{Key}$.*

The definition of constraint-satisficing key line sets provided by Definition 5.2 is dependent on the network structure graph $\mathfrak{G}$, a set of line power-flow bounds $\mathbf{P_{Max}}$, and a selection of expected operating range $\mathbb{P}$ (as per Definition 5.1). If a given key line set $\mathcal{E}_{Key}$ is constraint-satisficing, then satisfaction of its line power-flow constraints $(|P_{Line,k,m}| \leq P_{Max,k,m} \ \forall \ (k,m) \in \mathcal{E}_{Key})$ while the network operates in the expected operating range $((\mathbf{P_G}, \mathbf{P_L}) \in \mathbb{P})$ is sufficient to ensure that *all* of the line power-flow constraints are satisfied $(|P_{Line,k,m}| \leq P_{Max,k,m} \ \forall \ (k,m) \in \mathcal{E})$. Therefore, when the network operates on the expected range, then enforcement of the line power-flow constraints associated with *only the key lines* is sufficient to ensure that the condition of Theorem 3.5 holds, and therefore network frequency synchronization and power sharing are guaranteed. This principal will form the basis of our control method for sparse deployment of CED inverters in the next chapter.

5.3 A Sufficient Condition Test for Constraint-Satisficing Key Line Sets

In this section, we will show (based on the network power-flow equations for a given network) that bounds on the generation and load power values in a network (from the expected operating range $\mathbb{P}$), combined with assumption that line power-flow constraints on key lines are satisfied, implies bounds on the line power-flow values of remaining lines in the network. If the bounds on all non-key lines $((k,m) \in (\mathcal{E} \backslash \mathcal{E}_{Key}))$ meet the constraints (are within $\pm P_{Max,k,m}$), then Definition 5.2 holds and $\mathcal{E}_{Key}$ is a

constraint-satisficing key line set.

5.3.1   Setup for Line Power-Flow Bounds

In this section, we will assume a given line set $\mathcal{E}_{Key} \subset \mathcal{E}$ such that the line power-flow constraint $|P_{Line,k,m}| \leq P_{Max,k,m}$ is satisfied for each $(k,m) \in \mathcal{E}_{Key}$. Combined with the generation and load bounds in Definition 5.1 for a given expected operating range $\mathbb{P}$, our goal is to calculate constant bounds $P_{UBound,k,m} \geq 0$ and $P_{LBound,k,m} \leq 0$ for all $(k,m) \in \mathcal{E} \setminus \mathcal{E}_{Key}$ such that $P_{LBound,k,m} \leq P_{Line,k,m} \leq P_{UBound,k,m}$.

Notice that since $P_{Line,k,m} = -P_{Line,m,k}$, then $P_{UBound,k,m} = -P_{LBound,m,k}$ and $P_{LBound,k,m} = -P_{UBound,m,k}$. In the interests of simplicity of notation, we will use each of these pairs interchangeably throughout the following section.

If $(k,m) \in \mathcal{E}_{Key}$, then by assumption the line power-flow constraint $|P_{Line,k,m}| \leq P_{Max,k,m}$ is satisfied. Therefore, the following bounds are valid for $P_{Line,k,m}$ for all $(k,m) \in \mathcal{E}_{Key}$:

$$P_{Line,k,m} \leq P_{Max,k,m} = P_{UBound,k,m} \tag{94}$$

$$P_{Line,k,m} \geq -P_{Max,k,m} = P_{LBound,k,m} \tag{95}$$

In order to generate similar bounds for non-key lines, we must turn to the physical laws governing power flows in an AC network. Line power flows in an AC power network are governed by the well-known power-flow equations, which are derived from Kirchoff's law. In power form, Kirchoff's law states that the power flows out of a bus sum to zero. Consider the arbitrary line $(k,m) \in \mathcal{E}$ in a power network as illustrated in Figure 5.1. Remember that since (by assumption) the network is lossless, then $P_{Line,k,m} = -P_{Line,m,k}$.

Kirchoff's law applied to buses k and m produces the following:

$$P_{G,k} = P_{L,k} + \sum_{l \in \mathcal{N}(k)} P_{Line,k,l} \tag{96}$$

$$P_{G,m} = P_{L,m} + \sum_{p \in \mathcal{N}(m)} P_{Line,m,p} \tag{97}$$
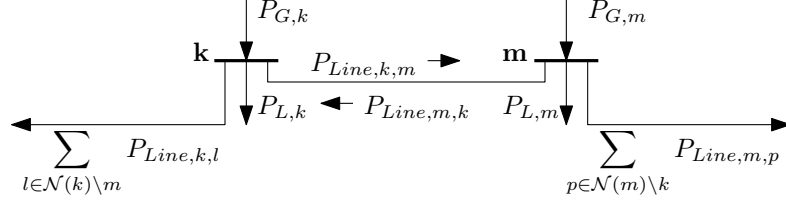
Figure 5.1: Line power flow on an arbitrary line (k, m)

Solving (96) and (97) for $P_{Line,k,m}$:

$$P_{Line,k,m} = P_{G,k} - P_{L,k} - \sum_{l \in \mathcal{N}(k) \setminus m} P_{Line,k,l} \tag{98}$$

$$P_{Line,k,m} = -P_{G,m} + P_{L,m} + \sum_{p \in \mathcal{N}(m) \setminus k} P_{Line,m,p} \tag{99}$$

Kirchoff's law in the form of (98) and (99) express line power flow $P_{Line,k,m}$ in terms of the generation and load at each of buses k and m, as well as the line power flows on all other lines incident to k and m.

Our goal is to bound the line power flow $P_{Line,k,m}$ both from above and below on the expected operating region. An upper bound can be placed on $P_{Line,k,m}$ by either the maximum power available to be sourced by bus k, or the maximum power available to be sunk by bus m. Since both methods are valid, we will calculate both bounds (the sourcing bound and the sinking bound), and select the stricter of the two. Similarly, a lowerbound can be placed on $P_{Line,k,m}$ (equivalent to an upper bound on $P_{Line,m,k}$) by either the maximum power available to be sunk by k or the maximum power available to be sourced by m (again selecting the stricter of the two).

More formally, the Non-Homogenous Farkas' Lemma (see [77], [57, Theorem 3.1.2]) states that a non-strict inequality follows from a set of other simultaenous non-strict inequalities if the former can be expressed as a conic combination (sum with all non-negative coefficients) of the later (and the tautologous inequality $0 \leq 1$). By Definition 5.1, on the expected operating range the generation and load bounds (90) - (93) apply. Since (98) and (99) can be expressed as a set of simultaneous non-strict inequalities, then the following bounds on $P_{Line,k,m}$ can be derived by conic

112

combinations of Kirhoff's law (98) - (99) combined with the generation and load bounds (90) - (93):

$$P_{Line,k,m} \leq P_{G,Max,k} - \sum_{l \in \mathcal{N}(k) \setminus m} P_{Line,k,l} \tag{100}$$

$$-P_{Line,k,m} \leq P_{G,Max,m} - \sum_{p \in \mathcal{N}_{In}(m) \setminus k} P_{Line,m,p} \tag{101}$$

$$P_{Line,k,m} \leq -P_{G,Min,m} + P_{L,Max,m} + \sum_{p \in \mathcal{N}(m) \setminus k} P_{Line,m,p} \tag{102}$$

$$-P_{Line,k,m} \leq -P_{G,Min,k} + P_{L,Max,k} + \sum_{k \in \mathcal{N}(k) \setminus m} P_{Line,k,l} \tag{103}$$

Inequality (100) places an upperbound on $P_{Line,k,m}$ in terms of the maximum power available to be sourced by bus k, while (101) places a lowerbound on $P_{Line,k,m}$ in terms of the maximum power available to be sourced by bus m. Similarly, inequality (102) places an upperbound on $P_{Line,k,m}$ in terms of the maximum power available to be sunk by bus m, and inequality (103) places a lowerbound on $P_{Line,k,m}$ in terms of the maximum power available to be sunk by k. Thus, (100) - (103) bound $P_{Line,k,m}$ in terms of generation and load bounds, but as they are in terms of other network power flows, do not yet provide the constant bounds that we seek.

5.3.2 Bounding Power Flow on Lines Incident to Leaf Buses

Assume that k is a leaf bus, that is, (k, m) is the only line incident to bus k. Then (100) and (103) can be rewritten as:

$$P_{Line,k,m} \leq P_{G,Max,k} = P_{UBound,Sourcing,k,m} \tag{104}$$

$$-P_{Line,k,m} \leq -P_{G,Min,k} + P_{L,Max,k} = P_{LBound,Sinking,k,m} \tag{105}$$

where $P_{UBound,Sourcing,k,m}$ and $P_{LBound,Sinking,k,m}$ are constant upper and lower bounds on the power flow $P_{Line,k,m}$. Thus, if k is a leaf bus, then the maximum generation on bus k is a valid constant upperbound on $P_{Line,k,m}$ and the maximum sinking at bus k is a valid constant lowerbound on $P_{Line,k,m}$. Recall that we select the

113

stricter of the sinking or sourcing bounds for both upper bound $P_{UBound,k,m}$ and lower bound $P_{LBound,k,m}$ for the line power flow $P_{Line,k,m}$. Therefore, if k is a leaf bus then both $P_{UBound,k,m}$ and $P_{LBound,k,m}$ exist, and $P_{UBound,k,m} \leq P_{UBound,Sourcing,k,m}$ and $P_{LBound,k,m} \geq P_{LBound,Sinking,k,m}$.

Similarly, if m is a leaf bus, then (102) and (101) can be rewritten as:

$$P_{Line,k,m} \leq -P_{G,Min,m} + P_{L,Max,m} = P_{UBound,Sinking,k,m} \tag{106}$$

$$-P_{Line,k,m} \leq P_{G,Max,m} = P_{LBound,Sourcing,k,m} \tag{107}$$

where $P_{UBound,Sinking,k,m}$ and $P_{LBound,Sourcing,k,m}$ are similarly valid bounds on $P_{Line,k,m}$. It then follows that if m is a leaf bus, then both $P_{UBound,k,m}$ and $P_{LBound,k,m}$ exist and $P_{UBound,k,m} \leq P_{UBound,Sinking,k,m}$ and $P_{LBound,k,m} \geq P_{LBound,Sourcing,k,m}$. Therefore, if either k or m is a leaf bus, then there exist valid constant bounds $P_{UBound,k,m}$ and $P_{LBound,k,m}$ for $P_{Line,k,m}$.

5.3.3 Bounding Power Flows on General Lines

We have now shown that constant bounds $P_{UBound,k,m}$ and $P_{LBound,k,m}$ exist for line $(k,m) \in \mathcal{E}$ if it is either a key line ((94) and (95)) or incident to a leaf bus ((104) - (107)). Now consider an arbitrary line $(k,m) \in \mathcal{E}$ such that the above do not apply (that is, $(k,m) \notin \mathcal{E}_{Key}$ and neither k nor m is a leaf bus). Assume that there exist valid bounds $P_{UBound,Sourcing,l,k}$ for all $l \in \mathcal{N}(k) \setminus m$. In this case, by combining (100) with the bounds $P_{Line,l,k} \leq P_{UBound,Sourcing,l,k}$ we find:

$$P_{Line,k,m} \leq P_{G,Max,k} + \sum_{l \in \mathcal{N}(k) \setminus m} P_{UBound,Sourcing,l,k} = P_{UBound,Sourcing,k,m} \tag{108}$$

Therefore, there exists a valid sourcing upper bound $P_{UBound,Sourcing,k,m}$ for arbitrary line $(k,m) \in \mathcal{E}$ if there exist valid sourcing upper bounds $P_{UBound,Sourcing,l,k}$ for all $l \in \mathcal{N}(k) \setminus m$ (notice that the upper bounds are on power flows *into* bus k). $P_{UBound,Sourcing,k,m}$ then represents the maximum power which is available to be

sourced to $P_{Line,k,m}$ from bus k (including the maximum value that can be imported into bus k on the other incident lines).

Similarly, assume that there exist valid bounds $P_{UBound,Sourcing,m,p}$ for each $p \in \mathcal{N}(m) \setminus k$. Then by combining (101) with the bounds $P_{Line,m,p} \leq P_{LBound,Sourcing,m,p}$ we find:

$$-P_{Line,k,m} \leq P_{G,Max,m} - \sum_{p \in \mathcal{N}(m) \setminus k} P_{LBound,Sourcing,p,m} = -P_{LBound,Sourcing,k,m} \quad (109)$$

Therefore, there exists a valid sourcing lower bound $P_{LBound,Sourcing,k,m}$ for arbitrary line $(k,m) \in \mathcal{E}$ if there exist valid sourcing lower bounds $P_{LBound,Sourcing,p,m}$ for all $p \in \mathcal{N}(m) \setminus k$. $P_{LBound,Sourcing,k,m}$ then represents the maximum power which can be sourced to $P_{Line,k,m}$ from bus m (including the maximum value that can be imported into bus m on the other incident lines).

It must then be determined whether the assumed bounds ($P_{UBound,Sourcing,l,k}$ for all $l \in \mathcal{N}(k) \setminus m$ or $P_{LBound,Sourcing,p,m}$ for all $p \in \mathcal{N}(m) \setminus k$) do in fact exist, and if so what their values are. We have already shown that any such line is either a key line, or is incident to a leaf bus, then its bounds exist and can be determined. If neither of these is the case, then we can recursively apply either (108) or (109) to determine if the bound exists for the new line, and if so what it's value is. A tree of recursions throughout the lines in the network is then formed, where recursive paths represent paths of lines in the AC network, and such paths terminate when either a key line or a leaf bus is reach.

Consider the recursion tree of the above method applied to an arbitrary line $(k,m) \in \mathcal{E}$. $P_{UBound,Sourcing,k,m}$ exists if each path descending the recursion tree terminates in either a leaf node or a line in $\mathcal{E}_{Key}$. Each such path corresponds to a path of lines through the graph $\mathfrak{G}$, which does not backtrack (since each recursive step excludes the previous line). Therefore, since $\mathfrak{G}$ is finite, any such path must eventually do one of the following:

1. Terminate at a line incident to a leaf bus.

2. Terminate in key line in $\mathcal{E}_{Key}$.

3. Enter a cycle in the graph $\mathfrak{G}$ (that doesn't contain a key line).

Either cases 1 or 2 terminates the recursion path, while 3 results in an infinite recursion. Therefore, if a cycle is entered which does not contain a key line, then recursion will fail to terminate unless this condition is detected and prevented. We must therefore track which lines are present in the recursion tree, and terminate with a failure when a line is reached which is already in the tree (indicating an unbounded cycle in the graph $\mathfrak{G}$). As an artifact of this case, the proposed method of bounding power flows only returns a valid result if each cycle in the graph $\mathfrak{G}$ contains at least one key line.

If each cycle in $\mathfrak{G}$ contains at least one key line, then each recursion path must terminate, resulting by induction in a valid value of $P_{UBound,Sourcing,k,m}$ for each $(k, m) \in \mathcal{E}$. This value represents the total maximum power that can be sourced by bus k, based on both its local sourcing capabilities, and the total power it can draw from the subnetwork to which it is attached (the network on the k side of k, m). The same method can be applied to show that a valid value of $P_{LBound,Sourcing,k,m}$ must also exist for each $(k, m) \in \mathcal{E}$ (representing the total power that bus m can source due to the subnetwork on the m side of k, m).

Applying the same method to the sinking bounds ((102) and (103)), we find:

$$P_{Line,k,m} \leq - P_{G,Min,m} + P_{L,m} + \sum_{p \in \mathcal{N}(m) \backslash k} P_{UBound,Sinking,m,p}$$

$$= P_{UBound,Sinking,k,m} \tag{110}$$

$$-P_{Line,k,m} \leq - P_{G,Min,k} + P_{L,k} - \sum_{l \in \mathcal{N}(k) \backslash m} P_{LBound,Sinking,k,l}$$

$$= -P_{LBound,Sinking,k,m} \tag{111}$$

116

where $P_{UBound,Sinking,k,m}$ represents the maximum power that bus m can sink (based on the subnetwork on the m side of (k,m)), and $P_{LBound,Sinking,k,m}$ represents the maximum power that bus k can sink (based on the subnetwork on the k side of (k,m)). Recursive trees can be built for each of $P_{UBound,Sinking,k,m}$ and $P_{LBound,Sinking,k,m}$ to show that they also must always exist for each $(k,m) \in \mathcal{E}$.

The above results show that two upperbounds and two lowerbounds (based on sourcing and sinking capabilities respectively) exist for each line $(k,m) \in \mathcal{E}$, and can be calculated by a line-recursive approach, corresponding to power-flow paths in the graph $\mathfrak{G}$. Since both both the sourcing and sinking bounds are valid, we will select the stricter of the two and designate it as line power-flow bound $P_{UBound,k,m}$ (or $P_{LBound,k,m}$) as follows:

$$P_{UBound,k,m} = \min(P_{UBound,Sourcing,k,m}, P_{UBound,Sinking,k,m}) \tag{112}$$

$$P_{UBound,k,m} = \min(P_{LBound,Sourcing,k,m}, P_{LBound,Sinking,k,m}) \tag{113}$$

This recursive method allows the sourcing and sinking line power-flow bounds in a network to be calculated in terms of generation and load bounds, combined with the assumption that line constraints are enforced on key lines.

5.3.4 Procedure for Calculating All Line Power-Flow Bounds in a Network

Using the above described method, it is possible to create a procedure which will calculate the values of $P_{UBound,k,m}$ and $P_{LBound,k,m}$ for each line $(k,m) \in \mathcal{E}$ in a given network.

Recall that since $P_{Line,k,m} = -P_{Line,m,k}$, then $P_{UBound,k,m} = -P_{LBound,m,k}$ and $P_{LBound,k,m} = -P_{UBound,m,k}$. Therefore, it is only necessary to calculate the bounding values in a single direction for each line in the network. Therefore, like in Chapter 3, we will arbitrarily assign a direction indicating positive power flow to each line in $\mathcal{E}$ and assign these directed lines to a directed edge set $\overrightarrow{\mathcal{E}}$.

The following procedure uses the above described recursive method to calculate the constants $P_{UBound,k,m}$ and $P_{LBound,k,m}$ for all $(k,m) \in \overrightarrow{\mathcal{E}}$. It requires inputs of the power-flow structure graph $\mathfrak{G}$, the generation and load bound vectors $\mathbf{P_{G,Max}}$, $\mathbf{P_{G,Min}}$, and $\mathbf{P_{L,Max}}$, the line power-flow constraints vector $\mathbf{P_{Max}} = [P_{Max,1} \ldots P_{Max,L}]^T$ (where $P_{Max,i} = P_{Max,k,m}$ for all $(k,m) \in \overrightarrow{\mathcal{E}}$ and $i \in \{1 \ldots L\}$ is the index assigned to (k,m)), and a given selection of $\mathcal{E}_{Key}$. This recursive procedure is summarized in Procedure 5.1 below.

Procedure 5.1 (Determination of Bounds on Non-Key Lines on Expected Operating Range Assuming Satisfaction of Key Line Constraints)**.**

Inputs:

- *Power-Flow Structure Graph* $\mathfrak{G} = (\mathcal{V}, \mathcal{E})$.

- *Directed edge set* $\overrightarrow{\mathcal{E}}$ *(representing the direction of positive power flow assigned to each line in* $\mathcal{E}$*). Each line* $(k,m) \in \overrightarrow{\mathcal{E}}$ *is assigned an index* $i \in \{1 \ldots L\}$.

- *Edge subset* $\mathcal{E}_{Key} \subset \mathcal{E}$. $\mathcal{E}_{Key}$ *represents the set of lines whose line power-flow constraints* $|P_{Line,k,m}| \leq P_{Max,k,m}$ *are assumed to be satisfied.*

- *Line power-flow constraint vector* $\mathbf{P_{Max}} = \begin{bmatrix} P_{Max,1} & \ldots & P_{Max,L} \end{bmatrix}^T \in \mathbb{R}^L$, *where* $P_{Max,i} = P_{Max,k,m} > 0$ *where* $i \in \{1 \ldots L\}$ *is the index assigned to line* $(k,m) \in \overrightarrow{\mathcal{E}}$.

- *Constant vector* $\mathbf{P_{G,Max}} \in \mathbb{R}^N = \begin{bmatrix} P_{G,Max,1} & \ldots P_{G,Max,N} \end{bmatrix}$ *where* $P_{G,Max,k}$ *represents the maximum generation at bus* $k \in \mathcal{V}$ *on the expected operating range* $\mathbb{P}$.

- *Constant vector* $\mathbf{P_{G,Min}} \in \mathbb{R}^N = \begin{bmatrix} P_{G,Min,1} & \ldots P_{G,Min,N} \end{bmatrix}$ *where* $P_{G,Min,k} \leq P_{G,Max,k}$ *represents the minimum generation at bus* $k \in \mathcal{V}$ *on the expected operating range* $\mathbb{P}$.

- *Constant vector* $\mathbf{P_{L,Max}} \in \mathbb{R}^N = \begin{bmatrix} P_{L,Max,1} & \dots P_{L,Max,N} \end{bmatrix}$ *where* $P_{L,Max,k} \geq 0$ *for all* $k \in \mathcal{V}$, *representing the maximum load power at each bus in the network on the expected operating range* $\mathbb{P}$.

Outputs:

- *Upper bound vector* $\mathbf{P_{UBound}} = \begin{bmatrix} P_{UBound,1} & \dots & P_{UBound,L} \end{bmatrix}^T \in \mathbb{R}^L$, *where* $P_{UBound,i} = P_{UBound,k,m}$ *where* $i \in \{1 \dots L\}$ *is the index assigned to line* $(k,m) \in \overrightarrow{\mathcal{E}}$. $P_{UBound,k,m}$ *represents an upperbound on* $P_{Line,k,m}$ *on the expected operating range* $\mathbb{P}$ *assuming that all key line power-flow constraints are met.*

- *Lower bound vector* $\mathbf{P_{LBound}} = \begin{bmatrix} P_{LBound,1} & \dots & P_{LBound,L} \end{bmatrix}^T \in \mathbb{R}^L$, *where* $P_{LBound,i} = P_{LBound,k,m}$ *where* $i \in \{1 \dots L\}$ *is the index assigned to line* $(k,m) \in \overrightarrow{\mathcal{E}}$. $P_{LBound,k,m}$ *represents a lowerbound on* $P_{Line,k,m}$ *on the expected operating range* $\mathbb{P}$ *assuming that all key line power-flow constraints are met.*

Procedure 5.1 (Determine Bound Vectors $\mathbf{P_{UBound}}$ and $\mathbf{P_{LBound}}$):

5.1.1 *Initialize the mutex variables* $M_{k,m} = 0$ *and validity variables* $V_{UBound,Sinking,k,m} = V_{LBound,Sinking,k,m} = V_{UBound,Sinking,k,m} = V_{LBound,Sinking,k,m} = 0$ *for all* $(k,m) \in \overrightarrow{\mathcal{E}}$.

5.1.2 *For each line* $(k,m) \in \overrightarrow{\mathcal{E}}$:

    5.1.2.1 *If* $V_{UBound,Sourcing,k,m} = 0$ *then call Subprocedure 5.1A to determine* $P_{UBound,Sourcing,k,m}$. *If a failure is returned, then end the procedure with a failure.*

    5.1.2.2 *If* $V_{UBound,Sinking,k,m} = 0$ *then call Subprocedure 5.1C to determine* $P_{UBound,Sinking,k,m}$. *If a failure is returned, then end the procedure with a failure.*

5.1.2.3 If $V_{LBound,Sourcing,k,m} = 0$ then call Subprocedure 5.1B to determine $P_{LBound,Sourcing,k,m}$. If a failure is returned, then end the procedure with a failure.

5.1.2.4 If $V_{LBound,Sinking,k,m} = 0$ then call Subprocedure 5.1D to determine $P_{LBound,Sinking,k,m}$. If a failure is returned, then end the procedure with a failure.

5.1.2.5 Set

$$P_{UBound,k,m} := min(P_{UBound,Sourcing,k,m}, P_{UBound,Sinking,k,m}), \quad (114)$$

and

$$P_{LBound,k,m} := max(P_{LBound,Sourcing,k,m}, P_{LBound,Sinking,k,m}). \quad (115)$$

5.1.3 End the procedure with a successful result, returning a value value of $P_{UBound,k,m}$ and $P_{UBound,k,m}$ for each $(k,m) \in \overrightarrow{\mathcal{E}}$.

Subprocedure 5.1A *(Determine $P_{UBound,Sourcing,k,m}$).*

5.1A.1 If $M_{k,m} = 1$ then return a failure. Otherwise set $M_{k,m} = 1$.

5.1A.2 If $(k,m) \in \mathcal{E}_{Key}$ then set

$$P_{UBound,Sourcing,k,m} := P_{Max,k,m}, \quad (116)$$

and go to 5.1A.6. Otherwise (if $(k,m) \notin \mathcal{E}_{Key}$) then proceed to step 5.1A.3.

5.1A.3 For each $l \in \mathcal{N}_{In}(k) \setminus m$: If $V_{UBound,Sourcing,l,k} = 0$ then recursively call Subrocedure 5.1A to calculate $P_{UBound,Sourcing,l,k}$. If any such call returns a failure, then set $M_{k,m} = 0$ and return a failure.

5.1A.4 For each $l \in \mathcal{N}_{Out}(k) \setminus m$: If $V_{LBound,Sourcing,k,l} = 0$ then recursively call Subprocedure 5.1B to calculate $P_{LBound,Sourcing,k,l}$. If any such call returns a failure, then set $M_{k,m} = 0$ and return a failure.

120

5.1A.5 Set:

$$P_{UBound,Sourcing,k,m} := P_{G,Max,k} + \sum_{l \in \mathcal{N}_{In}(k)} P_{UBound,Sourcing,l,k}$$

$$- \sum_{l \in \mathcal{N}_{Out}(k) \backslash m} P_{LBound,Sourcing,k,l}. \qquad (117)$$

5.1A.6 Set $V_{UBound,Sourcing,k,m} = 1$, set $M_{k,m} = 0$, and return a valid value of $P_{UBound,Sourcing,k,m}$.

Subprocedure 5.1B(*Determine $P_{LBound,Sourcing,k,m}$*).

5.1A.1 If $M_{k,m} = 1$ then return a failure. Otherwise set $M_{k,m} = 1$.

5.1A.2 If $(k,m) \in \mathcal{E}_{Key}$ then set

$$P_{LBound,Sourcing,k,m} := -P_{Max,k,m}, \qquad (118)$$

and go to 5.1B.6. Otherwise (if $(k,m) \notin \mathcal{E}_{Key}$) then proceed to step 5.1B.3.

5.1A.3 For each $p \in \mathcal{N}_{In}(m) \backslash k$: If $V_{UBound,Sourcing,p,m} = 0$ then recursively call Subprocedure 5.1A to calculate $P_{UBound,Sourcing,p,m}$. If any such call returns a failure, then set $M_{k,m} = 0$ and return a failure.

5.1A.4 For each $p \in \mathcal{N}_{Out}(m) \backslash k$: If $V_{LBound,Sourcing,m,p} = 0$ then recursively call Subprocedure 5.1B to calculate $P_{LBound,Sourcing,m,p}$. If any such call returns a failure, then set $M_{k,m} = 0$ and return a failure.

5.1A.5 Set:

$$P_{LBound,Sourcing,k,m} := -P_{G,Min,m} + P_{L,Max,m} + \sum_{p \in \mathcal{N}_{In}(m) \backslash k} P_{UBound,Sourcing,p,m}$$

$$- \sum_{p \in \mathcal{N}_{Out}(m) \backslash k} P_{LBound,Sourcing,m,p}. $$

$$(119)$$

5.1A.6 Set $V_{LBound,Sourcing,k,m} = 1$, set $M_{k,m} = 0$, and return a valid value of $P_{LBound,Sourcing,k,m}$.

Subprocedure 5.1C(*Determine $P_{UBound,Sinking,k,m}$*).

5.1C.1 If $M_{k,m} = 1$ then return a failure. Otherwise set $M_{k,m} = 1$.

5.1C.2 If $(k,m) \in \mathcal{E}_{Key}$ then set

$$P_{UBound,Sinking,k,m} := P_{Max,k,m}, \tag{120}$$

and go to 5.1C.6. Otherwise (if $(k,m) \notin \mathcal{E}_{Key}$) then proceed to step 5.1C.3.

5.1C.3 For each $p \in \mathcal{N}_{In}(m) \setminus k$: If $V_{LBound,Sinking,p,m} = 0$ then recursively call Subprocedure 5.1D to calculate $P_{LBound,Sinking,p,m}$. If any such call returns a failure, then set $M_{k,m} = 0$ and return a failure.

5.1C.4 For each $p \in \mathcal{N}_{Out}(m) \setminus k$: If $V_{UBound,Sinking,m,p} = 0$ then recursively call Subprocedure 5.1C to calculate $P_{UBound,Sinking,m,p}$. If any such call returns a failure, then set $M_{k,m} = 0$ and return a failure.

5.1C.5 Set:

$$P_{UBound,Sinking,k,m} := -P_{G,Min,m} + P_{L,Max,m} - \sum_{p \in \mathcal{N}_{In}(m) \setminus k} P_{LBound,Sinking,p,m}$$
$$+ \sum_{p \in \mathcal{N}_{Out}(m) \setminus k} P_{UBound,Sinking,m,p} \tag{121}$$

5.1C.6 Set $V_{UBound,Sinking,k,m} = 1$, set $M_{k,m} = 0$, and return a valid value of $P_{UBound,Sinking,k,m}$.

Subprocedure 5.1D(*Determine $P_{LBound,Sinking,k,m}$*).

5.1D.1 If $M_{k,m} = 1$ then return a failure. Otherwise set $M_{k,m} = 1$.

5.1D.2 If $(k,m) \in \mathcal{E}_{Key}$ then set

$$P_{LBound,Sinking,k,m} := -P_{Max,k,m}, \tag{122}$$

and go to 5.1D.6. Otherwise (if $(k,m) \notin \mathcal{E}_{Key}$) then proceed to step 5.1D.3.

5.1D.3 For each $l \in \mathcal{N}_{In}(k) \setminus m$: If $V_{LBound,Sinking,l,k} = 0$ then recursively call Subro-cedure 5.1D to calculate $P_{LBound,Sinking,l,k}$. If any such call returns a failure, then set $M_{k,m} = 0$ and return a failure.

5.1D.4 For each $l \in \mathcal{N}_{Out}(k) \setminus m$: If $V_{UBound,Sinking,k,l} = 0$ then recursively call Subpro-cedure 5.1C to calculate $P_{LBound,Sinking,k,l}$. If any such call returns a failure, then set $M_{k,m} = 0$ and return a failure.

5.1D.5 Set:

$$P_{LBound,Sinking,k,m} := -P_{G,Min,k} + P_{L,Max,k} + \sum_{l \in \mathcal{N}_{In}(k) \setminus m} P_{LBound,Sinking,l,k}$$

$$- \sum_{l \in \mathcal{N}_{Out}(k) \setminus m} P_{UBound,Sinking,k,l}.$$

$$(123)$$

5.1D.6 Set $V_{LBound,Sinking,k,m} = 1$, set $M_{k,m} = 0$, and return a valid value of $P_{LBound,Sinking,k,m}$.

Procedure 5.1 formalizes the recursive method for calculation of the bounds $P_{LBound,k,m}$ and $P_{UBound,k,m}$ for each *directed* line $(k,m) \in \overrightarrow{\mathcal{E}}$. The reverse-direction power-flow bounds can then be simply calculated by $P_{UBound,m,k} = -P_{LBound,k,m}$ and $P_{LBound,m,k} = P_{UBound,k,m}$. The use of the validity flags ($V_{UBound,Sourcing,k,m}$, $V_{LBound,Sourcing,k,m}$, $V_{UBound,Sinking,k,m}$, and $V_{LBound,Sinking,k,m}$ for each directed line $(k,m) \in \overrightarrow{\mathcal{E}}$) prevents redundancy of calculation, since each bound value ($P_{UBound,Sourcing,k,m}$, $P_{LBound,Sourcing,k,m}$, $P_{UBound,Sinking,k,m}$, and $P_{LBound,Sinking,k,m}$ for each $(k,m) \in \overrightarrow{\mathcal{E}}$) need only be calculated once, and can then be used many times in other calculations. Finally, the use of the line mutex flags $M_{k,m}$ for each $(k,m) \in \overrightarrow{\mathcal{E}}$ allows detection of unconstrained cycles in the graph, preventing the method from entering an infinite loop.

Lemma 5.1 below states formally the characteristics of Procedure 5.1: that $P_{UBound,k,m}$ and $P_{LBound,k,m}$ exist for all lines $(k,m) \in \overrightarrow{\mathcal{E}}$ (assuming a finite graph $\mathfrak{G}$ such that each cycle in $\mathfrak{G}$ contains at least one line in $\mathcal{E}_{Key}$), and that those bounds are valid on

the expected operating range assuming satisfaction of the line power-flow constraints for all key lines.

Lemma 5.1. *Consider an inverter-based power network whose structure is described by the finite graph $\mathfrak{G} = (\mathcal{V}, \mathcal{E})$. Define edge set $\mathcal{E}_{Key} \subset \mathcal{E}$, and assume that for each cycle $\mathcal{E}_C \subset \mathcal{E}$, then $\mathcal{E}_C \cap \mathcal{E}_{Key} \neq \emptyset$. Each line $(k, m) \in \mathcal{E}$ is assigned maximum power-flow constant $P_{Max,k,m}$ such that $0 < P_{Max,k,m} < Y_{k,m} V_k V_m$. Assume that there exists $P_{G,Min,k} \leq 0$, $P_{G,Max,k} \geq 0$, and $P_{L,Max,k} \geq 0$ for each $k \in \mathcal{V}$ defining the expected operating range $\mathbb{P}$ of the network (per Definition 5.1).*

Then:

5.1.A $P_{UBound,k,m} \geq 0$ *and* $P_{LBound,k,m} \leq 0$ *exist for all* $(k, m) \in \mathcal{E}$*, and Procedure 5.1 will terminate with a finite number of recursions.*

5.1.B *If* $(\mathbf{P_G}, \mathbf{P_L}) \in \mathbb{P}$*, then* $|P_{Line,k,m}| \leq P_{Max,k,m}$ *for all* $(k, m) \in \mathcal{E}_{Key}$ *implies that* $P_{LBound,k,m} \leq P_{Line,k,m} \leq P_{UBound,k,m}$ *for all* $(k, m) \in \mathcal{E}$*, where* $P_{LBound,k,m}$ *and* $P_{UBound,k,m}$ *are calculated by Procedure 5.1.*

5.1.C *The computational complexity of Procedure 5.1 is* $O(L\,\mathcal{N}_{Max})$*, where L is the number of lines in the graph $\mathfrak{G}$ and $\mathcal{N}_{Max} = \max_{k \in \mathcal{V}} |\mathcal{N}(k)|$ is the maximum number of neighbors of any single bus in $\mathfrak{G}$.*

Proof. Lemma 5.1.A:

We have shown that there are two cases in which a call to any of the Subprocedures 5.1A - 5.1D on line $(k, m) \in \overrightarrow{\mathcal{E}}$ terminates without any recursive calls: if $(k, m) \in \mathcal{E}_{Key}$, or if either bus k or bus m is a leaf bus (has only one incident line, which is (k, m)).

Since $|\mathcal{E}|$ (and therefore $|\overrightarrow{\mathcal{E}}|$) is finite, the number of calls in Procedure 5.1 is finite, so it only needs to be shown that any recursion path of Subprocedures 5.1A - 5.1D must have finite length. Consider the sequence of lines $\{e_{P,i}\}$ representing a

recursion path. At each recursion step, if $e_{P,i} = (k, m) \in \mathcal{E}_{Key}$, then the recursion (and the sequence) terminates immediately. Likewise, if $e_{P,i}$ is incident to a leaf bus, then recursion also terminates immediately. Otherwise, we select one of the lines on which a recursive call is made and append it to $\{e_{P,i}\}$.

Since $|\vec{\mathcal{E}}|$ is finite, one of three conditions must eventually occur:

(1) The line $e_{P,i} \in \mathcal{E}_{Key}$.

(2) $e_{P,i}$ is incident to a leaf bus.

(3) $e_{P,i}$ is already in the sequence.

In cases (1) or (2), recursion terminates immediately. Case (3) leads to a contradiction, since all of Subprocedures 5.1A - 5.1D exclude the preceeding line from the recursive calls (so recursion cannot backtrack along the same path in $\mathfrak{G}$), and we have assumed that each cycle in $\mathfrak{G}$ must contain at least one line in $\mathcal{E}_{Key}$. Therefore, any recursion path must terminate in a finite number of calls, resulting in a valid value of $P_{UBound,k,m}$ or $P_{LBound,k,m}$.

Finally, since for each $(k, m) \in \mathcal{E}$ there exists exactly one of (k, m) or (m, k) in $\vec{\mathcal{E}}$, then each member of $\mathcal{E}$ is either in $\vec{\mathcal{E}}$, or is the reverse of a directed line in $\vec{\mathcal{E}}$. The reverse-direction bounds $P_{UBound,m,k}$ and $P_{LBound,m,k}$ may be calculated by $P_{UBound,m,k} = -P_{LBound,k,m}$ and $P_{LBound,m,k} = P_{UBound,k,m}$. Therefore, the bounds $P_{UBound,k,m}$ and $P_{LBound,k,m}$ exist for each line $(k, m) \in \mathcal{E}$, and are calculated by Procedure 5.1.

Lemma 5.1.B:

We have already shown in the proof to Lemma 5.1.A above that the constant bounds $P_{UBound,Sourcing,k,m}$, $P_{LBound,Sourcing,k,m}$, $P_{UBound,Sinking,k,m}$, and $P_{LBound,Sinking,k,m}$ exist for each line $(k, m) \in \mathcal{E}$. By assumption (116), (118), (120), and (122) represent power-flow bounds on key lines $(k, m) \in \mathcal{E}_{Key}$. By appropriately substituting $P_{UBound,m,k} = -P_{LBound,k,m}$ and $P_{LBound,m,k} = -P_{UBound,k,m}$ into (117), (119), (121),

(123), we obtain (108), (109), (110), and (111) respectively, which we have shown by construction (in Section 5.3.3 above) are valid bounds on $P_{Line,k,m}$ for non-key lines $(k,m) \in \overrightarrow{\mathcal{E}} \setminus \mathcal{E}_{Key}$ when $(\mathbf{P_G}, \mathbf{P_L}) \in \mathbb{P}$ ($P_{G,Min,k} \leq P_{G,k} \leq P_{G,Max,k}$ and $0 \leq P_{L,k} \leq P_{L,Max,k}$ $\forall\ k \in \mathcal{V}$). Therefore, Subprocedures 5.1A - 5.1D calculate valid bounds $P_{UBound,Sourcing,k,m}$, $P_{LBound,Sourcing,k,m}$, $P_{UBound,Sinking,k,m}$, $P_{LBound,Sinking,k,m}$ such that $P_{LBound,Sourcing,k,m} \leq P_{Line,k,m} \leq P_{LBound,Sourcing,k,m}$ and $P_{UBound,Sinking,k,m} \leq P_{Line,k,m} \leq P_{LBound,Sinking,k,m}$ for each line $(k,m) \in \overrightarrow{\mathcal{E}}$.

Finally, for each $(k,m) \in \mathcal{E}$, we can define $P_{UBound,k,m}$ and $P_{LBound,k,m}$ by (114) and (115) such that $P_{LBound,k,m} \leq P_{Line,k,m} \leq P_{UBound,k,m}$. Therefore, Procedure 5.1 numerically calculates valid power-flow bounds for all $(k,m) \in \mathcal{E}$ in terms of the generation and load constraints, combined with a given selection of $\mathcal{E}_{Key}$.

Lemma 5.1.C:

The recursive subprocedures (Subprocedures 5.1A, 5.1C, 5.1B, and 5.1D) each require a summation over the neighbors of the incident buses, and therefore each such subprocedure call requires $O(\mathcal{N}_{Max})$ calculations (excluding the recursive calls). The use of the $V_{UBound,Sourcing,k,m}$, $V_{UBound,Sinking,k,m}$, $V_{LBound,Sourcing,k,m}$, and $V_{LBound,Sinking,k,m}$ flags ensures that each subprocedure is called only once for each line in $\mathfrak{G}$, and therefore there are a maximum of $4 * L$ subprocedure calls. Therefore, the computational complexity of Procedure 5.1 is $O(L\,\mathcal{N}_{Max})$. $\qquad\square$

5.3.5 Sufficient Condition Test for Constraint-Satisfying Key Line Sets

Procedure 5.1 above calculates the line power-flow bounds $P_{LBound,k,m}$ and $P_{UBound,k,m}$ for each line $(k,m) \in \mathcal{E}$, based on a set of generation constraints $P_{G,Min,k} \leq P_{G,k} \leq P_{G,Max,k}$ and load constraints $0 \leq P_{L,k} \leq P_{L,Max}$ for all buses $k \in \mathcal{V}$, and a set of lines $\mathcal{E}_{Key} \subset \mathcal{E}$ such that the constraint $|P_{Line,k,m}| \leq P_{Max,k,m}$ is assumed to be met for all $(k,m) \in \mathcal{E}_{Key}$. Therefore, if $\mathcal{E}_{Key}$ is selected such that $-P_{Max,k,m} \leq P_{LBound,k,m}$ and $P_{UBound,k,m} \leq P_{Max,k,m}$ for all $(k,m) \in \mathcal{E}$, then such a selection of $\mathcal{E}_{Key}$ is a

constraint-satisficing key line set per Definition 5.2.

We formalize this result in the following lemma:

Theorem 5.1 (Sufficient Condition Test for Constraint-Satisficing Key Line Sets).
*Consider an inverter-based power network whose structure is described by the finite
graph $\mathfrak{G} = (\mathcal{V}, \mathcal{E})$. Each line $(k, m) \in \mathcal{E}$ is assigned maximum power-flow constant
$P_{Max,k,m}$ such that $0 < P_{Max,k,m} < Y_{k,m}V_kV_m$. Assume that there exists $P_{G,Min,k} \leq 0$,
$P_{G,Max,k} \geq 0$, and $P_{L,Max,k} \geq 0$ for each $k \in \mathcal{V}$ defining the expected operating range
$\mathbb{P}$ of the network (per Definition 5.1).*

*Assume that there exists a subset of lines $\mathcal{E}_{Key} \subset \mathcal{E}$ such that $P_{UBound,k,m} \leq
P_{Max,k,m}$ and $P_{LBound,k,m} \geq -P_{Max,k,m}$ for all $(k, m) \in \mathcal{E}$, where $P_{UBound,k,m}$ and
$P_{LBound,k,m}$ are calculated by Procedure 5.1. Then $\mathcal{E}_{Key}$ is a constraint-satisficing key
line set (per Definition 5.2).*

Proof. We have already shown in Lemma 5.1 above that the constant bounds $P_{UBound,k,m}$
and $P_{LBound,k,m}$ exist for each line $(k, m) \in \mathcal{E}$, and further that $|P_{Line,k,m}| \leq P_{Max,k,m} \; \forall \, (k, m) \in
\mathcal{E}_{Key} \implies P_{LBound,k,m} \leq P_{Line,k,m} \leq P_{UBound,k,m} \; \forall \, (k, m) \in \mathcal{E}$. Since, by assumption
$P_{UBound,k,m} \leq P_{Max,k,m}$ and $P_{LBound,k,m} \geq -P_{Max,k,m}$ for all $(k, m) \in \mathcal{E}$, then it follows
that $-P_{Max,k,m} \leq P_{LBound,k,m} \leq P_{Line,k,m} \leq P_{UBound,k,m} \leq P_{Max,k,m} \; \forall \, (k, m) \in \mathcal{E}$, and
therefore $|P_{Line,k,m}| \leq P_{Max,k,m} \; \forall \, (k, m) \in \mathcal{E}$, that is, the line set $\mathcal{E}_{Key}$ meets the re-
quirements of Definition 5.2 and is therefore a constraint-satisficing key line set. $\square$

Theorem 5.1 shows that if the power-flow bounds $P_{UBound,k,m}$ and $P_{LBound,k,m}$ are
within $\pm P_{Max,k,m}$ for each line $(k, m) \in \mathcal{E}$ in a power network for a given selection
of $\mathcal{E}_{Key}$ and a given expected operating range $\mathbb{P}$, then the line power-flow constraints
$|P_{Line,k,m}| \leq P_{Max,k,m}$ for all $(k, m) \in \mathcal{E}$ will be satisfiied. Therefore, explicit en-
forcement of *only the line power-flow constraints associated with key lines* is sufficient
to *implicitly* ensure satisfaction of the remaining constraints. This result allows re-
laxation of the sufficient condition for synchronization (Theorem 3.5) so that only

a subset of the constraints need be enforced. In the final technical chapter, we will use this result to form the basis of a control method allowing sparse deployment of constraint-enforcing inverters while still providing the desired robust synchronziation and power sharing result.

5.3.6 Discussion on Procedure 5.1 and Sufficient Condition for Constraint-Satisficing Key Line Sets

Procedure 5.1 and Theorem 5.1 provide a direct test to determine whether a given selection of the key line set $\mathcal{E}_{Key}$ is constraint-satisficing for a given network power-flow structure $\mathfrak{G} = (\mathcal{V}, \mathcal{E})$, expected operating range $\mathbb{P}$, and power-flow constraints $\mathbf{P_{Max}}$. This test explicitly integrates both the network structure and expected operating conditions, and can be applied to networks of arbitrary size and structure. Any subset of the network lines can be tested, including the full line set $\mathcal{E}_{Key} = \mathcal{E}$ (where it confirms the principal that the complete line set is always trivially constraint-satisficing) or the empty set. Of interest is the fact that some network are constraint-satisficing for $\mathcal{E}_{Key} = \emptyset$, which we show in Section 5.5.

Procedure 5.1 avoids redundant calculations where possible, but still may be computationally expensive for large networks. It also requires access to the structure and expected operating range of the network, and therefore the test can only be performed with global knowledge of the network parameters. In addition, it requires the presence of at least one key line in each cycle of the graph $\mathfrak{G}$.

Procedure 5.1 determines the power-flow bounds for a line by using the maximum (and minimum) generation and load capacity available on the subnetworks on each side of the line (taking into account the limits imposed by the assumption of enforcement of key line constraints). Because it lacks a method for bounding power flows in cycles of the network, it is likely overly conservative for highly cyclical networks.

Therefore, the test provided by Procedure 5.1 and Theorem 5.1 is a sufficient condition only (not necessary and sufficient), and as such may designate as not constraint-satisficing some key line sets which might in fact be constraint-satisficing. Further study is required to develop a method to more tightly bound power flows in highly cyclical networks.

5.4 Generation of Constraint-Satisficing Key Line Sets

Procedure 5.1 and Theorem 5.1 together provide a sufficient condition test whether a given candidate key line set $\mathcal{E}_{Key}$ is constraint-satisficing for given network and expected operating range. In order to constrain the network within the safe region for across the entire expected operating range, it will be necessary to generate a constraint-satisficing key line set $\mathcal{E}_{Key}$ (or ideally an irreducable or minimal constraint-satisficing key line set) given the network structure and bounds. This goal can be accomplished by using the test provided by Procedure 5.1 and Theorem 5.1, combined with a few key realizations about the characteristics of constraint-satisficing key line sets. These realizations are that 1) the set of all lines of the network $\mathcal{E}$ is always trivially constraint-satisficing, and 2) the subsets of non-constraint-satisficing key line sets are also non-constraint-satisficing. We formalize these results below:

Lemma 5.2 (Characteristics of Constraint-Satisficing Key Line Sets). *Consider the definition of constraint-satisficing key line sets in Definition 5.2. Then:*

5.2.A Set of all lines is always constraint-satisficing: The key line set $\mathcal{E}_{Key} = \mathcal{E}$ is always a constraint-satisficing key line set for the network $(\mathfrak{G}, \mathbb{P}, \mathbf{P_{Max}})$.

5.2.B Subsets of non-constraint-satisficing key line sets are always non-constraint-satisficing: If $\mathcal{E}_{Key}$ is not a constraint-satisficing key line set for $(\mathfrak{G}, \mathbb{P}, \mathbf{P_{Max}})$, then neither are any of its subsets.

Proof. Lemma 5.2.A:

If $\mathcal{E}_{Key} = \mathcal{E}$ for a given network $(\mathfrak{G}, \mathbb{P}, \mathbf{P_{Max}})$, then the condition for a constraint-satisficing key line set becomes $|P_{Line,k,m}| \leq P_{Max,k,m} \ \forall \ (k,m) \in \mathcal{E} \implies |P_{Line,k,m}| \leq P_{Max,k,m} \ \forall \ (k,m) \in \mathcal{E}$ for all $(\mathbf{P_G}, \mathbf{P_L}) \in \mathbb{P}$, which is a tautology (of the form $A \implies (A$ restricted to $X))$. $\qquad\square$

Lemma 5.2.B:

Contradiction Hypothesis: Assume that $\mathcal{E}_{Key} \subset \mathcal{E}$ is NOT a constraint-satisficing key line set for some $(\mathfrak{G}, \mathbb{P}, \mathbf{P_{Max}})$ and that there exists $\mathcal{E}'_{Key} \subset \mathcal{E}_{Key}$ such that $\mathcal{E}'_{Key}$ is a constraint-satisficing key line set for the same network.

Then $|P_{Line,k,m}| \leq P_{Max,k,m} \ \forall \ (k,m) \in \mathcal{E}_{Key}$ implies that $|P_{Line,k,m}| \leq P_{Max,k,m} \ \forall \ (k,m) \in \mathcal{E}'_{Key}$ (since $\mathcal{E}'_{Key} \subset \mathcal{E}_{Key}$), which further implies that $|P_{Line,k,m}| \leq P_{Max,k,m} \ \forall \ (k,m) \in \mathcal{E}$ for all $(\mathbf{P_G}, \mathbf{P_L}) \in \mathbb{P}$ (since $\mathcal{E}'_{Key}$ is a constraint-satisficing key line set for $(\mathfrak{G}, \mathbb{P}, \mathbf{P_{Max}})$). Then by Definition 5.2, $\mathcal{E}_{Key}$ is a constraint-satisficing key line set for $(\mathfrak{G}, \mathbb{P}, \mathbf{P_{Max}})$, which is a contradiction. Therefore, if $\mathcal{E}_{Key}$ is not a constraint-satisficing key line set for some $(\mathfrak{G}, \mathbb{P}, \mathbf{P_{Max}})$, then there does not exist $\mathcal{E}'_{Key} \subset \mathcal{E}_{Key}$ such that $\mathcal{E}'_{Key}$ is a constraint-satisficing key line set for $(\mathfrak{G}, \mathbb{P}, \mathbf{P_{Max}})$. $\qquad\square$

5.4.1 Search Procedure for Constraint-Satisficing Key Line Sets

The two characteristics of constraint-satisficing key line sets described in Lemma 5.2, together with the test provided by Procedure 5.1 and Theorem 5.1, allow development of an inductive search method for constraint-satisficing key line sets for a specified network $(\mathfrak{G}, \mathbb{P}, \mathbf{P_{Max}})$. If a given $\mathcal{E}_{Key} \subset \mathcal{E}$ is a constraint-satisficing key line set, then by one-by-one removing each of its lines and performing the test of Procedure 5.1 and Theorem 5.1, we can determine if any of its one-less subsets is a constraint-satisficing key line set. If any such subsets are constraint-satisficing key line sets, then we can recursively perform the same test on each other their one-less subsets, thus forming a recursive search tree of candidate key line sets. Since $\mathcal{E}_{Key} = \mathcal{E}$ is always trivially constraint-satisficing (and all possible constraint-satisficing key line sets are subsets

of $\mathcal{E}$), then it makes sense to start the search there.

By Lemma 5.2.B, if a given candidate set $\mathcal{E}_{Key}$ is not constraint-satisficing, then it is not necessary to test any of its subsets (and so recursion terminates). If none of the one-less subsets of a constraint-satisficing key line set $\mathcal{E}_{Key}$ is constraint-satisficing, then $\mathcal{E}_{Key}$ is irreducably constraint-satisficing. Therefore, the branches of the recursive search tree terminate at irreducably constraint-satisficing key line sets. Once the entire space of candidate key line sets has been searched, the minimally constraint-satisficing key line sets are those containing the minimum number of lines.

We formalize this inductive search procedure below:

Procedure 5.2 (Generation of Constraint-Satisficing Key Line Sets for a Specifed Network and Expected Operating Range)**.**

Inputs:

- *Power-Flow Structure Graph* $\mathfrak{G} = (\mathcal{V}, \mathcal{E})$.

- *Directed edge set* $\overrightarrow{\mathcal{E}}$ *(representing the direction of positive power flow assigned to each line in* $\mathcal{E}$*). Each line* $(k, m) \in \overrightarrow{\mathcal{E}}$ *is assigned an index* $i \in \{1 \ldots L\}$.

- *Line power-flow constraint vector* $\mathbf{P_{Max}} = \begin{bmatrix} P_{Max,1} & \ldots & P_{Max,L} \end{bmatrix}^T \in \mathbb{R}^L$, *where* $P_{Max,i} = P_{Max,k,m} > 0$ *where* $i \in \{1 \ldots L\}$ *is the index assigned to line* $(k, m) \in \overrightarrow{\mathcal{E}}$.

- *Constant vector* $\mathbf{P_{G,Max}} \in \mathbb{R}^N = \begin{bmatrix} P_{G,Max,1} & \ldots P_{G,Max,N} \end{bmatrix}$ *where* $P_{G,Max,k}$ *represents the maximum generation at bus* $k \in \mathcal{V}$ *on the expected operating range* $\mathbb{P}$.

- *Constant vector* $\mathbf{P_{G,Min}} \in \mathbb{R}^N = \begin{bmatrix} P_{G,Min,1} & \ldots P_{G,Min,N} \end{bmatrix}$ *where* $P_{G,Min,k} \leq P_{G,Max,k}$ *represents the minimum generation at bus* $k \in \mathcal{V}$ *on the expected operating range* $\mathbb{P}$.

131

- *Constant vector* $\mathbf{P_{L,Max}} \in \mathbb{R}^N = \begin{bmatrix} P_{L,Max,1} & \ldots P_{L,Max,N} \end{bmatrix}$ *where* $P_{L,Max,k} \geq 0$ *for all* $k \in \mathcal{V}$, *representing the maximum load power at each bus in the network on the expected operating range* $\mathbb{P}$.

Outputs:

- *Set of constraint-satisfing key line sets* $\boldsymbol{\mathcal{E}_{Satisficing}}$ *for the network* $(\mathfrak{G}, \mathbb{P}, \mathbf{P_{Max}})$.

- *Set of* Irreducable *constraint-satisfing key line sets* $\boldsymbol{\mathcal{E}_{Irr}}$ *for the network* $(\mathfrak{G}, \mathbb{P}, \mathbf{P_{Max}})$.

- *Set of* Minimal *constraint-satisfing key line sets* $\boldsymbol{\mathcal{E}_{Min}}$ *for the network* $(\mathfrak{G}, \mathbb{P}, \mathbf{P_{Max}})$.

Procedure 5.2 (Generate All constraint-satisfing key line sets for the Specified Network):

5.2.1 Initialize the global variables $\boldsymbol{\mathcal{E}_{Satisficing}} = \emptyset$, $\boldsymbol{\mathcal{E}_{Irr}} = \emptyset$, $\boldsymbol{\mathcal{E}_{Min}} = \emptyset$, *and* $\boldsymbol{\mathcal{E}_{Tested}} = \emptyset$.

5.2.2 Call Subprocedure 5.2A with $\mathcal{E}_{Key} = \mathcal{E}$ *to generate all constraint-satisfing subsets of* $\mathcal{E}$ *(assigns the global variables* $\boldsymbol{\mathcal{E}_{Satisficing}}$ *and* $\boldsymbol{\mathcal{E}_{Irr}}$*).*

5.2.3 Assign

$$L_{Min} := \min_{\mathcal{E}_{Key} \in \boldsymbol{\mathcal{E}_{Irr}}} |\mathcal{E}_{Key}| \tag{124}$$

5.2.4 Assign

$$\boldsymbol{\mathcal{E}_{Min}} := \{\mathcal{E}_{Key} \in \boldsymbol{\mathcal{E}_{Irr}} \ s.t. \ |\mathcal{E}_{Key}| = L_{Min}\} \tag{125}$$

5.2.5 Return $\boldsymbol{\mathcal{E}_{Satisficing}}$, $\boldsymbol{\mathcal{E}_{Irr}}$, *and* $\boldsymbol{\mathcal{E}_{Min}}$.

Subprocedure 5.2A(*Generate All Constraint-Satisfing Key Line Subsets of* $\mathcal{E}_{Key}$).

Arguments:

- *Edge subset* $\mathcal{E}_{Key} \subset \mathcal{E}$. $\mathcal{E}_{Key}$ *is the candidate constraint-satisfing key line set.*

Returns:

- Boolean value $Is\_Satisficing$, indicating whether the candidate set $\mathcal{E}_{Key}$ is a constraint-satisficing key line set for $(\mathfrak{G}, \mathbb{P}, \mathbf{P_{Max}})$.

5.2A.1 Is $\mathcal{E}_{Key} \in \boldsymbol{\mathcal{E}_{Tested}}$? If so, then go to 1a. Otherwise, go on to 5.2A.2.

    (a) If $\mathcal{E}_{Key} \in \boldsymbol{\mathcal{E}_{Satisficing}}$ then return $Is\_Satisficing = true$. Otherwise, return $Is\_Satisficing = false$.

5.2A.2 Add $\mathcal{E}_{Key}$ to $\boldsymbol{\mathcal{E}_{Tested}}$.

5.2A.3 Call Procedure 5.1 on $(\mathfrak{G}, \mathbb{P}, \mathbf{P_{Max}}, \mathcal{E}_{Key})$ to determine the bounding vectors $\mathbf{P_{UBound}}$ and $\mathbf{P_{LBound}}$.

5.2A.4 Determine whether $(\mathfrak{G}, \mathbb{P}, \mathbf{P_{Max}}, \mathcal{E}_{Key})$ is constraint-satisficing by the test of Theorem 5.1 ($P_{UBound,k,m} \leq P_{Max,k,m}$ and $P_{LBound,k,m} \geq -P_{Max,k,m}$ for all $(k, m) \in \mathcal{E}$). If not, then return $Is\_Satisficing = false$. Otherwise, continue to 5.2A.5.

5.2A.5 Add $\mathcal{E}_{Key}$ to $\boldsymbol{\mathcal{E}_{Satisficing}}$.

5.2A.6 For each $(k, m) \in \mathcal{E}_{Key}$:

    (a) Recursively call Subprocedure 5.2A for $\mathcal{E}_{Key} \setminus (k, m)$.

5.2A.7 If no recursive calls from 6a return true, then add $\mathcal{E}_{Key}$ to $\boldsymbol{\mathcal{E}_{Irr}}$.

5.2A.8 Return $Is\_Satisficing = true$.

Because the use of the set $\boldsymbol{\mathcal{E}_{Tested}}$ prevents multiple tests for a single candidate key line set $\mathcal{E}_{Key}$, the number of calls to Subprocedure 5.2A is limited by the number of subsets of $\mathcal{E}$. Since each subset can be represented as a bitfield of length L (where L is the number of lines in the graph $\mathfrak{G}$ and each bit indicates membership of the

corresponding line in the subset), then there are 2^L possible subsets of $\mathcal{E}$. Each call to Subprocedure 5.2A also makes a single call to Procedure 5.1, which has already been shown in Lemma 5.1.C to have computational complexity $O(L \, \mathcal{N}_{Max})$. Therefore, the computational complexity of Procedure 5.2 is $O(2^L \, L \, \mathcal{N}_{Max})$. Because of its high computational complexity, it may be difficult to find constraint-satisficing key line sets for large (or highly interconnected) networks using Procedure 5.2.

5.4.2 Discussion on Procedure 5.2

Procedure 5.2 provides a simple search procedure to find all of the constraint-satisficing key line sets (as well as the irreducable and minimal constraint-satisficing key line sets) for a specified network $\mathfrak{G}$ on the expected operating range $\mathbb{P}$ with power-flow constraints $\mathbf{P_{Max}}$. It can be easily modified to search only until the first irreducable constraint-satisficing key line set below a certain size is found, which may be necessary for large networks.

Since (as was discussed in Section 5.3.6) the test provided by Procedure 5.1 and Theorem 5.1 is overly conservative for highly cyclical networks, then the search procedure provided by Procedure 5.2 may miss some valid constraint-satisficing key line sets for highly cyclical networks. Therefore, the sets $\mathcal{E}_{Satisficing}$ and $\mathcal{E}_{Irr}$ should be considered to represent a selection of the (irreducable) constraint-satisficing key line sets for a given network and expected operating range, not necessarily all possible such sets. In addition, $\mathcal{E}_{Min}$ represents the set of the minimal constraint-satisficing key line sets that were found, not necessarily the minimum possible. Improvements in the test procedure (based on tighter power-flow bounds) are needed to ensure that all possible constraint-satisficing key line sets are found.

5.5 Constraint-Satisficing Key Line Sets for Selected Example Networks

We will now present several simple example networks to illustrate the concept of constraint-satisficing key line sets and application of Procedure 5.1, Theorem 5.1, and Procedure 5.2.

5.5.1 Six-Bus Radial Network

Consider again the simple six-bus radial network used for simulation in Chapter 4, a single-line diagram of which is shown in Figure 5.2. In order to assess the find the constraint-satisficing key line sets of this network, we must define the expected operating range $\mathbb{P}$ (in terms of generation and load constraint values $P_{G,Max,k}$, $P_{G,Min,k}$, and $P_{L,Max,k}$ to each bus $k \in \mathcal{V}$), which is shown in Table 5.1 below.
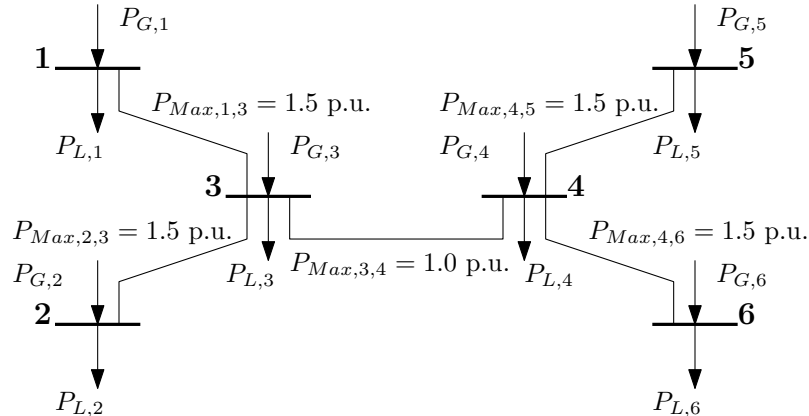
Figure 5.2: Single Line Diagram of Example Six-Bus Radial Network

In Simulation 4.5, this network lost synchronization due to violation of the line power-flow constraint on line $(3,4)$ using traditional droop control under conditions within the expected operating range defined in Table 5.1. Therefore, we would expect that Procedure 5.1 would show the bounding values on line $(3,4)$ to be outside of $\pm P_{Max,3,4}$. Table 5.2 shows the results of Procedure 5.1 applied to this network with $\mathcal{E}_{Key} = \emptyset$ (no constraint enforcement, as in Simulation 4.5), which does in fact show that the bounds on $P_{Line,3.4}$ are outside $\pm P_{Max,3,4}$. This is because the available

Table 5.1: Six-Bus Radial Network: Expected Operating Range Generation and Load Bound Values

Bus	$P_{G,Max}$	$P_{G,Min}$	$P_{L,Max}$
1	1.0	0.0	1.0
2	1.0	0.0	1.0
3	1.0	−1.0	4.0
4	1.0	−1.0	4.0
5	1.0	0.0	1.0
6	1.0	0.0	1.0

sourcing power in the subnetworks on either side of line $(3, 4)$ ($P_{UBound,Sourcing,3,4} = 3.0$ p.u. and $P_{LBound,Sourcing,3,4} = -3.0$ p.u.) are larger than $\pm P_{Max,3,4} = \pm 1.0$ p.u. (and therefore the structure of the network is not sufficient to enforce $|P_{Line,3,4}| \leq P_{Max,3,4}$). Therefore, (by Theorem 5.1) $\mathcal{E}_{Key} = \emptyset$ is not a constraint-satisficing key line set for this network and expected operating range $\mathbb{P}$ as defined in Table 5.1.

Table 5.2: Six-Bus Radial Network: Results of Procedure 5.1 for $\mathcal{E}_{Key} = \emptyset$

i	k	m	In $\mathcal{E}_{Key}$?	$P_{UBound,Sourcing}$	$P_{UBound,Sinking}$	$P_{LBound,Sourcing}$	$P_{LBound,Sinking}$	P_{UBound}	P_{LBound}	P_{Max}	Constraints Met?
1	1	3	False	1.0	13.0	−5.0	−1.0	1.0	−1.0	1.5	True
2	2	3	False	1.0	13.0	−5.0	−1.0	1.0	−1.0	1.5	True
3	3	4	False	3.0	7.0	−3.0	−7.0	3.0	−3.0	1.0	False
4	4	5	False	5.0	1.0	−1.0	−13.0	1.0	−1.0	1.5	True
5	4	6	False	5.0	1.0	−1.0	−13.0	1.0	−1.0	1.5	True

Since the line power flow on line $(3, 4)$ is not bounded within its constraint on the expected operating range, it makes sense that we should add it to the key line set $\mathcal{E}_{Key}$. In addition, all other lines in the network are incident to leaf buses, and therefore are constrained by the generation and load constraints on their incident leaf buses. Therefore, $\mathcal{E}_{key} = \{(3, 4)\}$ would seem to be an obvious candidate key

line set. Application of Procedure 5.2 to this network does in fact confirm that $\mathcal{E}_{key} = \{(3,4)\}$ is the unique irreducable (and unique minimal) constraint-satisficing key line set for this network. The results of Procedure 5.1 applied to this network with $\mathcal{E}_{key} = \{(3,4)\}$ are shown in Table 5.3, which reveal that enforcement of the line power-flow constraint $|P_{Line,3,4}| \leq P_{Max,3,4}$ is sufficient to ensure satisfaction of the line power-flow constraints on all lines in the network across the entire expected operating range.

Table 5.3: Six-Bus Radial Network: Results of Procedure 5.1 for $\mathcal{E}_{Key} = \{(3,4)\}$

i	k	m	In $\mathcal{E}_{Key}$?	$\mathbf{P}_{\text{UBound,Sourcing}}$	$\mathbf{P}_{\text{UBound,Sinking}}$	$\mathbf{P}_{\text{LBound,Sourcing}}$	$\mathbf{P}_{\text{LBound,Sinking}}$	$\mathbf{P}_{\text{UBound}}$	$\mathbf{P}_{\text{LBound}}$	$\mathbf{P}_{\text{Max}}$	Constraints Met?
1	1	3	False	1.0	7.0	-3.0	-1.0	1.0	-1.0	1.5	True
2	2	3	False	1.0	7.0	-3.0	-1.0	1.0	-1.0	1.5	True
3	3	4	True	1.0	1.0	-1.0	-1.0	1.0	-1.0	1.0	True
4	4	5	False	3.0	1.0	-1.0	-7.0	1.0	-1.0	1.5	True
5	4	6	False	3.0	1.0	-1.0	-7.0	1.0	-1.0	1.5	True

5.5.2 Six-Bus Meshed Network

Procedure 5.1 and Theorem 5.1 also apply to networks containing cycles, albeit with some limitations. Consider again the six-bus meshed network that was used for simulation in Chapter 3, a single-line diagram of which is shown in Figure 5.3. We define the expected operating range $\mathbb{P}$ of this network by the generation and load constraint values shown in Table 5.4.

Since this network contains a cycle (consisting of lines $\{(4,5),(5,6),(4,6)\}$), then in order to apply Procedure 5.1 we must select $\mathcal{E}_{Key}$ so that at least one line in the cycle is a key line. Recall that in Simulation 3.2, this network lost synchronization across the cut consisting of lines $(4,5)$ and $(4,6)$ due to a load step within the expected operating
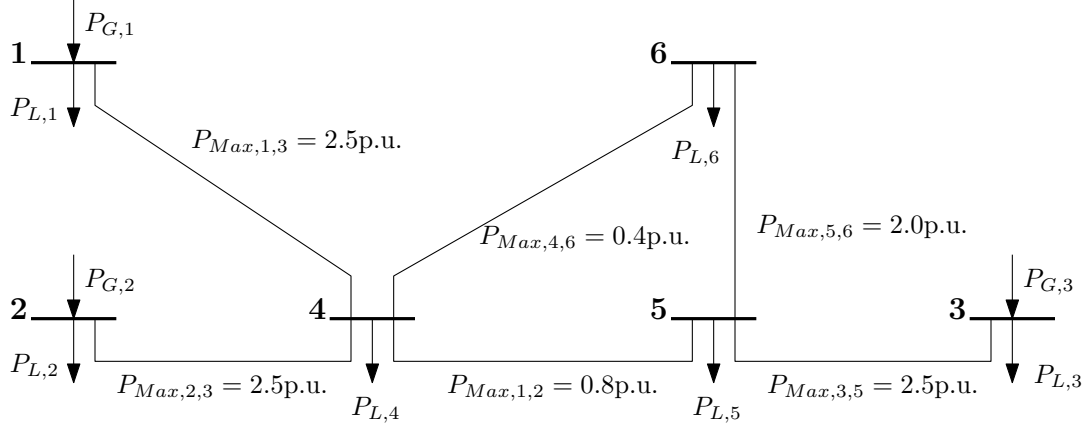
Figure 5.3: Single Line Diagram of Example Six-Bus Meshed Network

Table 5.4: Six-Bus Meshed Network: Expected Operating Range Generation and Load Bound Values

Bus	$P_{G,Max}$	$P_{G,Min}$	$P_{L,Max}$
1	1.0	0.0	1.0
2	1.0	0.0	1.0
3	1.0	−1.0	4.0
4	1.0	−1.0	4.0
5	1.0	0.0	1.0
6	1.0	0.0	1.0

range defined in Table 5.4. Application of Procedure 5.2 to this network reveals that $\mathcal{E}_{Key} = \{(4,5),(4,6)\}$ is the unique irreducable (and unique minimal) constraint-satisfising key line set for this network and expected operating range. Results of Procedure 5.1 applied to this network with $\mathcal{E}_{Key} = \{(4,5),(4,6)\}$ are shown in Table 5.5.

The results in Table 5.5 show that $\mathcal{E}_{Key} = \{(4,5),(4,6)\}$ is indeed a constraint-satisfising key line set for the example six-bus meshed network, since $P_{UBound,k,m} \leq P_{Max,k,m}$ and $P_{LBound,k,m} \geq -P_{Max,k,m}$ for all lines $(k,m) \in \mathcal{E}$. Therefore, explicit enforcement of *both* $|P_{Line,4,5}| \leq P_{Max,4,5}$ and $|P_{Line,4,6}| \leq P_{Max,4,6}$ is sufficient to ensure that all line power-flow constraints are met across the entire expected operating range of the network.

Table 5.5: Six-Bus Meshed Network: Results of Procedure 5.1 for $\mathcal{E}_{Key} = \{(4,5),(4,6)\}$

i	k	m	In $\mathcal{E}_{Key}$?	$P_{\text{UBound,Sourcing}}$	$P_{\text{UBound,Sinking}}$	$P_{\text{LBound,Sourcing}}$	$P_{\text{LBound,Sinking}}$	P_{UBound}	P_{LBound}	P_{Max}	Constraints Met?
1	4	1	False	2.2	2.0	-1.0	-5.2	2.0	-1.0	2.5	True
2	4	2	False	2.2	2.0	-1.0	-5.2	2.0	-1.0	2.5	True
3	5	3	False	1.2	2.0	-1.0	-4.7	1.2	-1.0	2.5	True
4	5	4	True	0.8	0.8	-0.8	-0.8	0.8	-0.8	0.8	True
5	6	4	True	0.4	0.4	-0.4	-0.4	0.4	-0.4	0.4	True
6	6	5	False	0.4	4.8	-1.8	-1.9	0.4	-1.8	2.0	True

5.5.3 Star Network

The following example is an interesting special case, which shows that for some networks, the key line set $\mathcal{E}_{Key} = \emptyset$ may be constraint-satisficing. Consider the network structure whose single-line diagram is shown in Figure 5.4. The underlying power-flow structure graph of this network is a *star graph*, meaning that it consists of a single center bus to which all other buses are directly connected (and no cycles are present). The center bus is a load bus, while all leaf buses are inverter buses. This type of power-flow structure might occur when a set of inverters are connected in parallel to power a single large load. Generation and load bounds defining the expected operating region $\mathbb{P}$ are shown in Table 5.6.

Results from application of Procedure 5.1 to this network with $\mathcal{E}_{Key} = \emptyset$ are shown in Table 5.7 below. Since all line flows are bounded within their respective constraints, then (by Theorem 5.1) $\mathcal{E}_{Key} = \emptyset$ is a constraint-satisficing key line set for this network under the expected operating range in Table 5.6. This reveals that for this network and expected operating range, *no explicit constraint enforcement is required to bound the network within the safe region.*

In fact, this result applies for most networks whose underlying graph is a star
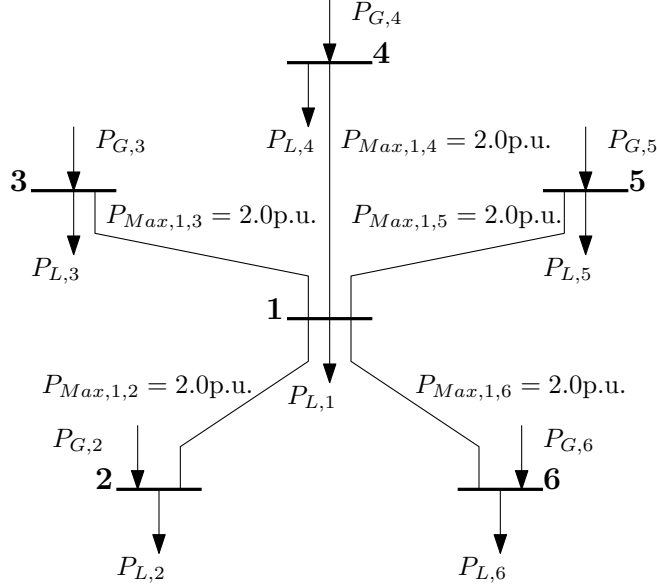
Figure 5.4: Single Line Diagram of Example Six-Bus Star Network

Table 5.6: Six-Bus Star Network: Generation and load bound values for Procedure 5.1

Bus	$\mathbf{P_{G,Max}}$	$\mathbf{P_{G,Min}}$	$\mathbf{P_{L,Max}}$
1	0.0	0.0	5.0
2	1.0	-1.0	1.0
3	1.0	-1.0	1.0
4	1.0	-1.0	1.0
5	1.0	-1.0	1.0
6	1.0	-1.0	1.0

configuration. This is because in a star configuration, each line is incident to a leaf bus, and therefore on the expected operating range each line power flow is bounded by the sourcing and sinking capacity of its incident leaf bus ((104) and (105)). For most power networks, the line capacity will be large enough to support the sourcing and sinking capacity of the incident leaf bus ($P_{G,Max,k} \leq P_{Max,k,1}$ and $-P_{G,Min,k} + P_{L,Max,k} \leq P_{Max,k,1}$ for each leaf bus $k \in \{2 \ldots N\}$, assuming the center bus is bus 1 and N total buses). In this case, then $P_{UBound,k,1} \leq P_{G,Max,k} \leq P_{Max,k,1}$ and $P_{LBound,k,1} \leq -P_{G,Min,k} + P_{L,Max,k} \leq P_{Max,k,1}$ for all $k \in \{2 \ldots N\}$, and therefore Theorem 5.1 applies. This confirms the result of [66], which found that for star-type

Table 5.7: Six-Bus Star Network: Results of Procedure 5.1 for $\mathcal{E}_{Key} = \emptyset$

i	k	m	In $\mathcal{E}_{Key}$?	$P_{\text{UBound,Sourcing}}$	$P_{\text{UBound,Sinking}}$	$P_{\text{LBound,Sourcing}}$	$P_{\text{LBound,Sinking}}$	P_{UBound}	P_{LBound}	P_{Max}	Constraints Met?
1	1	2	False	4.0	2.0	-1.0	-13.0	2.0	-1.0	2.0	True
2	1	3	False	4.0	2.0	-1.0	-13.0	2.0	-1.0	2.0	True
3	1	4	False	4.0	2.0	-1.0	-13.0	2.0	-1.0	2.0	True
4	1	5	False	4.0	2.0	-1.0	-13.0	2.0	-1.0	2.0	True
5	1	6	False	4.0	2.0	-1.0	-13.0	2.0	-1.0	2.0	True

networks of droop inverters, as long as the lines have larger capacity than the inverters then synchronization is guaranteed.

5.6 Chapter Conclusions

In this chapter, we have defined the concept of constraint-satisficing key line sets based on an expected operating range of the network and a set of key lines whose line power-flow constraints are assumed to be met. A constraint-satisficing key line set is a subset of the network lines such that satisfaction of the key line constraints, along with operation within the expected operating range, is sufficient to ensure that *all* line power-flow constraints are satisfied (Definition 5.2). By applying Kirchoff's law at each bus, we developed a procedure for bounding all line power flows in the network under the assumption of satisfaction of key line power-flow constraints and generation and load values within the expected operating range (Procedure 5.1). We then showed that if the resulting bound values for each line power-flow bounds are within its constraints, then the network is constraint-satisficing for the specified key line set and expected operating range (Theorem 5.1). Finally, we developed an inductive search procedure (Procedure 5.2) which allows generation of constraint-satisficing key line sets (as well as irreducable or minimal constraint-satisficing key

line sets) for a given network and expected operating range.

Both the generation of a constraint-satisficing key line set (via Procedure 5.2) and the test of its validity (via Procedure 5.1 and Theorem 5.1) require access to global network data: the entire network structure (represented by graph $\mathfrak{G}$), the expected operating range (represented by generation and load constraint vectors $\mathbf{P_{G,Max}}$, $\mathbf{P_{G,Min}}$, and $\mathbf{P_{L,Max}}$), and the line power-flow constraints (represented by the power-flow constraint vector $\mathbf{P_{Max}}$). Therefore, selection and validation of a constraint-satisficing key line set must be performed with global knowledge, preferably during power network design or refitting. However, as we will show in the following chapter, once a constraint-satisficing key line set $\mathcal{E}_{Key}$ has been found, then it is possible to use CED-controlled inverters to enforce the key line constraints (and therefore ensure robust synchronization and power sharing within the expected operating range) without need for communication or system level control.

CHAPTER VI

SPARSE APPLICATION OF CONSTRAINT-ENFORCING DROOP CONTROLLER FOR IMPROVED SYNCHRONIZATION OF INVERTER-BASED AC NETWORKS

In Chapter 4, a novel constraint-enforcing frequency-droop controller was introduced, and a method shown for its application to provide robust frequency synchronization and power sharing in all-active-bus, acyclic inverter-based power networks. This control method is based on the observation (from Chapter 3) that synchronization of an inverter-based network operating frequency-droop control can be ensured by enforcement of a specified line power-flow constraint on each line in the system (Theorem 3.5). However, while it is possible to construct a network of the type discussed in Chapter 4, most power networks are not acyclic in structure, nor is it feasible to place an inverter at each bus in a network, and therefore the method in Chapter 4 is not directly applicable to most power networks in practice. In this chapter, a less strict (and therefore much more practical) approach is presented, which allows sparse deployment of a few constraint-enforcing inverters in a network (which need not be acyclic) while maintaining most of the desirable properties produced by the approach of Chapter 4. This will be accomplished by application of CED-controlled inverters to enforce the power-flow constraints of *only the lines of a constraint-satisficing key line set* (as defined in Chapter 5), thereby ensuring satisfaction all of the power-flow constraints of the network (on the given expected operating range) and bounding its voltage-angle state trajectory to the safe region.

6.1 Challenges in Sparse Application of CED

In this chapter, we will generalize the class of networks we consider for application of CED for the purpose of guaranteeing frequency synchronization and power sharing. The networks considered in this chapter consist of a mix of inverter buses and network buses. In addition, some inverters may operate CED control, while others operate traditional frequency-droop. We will refer to networks of this class as *mixed-bus inverter-based networks*. Moving from the all-active-bus, acyclic networks considered in Chapter 4 to mixed-bus inverter-based networks will require a changes in both the control approach and the method of analysis required to show frequency synchronization and power sharing.

6.1.1 Implicit Enforcement of Line Power-Flow Constraints

The results of Chapter 3 show that guaranteed frequency synchronization requires enforcement of a specified line power-flow constraint on *each* line in the system. The control method presented in Chapter 4 provides this enforcement by placing a CED-controlled inverter at each bus and using it to enforce the constraint on each incident line, that is, by explicitly enforcing each line power-flow constraint with two incident CED-controlled inverters. However, a sparse application of CED-controlled inverters means that many lines will not be directly incident to a CED-controlled inverter, and therefore many such constraints will not be explicitly enforced. In Chapter 5, we developed the concept of *constraint-satisfying key line sets*, which show that enforcement of the line power-flow constraints associated with only the key lines in a network is sufficient to ensure satisfaction of all the constraints (assuming that the network generation and load are within a given expected operating range). In this chapter, we will develop a distributed control method that allows CED inverters to be placed and configured in the network so as to explicitly enforce only the line power-flow constraints associated with lines in a constraint-satisfying key line set.

This implicitly enforces the line power-flow constraint on each line in the network, thus bounding the network within the safe region of the voltage-angle space.

6.1.2 Assymetry of Adaptive Line Tensions

In addition, sparse deployment of CED-controlled inverters means that some lines may be incident to only a single CED-controlled inverter. Therefore, the adaptive line tension values (see Section 4.2) for some key lines may be line-asymmetric, that is, the line may effect the dynamics of one incident bus differently than the other. For example, consider a line $(k, m) \in \mathcal{E}$ where bus k is a constraint-enforcing inverter bus and bus m is a traditional droop inverter bus. The adaptive line tension associated with line (k, m) appearing in the dynamics of δ_k is $\gamma_{k,m} P_{Line,k,m}$, while that appearing in the dynamics of δ_m is simply $P_{Line,m,k}$. This means that the center-of-mass frequency $\Delta \omega_{COM}$ of a network with sparse CED deployment may *not* be independent of state, and that the network energy function U (41) may not be non-increasing everywhere on the safe region. Therefore, a more general method of showing the convergence of frequency (and therefore power sharing) of the network will be required.

6.1.3 Problems with Unbounded Line Gains

The control approach presented in Chapter 4 requires that each CED-controlled inverter apply an unbounded adaptive gain to each incident line (see Definition 4.2). This was due to the need for the adaptive line tension value to become "large enough" to overcome all other dynamic tensions as the line near its constraint. However, while in theory (and often in practice) this results in enforcement of the associated line power-flow constraint, in practice unbounded gains may interact with unmodeled feedback delays to result in oscillations, or even instability. Therefore, it is desirable to move to a bounded form of the adaptive line gain function, while ensuring that the associated line power-flow constraint is still enforced. In this chapter, we will present a class of bounded adaptive line gain functions, and show that it is still possible to

enforce the specified line power constraints using functions of that class.

6.1.4 Counterexample to Naive Approach for Sparse Deployment of CED Inverters

Finally, to allow sparse deployment of CED-controlled inverters, it is necessary (as we will show below) to modify the CED control law so that it applies an adaptive gain to only *a single incident line* (rather than all incident lines as in Definition 4.1). This is because it is not, in general, possible for a single constraint-enforcing inverter to enforce multiple constraints simultaneously without the assistance of similar inverters on the adjacent buses. To illustrate this phenominon, we will provide an example of a naive approach to sparse deployment of CED based on a given constraint-satisficing key line set in a network using the all-incident-line CED control law (50).

Consider the simple three-bus power network illustrated in Figure 6.1. The set of all lines $\mathcal{E}_{Key} = \mathcal{E} = \{(1,2),(2,3)\}$ is trivially a constraint-satisficing key line set for this network (Lemma 5.2.A). A naive approach to enforcement of the line power-flow constraints on $\mathcal{E}_{Key}$ might call for the inverter at bus 2 to operate the all-incident-lines CED control law (50) (thereby attempting to enforce both the constraints $|P_{Line,1,2}| \leq P_{Max,1,2}$ and $|P_{Line,2,3}| \leq P_{Max,2,3}$), while inverters 1 and 3 operate traditional frequency droop. As we will show below, under some conditions it is not possible for inverter 2 alone to enforce both of these constraints at the same time without the participation of inverters 1 and/or 3 in the constraint enforcement.
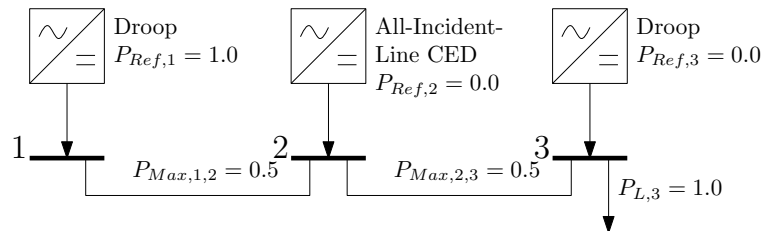
Figure 6.1: Three-Bus Network for Counterexample

Consider the inputs $\mathbf{P_{Ref}}$ and $\mathbf{P_L^0}$ as shown in Table 6.1, and select $P_{Max,1,2} =$

146

$P_{Max,2,3} = 0.5$ p.u.

Table 6.1: Bus Configuration for Three-Bus Counterexample

Bus #	Type	$\mathbf{P_{Ref}}$ (p.u.)	$\mathbf{P_L^0}$ (p.u.)
1	Droop	1.0	0.0
2	All-Incident-Line CED	0.0	0.0
3	Droop	0.0	1.0

By substituting the input conditions in Table 6.1 into the droop control law (4) and all-incident-lines CED control law (50), we obtain the dynamics of this network as follows:

$$\Delta\omega_1 = R_1[P_{Ref,1} - P_{L,1}^0 - P_{Line,1,2}] = R[1.0 - P_{Line,1,2}] \tag{126}$$

$$\Delta\omega_2 = R_2[P_{Ref,2} - P_{L,2}^0 + \gamma_{1,2}(|P_{Line,1,2}|)P_{Line,1,2} - \gamma_{2,3}(|P_{Line,2,3}|)P_{Line,2,3}]$$

$$= R[\gamma_{1,2}(|P_{Line,1,2}|)P_{Line,1,2} - \gamma_{2,3}(|P_{Line,2,3}|)P_{Line,2,3}] \tag{127}$$

$$\Delta\omega_3 = R_3[P_{Ref,3} - P_{L,3}^0 + P_{Line,2,3}] = R[-1.0 + P_{Line,2,3}] \tag{128}$$

where we have assumed that $R_1 = R_2 = R_3 = R > 0$

At steady state (frequency agreement, where $\Delta\omega_1 = \Delta\omega_2 = \Delta\omega_3$) the following simultaneous inequalities follow from (126) and (128):

$$\Delta\omega_2 \leq R[1.0 - P_{Line,1,2}] \tag{129}$$

$$\Delta\omega_2 \geq R[1.0 - P_{Line,1,2}] \tag{130}$$

$$\Delta\omega_2 \leq R[-1.0 + P_{Line,2,3}] \tag{131}$$

$$\Delta\omega_2 \geq R[-1.0 + P_{Line,2,3}] \tag{132}$$

In addition, if inverter 2 succeeds at enforcing its incident line power-flow constraints, then the following inequalities also apply:

$$P_{Line,1,2} \leq P_{Max,1,2} = 0.5 \tag{133}$$

$$P_{Line,2,3} \leq P_{Max,2,3} = 0.5 \tag{134}$$

147

By Nonhomogeneous Farkas Lemma (see [57, Theorem 3.1.2]), we can combine (130) with (133) and (131) with (134) respectively to obtain the following inequalities:

$$\Delta\omega_2 \geq R[1.0 - P_{Max,1,2}] = 0.5R \tag{135}$$

$$\Delta\omega_2 \leq R[-1.0 + P_{Max,2,3}] = -0.5R \tag{136}$$

Since $R > 0$, then (135) and (136) are in contradiction. Therefore, the polytope defined by the constraints (129)-(134) is infeasible, and so there does not exist a steady state solution to the example network such that the constraints on lines $(1,2)$ and $(3,4)$ are enforced. This is due to the fact that it is not possible for the single control variable $\Delta\omega_2$ to satisfy both the constraint associated with line $(1,2)$ and the constraint associated with line $(2,3)$ simultaneously; inverter 2 is "pulled" in opposite directions by the adaptive line tensions $\gamma_{1,2}P_{Line,1,2}$ and $\gamma_{2,3}P_{Line,2,3}$. Therefore, it is not possible for the CED inverter on bus 2 to simultaneously enforce the constraints $|P_{Line,1,2}| \leq P_{Max,1,2}$ and $|P_{Line,2,3}| \leq P_{Max,2,3}$ without the participation of inverters 1 and/or 3.

The preceeding example shows that a naive approach to sparse deployment of constraint-enforcing inverters, based on deployment of an inverter operating the all-incident-line CED control law (50) adjacent to each line in a constraint-satisficing key line set, is not (in general) capable of enforcing the line power-flow constraints on all of the the key lines, since a single control variable (the inverter output frequency) may not in general be capable of satisfying all of the necessary constraints simulate-nously. Therefore, is not capable of enforcing the line power-flow constraints on the lines in $\mathcal{E}_{Key}$, and so cannot provide the desired property of guaranteed frequency synchronization and power sharing. In this chapter, we will show that this limitation can be overcome by modifying the CED control law so that it applies an adaptive gain to only a single incident line, thereby ensuring that conflicts between the constraints never occur and allowing each CED inverter to sucessfully enforce only its

single assigned line power-flow constraint.

6.2 Approach to Sparse Application of CED in Inverter-Based Networks

In order to overcome the issues described in the previous section, of an inverter-based network, and provide guaranteed frequency synchronization and power sharing (on the expected operating range) by sparse application of CED-controlled inverters, it will be necessary to develop a more nuanced approach to both the method of control and of analysis. In particular, a *bounded gain, single-line-constraint-enforcing* form of the CED control law must be developed, and the concept of a *constraint-satisficing droop control configuration* developed and validated.

6.2.1 Class of Networks Under Considertion

In this chapter, we will consider a more general class of networks than in the previous chapters. Our new class of networks consists of a mix of inverter buses and network buses. In addition, some inverters will operate the traditional frequency-droop control law (4), while others will operate a novel form of the CED control law (specified below). More formally, we define a *mixed-bus inverter-based network* as follows:

Definition 6.1 (Mixed-Bus Inverter-Based Networks)**.** *A* mixed-bus inverter-based network *is a 3-phase AC power network, which is identical to a lossless droop inverter-based power network with ideal voltage regulation (Definition 3.1) with the following differences:*

6.1.A Each bus $k \in \mathcal{V}$ is exactly one of the following:

(a) A droop-inverter bus, in which case $k \in \mathcal{V}_{Droop}$, and inverter k implements the traditional frequency-droop control law (4).

(b) A CED-inverter bus, in which case $k \in \mathcal{V}_{CED}$, and inverter k implements the bounded, single-line CED control law (to be defined).

149

(c) A network bus, in which case $k \in \mathcal{V}_{Net}$, and there is no inverter at bus k.

6.1.B Each line $(k, m) \in \mathcal{E}$ is assigned a line-even, constant maximum power-flow value $P_{Max,k,m} = P_{Max,m,k}$, where $0 < P_{Max,k,m} < Y_{k,m} V_k V_m$.

6.1.C Each bus $k \in \mathcal{V}$ has assigned generation and load bounds $P_{G,Max,k}$, $P_{G,Min,k}$, and $P_{L,Min,k}$, which defining the network expected operating range $\mathbb{P}$ as by Definition 5.1.

Similar to the previous chapters, the underlying structure of the power network is represented by the graph $\mathfrak{G} = (\mathcal{V}, \mathcal{E})$. As such, a mixed-bus inverter-based network can be identified by the triple $(\mathfrak{G}, \mathbb{P}, \mathbf{P_{Max}})$, where $\mathfrak{G}$ represents its power-flow structure, $\mathbb{P}$ represents its expected operating range, and the vector $\mathbf{P}_{Max} \in \mathbb{R}^L$ represents its assigned line power-flow constraints.

In this chapter, we will develop a control method to enforce the line-power flow constraints associated with a a selected constraint-satisficing key line set $\mathcal{E}_{Key}$ for a power network $\mathfrak{G}$ on the expected operating range $\mathbb{P}$. The key line set $\mathcal{E}_{Key}$ should be selected from the set of constraint-satisficing key line sets for $(\mathfrak{G}, \mathbb{P}, \mathbf{P_{Max}})$ determined by Procedure 5.2. In general there may exist many such constraint-satisficing key line sets for a given network, and a strict method for determination of the "best" such set is beyond the scope of this work (since the definition of the "best" constraint-satisficing key line set for any given network is highly application-dependent). For most appliations, an irreducable constraint-satisficing key line set should be selected (since otherwise it might be possible to reduce cost by eliminating some CED-controlled inverters), and often a minimal constraint-satisficing key line set should be selected. In the remainder of this chapter, we will assume that a constraint-satisficing key line set $\mathcal{E}_{Key}$ has been selected and treat it as given.

6.2.2 Approach to Sparse Application of CED

Successful guarantee of frequency synchronization and power sharing in an inverter-based network with sparse deployment of CED-controlled inverters involves the careful placement and configuration of CED-controlled inverters in the network. Such a configuration of CED inverters in the network is known as a *constraint-satisficing droop control configuration*. In a constraint-satisficing droop control configuration, CED inverters are placed and configured so that they are able to enforce the line power-flow constraints associated with the key lines in the selected constraint-satisficing key line set $\mathcal{E}_{Key}$, thereby implicitly enforcing the line power-flow constraints on *all* lines in the network on the expected operating range $\mathbb{P}$. We will show that this in turn bounds the network voltage-angle trajectory onto the safe region Θ_{Safe} (as defined in Definition 3.8) and provides the desired properties of guaranteed frequency synchronization and constrained power sharing on the entire expected operating range $\mathbb{P}$.

Because of its non-local dependence on the graph structure and parameters, the creation and validation of a constraint-satisficing droop control configuration is *not* a distributed operation, and must be performed using global knowledge of the network structure and parameters. However, once this operation has been performed and CED-controlled inverters placed and configured, it is possible for them to enforce the line power-flow constraints and guarantee frequency synchronization and power sharing using only local measurements and control. Therefore, the sparse deployment of CED-controlled inverters requires a two-stage approach: A placement and configuration stage (performed with global knowledge), followed by an operation stage (which is purely distributed). In this dissertation, we assume that the placement and configuration stage is performed during power network design (either of a new network or retrofitting an existing one).

In Section 6.1.4, it was shown that the all-incident-line CED control law developed

in Chapter 4 is not necessarily capable of enforcing line power-flow constraints on its incident lines when deployed sparsely in a network, and that this is due to conflicts that can arise between the constraints. To avoid this issue, we will introduce a new form of the CED control law that enforces only a single incident line power-flow constraint. In addition, this form of the CED control law uses a bounded adaptive gain function, which improves performance under control delays. This requires a selection of the maximum adaptive gain, which must be sufficiently large to overcome any dynamic tension that could cause the line constraint to be violated. As we will show, the maximum possible tension that could cause constraint violation is bounded on the expected operating range, and therefore a bounded maximum gain can be selected so as to overcome it. Determination of this maximum gain, and proof that it is capable of enforcing the (single) designated incident power-flow constraint, appears later in this chapter.

Finally, it is necessary to show that once CED inverters have been deployed and configured so as to enforce the key line constraints (and thereby implicitly all of the line constraints), then frequency synchronization and constrained sharing of real power between inverters will necessarily follow. Since the class of networks now under consideration does not necessarily exhibit symmetric adaptive line tensions, then the energy-function based method developed in Chapters 3 and 4 is no longer applicable. Therefore, a more general approach based on the Contraction Property (see [81]) of the class of network under consideration will be developed later in this chapter, which will show that deployment of CED inverters to enforce key line constraints is sufficient to guarantee frequency synchronization and (constrained) power sharing on the expected operating range.

6.2.3   Constraint-Satisficing Droop Control Configuration

A constraint-satisficing droop control configuration (associated with a given expected operating range $\mathbb{P}$ and constraint-satisficing key line set $\mathcal{E}_{Key}$) is a specification of how CED-controlled inverters are to be deployed in a network and configured so that line power-flow constraints associated with the lines in the selected constraint-satisficing key line set $\mathcal{E}_{Key}$ can be enforced, thereby bounding the network within the safe region of the voltage-angle state space.

Once a constraint-satisficing key line set $\mathcal{E}_{Key}$ has been determined for a given mixed-bus network $(\mathfrak{G}, \mathbb{P}, \mathbf{P_{Max}})$, in order to form a constraint-satisficing droop control configuration, CED-controlled inverters must be placed and configured to enforce the power-flow constraints for all key lines $(k, m) \in \mathcal{E}_{Key}$. Since we now employ a form of the CED control law that only enforces a single line power-flow constraint per CED inverter, it is necessary to place a CED-controlled inverter incident to each line in $\mathcal{E}_{Key}$, and to configure that inverter so that it enforces the key constraint. We represent the placement of the CED-controlled inverters with the CED inverter bus set $\mathcal{V}_{CED} \subset \mathcal{V}$, where $k \in \mathcal{V}_{CED}$ indicates that bus k has an attached inverter operating the new single-incident-line CED control law. We will also introduce the *CED assignment function* $\sigma(k)$ to map each CED-controlled inverter $k \in \mathcal{V}_{CED}$ to the line whose constraint it is assigned to enforce:

Definition 6.2 (CED Assignment Function $\sigma(k)$)**.** *The CED Assignment Function $\sigma : \mathcal{V}_{CED} \mapsto \mathcal{V}$ is a map of CED inverters to buses, where $\sigma(k) = m$ indicates that the CED inverter at bus k is assigned to enforce the line power-flow constraint on the line $(k, m) \in \mathcal{E}$. $\sigma(k)$ must be a member of $\mathcal{N}(k)$.*

Since we now use bounded adaptive gains in the CED control law, the adaptive gain $\gamma_{k,m}$ for a key line $(k, m) \in \mathcal{E}_{Key}$ increases to a bounded constant $\gamma_{Max,k,m}$ (rather

than to ∞ as for the unbounded form) as $|P_{Line,k,m}|$ approaches $P_{Max,k,m}$. As in Chapter 4, the adaptive gain function $\gamma_{k,m}(|P_{Line,k,m}|)$ must be designed so that the line adaptive tension $\gamma_{k,m}P_{Line,k,m}$ becomes large enough as $|P_{Line,k,m}|$ approaches $P_{Max,k,m}$ to overcome the opposing tensions and thereby enforce the constraint. Therefore, we must select the constant $\gamma_{Max,k,m}$ for each key line $(k,m) \in \mathcal{E}_{Key}$ large enough (but still bounded) to overcome the maximum opposing tensions. This is possible, since (as we will show later in this chapter) the maximum opposing tension is bounded on the expected operating range.

More formally, we define a constraint-satisficing droop control configuration as follows:

Definition 6.3 (Constraint-Satisficing Droop Control Configurations and Constraint-Satisficing Droop Inverter Networks)**.** *Consider a given mixed-bus inverter-based power network* $(\mathfrak{G}, \mathbb{P}, \mathbf{P_{Max}})$ *(Definition 6.1) and assume that there exists a given constraint-satisficing key line set* $\mathcal{E}_{Key}$ *for the network on* $\mathbb{P}$. *Then a* constraint-satisficing droop control configuration *consists of the following:*

6.3.A A Constraint-Satisficing CED Inverter Placement and Assignment: A placement $\mathcal{V}_{CED}$ *and assignment function* $\sigma : \mathcal{V}_{CED} \mapsto \mathcal{V}$ *meeting the requirements of Definition 6.6.*

6.3.B A Set of Key-line-enforcing $\gamma_{k,m}$ *Selections: A selection of key line adaptive gain function* $\gamma_{k,m}$ *(meeting the requirements of Definition 6.5) and associated enforcing bound constant* $\gamma_{Max,k,m}$ *(meeting the requirements of Definition 6.7) for each key line* $(k,m) \in \mathcal{E}_{Key}$.

A mixed-bus inverter-based network to which a constraint-satisficing droop control configuration has been applied is called a constraint-satisficing droop inverter network.

The primary goal of this chapter is to show that a deployment of CED inverters

meeting the requirements of Definition 6.3 is sufficient to guarantee frequency syn-chronziation and power sharing in an inverter-based power network on the expected operating range. In Section 6.3, we define the single-line CED control law, along with the class of bounded adaptive gain functions, and a specification for constraint-satisficing placement and assignments of such CED inverters. In Section 6.4, we develop a parametric condition for the bounded gain constant $\gamma_{Max,k,m}$ for each key line $(k, m) \in \mathcal{E}_{Key}$, and show that if the value of $\gamma_{Max,k,m}$ for each CED inverter bus k is selected accordingly then each line power-flow constraint in $\mathcal{E}_{Key}$ can be enforced by a single incident CED inverter, implying that the network voltage-angle state trajectory will be bounded in the safe region, in which all line constraints are met. In Section 6.5 we show that bounding operation within this safe region is sufficient to ensure frequency synchronization between inverters for the entire expected operating range. In Section 6.6, we derive the power sharing characteristics of constraint-satisficing droop inverter networks. Finally, in Section 6.7 we present several example applications of our method to guarantee frequency synchronization and power sharing of mixed-bus inverter-based networks for several different network structures.

6.3 Single-Line CED Control Law and Its Placement and Assignment

Once a valid constraint-satisficing key line set $\mathcal{E}_{Key}$ has been identified for a given network (as by Procedure 5.2A), then CED-controlled inverters must be placed and configured so as to explicitly enforce the line power-flow constraints $|P_{Line,k,m}| \leq P_{Max,k,m}$ on each key line $(k, m) \in \mathcal{E}_{Key}$. However, we have already shown that a naive approach to such placement (based on the all-incident-lines CED control law in Definition 4.1) is not sufficient to ensure the enforcement of the key line constraints in a mixed-bus network. Therefore, in this section, we introduce a new form of the CED control law in order to overcome challenges in its sparse deployment, as well as making it more robust in practice.

6.3.1 Bounded Gain, Single-Line-Constraint-Enforcing Droop Control Law

In the new form of the CED control law, an adaptive gain $\gamma_{k,m}$ is applied only to the line power flow associated with single assigned key line $(k,m) \in \mathcal{E}_{Key}$ where $m = \sigma(k)$, while all other line power-flow values are left at unity gain. This causes each CED-controlled inverter to be "responsible" for enforcing only a single incident line constraint, thus avoiding the possibility of fighting between the constraints as occured in the counterexample in Section 6.1.4. In addition, a bounded form of the adaptive gain function $\gamma_{k,m}$ is used. This makes the CED inverter response more robust to feeback delays. We therefore refer to the new form of the CED control law as the *bounded gain, single-line CED control law*.

We have already defined the the CED Assignment Function $\sigma(k)$, which maps each CED-controlled inverter $k \in \mathcal{V}_{CED}$ to the (single) line that it is assigned to enforce (Definition 6.2). Based on $\sigma(k)$, the new form of the CED control law is as follows:

Definition 6.4 (Single-Incident-Line CED Control Law). *The Single-Incident-Line form of the CED Control Law (at an arbitrary bus $k \in \mathcal{V}_{CED}$) is as follows:*

$$\Delta\omega_k = R_k \left[P_{Ref,k} - P_{L,k} - \sum_{m \in \mathcal{N}(k) \backslash \sigma(k)} P_{Line,k,m} - \gamma_{k,\sigma(k)}(|P_{Line,k,\sigma(k)}|)P_{Line,k,\sigma(k)} \right]$$

(137)

The Single-Incident-Line CED control law in Definition 6.4 differs from the All-Active-Bus CED control law in Definition 4.1 in that it applies an adaptive gain only to the single line power flow $P_{Line,k,m}$ where $m = \sigma(k)$. In addition, the adaptive gain function $\gamma_{k,m}(|P_{Line,k,m}|)$ will be selected from a bounded class of functions, rather than the unbounded class $\mathbf{\Gamma}_{Unbounded}$ in Definition 4.2. We will show in this chapter that the single-incident-line CED control law is capable of enforcing its assigned line power-flow constraint $|P_{Line,k,m}| \leq P_{Max,k,m}$ when deployed properly in a network (that is, when $\mathcal{V}_{CED}$, σ, and $\gamma_{Max,k,m}$ are selected to meet specified requirements).

6.3.2 Selection of Bounded Adaptive Gain Function $\gamma_{k,m}$

Similar to our approach in Chapter 4, the adaptive gain function $\gamma_{k,m}(|P_{Line,k,m}|)$ for each CED-controlled inverter $k \in \mathcal{V}_{CED}$ where $m = \sigma(k)$ is selected during control design so that it has a set of characteristics needed to enforce the *single* assigned line power-flow constraint $|P_{Line,k,m}| \leq P_{Max,k,m}$, and so that the CED-controlled inverter behaves identically to a traditional-droop-controlled inverter when the assigned constraint is inactive. In particular, we require that $\gamma_{k,m}$ be selected from the following class of functions:

Definition 6.5 (Feasible Class $\mathbf{\Gamma}_{Bounded}$ for $\gamma_{k,m}$). *A function $\gamma_{k,m} : [0 \quad \infty) \mapsto [1 \quad \gamma_{Max,k,m}]$ is a member of the class $\mathbf{\Gamma}_{Bounded}$ for given constants $P_{Max,k,m} > 0$ and $\gamma_{Max,k,m} \geq 1$ if it has the following characteristics:*

6.5.A $\gamma_{k,m}$ is Lipschitz continuous with respect to $|P_{Line,k,m}|$ for all $|P_{Line,k,m}|$.

6.5.B $\gamma_{k,m}$ is bounded by $\gamma_{Max,k,m}$:

$$1 \leq \gamma_{k,m}(|P_{Line,k,m}|) \leq \gamma_{Max,k,m} \text{ for all } |P_{Line,k,m}|.$$

6.5.C $\gamma_{k,m}$ equals unity for small $|P_{Line,k,m}|$:

$$\exists \ \epsilon_{k,m} \in (0 \quad 1) \text{ such that } \gamma_{k,m}(|P_{Line,k,m}|) = 1 \text{ for all } |P_{Line,k,m}| \leq (1 - \epsilon_{k,m})P_{Max,k,m}.$$

6.5.D $\gamma_{k,m}(|P_{Line,k,m}|)$ goes to $\gamma_{Max,k,m}$ as $|P_{Line,k,m}|$ approaches $P_{Max,k,m}$:

$$\lim_{|P_{Line,k,m}| \to P_{Max,k,m}} \gamma_{k,m}(|P_{Line,k,m}|) = \gamma_{Max,k,m}.$$

6.5.E $\gamma_{k,m}$ is non-decreasing in $|P_{Line,k,m}|$:

$$\frac{\partial \gamma_{k,m}}{\partial |P_{Line,k,m}|} \geq 0 \ \forall \ |P_{Line,k,m}|.$$

Any function that meets the requirements of Definition 6.5 (and is therefore a member of the set $\Gamma_{Bounded}$) may be selected for the adaptive gain function $\gamma_{k,m}$ for $(k, m) \in \mathcal{E}_{Key}$. We will show in this chapter that for a properly deployed CED

inverter k, the selection of an adaptive gain function $\gamma_{k,m}$ meeting the requirements of Definition 6.5 is sufficient to ensure that the single assigned line power-flow constraint $|P_{Line,k,m}| \leq P_{Max,k,m}$ where $m = \sigma(k)$ when $\gamma_{Max,k,m}$ is chosen to meet specified requirements.

Consider the example function $\gamma_{k,m}$ as defined in (138), a plot of which is shown in Figure 6.2. This function meets the requirements of Definition 6.5, and therefore is a valid choice for $\gamma_{k,m}$ for given values of $P_{Max,k,m}$, $\gamma_{Max,k,m}$, and $\epsilon_{k,m}$. Throughout the examples presented in this chapter, we will use the function (138) for the adaptive gain function $\gamma_{k,m}$ for each $(k,m) \in \mathcal{E}_{Key}$.

In Chapter 4, the unbounded-gain CED control law was introduced with the idea that as the line power-flow magnitude $|P_{Line,k,m}|$ approached its constraint $P_{Max,k,m}$ for any line $(k,m) \in \mathcal{E}$, then the associated line adaptive tension value $\gamma_{k,m}P_{Line,k,m}$ (which always opposes the increase of $|P_{Line,k,m}|$) grows to become *large enough* to overcome any dynamic tension that could cause the increase of $|P_{Line,k,m}|$, thus enforcing the constraint. The unbounded growth of $\gamma_{k,m}$ ensured that the line adaptive tension is always large enough. However, in the case of bounded gain functions, the maximum gain $\gamma_{Max,k,m}$ must be selected so that it is just large enough to enforce the associated line power-flow constraint. In the next section, we develop a parametric condition on $\gamma_{Max,k,m}$ which ensures that it is sufficiently large to overcome the

Example adaptive gain function $\gamma_{k,m} \in \mathbf{\Gamma}_{Bounded}$ (for given values of $P_{Max,k,m}$, $\gamma_{Max,k,m}$, and $\epsilon_{k,m}$):

$$\gamma_{k,m}(|P_{Line,k,m}|) =$$
$$\begin{cases} 1 & |P_{Line,k,m}| \leq (1 - \epsilon_{k,m})P_{Max,k,m} \\ \left. \begin{array}{l} 1 + \dfrac{\gamma_{Max,k,m} - 1}{\epsilon_{k,m}P_{Max,k,m}}(|P_{Line,k,m}| \\ \qquad - (1 - \epsilon_{k,m})P_{Max,k,m}) \end{array} \right\} & (1 - \epsilon_{k,m})P_{Max,k,m} < |P_{Line,k,m}| \leq P_{Max,k,m} \\ \gamma_{Max,k,m} & |P_{Line,k,m}| > P_{Max,k,m} \end{cases}$$
$$\tag{138}$$
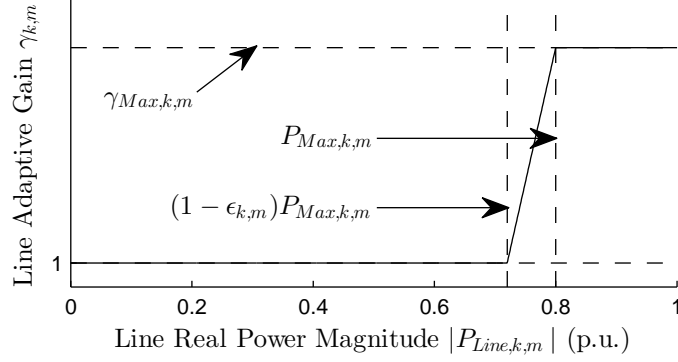
Figure 6.2: Example selection of $\gamma_{k,m} \in \mathbf{\Gamma}_{Bounded}$ as in (138) with $P_{Max,k,\sigma(k)} = 0.8$, $\epsilon_{k,m} = 0.2$, and $\gamma_{Max,k,m} = 10$.

maximum possible dynamic tension which could cause violation of the assigned key constraint $|P_{Line,k,m}| \leq P_{Max,k,m}$, thereby enforcing the constraint.

6.3.3 Placement and Assignment of CED-Controlled Inverters

In Chapter 3, we defined the safe region Θ_{Safe} of the voltage-angle state space (Definition 3.8), which represents the subset of the principal region in which all of the line power-flow constraints $|P_{Line,k,m}| \leq P_{Max,k,m}$ are satisfied. Our goal is to bound the network state trajectory $\boldsymbol{\theta}(t)$ in the safe region Θ_{Safe}, which corresponds to enforcement of all line power-flow constraints $|P_{Line,k,m}| \leq P_{Max,k,m}$ for all $(k,m) \in \mathcal{E}$. Since by assumption $\mathcal{E}_{Key}$ is a constraint-satisfying key line set (per Definition 5.2), then enforcement of only the line power-flow constraints associated with key lines is sufficient to also bound it into Θ_{Safe}, that is, explicit enforcement of $|P_{Line,k,m}| \leq P_{Max,k,m}$ for all *key* lines $(k,m) \in \mathcal{E}_{Key}$ on the expected operating range $\mathbb{P}$ also implicitly enforces the remaining constraints.

In order to enforce the key line constraints, we will place at least one CED inverter incident to each key line (member of $\mathcal{E}_{Key}$) and assign the inverter to enforce the key line constraint. Without loss of generality, for each key line $(k,m) \in \mathcal{E}$ we can assume that k is the CED inverter assigned to enforce the constraint on (k,m), since we can simply swap the (arbitrary) positive power-flow direction assigned to (k,m). Making

159

this assumption, there are four possible configurations for each key line $(k, m) \in \mathcal{E}_{Key}$, which are illustrated in Figure 6.3:

1. Bus m is a network bus ($m \in \mathcal{V}_{Net}$).

2. Bus m is a traditional droop inverter bus ($m \in \mathcal{V}_{Droop}$).

3. Bus m is a CED bus, and it is assigned to enforce the constraint on (k, m) ($m \in \mathcal{V}_{CED}$ and $\sigma(m) = k$).

4. Bus m is a CED bus, but it is assigned to enforce the constraint on another line ($m \in \mathcal{V}_{CED}$ and $\sigma(m) \neq k$).

Cases 1 and 4 above are not recommended, since they result in requirements on the CED inverter configuration which are difficult to meet in practice. Therefore, we will focus on Case 2 and Case 3, which we will call the *asymmetric CED placement* (Figure 6.3b) and the *symmetric CED placement* (Figure 6.3c) cases respectively. More formally, we define a *Constraint-Satisficing CED Inverter Placement and Assignment* as follows:

Definition 6.6 (Constraint-Satisficing CED Inverter Placement and Assignment). *A placement of inverters $\mathcal{V}_{CED}$ and associated CED assignment function $\sigma : \mathcal{V}_{CED} \to \mathcal{V}$ is a* constraint-satisficing CED inverter placement and assignment *for a given network $(\mathfrak{G}, \mathbb{P}, \mathbf{P_{Max}})$ and an associated constraint-satisficing key line set $\mathcal{E}_{Key}$ (per Definition 5.2) if for each $(k, m) \in \mathcal{E}_{Key}$ one of the following applies:*

6.6.A Asymmetric CED Placement: $k \in \mathcal{V}_{CED}$, $\sigma(k) = m$, and $m \in \mathcal{V}_{Droop}$.

6.6.B Symmetric CED Placement: $k, m \in \mathcal{V}_{CED}$, $\sigma(k) = m$, and $\sigma(m) = k$.

If the set of CED-inverter buses $\mathcal{V}_{CED}$ and CED assignment function σ are chosen according to Definition 6.6, then each key line $(k, m) \in \mathcal{E}_{Key}$ is assigned to at least one incident CED inverter. In the following section, we will show that appropriately
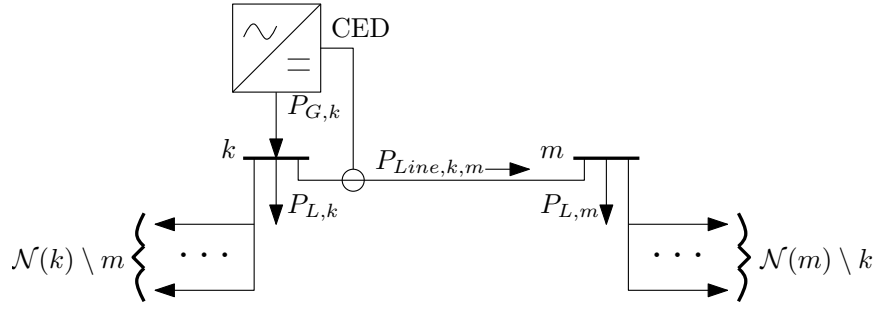
(a) Case 1: Bus m is a network bus ($m \in \mathcal{V}_{Net}$)
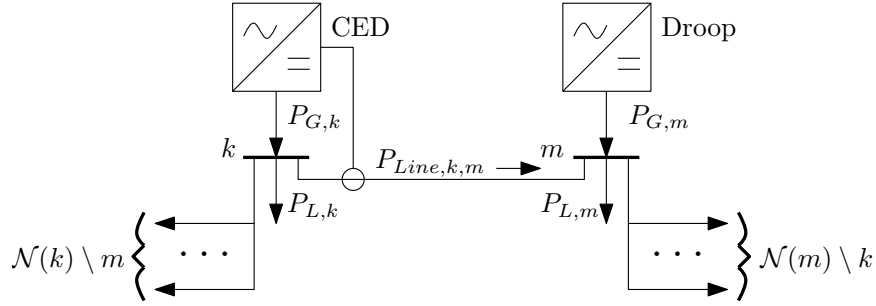
(b) Case 2 (Asymmetric CED Placement): Bus m is a traditional droop inverter bus ($m \in \mathcal{V}_{Droop}$)
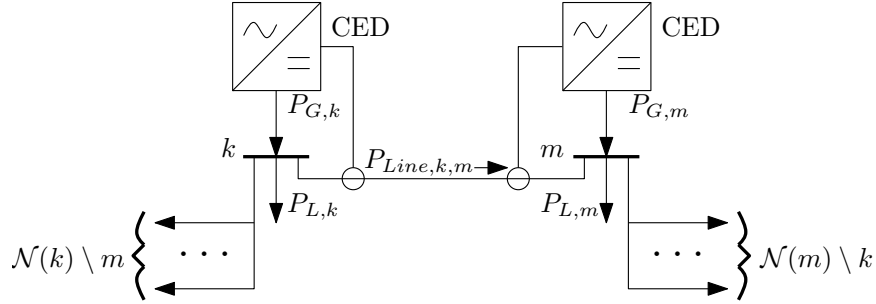
(c) Case 3 (Symmetric CED Placment): Bus m is a CED inverter bus, and it's also assigned to enforce the constraint on (k, m) ($m \in \mathcal{V}_{CED}$ and $\sigma(m) = k$)
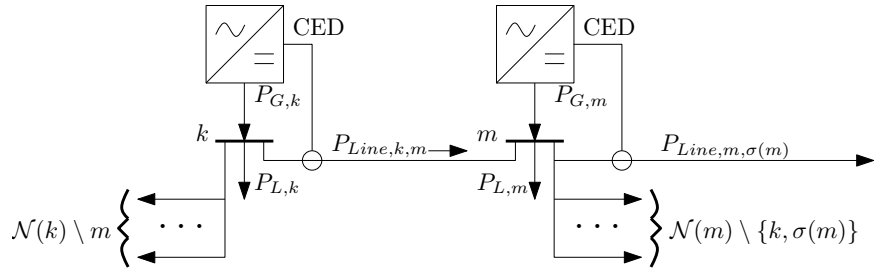
(d) Case 4: Bus m is a CED inverter bus, but it's assigned to enforce a different line constraint ($m \in \mathcal{V}_{CED}$ and $\sigma(m) \neq k$)

Figure 6.3: Possible Configurations for key line $(k, m) \in \mathcal{E}_{CED}$ assuming $k \in \mathcal{V}_{CED}$ and $\sigma(k) = m$

selecting their control parameters, we can ensure that the CED inverters will be capable of enforcing their assigned line power-flow constraints, thus implicitly enforcing the line power-flow constraints on *all* lines in the network and bounding it within the safe region of the voltage-angle state space.

6.4 Sparse Enforcement of Key Line Constraints

In this section, we develop a parametric requirement on the gain bound constants $\gamma_{Max,k,m}$ for each CED inverter bus $k \in \mathcal{V}_{CED}$ that ensures that the line power-flow constraint $|P_{Line,k,m}| \leq P_{Max,k,m}$ associated with each key line $(k,m) \in \mathcal{E}_{Key}$ are all enforced for the entire expected operating range $\mathbb{P}$ of the network. This will ensure that the line power-flow constraints associated with *all* lines in the network are satisfied, thereby bounding its operation within the safe region Θ_{Safe} (as in Definition 3.8), that is, the safe region becomes invariant to the network dynamics.

6.4.1 Modeling of Synchronization in Mixed-Bus Inverter-Based Networks

The class of networks under consideration is mixed-bus inverter-based networks (Definition 6.1), which contain a mix of CED-inverter buses, traditional-droop inverter buses, and network buses. We will therefore modify the structure-preserving dynamic model presented in Chapter 3 to represent a mixed-bus inverter-based network. As in Chapter 3, network buses ($k \in \mathcal{V}_{Net}$) or traditional frequency-droop inverter buses ($k \in \mathcal{V}_{Droop}$) are represented by the scalar dynamic equation (7). By substituting the frequency-dependent load model (3) into the single-line CED control law (137) and solving for $\dot{\delta}_k = \Delta\omega_k$, we find the scalar dynamic model of a single-line-CED-inverter bus:

$$\dot{\delta}_k = \Delta\omega_k = D_k^{-1}\Big[P_{Ref,k}(t) - P_{L,k}^0(t) - \sum_{m \in \mathcal{N}(k)\backslash\sigma(k)} P_{Line,k,m}(\delta_k - \delta_m)$$

$$- \gamma_{k,\sigma(k)}\big(|P_{Line,k,\sigma(k)}|\big)\, P_{Line,k,\sigma(k)}(\delta_k - \delta_{\sigma(k)})\Big] \tag{139}$$

where $D_k = R_k^{-1} + D_k'$ for each single-line-CED-controlled inverter bus $k \in \mathcal{V}_{CED}$. Notice that we now allow for time-varying forcing inputs $P_{Ref,k}$ and $P_{L,k}$.

The scalar dynamic equation associated with any bus ((7) for a network or droop bus or (139) for a CED-inverter bus) may be viewed as a (time-dependent) local forcing term $(P_{Ref,k}(t) - P_{L,k}^0(t))$ summed with "tension" terms representing the coupling between buses, each term associated with a line. Notice that in the dynamic equation (7) from Chapter 3 (representing either a network bus or a traditional droop inverter bus), the line tension value associated with each incident line $m \in \mathcal{N}(k)$ equals $P_{Line,k,m}$, while in (139) (representing a CED inverter bus) one line $((k, \sigma(k))$ for CED-inverter bus $k)$ has associated the dynamic tension $\gamma_{k,m}(|P_{Line,k,\sigma(k)}|) \, P_{Line,k,\sigma(k)}$. To simplify our notation, we will therefore introduce the line adaptive tension function $\tau_{k,m}$ for each $(k, m) \in \mathcal{E}$, defined as follows:

$$\tau_{k,m}(\theta_{k,m}) = \begin{cases} D_k^{-1} P_{Line,k,m}(\theta_{k,m}) & \begin{aligned} & k \notin \mathcal{V}_{CED} \text{ or} \\ & \big[k \in \mathcal{V}_{CED} \text{ and } \sigma(k) \neq m \big] \end{aligned} \\ D_k^{-1} \gamma_{k,m}(|P_{Line,k,m}|) \, P_{Line,k,m}(\theta_{k,m}) & k \in \mathcal{V}_{CED} \text{ and } \sigma(k) = m \end{cases}$$

$$(140)$$

where (as in the previous chapters) $\theta_{k,m} = \delta_k - \delta_m$ for all lines $(k, m) \in \mathcal{E}$. Since (by assumption) $D_k > 0$ for all $k \in \mathcal{V}$, $P_{Line,k,m}(\theta_{k,m})$ is odd with respect to $\theta_{k,m}$ on the principal region (see (2)), and $\gamma_{k,m}(|P_{Line,k,m}|) \geq 1$ for all $|P_{Line,k,m}|$ (Definition 6.5.B), then $\tau_{k,m}$ is also odd with respect to $\theta_{k,m}$, that is, $\tau_{k,m}(\theta_{k,m})$ has the same sign as $\theta_{k,m}$ on $\theta_{Principal}$. However, $\tau_{k,m}$ is not necessarily line-symmetric (that is, $\tau_{k,m}$ does not necessarily equal $\tau_{m,k}$).

As in the preceeding chapters, we define the line-oriented state vector $\boldsymbol{\theta} = \begin{bmatrix} \theta_1 & \dots & \theta_L \end{bmatrix}^T \in \mathbb{R}^L$ in terms of an arbitrary line orientation $\overrightarrow{\mathcal{E}}$ and line indices $i \in \{1 \dots L\}$, where $\theta_i = \theta_{k,m}$ for each $(k, m) \in \overrightarrow{\mathcal{E}}$ that was assigned index i. Then, using the line adaptive tension functions $\tau_{k,m}$ and $\tau_{m,k}$ for each line $(k, m) \in \overrightarrow{\mathcal{E}}$, we can form the following

line-oriented dynamic system-of-equations model for the state vector $\boldsymbol{\theta}$:

$$\left.\begin{aligned}
\dot{\theta}_{k,m} =& D_k^{-1} P_{Ref,k}(t) - D_k^{-1} P_{L,k}^0(t) - D_m^{-1} P_{Ref,m}(t) + D_m^{-1} P_{L,m}^0(t) \\
& - D_k^{-1} \sum_{l \in \mathcal{N}(k)\setminus m} \tau_{k,l}(\theta_{k,l}) + D_m^{-1} \sum_{p \in \mathcal{N}(m)\setminus k} \tau_{m,p}(\theta_{m,p}) \\
& - \tau_{k,m}(\theta_{k,m}) - \tau_{m,k}(\theta_{k,m})
\end{aligned}\right\} \quad \forall\, (k,m) \in \mathcal{E}$$

$$(141)$$

Notice that the dynamic equation (141) for each line consists of a *local forcing* (based on $\mathbf{P_{Ref}}(t)$ and $\mathbf{P_L^0}(t)$), line coupling terms (in terms of the line adaptive tensions associated with adjacent lines), and a self-tension (its own line adaptive tension values, one in each direction). Further, since $\tau_{k,m}$ always has the same sign as $\theta_{k,m}$, then the line self-tension $[-\tau_{k,m}(\theta_{k,m}) - \tau_{m,k}(\theta_{k,m})]$ *always opposes the increase of* $|\theta_{k,m}|$ for any line $(k,m) \in \mathcal{E}$.

Also notice from (140) that $\tau_{k,m}(\theta_{k,m})$ is globally Lipschitz continuous with respect to $\theta_{k,m}$, since (by Definition 6.5.A) $\gamma_{k,m} \in \mathbf{\Gamma}_{Bounded}$ must be globally Lipschitz continous with respect to $|P_{Line,k,m}|$, which is in turn globally Lipschitz continuous with respect to $\theta_{k,m}$ (see (2)). Therefore, the dynamic equation (141) is also globally Lipschitz with respect to $\theta_{k,m}$ (and so $\theta_{k,m}(t)$ exists and is continuous).

6.4.2 Local Enforcment of Key Line Constraints

Consider the dynamic equation (141) for the line voltage angle $\theta_{k,m}$ associated with a key line $(k,m) \in \mathcal{E}_{Key}$. By assumption, at least one bus incident to (k,m) must be a CED-inverter bus, and without loss of generality we can assume it be be k (and therefore $k \in \mathcal{V}_{CED}$ and $\sigma(k) = m$). We observed above that the self-tension term $[-\tau_{k,m}(\theta_{k,m}) - \tau_{m,k}(\theta_{k,m})]$ always opposes the increase of $|\theta_{k,m}|$ (and therefore $|P_{Line,k,m}|$) on the principal region. Therefore, if the self-tension term is larger than the sum of the other line tension terms and the forcing terms (which we will call the non-self-tension terms), then $|\theta_{k,m}|$ and $|P_{Line,k,m}|$ are both decreasing.

Since the network state trajectory $\boldsymbol{\theta}(t)$ is continuous, in order for the network state

trajectory $\boldsymbol{\theta}(t)$ to leave the safe region Θ_{Safe} (which is a subset of $\Theta_{Principal}$), the line power-flow constraint $|P_{Line,k,m}| \leq P_{Max,k,m}$ for some key line $(k,m) \in \mathcal{E}_{Key}$ must be violated. Consider the boundary condition $|P_{Line,k,m}| = P_{Max,k,m}$ for such a key line. If at that condition the self-tension $[-\tau_{k,m}(\theta_{k,m}) - \tau_{m,k}(\theta_{k,m})]$ is greater than the sum of the non-self-tension terms, then $|P_{Line,k,m}|$ is decreasing, and the network dynamics will return to the interior of Θ_{Safe}, thus enforcing the constraint. Since k is a CED-inverter bus that is responsible for enforcing the key line constraint $(k,m) \in \mathcal{E}_{Key}$, then as $|P_{Line,k,m}|$ approaches $P_{Max,k,m}$, $\gamma_{k,m}$ approaches $\gamma_{Max,k,m}$ (Definition 6.5.D), and so $\tau_{k,m}(\theta_{k,m})$ approaches $\pm D_k^{-1}\gamma_{Max,k,m}P_{Max,k,m}$. Therefore, by select $\gamma_{Max,k,m}$ such that $\tau_{k,m}$ is always larger than the sum of the maximum value of the non-self-tension terms when $|P_{Line,k,m}| = P_{Max,k,m}$, we can enforce the key line constraint $|P_{Line,k,m}| \leq P_{Max,k,m}$ and bound the network state trajectory within Θ_{Safe}. As we will show below, this is possible because the maximum value of the non-self-tension terms is bounded on the safe region Θ_{Safe} under the expected operating range $\mathbb{P}$.

6.4.3 Maximum and Minimum Non-Self-Tension

Consider again the dynamic equation (141) for the line voltage angle $\theta_{k,m}$ associated with a key line $(k,m) \in \mathcal{E}_{Key}$. If the network inputs are on the expected operating range, then (by Definition 5.1) $P_{G,Min,k} \leq P_{G,k}(t) \leq P_{G,Max,k}$ and $0 \leq P_{L,k}(t) \leq P_{L,Max,k}$ for all buses $k \in \mathcal{V}$ and for all t. It is reasonable to also assume that the value of $P_{Ref,k}$ assigned to each bus $k \in \mathcal{V}$ is bounded by $P_{G,Min,k} \leq P_{Ref,k}(t) \leq P_{G,Max,k}$ for all t, since it doesn't make sense to assign a reference power to an inverter which the inverter isn't capable of sourcing or sinking. Further, we will assume that the nominal-frequency load $P_{L,k}^0$ is also bounded by $0 \leq P_{L,k}^0(t) \leq P_{L,Max,k}$ (that is, $(\mathbf{P_{Ref}}(t), \mathbf{P_L^0}(t)) \in \mathbb{P}$) for all t .

In addition, on the safe region Θ_{Safe}, by definition all of the key line power-flow constraints are met ($|P_{Line,l,p}| \leq P_{Max,l,p} \; \forall \; (l,p) \in \mathcal{E}_{Key}$). Since by assumption $\mathcal{E}_{Key}$ is

a constraint-satisficing key line set for $(\mathfrak{G}, \mathbb{P}, \mathbf{P_{Max}})$, then by Lemma 5.1.B the bounds $P_{LBound,l,p} \leq P_{Line,l,p} \leq P_{UBound,l,p}$ apply for each line $(l, p) \in \mathcal{E}$, where $P_{LBound,k,m}$ and $P_{UBound,k,m}$ are calculated by Procedure 5.1. Therefore, there exist bounds on all of the non-self tension terms that appear in (146), bounding the total tension that can oppose the self-tension and cause the associated line power-flow constraint to be violated. We formalize this result as follows:

Lemma 6.1 (Bounding of Non-Self-Tensions on Θ_{Safe}). *Consider a given constraint-satisficing droop inverter network (Definition 6.3). If $\boldsymbol{\theta} \in \Theta_{Safe}$ and $(\mathbf{P_{Ref}}, \mathbf{P_L^0}) \in \mathbb{P}$ then $\dot{\theta}_{k,m}$ may be bounded by:*

$$\dot{\theta}_{k,m} \leq \tau_{Max,k,m} - \tau_{k,m}(\theta_{k,m}) - \tau_{m,k}(\theta_{k,m}) \tag{142}$$

$$\dot{\theta}_{k,m} \geq \tau_{Min,k,m} - \tau_{k,m}(\theta_{k,m}) - \tau_{m,k}(\theta_{k,m}) \tag{143}$$

where constants $\tau_{Max,k,m}$ and $\tau_{Min,k,m}$ are defined as:

$$
\begin{aligned}
\tau_{Max,k,m} =& D_k^{-1} P_{G,Max,k} - D_m^{-1} P_{G,Min,m} + D_m^{-1} P_{L,Max,m} \\
& - D_k^{-1} \sum_{l \in \mathcal{N}(k) \backslash m} P_{LBound,k,l} + D_m^{-1} \sum_{p \in \mathcal{N}(m) \backslash k} P_{UBound,m,p}
\end{aligned}
\tag{144}
$$

$$
\begin{aligned}
\tau_{Min,k,m} =& D_k^{-1} P_{G,Min,k} - D_k^{-1} P_{L,Max,k} - D_m^{-1} P_{G,Max,m} \\
& - D_k^{-1} \sum_{l \in \mathcal{N}(k) \backslash m} P_{UBound,k,l} + D_m^{-1} \sum_{p \in \mathcal{N}(m) \backslash k} P_{LBound,m,p}
\end{aligned}
\tag{145}
$$

for all $(k, m) \in \mathcal{E}_{Key}$.

Proof. Then the dynamic equation (141) for $(k, m) \in \mathcal{E}_{Key}$ can be rewritten as follows:

$$
\begin{aligned}
\dot{\theta}_{k,m} =& D_k^{-1} P_{Ref,k}(t) - D_k^{-1} P_{L,k}^0(t) - D_m^{-1} P_{Ref,m}(t) + D_m^{-1} P_{L,m}^0(t) \\
& - D_k^{-1} \sum_{l \in \mathcal{N}(k) \backslash m} P_{Line,k,l}(\theta_{k,l}) + D_m^{-1} \sum_{p \in \mathcal{N}(m) \backslash k} P_{Line,m,p}(\theta_{m,p}) \\
& - \tau_{k,m}(\theta_{k,m}) - \tau_{m,k}(\theta_{k,m})
\end{aligned}
\tag{146}
$$

By Definition 5.1, the assumption that $(\mathbf{P_{Ref}}, \mathbf{P_L^0}) \in \mathbb{P}$ implies bounds on the reference and nominal-frequency load at each bus. By combining the bounds on reference and load with (146) using Non-homogeneous Farkas' Lemma (see [57, Theorem 3.1.2]), we find the following upper and lower bounds on $\dot{\theta}_{k,m}$ on the expected operating range $\mathbb{P}$:

$$
\begin{aligned}
\dot{\theta}_{k,m} \leq & D_k^{-1} P_{G,Max,k} - D_m^{-1} P_{G,Min,m} + D_m^{-1} P_{L,Max,m} \\
& - D_k^{-1} \sum_{l \in \mathcal{N}(k) \backslash m} P_{Line,k,l}(\theta_{k,l}) + D_m^{-1} \sum_{p \in \mathcal{N}(m) \backslash k} P_{Line,m,p}(\theta_{m,p}) \\
& - \tau_{k,m}(\theta_{k,m}) - \tau_{m,k}(\theta_{k,m})
\end{aligned}
\tag{147}
$$

and

$$
\begin{aligned}
\dot{\theta}_{k,m} \geq & D_k^{-1} P_{G,Min,k} - D_k^{-1} P_{L,Max,k} - D_m^{-1} P_{G,Max,m} \\
& - D_k^{-1} \sum_{l \in \mathcal{N}(k) \backslash m} P_{Line,k,l}(\theta_{k,l}) + D_m^{-1} \sum_{p \in \mathcal{N}(m) \backslash k} P_{Line,m,p}(\theta_{m,p}) \\
& - \tau_{k,m}(\theta_{k,m}) - \tau_{m,k}(\theta_{k,m})
\end{aligned}
\tag{148}
$$

On the safe region Θ_{Safe}, by Definition 3.8 all of the key line power-flow constraints are met ($|P_{Line,l,p}| \leq P_{Max,l,p} \ \forall \ (l,p) \in \mathcal{E}_{Key}$). Since by assumption $\mathcal{E}_{Key}$ is a constraint-satisfying key line set for $(\mathfrak{G}, \mathbb{P}, \mathbf{P_{Max}})$, then by Lemma 5.1.B the bounds $P_{LBound,l,p} \leq P_{Line,l,p} \leq P_{UBound,l,p}$ apply for each line $(l,p) \in \mathcal{E}$, where $P_{LBound,k,m}$ and $P_{UBound,k,m}$ are calculated by Procedure 5.1. We may again combine these line power-flow bounds with (147) and (148) to further bound $\dot{\theta}_{k,m}$ by:

$$
\begin{aligned}
\dot{\theta}_{k,m} \leq & D_k^{-1} P_{G,Max,k} - D_m^{-1} P_{G,Min,m} + D_m^{-1} P_{L,Max,m} \\
& - D_k^{-1} \sum_{l \in \mathcal{N}(k) \backslash m} P_{LBound,k,l} + D_m^{-1} \sum_{p \in \mathcal{N}(m) \backslash k} P_{UBound,m,p} \\
& - \tau_{k,m}(\theta_{k,m}) - \tau_{m,k}(\theta_{k,m}) \\
= & \tau_{Max,k,m} - \tau_{k,m}(\theta_{k,m}) - \tau_{m,k}(\theta_{k,m})
\end{aligned}
\tag{149}
$$

$$\dot{\theta}_{k,m} \geq D_k^{-1} P_{G,Min,k} - D_k^{-1} P_{L,Max,k} - D_m^{-1} P_{G,Max,m}$$

$$- D_k^{-1} \sum_{l \in \mathcal{N}(k) \backslash m} P_{UBound,k,l} + D_m^{-1} \sum_{p \in \mathcal{N}(m) \backslash k} P_{LBound,m,l}$$

$$- \tau_{k,m}(\theta_{k,m}) - \tau_{m,k}(\theta_{k,m})$$

$$= \tau_{Min,k,m} - \tau_{k,m}(\theta_{k,m}) - \tau_{m,k}(\theta_{k,m}) \tag{150}$$

where $\tau_{Max,k,m}$ and $\tau_{Min,k,m}$ are as defined in (144) and (145) respectively. $\qquad \square$

Lemma 6.1 shows that the sum of the non-self-tension terms in the dynamics of $\theta_{k,m}$ for a key line $(k,m) \in \mathcal{E}_{Key}$ is bounded on Θ_{Safe} and the expected operating range $\mathbb{P}$. Based on this result, we will show below that there exist values of $\gamma_{Max,k,m}$ (and $\gamma_{Max,m}$ in the case of symmetric CED placement) such that the self-tension term is always "large enough" to overcome the maximum possible other tensions, thus enforcing the key line constraint $|P_{Line,k,m}| \leq P_{Max,k,m}$.

6.4.4 Parametric Requirement for $\gamma_{Max,k,m}$

Assume that the network state trajectory $\boldsymbol{\theta}(t)$ approaches the boundary of Θ_{Safe} from inside. By assumption, $\mathcal{E}_{Key}$ is a constraint-satisficing key line set, and so $\boldsymbol{\theta}(t)$ approaching the boundary of Θ_{Safe} corresponds to some key line $(k,m) \in \mathcal{E}_{Key}$ approaching its line power-flow constraint ($|P_{Line,k,m}|$ approaches $P_{Max,k,m}$ while $d|P_{Line,k,m}|/dt > 0$). On the principal region, $d|P_{Line,k,m}|/dt > 0$ corresponds to $d|\theta_{k,m}|/dt > 0$ (see Lemma 3.3), and therefore if we select $\gamma_{Max,k,m}$ so that $d|\theta_{k,m}|/dt \leq 0$ when $|P_{Line,k,m}| = P_{Max,k,m}$ for the maximum and minimum tensions in (142) and (143), then at some point before it exits Θ_{Safe}, $\theta_{k,m}$ will be pulled back into Θ_{Safe}, and therefore the key line power-flow constraint $|P_{Line,k,m}| \leq P_{Max,k,m}$ will be enforced.

By Lemma 6.1, when $\boldsymbol{\theta} \in \partial\Theta_{Safe}$ (the boundary of Θ_{Safe}) and $(\mathbf{P_{Ref}}, \mathbf{P_L^0}) \in \mathbb{P}$, $\dot{\theta}_{k,m}$ can be bounded by (142) and (143). By Definition 6.6, if $\mathcal{V}_{CED}$ and σ constitute a constraint-satisficing CED inverter placement and assignment, then we use either asymmetric or symmetric CED placement for the key line $(k,m) \in \mathcal{E}_{Key}$. Substituting

the appropriate values of $\tau_{k,m}$ and $\tau_{m,k}$ into (142) and (143) for the key line $(k,m) \in \mathcal{E}$:

$$\dot{\theta}_{k,m} \leq \tau_{Max,k,m} + \begin{cases} \begin{rcases} - D_k^{-1}\gamma_{k,m}(|P_{Line,k,m}(\theta_{k,m})|)\, P_{Line,k,m}(\theta_{k,m}) \\ - D_m^{-1}P_{Line,k,m}(\theta_{k,m}) \end{rcases} & m \in \mathcal{V}_{Droop} \\ \begin{rcases} - D_k^{-1}\gamma_{k,m}(|P_{Line,k,m}(\theta_{k,m})|)\, P_{Line,k,m}(\theta_{k,m}) \\ - D_m^{-1}\gamma_{m,k}(|P_{Line,k,m}(\theta_{k,m})|)\, P_{Line,k,m}(\theta_{k,m}) \end{rcases} & \begin{matrix} m \in \mathcal{V}_{CED} \\ \text{and } \sigma(m) = k \end{matrix} \end{cases}$$

$$(151)$$

$$\dot{\theta}_{k,m} \geq \tau_{Min,km} + \begin{cases} \begin{rcases} - D_k^{-1}\gamma_{k,m}(|P_{Line,k,m}(\theta_{k,m})|)\, P_{Line,k,m}(\theta_{k,m}) \\ - D_m^{-1}P_{Line,k,m}(\theta_{k,m}) \end{rcases} & m \in \mathcal{V}_{Droop} \\ \begin{rcases} - D_k^{-1}\gamma_{k,m}(|P_{Line,k,m}(\theta_{k,m})|)\, P_{Line,k,m}(\theta_{k,m}) \\ - D_m^{-1}\gamma_{m,k}(|P_{Line,k,m}(\theta_{k,m})|)\, P_{Line,k,m}(\theta_{k,m}) \end{rcases} & \begin{matrix} m \in \mathcal{V}_{CED} \\ \text{and } \sigma(m) = k \end{matrix} \end{cases}$$

$$(152)$$

Assume that $\boldsymbol{\theta}$ is in the boundary of Θ_{Safe} such that $P_{Line,k,m} = P_{Max,k,m}$ for line $(k,m) \in \mathcal{E}_{Key}$. By Definition 6.5.D, then $\gamma_{k,m} = \gamma_{m,k} = \gamma_{Max,k,m}$. To enforce the line power-flow constraint $|P_{Line,k,m}| \leq P_{Max,k,m}$, we should select $\gamma_{Max,k,m}$ such that $\dot{\theta}_{k,m} \leq 0$. Substituting into the inequality (151):

$$\dot{\theta}_{k,m} \leq \tau_{Max,k,m} + \begin{cases} -(D_k^{-1}\gamma_{Max,k,m} + D_m^{-1})P_{Max,k,m} & m \in \mathcal{V}_{Droop} \\ -(D_k^{-1} + D_m^{-1})\gamma_{Max,k,m}P_{Max,k,m} & m \in \mathcal{V}_{CED} \text{ and } \sigma(m) = k \end{cases}$$

$$\leq 0 \qquad\qquad (153)$$

Solving the inequality (153) for $\gamma_{Max,k,m}$:

$$\gamma_{Max,k,m} \geq \begin{cases} D_k\left(\dfrac{\tau_{Max,k,m}}{P_{Max,k,m}} - D_m^{-1}\right) & m \in \mathcal{V}_{Droop} \\ \dfrac{\tau_{Max,k,m}}{P_{Max,k,m}}(D_k^{-1} + D_m^{-1})^{-1} & m \in \mathcal{V}_{CED} \text{ and } \sigma(m) = k \end{cases}$$

$$(154)$$

Alternatively, assume that $\boldsymbol{\theta}$ is in the boundary of Θ_{Safe} such that $P_{Line,k,m} = -P_{Max,k,m}$ for line $(k,m) \in \mathcal{E}_{Key}$ (and so again $\gamma_{k,m} = \gamma_{m,k} = \gamma_{Max,k,m}$). For this case,

169

we should select $\gamma_{Max,k,m}$ such that $\dot{\theta}_{k,m} \geq 0$. Substituting into (151):

$$\dot{\theta}_{k,m} \geq \tau_{Min,km} + \begin{cases} (D_k^{-1}\gamma_{Max,k,m} + D_m^{-1})P_{Max,k,m} & m \in \mathcal{V}_{Droop} \\ (D_k^{-1} + D_m^{-1})\gamma_{Max,k,m}P_{Max,k,m} & m \in \mathcal{V}_{CED} \text{ and } \sigma(m) = k \end{cases}$$

$$\geq 0 \tag{155}$$

Solving the inequality (155) for $\gamma_{Max,k,m}$:

$$\gamma_{Max,k,m} \geq \begin{cases} D_k \left(\dfrac{-\tau_{Min,k,m}}{P_{Max,k,m}} - D_m^{-1} \right) & m \in \mathcal{V}_{Droop} \\ -\dfrac{\tau_{Min,k,m}}{P_{Max,k,m}}(D_k^{-1} + D_m^{-1})^{-1} & m \in \mathcal{V}_{CED} \text{ and } \sigma(m) = k \end{cases} \tag{156}$$

If we select $\gamma_{Max,k,m}$ according to the stricter of (154) and (156), then we ensure that the self-tension associated with the key line $(k,m) \in \mathcal{E}_{Key}$ is always large enough to overcome the other tensions (on the expected operating range) so as to bound $|P_{Line,k,m}| \leq P_{Max,k,m}$, thus enforcing the key line power-flow constraint. Therefore, we call a selection of $\gamma_{Max,k,m}$ satisfying (154) and (156) as an *enforcing* $\gamma_{Max,k,m}$ *selection*:

Definition 6.7 (Enforcing $\gamma_{Max,k,m}$ Selection). *A selection of* $\gamma_{Max,k,m} = \gamma_{Max,m,k}$ *for a key line* $(k,m) \in \mathcal{E}_{Key}$ *is an* enforcing $\gamma_{Max,k,m}$ *selection if it satisfies the following:*

$$\gamma_{Max,k,m} \geq \begin{cases} \max \left(D_k \left[\dfrac{\tau_{Max,k,m}}{P_{Max,k,m}} - D_m^{-1} \right], -D_k \left[\dfrac{\tau_{Min,k,m}}{P_{Max,k,m}} - D_m^{-1} \right], 1 \right) & m \in \mathcal{V}_{Droop} \\ \max \left(\dfrac{\tau_{Max,k,m}}{P_{Max,k,m}}(D_k^{-1} + D_m^{-1})^{-1}, \dfrac{-\tau_{Min,k,m}}{P_{Max,k,m}}(D_k^{-1} + D_m^{-1})^{-1}, 1 \right) & \begin{array}{l} m \in \mathcal{V}_{CED} \\ \text{and } \sigma(m) = k \end{array} \end{cases} \tag{157}$$

where $\tau_{Max,k,m}$ *and* $\tau_{Min,k,m}$ *are calculated as in* (144) *and* (145) *respectively.*

Notice in Definition 6.7 that we include the requirement (from Definition 6.5.B), that $\gamma_{Max,k,m} \geq 1$. If the selection of $\gamma_{Max,k,m}$ for a key line $(k,m) \in \mathcal{E}_{Key}$ meets the requirements of Definition 6.7, then the self-tension for (k,m) will become large enough as $|P_{Line,k,m}|$ approaches $P_{Max,k,m}$ so that $\theta_{k,m}$ will be pulled back into the safe region Θ_{Safe}, thus enforcing the line power-flow constraint $|P_{Line,k,m}| \leq P_{Max,k,m}$.

170

6.4.5 Invariance of the Safe Region Θ_{Safe}

Assume that a CED inverter has been placed and assigned to enforce each line power-flow constraint in a constraint-satisficing key line set $\mathcal{E}_{Key}$ (per Definition 6.6), and that each such inverter $k \in \mathcal{V}_{CED}$ has assigned an enforcing $\gamma_{Max,k,m}$ selection (per Definition 6.7). Then each key line power-flow constraint should be enforced on the entire expected operating range, and therefore *all* of the line power-flow constraints should be enforced. Therefore, if the network begins within the safe region, then its operation should be bounded within the safe region, that is, the safe region should be invariant with respect to the network dynamics. We show this result formally in Lemma 6.2 below:

Lemma 6.2 (Invariance of Θ_{Safe} w.r.t. Constraint-Satisficing Droop Inverter Network Dynamics). *Consider the set Θ_{Safe} as defined in Definition 3.8 for a given constraint-satisficing droop inverter network (Definition 6.3), and assume that there exists trajectory $\boldsymbol{\theta}(t)$ of the network dynamics (141) for $t \geq 0$ such that $\boldsymbol{\theta}(0) \in \Theta_{Safe}$. Then if $(\mathbf{P_G}(t), \mathbf{P_L}(t)) \in \mathbb{P}$ and $(\mathbf{P_{Ref}}(t), \mathbf{P_L^0}(t)) \in \mathbb{P}$ for all $t \geq 0$ then $\boldsymbol{\theta}(t) \in \Theta_{Safe}$ for all $t \geq 0$, that is, Θ_{Safe} is positively-invariant with respect to the dynamics in (141).*

Proof. Consider the following set on $\mathbb{R}_L$:

$$\Theta_{Safe,Key} = \{\boldsymbol{\theta} \in \Theta_{Principal} \text{ s.t. } |P_{Line,k,m}(\theta_{k,m})| \leq P_{Max,k,m} \ \forall \ (k,m) \in E_{Key}\} \quad (158)$$

The set $\Theta_{Safe,Key}$ represents the subset of the principal region where the line power-flow constraints associated with the key lines in $\mathcal{E}_{Key}$ are satisfied.

We will first show that $\Theta_{Safe} = \Theta_{Safe,Key}$ for a constraint-satisficing droop inverter network. It trivially follows from the Definition 3.8 and (158) that $\Theta_{Safe} \subset \Theta_{Safe,Key}$, since the membership criterion of Θ_{Safe} implies the membership criterion of $\Theta_{Safe,Key}$. Further, since by assumption $\mathcal{E}_{Key}$ is a constraint-satisficing key line set

and $(\mathbf{P_G}, \mathbf{P_L}) \in \mathbb{P}$, then (by Definition 5.2) $|P_{Line,k,m}| \leq P_{Max,k,m} \ \forall \ (k,m) \in \mathcal{E}_{Key}$ (the membership criterion for $\Theta_{Safe,Key}$) implies that $|P_{Line,k,m}| \leq P_{Max,k,m} \ \forall \ (k,m) \in \mathcal{E}$ (the membership criterion for Θ_{Safe}), and therefore $\Theta_{Safe,Key} \subset \Theta_{Safe}$. Since $\Theta_{Safe} \subset \Theta_{Safe,Key}$ and $\Theta_{Safe,Key} \subset \Theta_{Safe}$, then $\Theta_{Safe} = \Theta_{Safe,Key}$.

Contradiction Hypothesis: There exists a trajectory $\boldsymbol{\theta}(t)$ of the dynamics (141) and a time $T_1 > 0$ such that $\boldsymbol{\theta}(0) \in \Theta_{Safe,Key}$ and $\boldsymbol{\theta}(T_1) \notin \Theta_{Safe,Key}$ (that is, $\boldsymbol{\theta}(t)$ exits $\Theta_{Safe,Key}$ sometime between $t = 0$ and $t = T_1$).

We have already shown that the dynamics of $\dot{\boldsymbol{\theta}}$ are globally Lipschitz, so $\boldsymbol{\theta}(t)$ is continuous. Therefore, it follows from the contradiction hypothesis there exists T such that $0 < T < T_1$, $\boldsymbol{\theta}(t) \in \Theta_{Safe,Key}$ for all $t \leq T$, and $\boldsymbol{\theta}(T) \in \partial\Theta_{Safe,Key}$. Time T is the instant at which $\boldsymbol{\theta}(t)$ first crosses the boundary of $\Theta_{Safe,Key}$, that is, there exists some line $(k,m) \in E_{Key}$ such that $|P_{Line,k,m}(\theta_{k,m}(T))| = P_{Max,km}$. By Definition 6.5.D, $|P_{Line,k,m}(\theta_{k,m}(T))| = P_{Max,k,m}$ implies that $\gamma_{k,m}(|P_{Line,k,m}(\theta_{k,m}(T))|) = \gamma_{Max,k,m}$.

In addition, the contradiction hypothesis implies that $|P_{Line,k,m}|$ must be increasing at $t = T$, that is:

$$\left.\frac{d|P_{Line,km}|}{dt}\right|_{t=T} = \left.\frac{\partial|P_{Line}|}{\partial|\theta_{km}|}\right|_{t=T} \left.\frac{d|\theta_{km}|}{dt}\right|_{t=T} = \left.\frac{\partial P_{Line}}{\partial\theta_{km}}\right|_{t=T} \left.\frac{d|\theta_{km}|}{dt}\right|_{t=T} > 0 \qquad (159)$$

We showed in Lemma 3.3 that $\partial P_{Line}/\partial\theta_{km} > 0$ on $\Theta_{Principal} \supset \Theta_{Safe,Key}$ for all $(k,m) \in \mathcal{E}$. Therefore, we find that:

$$\left.\frac{d|\theta_{k,m}|}{dt}\right|_{t=T} = sign(\theta_{k,m}(T)) \left.\dot{\theta}_{k,m}\right|_{t=T} > 0 \qquad (160)$$

There are two cases when $|P_{Line,k,m}(\theta_{k,m}(T))| = P_{Max,km}$: $P_{Line,k,m}(T) = P_{Max,k,m}$ and $P_{Line,k,m}(T) = -P_{Max,k,m}$. Consider the case where $P_{Line,k,m}(T) = P_{Max,k,m}$. Since (k,m) is a key line, then (by Definition 6.6) $k \in \mathcal{V}_{CED}$ and $\sigma(k) = m$. Substituting into (140):

$$\tau_{k,m}(\theta_{k,m}(T)) = \gamma_{k,m}(P_{Line,k,m}(\theta_{k,m}(T)))P_{Line,k,m}(\theta_{k,m}(T)) = \gamma_{Max,k,m}P_{Max,k,m}$$

$$(161)$$

By Lemma 6.1, we can bound $\dot\theta_{k,m}$ by (142) on Θ_{Safe} when $(\mathbf{P_{Ref}}, \mathbf{P_L^0}) \in \mathbb{P}$. Substituting (161) into (142):

$$\dot\theta_{k,m} \leq \tau_{Max,k,m} + \begin{cases} -(D_k^{-1}\gamma_{Max,k,m} + D_m^{-1})P_{Max,k,m} & m \in \mathcal{V}_{CED} \\ -(D_k^{-1}\gamma_{Max,k,m} + D_m^{-1}\gamma_{Max,k,m})P_{Max,k,m} & m \in \mathcal{V}_{CED} \text{ and } \sigma(m) = k \end{cases} \tag{162}$$

By substititing the upper bound (153) on $\gamma_{Max,k,m}$, we find that $P_{Line,k,m}(T) = P_{Max,k,m}$ implies that $\dot\theta_{k,m}|_{t=T} \leq 0$, and therefore:

$$\frac{d|\theta_{k,m}|}{dt}\bigg|_{t=T} = \dot\theta_{k,m}(T) \leq 0 \tag{163}$$

which contradicts the observation (160).

Alternatively, consider the case where $P_{Line,k,m}(T) = -P_{Max,k,m}$. It then follows that

$$\tau_{k,m}(\theta_{k,m}(T)) = \gamma_{k,m}(P_{Line,k,m}(\theta_{k,m}(T)))P_{Line,k,m}(\theta_{k,m}(T))) = -\gamma_{Max,k,m}P_{Max,k,m} \tag{164}$$

By Lemma 6.1, we can bound $\dot\theta_{k,m}$ by (143) on Θ_{Safe} when $(\mathbf{P_{Ref}}, \mathbf{P_L^0}) \in \mathbb{P}$. Substituting (164) into (143):

$$\dot\theta_{k,m}(T) \geq \tau_{Min,k,m} - \begin{cases} -(D_k^{-1}\gamma_{Max,k,m} + D_m^{-1})P_{Max,k,m} & m \in \mathcal{V}_{CED} \\ -(D_k^{-1}\gamma_{Max,k,m} + D_m^{-1}\gamma_{Max,k,m})P_{Max,k,m} & m \in \mathcal{V}_{CED} \text{ and } \sigma(m) = k \end{cases} \tag{165}$$

Similarly by substititing the lower bound (155) on $\gamma_{Max,k,m}$, we find that $P_{Line,k,m}(T) = -P_{Max,k,m}$ implies:

$$\dot\theta_{k,m}(T) \geq 0 \tag{166}$$

and therefore

$$\frac{d|\theta_{k,m}|}{dt}\bigg|_{t=T} = -\dot\theta_{k,m} \leq 0 \tag{167}$$

which also contradicts the observation (160).

Therefore, the contradiction hypothesis is shown false, and instead $\boldsymbol{\theta}(0) \in \Theta_{Safe,Key}$ implies that $\boldsymbol{\theta}(t) \in \Theta_{Safe,Key}$ for all $t \geq 0$, that is, $\Theta_{Safe,Key} = \Theta_{Safe}$ is positively invariant w.r.t. the dynamics (141). □

Lemma 6.2 formalizes our statement that the following are sufficient enforce all line power-flow constraints in the network for the entire expected operating range $\mathbb{P}$:

1. $\mathcal{E}_{Key}$ is a constraint-satisficing key line set (per Definition 5.2)

2. $(\mathcal{V}_{CED}, \sigma)$ is a constraint-satisficing CED inverter placement and assignment (per Definition 6.6).

3. $\gamma_{Max,k,m}$ for each key line $(k,m) \in \mathcal{E}_{Key}$ is selected as an enforcing $\gamma_{Max,k,m}$ selection (per Definition 6.7).

Therefore, the CED configuration specified by $\mathcal{V}_{CED}$, σ, and the set of $\gamma_{Max,k,m}$ values for all $k \in \mathcal{V}_{CED}$ is a *constraint-satisficing droop control configuration* (Definition 6.3), and it bounds the voltage-angle trajectory of the network in the safe region on the expected operating range. In the following sections, we will show that this result is also sufficient to ensure frequency synchronization and constrained power sharing of the network.

6.4.6 Constraint-Satisficing Droop Control Configurations for Example Networks

To better illustrate the concept of a constraint-satisficing droop control configuration, we will now form constraint-satisficing droop control configurations for some example networks.

6.4.6.1 Six-Bus Radial Microgrid

Consider again the six-bus radial microgrid whose single-line diagram is shown in Figure 5.2, which was used for simulation in Chapter 4. In Section 5.5.1, we showed that

$\mathcal{E}_{Key} = \{(3,4)\}$ is a valid constraint-satisficing key line set (per Definition 5.2) for this network under the expected operating range defined in Table 5.1. We will now create two constraint-satisficing droop control configurations (one based on asymmetric placement and one symmetric placement) for $\mathcal{E}_{Key} = \{(3,4)\}$.

Asymmetric CED placement (Definition 6.6.A) for line $(3,4)$ requires that we should select exactly one of buses 3 or 4 to be a CED-inverter bus and assign it to line $(3,4)$, while the other is a traditional droop inverter bus. We will arbitrarily select $3 \in \mathcal{V}_{CED}$, $\sigma(3) = 4$, and $4 \in \mathcal{V}_{Droop}$. Similarly for symmetric CED placement (Definition 6.6.B), we should select both buses 3 and 4 as CED-inverter buses and assign them both to line $(3,4)$ $(3,4 \in \mathcal{V}_{CED}$, $\sigma(3) = 4$, and $\sigma(4) = 3)$. Both configurations are shown in Figure 6.4, where Figure 6.4a shows the selected assymetric CED placement for the single key line $(3,4)$, and Figure 6.4b shows the symmetric CED placement for the same line.

Now consider the maximum and minimum tension constants $\tau_{Max,k,m}$ and $\tau_{Min,k,m}$ for the single key line $(3,4) \in \mathcal{E}_{Key}$, which may be calculated by (144) and (145) respectively. Substituting the generation and load bounds from Table 5.1, the line flow bounds calculated by Procedure 5.1 in Table 5.3, and assuming $D_3^{-1} = D_4^{-1} = 1/(2\,\pi\,0.5) + 1e - 2$ rad/sec, we can calculate numerical values of $\tau_{Max,3,4}$ and $\tau_{Min,3,4}$ as follows:

$$
\begin{aligned}
\tau_{Max,3,4} =& D_3^{-1} P_{G,Max,3} - D_4^{-1} P_{G,Min,4} + D_4^{-1} P_{L,Max,4} \\
& + D_3^{-1} P_{UBound,1,3} + D_3^{-1} P_{UBound,2,3} - D_4^{-1} P_{LBound,5,4} - D_4^{-1} P_{LBound,6,4} \\
=& 3.7699 \text{ rad/sec}
\end{aligned}
\tag{168}
$$

$$
\begin{aligned}
\tau_{Min,3,4} =& D_3^{-1} P_{G,Min,3} - D_3^{-1} P_{L,Max,3} - D_4^{-1} P_{G,Max,4} \\
& + D_3^{-1} P_{LBound,1,3} + D_3^{-1} P_{LBound,2,3} - D_4^{-1} P_{UBound,5,4} - D_4^{-1} P_{UBound,6,4} \\
=& - 3.7699 \text{ rad/sec}
\end{aligned}
\tag{169}
$$
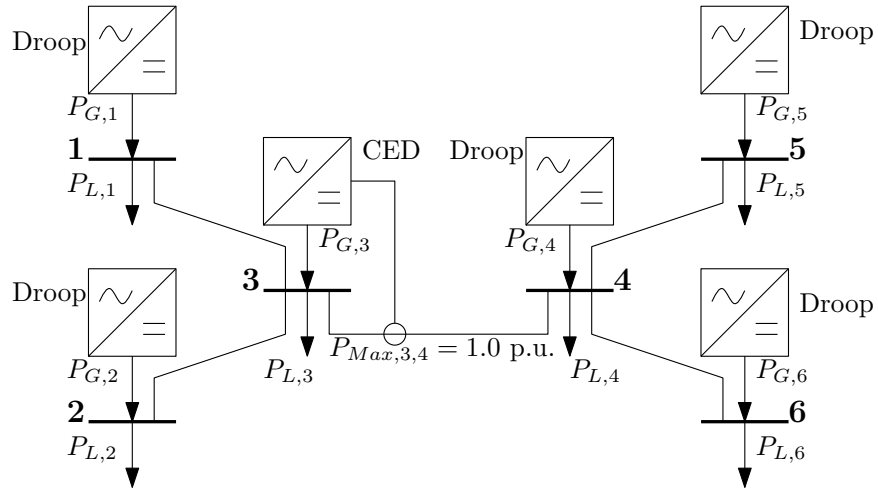
(a) Asymmetric CED: $\mathcal{V}_{CED} = \{3\}$, $\sigma(3) = 4$, and $4 \in \mathcal{V}_{Droop}$
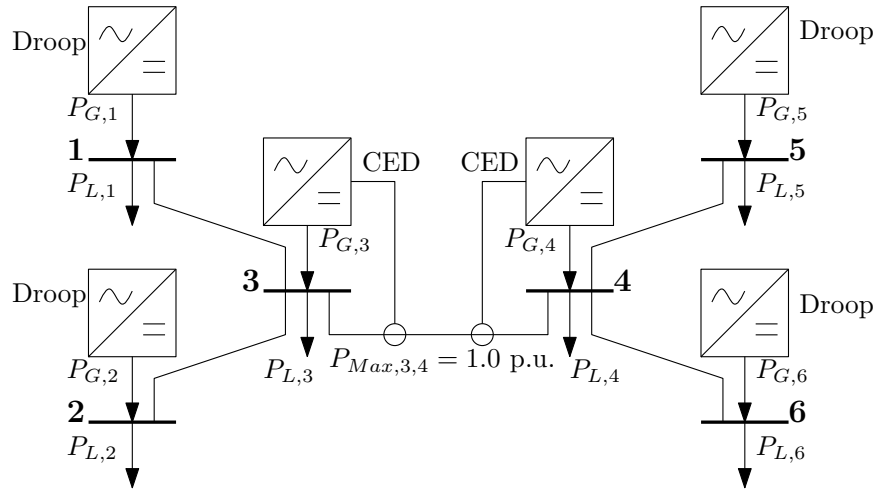
(b) Symmetric CED: $\mathcal{V}_{CED} = \{3, 4\}$, $\sigma(3) = 4$, and $\sigma(4) = 3$

Figure 6.4: Six-Bus Radial Network: Sparse CED Placement and Assignment

In this case, because the network is symmetric about the line $(3, 4)$, $\tau_{Max,3,4}$ and $\tau_{Min,3,4}$ have equal magnitudes, but for other networks this may not be the case.

By Definition 6.7 in order for $\gamma_{Max,3,4} = \gamma_{Max,4,3}$ to be an enforcing selection we should select $\gamma_{Max,3,4}$ according to:

$$\gamma_{Max,3,4} \geq \begin{cases} \max\left(D_3\left[\dfrac{\tau_{Max,3,4}}{P_{Max,3,4}} - D_4^{-1}\right], D_3\left[\dfrac{-\tau_{Min,3,4}}{P_{Max,3,4}} - D_4^{-1}\right], 1\right) & 4 \in \mathcal{V}_{Droop} \\[2em] \max\left(\dfrac{\tau_{Max,3,4}}{P_{Max,3,4}}(D_3^{-1} + D_4^{-1})^{-1}, \dfrac{-\tau_{Min,3,4}}{P_{Max,3,4}}(D_3^{-1} + D_4^{-1})^{-1}, 1\right) & \begin{aligned} &4 \in \mathcal{V}_{CED} \\ &\text{and } \sigma(4) = 3 \end{aligned} \end{cases}$$

$$= \begin{cases} \max(5, 5, 1) & 4 \in \mathcal{V}_{Droop} \\ \max(3, 3, 1) & 4 \in \mathcal{V}_{CED} \text{ and } \sigma(4) = 3 \end{cases} \tag{170}$$

Therefore, we should choose $\gamma_{Max,3,4} \geq 5$ for the asymmetric CED placement (Figure 6.4a), or $\gamma_{Max,3,4} = \gamma_{Max,4,3} \geq 3$ for the symmetric CED placement (Figure 6.4b).

We have therefore constructed two constraint-satisficing droop control configurations for the six-bus radial microgrid under the expected operating range in Table 5.1:

1. Symmetric configuration: $\mathcal{V} = \{3, 4\}$, $\sigma(3) = 4$, $\sigma(4) = 3$, and $\gamma_{Max,3,4} = \gamma_{Max,4,3} = 3$.

2. Asymmetric configuration: $\mathcal{V}_{CED} = \{3\}$, $\sigma(3) = 4$, and $\gamma_{Max,3,4} = 5$.

6.4.6.2 Three-Bus Grid-Tied Microgrid

Consider the three-bus, grid-tied microgrid whose single-line diagram is shown in Figure 6.5. This microgrid has two buses (buses 1 and 2) which each have a connected inverter, one bus (bus 3) which is passive, and a single connection to an external grid, modeled by the infinite bus 4 where $D_4 = \infty$. This represents a typical case of a multi-inverter grid-tied microgrid, and allows for multiple configurations of inverter control type. The expected operating range for this network is shown in Table 6.2 below.

Table 6.2: Expected Operating Range for Three-Bus Microgrid w/ External Infinite Bus

Bus	$P_{G,Max}$	$P_{G,Min}$	$P_{L,Max}$
1	1.0	0.0	5.0
2	2.0	-2.0	6.0
3	0.0	0.0	6.0
4	∞	$-\infty$	0.0
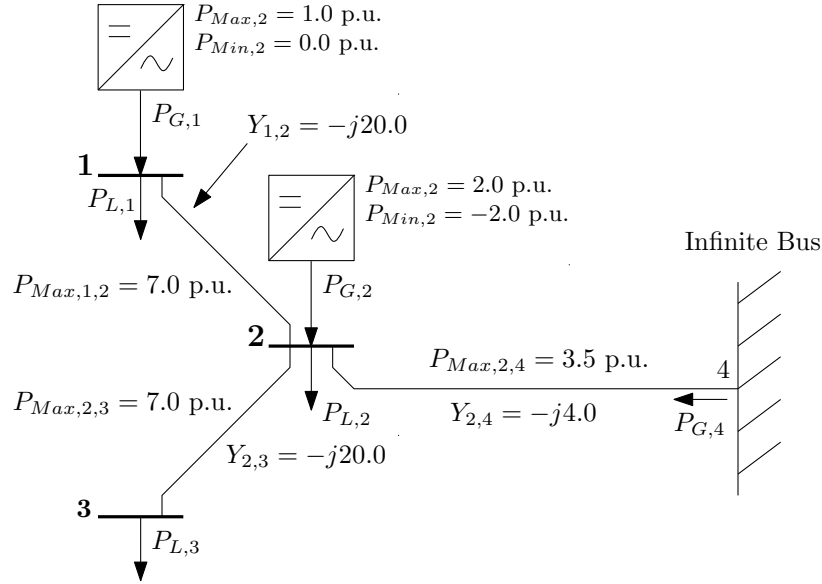
Figure 6.5: Single-Line Diagram of Lossless Three-Bus Grid-Tied Microgrid

Application of the search procedure for constraint-satisficing key line sets (Procedure 5.2) determines that the key line set $\mathcal{E}_{Key} = \{(2,4)\}$ is the unique irreducable (and unique minimal) constraint-satisficing key line set for this network under the expected operating range in Table 6.2. Results of Procedure 5.1 applied to this network for the expected operating range in Table 6.2 for the selection $\mathcal{E}_{Key} = \{(2,4)\}$ are shown in Table 6.3.

Assume that we create a constraint-satisficing droop control configuration for this network by using asymmetric CED at bus 2 to enforce the line power-flow constraint on line $(2,4)$ ($\mathcal{V}_{CED} = \{2\}$ and $\sigma(2) = 4$). We can calculate the maximum and minimum tension values on line $(2,4)$ by substituting the reference and load constraints

Table 6.3: Results of Procedure 5.1 for Three-Bus Microgrid w/ External Infinite Bus with $\mathcal{E}_{Key} = \{(2,4)\}$

i	k	m	In $\mathcal{E}_{Key}$?	$P_{UBound,Sourcing}$	$P_{UBound,Sinking}$	$P_{LBound,Sourcing}$	$P_{LBound,Sinking}$	P_{UBound}	P_{LBound}	P_{Max}	Constraints Met?
1	1	2	False	1.0	17.5	-5.5	-5.0	1.0	-5.0	7.0	True
2	2	3	False	6.5	6.0	0.0	-16.5	6.0	0.0	7.0	True
3	2	4	True	3.5	3.5	-3.5	-3.5	3.5	-3.5	3.5	True

from Table 6.2, the line power-flow bounds from Table 6.3, and the bus total frequency dependence coefficients $D_2 = 1/(2\pi 0.05) + 1e - 2$ sec/rad and $D_4 = \infty$ into (144) and (145) as follows:

$$\tau_{Max,2,4} = D_2^{-1} P_{G,Max,2} - D_4^{-1} P_{G,Min,4} + D_4^{-1} P_{L,Max,4}$$

$$+ D_2^{-1} P_{UBound,1,2} - D_2^{-1} P_{LBound,2,3}$$

$$= 0.9422 \text{ rad/sec} \tag{171}$$

$$\tau_{Min,2,4} = D_2^{-1} P_{G,Min,2} - D_2^{-1} P_{L,Max,2} - D_4^{-1} P_{G,Max,4}$$

$$+ D_2^{-1} P_{LBound,1,2} - D_2^{-1} P_{LBound,2,3}$$

$$= -5.9672 \text{ rad/sec} \tag{172}$$

Notice that since $D_4^{-1} = 0$, then bus 4 does not contribute towards the total tension on line $(2,4)$.

By Definition 6.7, in order for $\gamma_{Max,2,4}$ to be an enforcing selection, we should select it according to:

$$\gamma_{Max,2,4} \geq \max\left(-D_2 \left[\frac{\tau_{Max,2,4}}{P_{Max,2,4}} - D_4^{-1}\right], D_2 \left[\frac{\tau_{Min,2,4}}{P_{Max,2,4}} - D_4^{-1}\right], 1\right)$$

$$= \max\left(0.8571, 5.4286, 1\right) = 5.4286 \tag{173}$$

We therefore select $\gamma_{Max,2,4} = 5.5$ to form the a constraint-satisficing droop control configuration $\mathcal{V}_{CED} = \{2\}$, $\sigma(2) = 4$, $\gamma_{Max,2,4} = 5.5$ for the example three-bus grid-tied microgrid in Figure 6.5.

6.5 *Improved Frequency Synchronization and Power Sharing of Constraint-Satisficing Droop Inverter Networks*

We have shown that applying a constraint-satisficing droop control configuration to a mixed-bus inverter-based network (thus creating a constraint-satisficing droop inverter network, see Definition 6.3), we can explicitly enforce the key line constraints, and thereby bound the network state trajectory $\boldsymbol{\theta}(t)$ into the safe region Θ_{Safe}. We will now show that this is also sufficient to guarantee frequency synchronization for the network on the expected operating range.

In Chapter 4, we used a modified form of LaSalle's Theorem to show convergence of the bus frequency values on closed subsets of the safe region. Because we now include the possibility of network cycles and asymmetric application of CED, this method is no longer sufficient to prove convergence (since the assumption of an acyclic network and symmetric line tensions were necessary, see the proof to Theorem 4.5). In order to show frequency synchronization of constraint-satisficing droop inverter networks, we will use a method based on the Contraction Property (for a full explanation, [49, 81, 55]). Conceptually, the Contraction property of a system of coupled subsystems states that under some mild assumptions, if the dynamics of each subsystem always are always directed into the interior of the convex hull of the subsystem states, then the convex hull of the states must contract, eventually reaching a point (corresponding to state agreement).

We will apply the Contraction property method to the dynamics of the bus frequencies in a mixed-bus inverter-based network under a constraint-satisficing droop control configuration, and show that on the safe region, these frequencies are coupled in such a way that the maximum and minimum bus frequencies are always converging,

and as such must eventually converge to agreement (frequency synchronization). The Convergence property as strictly stated does not directly apply to our network bus frequency dynamics, since the bus frequency dynamics have non-linear state and time dependences. However, by constructing a ficticious auxiliary system with minimum convergence, we can show that the actual frequencies are always contained within the interior of the auxiliary system, and that the Convergence property does directly apply to the auxilliary system. Therefore, the auxiliary system must converge to a point, and so the actual bus frequencies it contains must converge as well.

6.5.1 Modeling of Bus Frequency Dynamics

In this section, we are concerned with the dynamics of the bus frequency offset values $\Delta\omega_k$ for each bus $k \in \mathcal{V}$. We have shown in Lemma 6.2 above that by correctly selecting $\mathcal{E}_{Key}$ and applying a constraint-satisficing droop control configuration to the network (consisting of correctly chosen $\mathcal{V}_{CED}$, σ, and $\gamma_{Max,k,m}$ for each $(k, m) \in \mathcal{E}_{Key}$), it is possible to restrict the operation of the network to the safe region Θ_{Safe} of the voltage-angle state space. Therefore, we will restrict our analysis of the frequency dynamics to the region where $\boldsymbol{\theta} \in \Theta_{Safe}$.

We showed in Chapter 3 that the dynamics of bus synchronous voltage angle δ_k may be modeled by the dynamic equation (6) if k is a network bus or a traditional-droop inverter bus. Since $\Delta\omega_k = \dot{\delta}_k$, we may find the dynamics of $\Delta\omega_k$ by taking the time-derivative of (6):

$$\dot{\Delta\omega}_k = D_k^{-1}\left[\dot{P_{Ref,k}} - \dot{P_{L,k}^0} - \sum_{m\in\mathcal{N}(k)} \frac{\partial P_{Line,k,m}}{\partial\theta_{k,m}}\dot{\theta}_{k,m}\right] \tag{174}$$

for each $k \in (\mathcal{V} \setminus \mathcal{V}_{CED})$

Now consider the synchronous voltage-angle dynamic equation (139) for a CED inverter bus. Taking the time-derivative, we find the bus frequency dynamics for a

CED inverter bus:

$$\dot{\Delta\omega}_k = D_k^{-1}\left[\dot{P}_{Ref,k} - \dot{P}_{L,k}^0 - \sum_{m\in\mathcal{N}(k)\setminus\sigma(k)} \frac{\partial P_{Line,k,m}}{\partial\theta_{k,m}}\dot{\theta}_{k,l}\right.$$

$$- \gamma_{k,\sigma(k)}(|P_{Line,k,\sigma(k)}|)\frac{\partial P_{Line,k,\sigma(k)}}{\partial\theta_{k,\sigma(k)}}\dot{\theta}_{k,\sigma(k)}$$

$$\left.- \frac{\partial\gamma_{k,\sigma(k)}}{\partial|P_{Line,k,\sigma(k)}|}\frac{\partial P_{Line,k,\sigma(k)}}{\partial\theta_{k,\sigma(k)}}|P_{Line,k,\sigma(k)}|\dot{\theta}_{k,\sigma(k)}\right] \tag{175}$$

for each $k \in \mathcal{V}_{CED}$.

The dynamic equations (174) and (175) together form the bus frequency dynamics for a mixed-bus inverter-based AC network. Both consist of two forcing terms $(\dot{P}_{Ref,k} - \dot{P}_{L,k}^0)$ plus a summation of coupling terms to other buses. Further, we can combine the two equations, and represent them as a summation of weighted frequency-coupling terms as follows:

$$\dot{\Delta\omega}_k = D_k^{-1}[\dot{P}_{Ref,k} - \dot{P}_{L,k}^0] - \sum_{m\in\mathcal{N}(k)} \alpha_{k,m}(\theta_{k,m})\theta_{k,m}$$

$$= D_k^{-1}[\dot{P}_{Ref,k} - \dot{P}_{L,k}^0] - \sum_{m\in\mathcal{N}(k)} \alpha_{k,m}(\theta_{k,m})(\Delta\omega_k - \Delta\omega_m) \tag{176}$$

for all $k \in \mathcal{V}$, where

$$\alpha_{k,m}(\theta_{k,m}) = \begin{cases} D_k^{-1}\left[\gamma_{k,m}(|P_{Line,k,m}|) + \frac{\partial\gamma_{k,m}}{\partial|P_{Line,k,m}|}|P_{Line,k,m}|\right]\frac{\partial P_{Line,k,m}}{\partial\theta_{k,m}} & k \in \mathcal{V}_{CED} \\ & \text{and } \sigma(k) = m \\ D_k^{-1}\frac{\partial P_{Line,k,m}}{\partial\theta_{k,m}} & \text{Otherwise} \end{cases} \tag{177}$$

is a state-dependent weight term for each line, where the weight $\alpha_{k,m}$ is a function of the associated line voltage-angle difference $\theta_{k,m}$, and is not necessarily line-symmetric ($\alpha_{k,m}$ does not necessarily equal $\alpha_{m,k}$).

In Lemma 3.3, we showed that partial derivative $\partial P_{Line,k,m}/\partial\theta_{k,m}$ is strictly positive on the principal region (and therefore on the safe region since $\Theta_{Safe} \subset \Theta_{Principal}$). By assumption $D_k^{-1} > 0$ for all $k \in \mathcal{V}$, and by Definition 6.5, $\gamma_{k,m}(|P_{Line,k,m}|)$ is strictly

positive and $\partial\gamma_{k,m}/\partial|P_{Line,k,m}|$ non-negative. Therefore, the state-dependent weight is strictly positive ($\alpha_{k,m}(\theta_{k,m}) > 0$) for all lines $(k, m) \in \mathcal{E}$ on the safe region $\boldsymbol{\theta} \in \Theta_{Safe}$. Thus, the bus frequency dynamics of any bus can be represented as a conic combination (summation with all non-negative weights) of the differences between bus frequencies across each incident line (plus a forcing term).

Consider the vector of bus frequency values $\boldsymbol{\Delta\omega} = \begin{bmatrix} \Delta\omega_1 & \dots & \Delta\omega_N \end{bmatrix}^T \in \mathbb{R}^N$, and imagine its members as points on a line. Then their convex hull is a line segment between the maximum and minimum values of $\Delta\omega_k$. The terms of the bus frequency dynamics (176) can then be imagined as tensions, which pull the bus frequencies towards each other on Θ_{Safe} (since the coefficients $\alpha_{k,m}(\theta_{k,m})$ are always positive on Θ_{Safe}). If the forcing terms decay to zero (as when $P_{Ref,k}$ and $P_{L,k}^0$ converge to constants), then the total dynamics $\Delta\omega_k$ for each $k \in \mathcal{V}$ should be directed into the convex hull. However, this property is not sufficient to ensure synchronization of the bus frequencies, since the Contraction Property Theorem [49, Theorem 3.8] as stated applies only to networked systems where the weight depends only on the consensus variable ($\boldsymbol{\Delta\omega}$ in this case), and not when it depends on time or an external variable ($\boldsymbol{\theta}$ in this case). Therefore, we will introduce below a ficticious "auxiliary system", such that the convex hull of the auxiliary system always contains the actual bus frequency values, and the Contraction Property Theorem can be shown to apply directly to the auxiliary system.

6.5.2 Development of Auxiliary Bounding System

Consider again the state-dependent weight functions $\alpha_{k,m}$ for each line $(k, m) \in \mathcal{E}$ in (177). Finding the partial derivative $\partial P_{Line,k,m}/\partial\theta_{k,m}$ from (2) and substituting into

(177):

$$
\alpha_{k,m}(\theta_{k,m}) = \begin{cases} D_k^{-1}\left[\gamma_{k,m}(|P_{Line,k,m}|) + \dfrac{\partial \gamma_{k,m}}{\partial |P_{Line,k,m}|}|P_{Line,k,m}|\right]Y_{k,m}V_kV_m\cos(\theta_{k,m}) & \begin{array}{l} k \in \mathcal{V}_{CED} \\ \text{and } \sigma(k) = m \end{array} \\ \\ D_k^{-1}Y_{k,m}V_kV_m\cos(\theta_{k,m}) & \text{Otherwise} \end{cases}
$$
$$(178)$$

Recall that $Y_{k,m}$, V_k, V_m, and D_k^{-1} are all (by assumption) strictly positive. By Definition 6.5, $\gamma_{k,m}(|P_{Line,k,m}|) \geq 1$ and $\partial \gamma_{k,m}/\partial |P_{Line,k,m}| \geq 0$. Therefore, we may bound $\alpha_{k,m}$ from below by:

$$
\alpha_{k,m}(\theta_{k,m}) \geq D_k^{-1}Y_{k,m}V_kV_m\cos(\theta_{k,m}) \tag{179}
$$

Further, by Corollary 3.2, $|\theta_{k,m}| \leq \theta_{Max,k,m}$ on Θ_{Safe} for each $(k,m) \in \mathcal{E}$, and therefore, we can further bound $\alpha_{k,m}$ by:

$$
\alpha_{k,m}(\theta_{k,m}) \geq D_k^{-1}Y_{k,m}V_kV_m\cos(\theta_{Max,k,m}) = \alpha_{Min,k,m}, \; \boldsymbol{\theta} \in \Theta_{Safe} \tag{180}
$$

where $\alpha_{Min,k,m} > 0$ is a constant, which represents the minimum value of the coefficient $\alpha_{k,m}(\theta_{k,m})$ on Θ_{Safe}.

Imagine a fictitious auxiliary variable $v_k(t)$ associated with each bus $k \in \mathcal{V}$, where $v_k(T) = \Delta\omega_k(T)$ for some time T. However, while $\Delta\omega_k$ evolves in $t \geq T$ according to the dynamics (176) (based on the state-dependent tension weights $\alpha_{k,m}(\theta_{k,m})$), $v_k(t)$ evolves according to the same dynamics *but with the constant minimum tension weights $\alpha_{Min,k,m}$*). The auxiliary system $\boldsymbol{v}(t)$ therefore represents a "minimum coupling" version of the frequency dynamics.

Figure 6.6 below shows the elements of the vector of bus frequency values $\Delta\boldsymbol{\omega}$ and auxiliary variables $\boldsymbol{v} = \begin{bmatrix} v_1 & \cdots & v_N \end{bmatrix}^T$ for an example system as points on a line. Notice that at time $t = T$ (Figure 6.6a), $\Delta\boldsymbol{\omega}(T) = \boldsymbol{v}(T)$. However, v_{Max} (the maximum element of $\boldsymbol{v}$) is decreasing more slowly than $\Delta\omega_{Max}$ (the maximum element of $\Delta\boldsymbol{\omega}$), since the tension weights in the dynamics of $\boldsymbol{v}$ are always less than

or equal to those in the dynamics of $\boldsymbol{\Delta\omega}$. Similarly, v_{Min} is increasing more slowly than $\Delta\omega_{Min}$ (for the same reason). Therefore, at time $t = T + \Delta T$ (Figure 6.6b), $v_{Max} \geq \Delta\omega_{Max}$ and $v_{Min} \leq \Delta\omega_{Min}$. Therefore, the line segment between v_{Min} and v_{Max} (convex hull of $\boldsymbol{v}$) always contains all of the bus frequency values. We formalize this result in Lemma 6.3 below.

(a) $\boldsymbol{\Delta\omega}$ and $\boldsymbol{v}$ at time $t = T$

(b) $\boldsymbol{\Delta\omega}$ and $\boldsymbol{v}$ at time $t = T + \Delta T$ for some $\Delta T > 0$
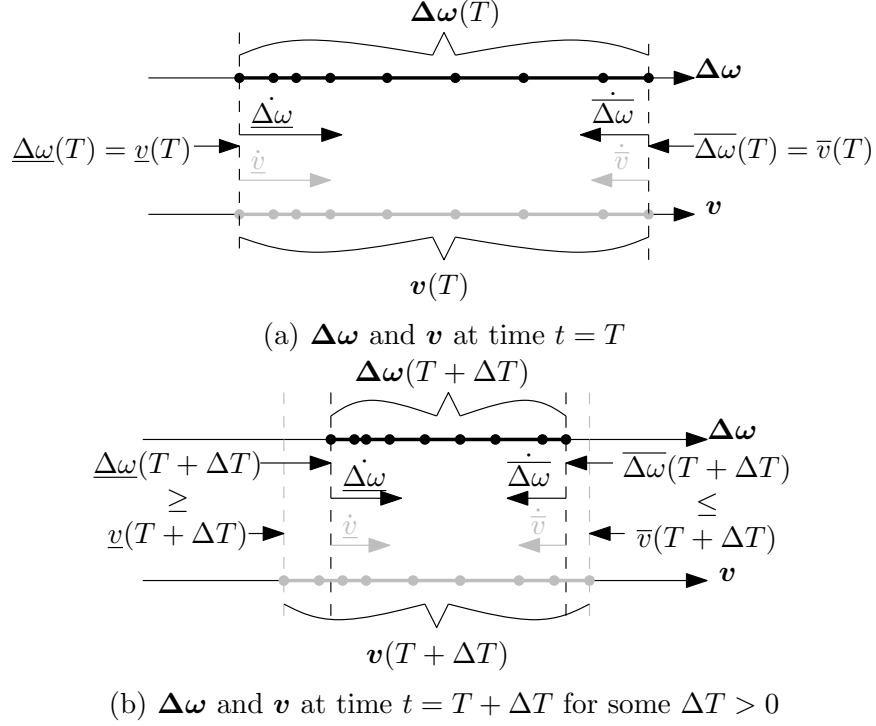
Figure 6.6: Example bus frequencies and auxiliary variables

Lemma 6.3 (Bus frequencies are always contained inside auxiliary system convex hull). *Consider a trajectory $\boldsymbol{\Delta\omega}(t)$ of the bus frequency offset dynamics* (176) *with weight coefficients* (177), *and assume that $\boldsymbol{\theta}(t) \in \Theta_{Safe}$ for all $t \geq T$ and that $\mathbf{\dot{P}_{Ref}} = \mathbf{\dot{P}_L^0} = \mathbf{0}_N$. Consider the trajectory $\mathbf{v}(t) = \left[v_1(t) \ldots v_N(t) \right]^T \in \mathbb{R}^N$ where $\mathbf{v}(T) = \boldsymbol{\Delta\omega}(T)$ and*

$$\dot{v}_k = - \sum_{m \in \mathcal{N}(k)} \alpha_{Min,k,m}(v_k - v_m) \tag{181}$$

where

$$\alpha_{Min,k,m} = D_k^{-1} V_k V_m \cos(\theta_{Max,k,m}) > 0 \tag{182}$$

185

Consider also the following values:

$$\Delta\omega_{Max}(t) = \max_{k \in \mathcal{V}}\{\boldsymbol{\Delta\omega}(t)\} \tag{183}$$

$$\Delta\omega_{Min}(t) = \min_{k \in \mathcal{V}}\{\boldsymbol{\Delta\omega}(t)\} \tag{184}$$

$$v_{Max}(t) = \max_{k \in \mathcal{V}}\{\mathbf{v}(t)\} \tag{185}$$

$$v_{Min}(t) = \min_{k \in \mathcal{V}}\{\mathbf{v}(t)\} \tag{186}$$

Then the following inequality holds for all for all $k \in \mathcal{V}$ and for all $t \geq T$:

$$v_{Min}(t) \leq \Delta\omega_{Min}(t) \leq \Delta\omega_k(t) \leq \Delta\omega_{Max}(t) \leq v_{Max}(t) \tag{187}$$

that is, the convex hull of the frequency error $\boldsymbol{\Delta\omega}(t)$ is contained within the convex hull of $\boldsymbol{v}(t)$.

Proof. Consider the frequency dynamics (176) where $\mathbf{P_{Ref}}$ and $\mathbf{P_L^0}$ are constant. Observe that these dynamics are of the form:

$$\dot{\Delta\omega}_k = -\sum_{m \in \mathcal{N}(k)} \alpha_{k,m}(\theta_{k,m}(t))(\Delta\omega_k - \Delta\omega_m) = f_k(\boldsymbol{\Delta\omega}, t) \ \forall \ k \in \mathcal{V} \tag{188}$$

where the state-dependent weight term $\alpha_{k,m}(\theta_{k,m})$ is found as in (177). We have shown above that $\alpha_{k,m}(\theta_{k,m}) \geq \alpha_{Min,k,m}$ for all $\boldsymbol{\theta} \in \Theta_{Safe}$, where the constant $\alpha_{Min,k,m}$ is calculated as in (180).

Now consider the dynamic variables $\Delta\omega_{Max}(t)$ and $v_{Max}(t)$. For each $t \geq T$, there exists $k_{Max}(t) \in \mathcal{V}$ such that $v_{Max}(t) = v_{k_{Max}(t)}$ and $\dot{v}_{Max}(t) = \dot{v}_{k_{Max}(t)}$. Since (by definition) $(v_{k_{Max}(t)}(t) - v_m(t)) \geq 0$ for all $m \in \mathcal{V}$ and $\alpha_{k,m}(\theta_{k,m}) \geq \alpha_{Min,k,m} > 0$ for all $(k, m) \in \mathcal{E}$, then

$$\dot{v}_{Max}(t) = \dot{v}_{k_{Max}(t)} = -\sum_{m \in \mathcal{N}(k_{Max}(t))} \alpha_{Min,k_{Max}(t),m} \left(v_{k_{Max}(t)} - v_m\right)$$

$$\geq -\sum_{m \in \mathcal{N}(k_{Max}(t))} \alpha_{k_{Max}(t),m}(\theta_{k_{Max}(t),m}) \left(v_{k_{Max}(t)}(t) - v_m\right)$$

$$= f_{k_{Max}(t)}(\boldsymbol{v}(t), t) \tag{189}$$

Since $\Delta\omega_{Max}(T) = v_{Max}(T)$ and $\dot{v}_{Max}(t) \geq f_{k_{Max}(t)}(\boldsymbol{v}(t), t)$ for all $t \geq T$, then (by the Comparison Principal [43, Ch. 3]) $v_{Max}(t) \geq \Delta\omega_{Max}(t)$ for all $t \geq T$.

Similarly for each $t \geq T$, there exists $k_{Min}(t) \in \mathcal{V}$ such that $v_{Min}(t) = v_{k_{Min}(t)}$ and $\dot{v}_{Min}(t) = \dot{v}_{k_{Min}(t)}$, and since $(v_{k_{Min}(t)}(t) - v_m(t)) \leq 0$ for all $m \in V$, then

$$\dot{v}_{Min}(t) = \dot{v}_{k_{Min}(t)} = -\sum_{m \in \mathcal{N}(k_{Min}(t))} \alpha_{Min,k_{Min}(t),m} \left(v_{k_{Min}(t)} - v_m\right)$$

$$\leq -\sum_{m \in \mathcal{N}(k_{Min}(t))} \alpha_{k_{Min}(t),m}(\theta_{k_{Min}(t),m}) \left(v_{k_{Min}(t)} - v_m\right)$$

$$= f_{k_{Min}(t)}(\boldsymbol{v}(t), t) \tag{190}$$

Since $v_{Min}(T) = \Delta\omega_{Min}(T)$ and $\dot{v}_{Min}(t) \leq f_{k_{Min}(t)}(\boldsymbol{v}(t), t)$ for all $t \geq T$, then (by the Comparison Principal [43, Ch. 3]) $v_{Min}(t) \leq \Delta\omega_{Min}(t)$ for all $t \geq T$.

By definition $\Delta\omega_{Min}(t) \leq \Delta\omega_k(t) \leq \Delta\omega_{Max}(t)$ for all $k \in \mathcal{V}$ and all t. Therefore:

$$v_{Min}(t) \leq \Delta\omega_{Min}(t) \leq \Delta\omega_k(t) \leq \Delta\omega_{Max}(t) \leq v_{Max}(t) \tag{191}$$

for all $k \in \mathcal{V}$ and for all $t \geq T$. $\qquad\qquad \square$

Lemma 6.3 shows that the line segment between the maximum and minimum values of $\Delta\omega_k(t)$ for all $k \in \mathcal{V}$ (the convex hull of $\boldsymbol{\Delta\omega}(t)$) is always contained within the line segment between the maximum and minimum values of $v_k(t)$ (the convex hull of $\boldsymbol{v}(t)$). Conceptually, this is because v_{Min} and v_{Max} are pulled towards the interior of $\boldsymbol{v}$ *more slowly* than $\Delta\omega_{Min}$ and $\Delta\omega_{Max}$ are pulled towards the interior of $\boldsymbol{\Delta\omega}$ (since the tension weights are smaller).

6.5.3 Frequency Synchronization

In Lemma 6.2, we showed that in a constraint-satisfying droop inverter network (Definition 6.3), the network voltage-angle trajectory is constrained to the safe region Θ_{Safe}, on which all line power-flow constraints are met ($|P_{Line,k,m}| \leq P_{Max,k,m} \; \forall \; (k, m) \in \mathcal{E}$). We further showed in Lemma 6.3 that on Θ_{Safe}, the bus frequency values $\boldsymbol{\Delta\omega}(t)$

are contained in the convex hull of a simple linear auxiliary system $\mathbf{v}(t)$. Therefore, in order to show that a constraint-satisficing droop control configuration is sufficient to guarantee frequency synchronization on the expected operating range, we need only show that $\mathbf{v}(t)$ must converge to state agreement. We show this result via the Contraction Theorem (see [49, Theorem 3.8], which applies directly to the auxiliary system $\mathbf{v}(t)$. We show this result formally below:

Theorem 6.1 (Improved Frequency Synchronization of Constraint-Satisficing Droop Inverter Networks). *Consider a given constraint-satisficing droop inverter network (Definition 6.3), and assume that $(\mathbf{P_G}(t), \mathbf{P_L}(t)) \in \mathbb{P}$ and $(\mathbf{P_{Ref}}(t), \mathbf{P_L^0}(t)) \in \mathbb{P}$ for all $t \geq 0$. Further assume that there exists time $T > 0$ such that $\dot{\mathbf{P}}_{\mathbf{Ref}}(t) = 0$ and $\dot{\mathbf{P}}_{\mathbf{L}}^{\mathbf{0}}(t) = 0$ for all $t \geq T$. Consider the trajectory $\boldsymbol{\theta}(t)$ of the network dynamics (141) for $t \geq 0$ such that $\boldsymbol{\theta}(0) \in \Theta_{Safe}$. Then there exists $\Delta\omega_{Sys} \in \mathbb{R}$ such that $\Delta\boldsymbol{\omega}(t) \to \Delta\omega_{Sys}\mathbf{1}_N$ (frequency synchronization) and there exists $\boldsymbol{\theta}_F \in \Theta_{Safe}$ such that $\boldsymbol{\theta}(t) \to \boldsymbol{\theta}_F$ (phase coherency).*

Proof. We have shown (in Lemma 6.2) that the line voltage-angle $\boldsymbol{\theta}$ dynamics (141) of a network meeting the assumptions in Theorem 6.1 are invariant to the set Θ_{Safe}. Since (by assumption) $\boldsymbol{\theta}(0) \in \Theta_{Safe}$, then $\boldsymbol{\theta}(t) \in \Theta_{Safe} \subset \Theta_{Principal}$ for all $t \geq 0$.

Now consider the dynamics of the bus frequency dynamics $\Delta\boldsymbol{\omega}(t)$ in (176) with tension weights (177). By assumption, $\dot{P}_{Ref,k}(t) = 0$ and $\dot{P}_{L,k}(t) = 0$ for $t \geq T > 0$. Therefore, for $t \geq T$:

$$\dot{\Delta\omega}_k = -\sum_{m\in\mathcal{N}(k)} \alpha_{k,m}(\theta_{k,m})(\Delta\omega_k - \Delta\omega_m) \,\forall\, k \in \mathcal{V} \tag{192}$$

Since $T > 0$, then $\boldsymbol{\theta}(T) \in \Theta_{Safe}$. Therefore the results of Lemma 6.3 apply, showing that the bus frequency values $\Delta\omega_k(t)$ for all $k \in \mathcal{V}$ are contained within the convex hull of a simpler system $\mathbf{v}(t) = \begin{bmatrix} v_1(t) \dots v_N(t) \end{bmatrix}^T \in \mathbb{R}^N$ for $t \geq T$, where the dynamics of $\mathbf{v}(t)$ are shown in (181) and $\mathbf{v}(T) = \Delta\boldsymbol{\omega}(T)$. Therefore, if $\mathbf{v}(t)$ converges

to state agreement (and so its convex hull contracts to a point), then $\boldsymbol{\Delta\omega}(t)$ must as well.

We will show that for $t \geq T$, the *Contraction Thorem* [49, Theorem 3.8] applies to the bounding system $\mathbf{v}(t)$. The Contraction Theorem considers a system of non-linear coupled subsystems with dynamics in the following form:

$$\dot{v}_k = - \sum_{m \in \mathcal{N}_{In}(k)} \alpha_{k,m}(\boldsymbol{v})(v_k - v_m) \tag{193}$$

where $\mathcal{N}_{In}(k)$ the in-neighborhood for bus $k \in \mathcal{V}$ in a directed network, that is, the set of all other buses such that there exists a line from m to k (*not* from k into m).

The dynamics in (188) are similar to (193), except that in (188) each $\dot{\Delta\omega}_k$ depends on all its neighbors in the power-flow structure graph $\mathfrak{G}$ ($\mathcal{N}(k)$) rather than just $\mathcal{N}_{In}(k)$. Therefore, we will form the directed *dynamic iteraction graph* $\mathfrak{G}' = (\mathcal{V}, \mathcal{E}')$ where $\mathcal{E}' = \{\mathcal{E}, reverse(\mathcal{E})\}$ such that (181) can be written in the form (193) using $\mathfrak{G}'$ as the underlying dynamic-interaction graph. Further, observe that since the power-flow structure graph $\mathfrak{G}$ is assumed to be connected, then $\mathfrak{G}'$ is strongly connected for all t (and therefore uniformly quasi-strongly connected).

The contraction property states that if $\alpha_{k,m}(\boldsymbol{v}) > 0$ and locally Lipschitz for all $(k, m) \in \mathcal{E}$ and the underlying dynamic interaction graph is uniformly quasi-strongly connected then the network state $\boldsymbol{v}$ will converge to the agreement subspace $span\{\mathbf{1}_N\}$. Therefore, the Contraction Theorem [49, Theorem 3.8] applies to the auxiliary system $\boldsymbol{v}(t)$ since:

1. The network dynamics (181) are globally Lipschitz, satifying [49, Assumption A1]).

2. The coupling weight term $\alpha_{Min,k,m}$ for all $(k, m) \in \mathcal{E}$ of the $\mathbf{v}(t)$ dynamics is strictly positive, satisfying the *strict subtangentiality condition* [49, Assumption A2]).

189

3. The dynamic interaction graph $\mathfrak{G}'$ (*not* the power-flow structure graph $\mathfrak{G}$) is statically strongly connected (and therefore uniformly quasi-strongly connected, satisfying [49, Assumption A3]).

The above show that [49, Theorem 3.8] applies to the bounding system $\mathbf{v}(t)$ with dynamics (181), and therefore there exists $\Delta\omega_{Sys} \in \mathbb{R}$ such that $\lim_{t\to\infty} \mathbf{v}(t) = \Delta\omega_{Sys}\mathbf{1}_N$. Since we have also shown (Lemma 6.3) that $v_{Min}(t) \leq \Delta\omega_k(t) \leq v_{Max}(t)$, then $\lim_{t\to\infty} v_{Min}(t) = \lim_{t\to\infty} \Delta\omega_k(t) = \lim_{t\to\infty} v_{Max}(t) = \Delta\omega_{Sys}$ for all $k \in \mathcal{V}$, that is, $\lim_{t\to\infty} \mathbf{\Delta\omega} = \Delta\omega_{Sys}\mathbf{1}_N$.

Finally, since $\dot{\boldsymbol{\theta}} = \mathfrak{D}^T\dot{\boldsymbol{\delta}} = \mathfrak{D}^T\mathbf{\Delta\omega}$ and $\mathfrak{D}^T\mathbf{1}_N = \mathbf{0}_L$, then $\lim_{t\to\infty} \dot{\boldsymbol{\theta}} = \mathfrak{D}^T \lim_{t\to\infty} \mathbf{\Delta\omega} = \mathbf{0}_L$. Since we have shown that $\boldsymbol{\theta}(t) \in \Theta_{Safe}$ for all $t \geq 0$ and Θ_{Safe} is compact (Corollary 3.2), then there exists $\boldsymbol{\theta}_F \in \Theta_{Safe}$ such that $\lim_{t\to\infty} \boldsymbol{\theta}(t) = \boldsymbol{\theta}_F$. $\qquad\square$

Theorem 6.1 confirms the expectation that application of a constraint-satisficing droop control configuration (per Definition 6.3), which was already shown to bound the network operation into the safe region Θ_{Safe}, is also sufficient to ensure frequency synchronization of the network for any condition with the expected operating range $\mathbb{P}$. It extends Theorem 3.5 (which only applied to droop inverter-based network) to the much more general case encompased by mixed-bus inverter-based networks. In addition, it provides a much stronger result: by applying a constraint-satisficing droop control configuration, it is possible to ensure frequency synchronization for *any initial condition and any operating conditions within the expected operating range.*

6.6 Power Sharing in Constraint-Satisficing Droop Inverter Networks

Throughout this work, we have attempted to use frequency synchronization of the network to ensure equitable sharing of real power between the inverter sources (according to their assigned reference and droop values). In Chapter 3 we showed that frequency synchronization of traditional droop inverter-based networks is sufficient to

ensure power sharing between inverters, which we termed the simple power sharing property. We extended this result in Chapter 4 by showing that in all-active-bus, acyclic CED networks, a similar property applies, but when a constraint is active the incident inverter must adjust their real power output to enforce the constraint, which we termed the constrained power sharing property. In this section, we consider the convergence properties of a mixed-bus inverter-based network under a constraint-satisficing droop control configuration, and show that it also possess properties ensuring the sharing of real power between inverters. Further, since such a network has been shown to have significantly improved frequency synchronization behavior (as compared with traditional frequency-droop), it follows that its power sharing will also be much more robust.

6.6.1 Center-of-Mass Frequency for Constraint-Satisficing Droop Inverter Network

In Lemma 3.1, we showed that a traditional droop inverter-based network possesses the *static center-of-mass frequency property*, that is, its center-of-mass frequency (defined in Definition 3.2) is static (independent of state) for constant inputs $\mathbf{P_{Ref}}$ and $\mathbf{P_L^0}$. We showed in Lemma 4.2 that the same property also holds for all-active-bus, acyclic CED networks. In both cases, this property is due to the fact that all line dynamic tensions ($P_{Line,k,m}$ in traditional droop and $\gamma_{k,m} P_{Line,k,m}$ for all-active-bus CED) are line-odd, and therefore cancel in the center-of-mass frequency summation. However, as we will show below, this property only holds for constraint-satisficing droop inverter networks *only under certain conditions*, due to the asymmetry of some line dynamic tensions.

Lemma 6.4 (Conditional Static Center-of-Mass Frequency for Constraint-Satisficing Droop Inverter Networks)**.** *Consider the center-of-mass frequency $\Delta\omega_{COM}(t)$ defined in Definition 3.2 for a state trajectory $\boldsymbol{\theta}(t) \in \Theta_{Safe}$ for $t \geq 0$ of a given constraint-satisficing droop inverter network (Definition 6.3) where $(\mathbf{P_G}(t), \mathbf{P_L}(t)) \in \mathbb{P}$ and*

191

$(\mathbf{P_{Ref}}(t), \mathbf{P_L^0}(t)) \in \mathbb{P}$ *for all* $t \geq 0$. *Further assume that there exists time* $T > 0$ *such that* $\dot{\mathbf{P}}_{\mathbf{Ref}}(t) = 0$ *and* $\dot{\mathbf{P}}_{\mathbf{L}}^{\mathbf{0}}(t)$ *for all* $t \geq T$. *Then* $\Delta\omega_k(t) \to \Delta\omega_{COM}(t) = 0$ *for each* $k \in \mathcal{V}$. *Further, the static center-of-mass frequency property:*

$$\Delta\omega_{COM}(t) = \frac{\sum_{k\in\mathcal{V}} P_{Ref,k}(t) - \sum_{k\in\mathcal{V}} P_{L,k}^0(t)}{\sum_{k\in\mathcal{V}} D_k} = \frac{\Delta\mathcal{P}_{Ref}}{\mathcal{D}}, \qquad (194)$$

holds if Symmetric CED Placement (Definition 6.6.B) is used for each key line $(k,m) \in \mathcal{E}_{Key}$.

Proof. We have already shown in Theorem 6.1 above that for the condition in Theorem 6.2, then there exists $\Delta\omega_{Sys} \in \mathbb{R}$ and $\boldsymbol{\theta}_F \in \Theta_{Safe}$ such that $\boldsymbol{\Delta\omega}(t) \to \Delta\omega_{Sys}\mathbf{1}_N$ and $\boldsymbol{\theta}(t) \to \boldsymbol{\theta}_F$.

Taking the limit of $\Delta\omega_{COM}(t)$ as $t \to \infty$:

$$\lim_{t\to\infty} \Delta\omega_{COM}(t) = \frac{\sum_{k\in\mathcal{V}} D_k \lim_{t\to\infty} \Delta\omega_k(t)}{\sum_{k\in\mathcal{V}} D_k} = \frac{\sum_{k\in\mathcal{V}} D_k \Delta\omega_{Sys}}{\sum_{k\in\mathcal{V}} D_k}$$

$$= \Delta\omega_{Sys} = \lim_{t\to\infty} \Delta\omega_k(t) \; \forall \; k \in \mathcal{V} \qquad (195)$$

Therefore, $\Delta\omega_k(t) \to \Delta\omega_{Sys}$ for all $k \in \mathcal{V}$ implies that $\Delta\omega_k(t) \to \Delta\omega_{COM}(t)$ for all $k \in \mathcal{V}$.

Consider again the center-of-mass frequency $\Delta\omega_{COM}$ as in Definition 3.2. Substituting the dynamic equation (7) for $k \in (\mathcal{V}_{Droop} \cup V_{Net})$ and (139) for $k \in \mathcal{V}_{CED}$:

$$\Delta\omega_{COM}(t) = \frac{1}{\sum_{k\in\mathcal{V}} D_k} \sum_{k\in(\mathcal{V}_{Droop}\cup\mathcal{V}_{Net})} \left[P_{Ref,k} - P_{L,k}^0 - \sum_{m\in\mathcal{N}(k)} P_{Line,k,m} \right]$$

$$+ \frac{1}{\sum_{k\in\mathcal{V}} D_k} \sum_{k\in\mathcal{V}_{CED}} \left[P_{Ref,k} - P_{L,k}^0 - \sum_{m\in\mathcal{N}(k)\backslash\sigma(k)} P_{Line,k,m} \right.$$

$$\left. - \gamma_{k,\sigma(k)}(|P_{Line,k,\sigma(k)}|) P_{Line,k,\sigma(k)} \right] \qquad (196)$$

Since the network is constraint-satisficing, then by Definition 6.6 each key line is enforced either by asymmetric or symmetric CED placement. Let $\mathcal{E}_{Key,Sym}$ by the set of key lines enforced by symmetric CED placement and let $\mathcal{E}_{Key,Asym}$ by the set of

key line enforced by asymmetric CED placement. Then the summation in (196) may be rearranged by lines as follows:

$$\Delta\omega_{COM}(t) = \frac{1}{\sum_{k\in\mathcal{V}} D_k} \left[\sum_{k\in\mathcal{V}} \left[P_{Ref,k} - P_{L,k}^0 \right] \right.$$

$$+ \sum_{(k,m)\in(\mathcal{E}\backslash\mathcal{E}_{Key})} \left[P_{Line,k,m} + P_{Line,m,k} \right]$$

$$+ \sum_{(k,m)\in\mathcal{E}_{Key,Sym}} \left[\gamma_{k,m}(|P_{Line,k,m}|)P_{Line,k,m} + \gamma_{m,k}(|P_{Line,m,k}|)P_{Line,m,k} \right]$$

$$+ \left. \sum_{(k,m)\in\mathcal{E}_{Key,Asym}} \left[\gamma_{k,m}(|P_{Line,k,m}|)P_{Line,k,m} + P_{Line,m,k} \right] \right]$$

$$(197)$$

By assumption, $\gamma_{k,m}(|P_{Line,k,m}|) = \gamma_{m,k}(|P_{Line,m,k}|)$, and by (2) $P_{Line,k,m} = -P_{Line,m,k}$. Therefore, the summations associated with the non-key lines and symmetric CED key lines cancel:

$$\Delta\omega_{COM}(t) = \frac{1}{\sum_{k\in\mathcal{V}} D_k} \left[\sum_{k\in\mathcal{V}} \left[P_{Ref,k} - P_{L,k}^0 \right] \right.$$

$$+ \left. \sum_{(k,m)\in\mathcal{E}_{Key,Asym}} \left[\gamma_{k,m}(|P_{Line,k,m}|)P_{Line,k,m} + P_{Line,m,k} \right] \right]$$

$$(198)$$

Now consider the condition where Symmetric CED Placement is used for all key lines. Then $\mathcal{E}_{Key,Asym} = \emptyset$, and so (198) reduces to (194). $\qquad\square$

Lemma 6.4 shows that a constraint-satisficing droop inverter network using symmetric CED placement has the same static center-of-mass frequency $\Delta\omega_{COM}$ as either a traditional droop network (see Lemma 3.1) or an all-active-bus CED network (see Lemma 4.2).

6.6.2 Constrained Power Sharing of Constraint-Satisficing Droop Inverter Networks

The inverter sources in a constraint-satisficing droop inverter network are a mix of traditional frequency-droop inverters and bounded, single-line CED inverters. We

showed in Lemma 3.2 that because the traditional frequency-droop control law creates an explicit relationship between inverter output power and frequency, frequency synchronization of the network is sufficient to ensure that traditional droop inverters share power according to their assigned reference and droop constant values. Like the all-incident-line CED control law, the single-line CED control law produces dynamics identical to traditional droop when no incident line constraints are active. As such, all droop inverters and all CED inverters not incident to lines with active constraints should share power similarly to inverters in a traditional droop network. We formalize this result as follows:

Theorem 6.2 (Constrained Power Sharing of Constraint-Satisficing Droop Inverter Networks). *Consider a given constraint-satisficing droop inverter network (Definition 6.3), and assume that $(\mathbf{P_G}(t), \mathbf{P_L}(t)) \in \mathbb{P}$ and $(\mathbf{P_{Ref}}(t), \mathbf{P_L^0}(t)) \in \mathbb{P}$ for all $t \geq 0$. Further assume that there exists time $T > 0$ such that $\dot{\mathbf{P}}_{\mathbf{Ref}}(t) = 0$ and $\dot{\mathbf{P}}_{\mathbf{L}}^{\mathbf{0}}(t) = 0$ for all $t \geq T$. Consider the trajectory $\boldsymbol{\theta}(t)$ of the network dynamics (141) for $t \geq 0$ such that $\boldsymbol{\theta}(0) \in \Theta_{Safe}$. Then for each $k \in \mathcal{V}_{Droop}$ and each $k \in \mathcal{V}_{CED}$ such that $|P_{Line,k,\sigma(k)}(\theta_{F,k,\sigma(k)})| \leq (1 - \epsilon_{k,m})P_{Max,k,\sigma(k)}$:*

$$\lim_{t \to \infty} P_{G,k}(t) = P_{Ref,k} - R_k^{-1}\Delta\omega_{Sys} \tag{199}$$

for some $\Delta\omega_{Sys} \in \mathbb{R}$. Further,

$$\lim_{t \to \infty} P_{G,k}(t) = P_{Ref,k} - R_k^{-1}\frac{\Delta\mathcal{P}_{Ref}}{\mathcal{D}} = P_{F,k} \tag{200}$$

(where $P_{F,k}$ is defined in (20)) if Symmetric CED Placement (Definition 6.6.B) is used for each key line $(k, m) \in \mathcal{E}_{Key}$.

Proof. We have already shown in Theorem 6.1 above that for the condition in Theorem 6.2, then there exists $\Delta\omega_{Sys} \in \mathbb{R}$ and $\boldsymbol{\theta}_F \in \Theta_{Safe}$ such that $\Delta\omega(t) \to \Delta\omega_{Sys}\mathbf{1}_N$ and $\boldsymbol{\theta}(t) \to \boldsymbol{\theta}_F$.

Consider the traditional frequency droop control law (4), which applies at each $k \in \mathcal{V}_{Droop}$. Solving for for $P_{G,k}(t)$:

$$P_{G,k}(t) = P_{Ref,k} - R_k^{-1}\Delta\omega_k(t) \tag{201}$$

We have shown in Theorem 6.1 that under the conditions in Theorem 6.2, $\Delta\omega_k \to \Delta\omega_{Sys}$ for all $k \in \mathcal{V}$. Taking the limit of (201) as $t \to \infty$ and substituting $\lim_{t\to\infty} \Delta\omega_k(t) = \Delta\omega_{Sys}$ yields (199).

Now consider the single-line CED control law (137), which applies at each $k \in \mathcal{V}_{CED}$. If $|P_{Line,k,\sigma(k)}(\theta_{F,k,\sigma(k)})| \leq (1 - \epsilon_{k,m})P_{Max,k,\sigma(k)}$, then by Definition 6.5.C, $\lim_{t\to\infty} \gamma_{k,\sigma(k)}(|P_{Line,k,\sigma(k)}(\theta_{k,m}(t))|) = 1$. Substiting into (137) and simplifying:

$$\Delta\omega_k = D_k^{-1}\left[P_{Ref,k} - P_{L,k}^0 - \sum_{k\in\mathcal{N}(k)} P_{Line,k,m} \right] \tag{202}$$

Recall that $P_{L,k} = P_{L,k}^0 + D_k'\Delta\omega_k$, $D_k = R_k^{-1} + D_k'$, and $P_{G,k} = P_{L,k} + \sum_{m\in\mathcal{N}(k)} P_{Line,k,m}$. Substituting into (202) and solving for $P_{G,k}(t)$:

$$P_{G,k}(t) = P_{Ref,k} - R_k^{-1}\Delta\omega_k(t) \tag{203}$$

Taking the limit as $t \to \infty$ and substituting $\lim_{t\to\infty} \Delta\omega_k(t) = \Delta\omega_{Sys}$ again yields (199). Therefore, (199) holds either when $k \in \mathcal{V}_{Droop}$ or when $k \in \mathcal{V}_{CED}$ and $|P_{Line,k,\sigma(k)}| \leq (1 - \epsilon_{k,m})P_{Max,k,\sigma(k)}$.

Finally, we have shown in Lemma 6.4 that if symmetric CED placement is used for each key line $(k, m) \in \mathcal{E}_{Key}$, then $\lim_{t\to\infty} \Delta\omega_{COM}(t) = \Delta\omega_{Sys} = \Delta\mathcal{P}_{Ref}/\mathcal{D}$. Substituting into (199) yields $\lim_{t\to\infty} P_{G,k}(t) = P_{F,k}$, where $P_{F,k}$ if the final power value in (20). $\square$

Thorem 6.2 shows that for a constraint-satisficing droop inverter network, a form of constrained power sharing is guaranteed for any operating condition within the safe region. In this form of power sharing, each traditional droop inverter and each CED inverter not enforcing an active constraint must converge to a state such that each

sources its reference power plus an offset inverse-proportional to its droop constant. However, the frequency (and therefore offset term of each inverter's output power) does not necessarily converge to the same value as in the traditional droop or all-active-bus, acyclic CED networks. This is due to the power injection associated with active constraints on key lines being enforcing by asymmetric CED: the single inverter asymemtrically enforcing a key line constraint must inject power which is not balanced by complementary injection on the other end of the line, thus unbalancing the center-of-mass frequency summation and skewing its results. If there are no key lines to which were assigned asymmetric CED placements, or if no constraints are active, then the center-of-mass frequency is the same as that in traditional droop or all-active-bus, acyclic CED networks. As we will show in the following example section, this constitutes an advantage associated with symmetric CED placement, which may justify its increased cost as compared to asymmetric CED placement.

6.6.3 Discussion on Frequency Synchronization and Power Sharing in Constraint-Satisficing Droop Inverter Networks

Together, Theorems 6.1 and 6.2 describe the synchronization and power sharing behavior of constraint-satisficing droop inverter networks. As compared with Theorem 3.5, they show that a constraint-satisficing droop inverter network has significantly improved synchronization behavior as compared with a similar traditional frequency-droop inverter network. While a traditional droop network may lose synchronization (and therefore power sharing) due to network non-linearities and constraints, the CED inverters in a constraint-satisficing droop inverter network enforce the specified key line constraints, thereby bounding the network voltage-angle trajectory within the safe region and ensuring synchronization and constrained power sharing.

However, the results of Theorems 6.1 and 6.2 still fall short of formal control-theoretic robustness to changing operating conditions. This is because, in addition to requiring the bounding of the network inputs $\mathbf{P_{Ref}}(t)$ and $\mathbf{P_L^0}(t)$ within the compact

196

set $\mathbb{P}$ (representing the network expected operating range), we also require the quantities $\mathbf{P_G}(t)$ and $\mathbf{P_L}(t)$ (the network generation and load vectors) to be bounded within the same range. Because $\mathbf{P_G}(t)$ and $\mathbf{P_L}(t)$ are state-dependent quantities, Theorems 6.1 and 6.2 still constitute dynamic conditions for synchronization and power sharing.

Despite this limitation, we argue that the results of Theorems 6.1 and 6.2 still constitute significantly improved synchronization behavior as compared with traditional frequency-droop, since bounding generation and load is much simpler to accomplish than bounding the network voltage-angle trajectory. Almost all inverter sources in practice implement power-limiting behavior (which limits $P_{G,k}$ within its specified range), and almost all load circuits are equipped with relays or circuit breakers to limit the maximum load power within its specified range. Since power flows in a network are bounded on the expected operating range, the power injections required of CED inverters to enforce key line power-flow constraints are also bounded. Therefore, by extending the dynamic model used to encompass power limiting behavior and by requiring that CED inverters possess sufficient capacity to enforce the assigned key line constraint under worst-case conditions, it should be possible to relax the assumption that generation and load remain within the safe region, and instead show that it follows from the network dynamics, resulting in formally robust synchronization and power sharing behavior.

In addition, Lemma 6.4 and Theorem 6.2 reveal the trade-off inherent in choosing symmetric vs. asymmetric CED configuration for key lines. In symmetric CED configuration, a CED inverter is placed on each end of the key line, and the two inverters share the responsibility for enforcing its constraint. In asymmetric CED configuration, only a single CED inverter is placed at one incident bus, which is responsible for the enforcement by itself. Symmetric CED configuration has the advantage that when the constraint is active, the two CED inverters provide symmetric power injections

whose effects cancel each other, and so the network maintains the static center-of-mass frequency property and all other inverters are uneffected. Asymmetric CED configuration results in an asymmetric power injection when the constraint is active, which displaces the center-of-mass frequency as well as the final output power of the other inverters. However, symmetric CED configuration requires two inverters and more measurements, increasing cost.

6.7 Simulation Results for CED Sparse Configuration in Example Networks

In this section, we present the development of a constraint-satisfying droop control configuration for several example networks, and present simulation results verifying the claim of guaranteed frequency synchronization and power sharing on the expected operating range, as well as exploring the response of such a network to a variety of input conditions. In the following examples, we use the example gain function $\gamma_{k,m}$ as defined in (138) with $\epsilon_{k,m} = 0.2$ and $C_{k,m} = 0.1$ for all $(k,m) \in \mathcal{E}_{Key}$.

6.7.1 Six-Bus Radial Microgrid

In Chapter 4, we considered the six-bus radial microgrid network whose single-line diagram is shown in Figure 4.2. In this network, two subnetworks ($\{1, 2, 3\}$ and $\{4, 5, 6\} \subset \mathcal{V}$) are connected by a single line $(3, 4)$. In Simulation 4.5, we showed that this network may lose synchronization under traditional frequency-droop control due to a significant imbalance between the reference power injection totals between the two subnetworks. In Simulation 4.6, all-active-bus CED was applied, resulting in frequency sychronization and constrained power sharing under the same conditions, in which inverters 3 and 4 provided complementary power injections to enforce the line constraint $|P_{Line,3,4}| \leq P_{Max,3,4}$, while all other inverters converged to their respective final power values. In Chapter 5, we showed that the key line set $\mathcal{E}_{Key} = \{(3, 4)\}$ is a constraint-satisfying key line set for this network under the expected operating range

in Table 5.1. In Section 6.4.6.1, we developed two constraint-satisficing droop control configurations, one symmetric (Figure 6.4b) and one asymmetric (Figure 6.4a) for this network and expectedc operating range.

We will now simulate this network under both the symmatric and asymmetric constraint-satisficing droop control configurations for the same load step condition as in Simulation 4.5 and 4.6 (post-step conditions reprinted in Tables 6.4 and 6.5). Notice that the (post-step) value of $\Delta \mathcal{P}_{Eq,3,4}$ is greater than $Y_{3,4}V_3V_4$, and as a result then without constraint enforcement, this network will lose synchronization across line $(3, 4)$ after the step (as occured in Simulation 4.5).

Table 6.4: Post-Step Bus Configuration for Simulations 6.1 and 6.2

k	$\mathbf{P_{Ref}}$ (p.u)	$\mathbf{P_L^0}$ (p.u)	$\mathbf{P_F}$ (p.u)
1	1.00	0.00	1.00
2	1.00	0.00	1.00
3	0.00	0.25	0.00
4	0.00	2.75	0.00
5	1.00	0.50	1.00
6	1.00	0.50	1.00

Table 6.5: Post-Step Line Configuration for Simulations 6.1 and 6.2

i	k	m	$Y_{Line}(p.u)$	$\mathbf{P_{Max}}(p.u)$	$\mathbf{\Delta P_{Eq}}$ (p.u)
1	1	3	2.00	1.50	1.00
2	2	3	2.00	1.50	1.00
3	3	4	1.50	1.00	1.75
4	5	4	2.00	1.50	0.50
5	6	4	2.00	1.50	0.50

Simulation 6.1 applies the same load step as Simulations 4.5 and 4.6, but with the symmetric CED configuration (Figure 6.4b) developed in Section 6.4.6.1 applied. In this configuration, inverters 3 and 4 both implement the bounded, single-line form of the CED control law (Definition 6.4) with $\gamma_{Max,3,4} = \gamma_{Max,4,3} = 3$, while all other inverters implement traditional frequency-droop. By Theorems 6.1 and 6.2, this configuration should be sufficient to enforce the line power-flow constraints and guarantee

synchronization and constrained power sharing for the entire operating range defined by Table 5.1.

In Simulation 6.1, the load step is applied at $t = 0$ to the network under the symmetric CED configuration developed in Section 6.4.6.1 (Figure 6.4b), and the network response is shown in Figure 6.7. Notice that in this sparse placement of CED inverters, inverters 3 and 4 respond to the approach of $|P_{Line,3,4}|$ to $P_{Max,3,4}$ by increasing the adaptive gain $\gamma_{3,4} = \gamma_{4,3}$, thereby enforcing the constraint and bounding the network within the safe region of the voltage-angle space. The participation of inverters 1, 2, 5, and 6 in the constraint-enforcement is not necessary, since the constraints on their incident lines are implicitly enforced by the generation and load constraints in Table 5.1. Therefore, the bus frequencies all synchronize to the center-of-mass frequency, which is equal to that of the equivalent traditional-droop (or all-active-bus, acyclic CED network) network, since all symmetric CED configuration is used. Finally, the inverter output power values all converge to constants. Since inverters 1, 2, 5, and 6 are operating traditional frequency-droop, their output power values all converge to their respective $P_{F,k}$ values found by (20), while inverters 3 and 4 provide complimentary power injections to enforce the constraint $|P_{Line,3,4}| \leq P_{Max,3,4}$. Overall, Simulation 6.1 shows that the sparse, symmetric CED placement in Figure 6.4b provides almost identical behavior to that of all-active-bus deployment of CED inverters, but only two CED inverters (and many fewer measurements) are required.

In contrast, Simulation 6.2 applies the same load step, but the asymmetric CED configuration (Figure 6.4a) developed in Section 6.4.6.1 is used. In this configuration, only inverter 3 implements the bounded, single-line CED control law with $\gamma_{Max,3,4} = 5$, while all other inverters implement traditional frequency-droop. Figure 6.8 shows the simulation results for this network with the load step applied at $t = 0$. In this case, inverter 3 increases the adaptive gain $\gamma_{3,4}$ to enforce the constraints $|P_{Line,3,4}| \leq P_{Max,3,4}$, bounding the network in the safe region and again resulting

in frequency synchronization. However, in this case, the center-of-mass frequency $\Delta\omega_{COM}$ does *not* remain static for static reference and load inputs after the step, and as such does not equal $\Delta\mathcal{P}_{Ref}/\mathcal{D}$ (that is, the static center-of-mass frequency property does not hold). This is due the fact that inverter 3 must asymmetrically enforce the constraint on line $(3,4)$, and inverter 4 does not provide a complimentary power injection. Further, while all of the inverters output power values converge to a constant, none of them (including those of inverters operating traditional frequency-droop) converge to their respective final power values $P_{F,k}$. Finally, because inverter 3 must enforce the constraint without the participation of inverter 4, it must provide a much larger power injection than under symmetric CED configuration (Simulation 6.1), and as such must have a higher power rating, and the values of $P_{G,Min,3}$ and $P_{G,Max,3}$ must be set accordingly.

In summary, Simulations 6.1 and 6.2 confirm the following:

1. Both symmetric and asymmetric constraint-satisficing droop control configurations are able to (either explicitly or implicitly) enforce the network line power-flow constraints, thus rendering invariant the safe region of the voltage-angle state space (Theorem 6.2).

2. Both symmetric and asymmetric constraint-satisficing droop control configurations ensure network frequency synchronization (Theorem 6.1).

3. Symmetric CED configuration has the advantage that it ensures that the static center-of-mass frequency property holds, while asymmetric CED configuration does not necessarily provide this behavior (Lemma 6.4).

4. As a result, symmetric CED configuration ensures the convergence of the output power values of droop inverters (or CED inverters assigned to inactive constraints) to their associated final power values, while asymmetric CED configuration does not (Theorem 6.2).
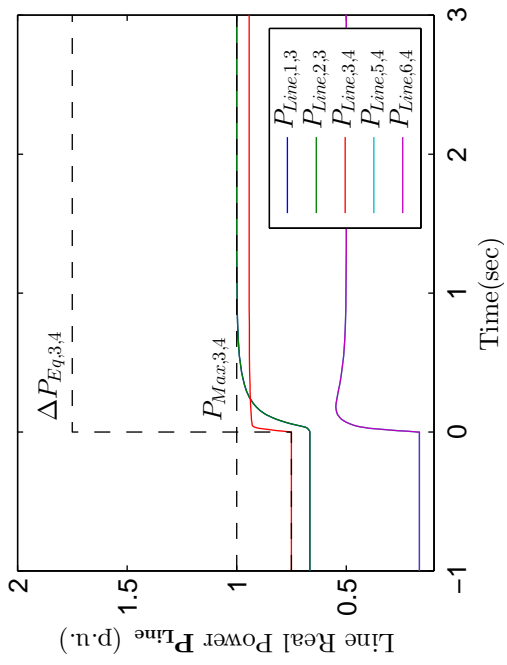
(a) Bus Frequency Error $\mathbf{\Delta\omega}$
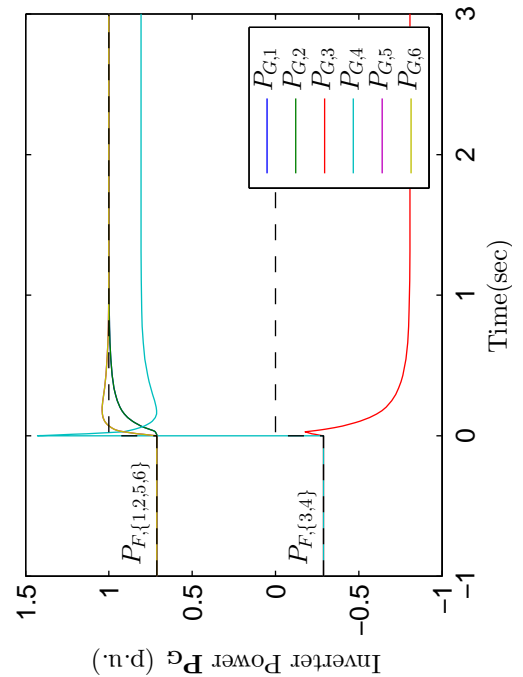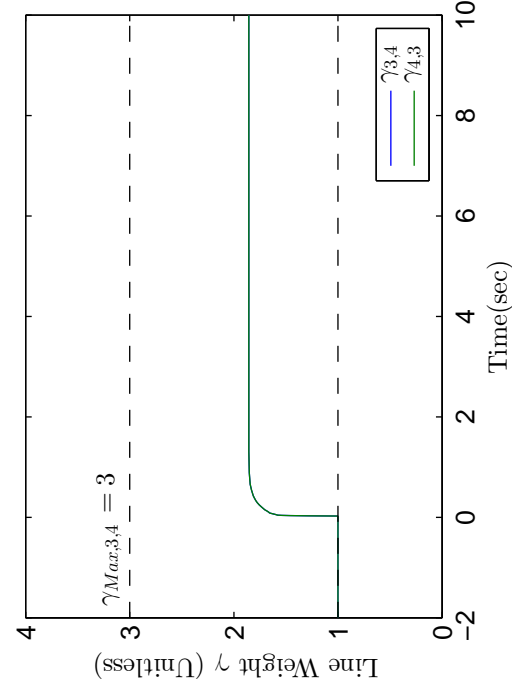
(b) Line Power Flows $\mathbf{P_{Line}}$

(c) Inverter Generated Power $\mathbf{P_G}$
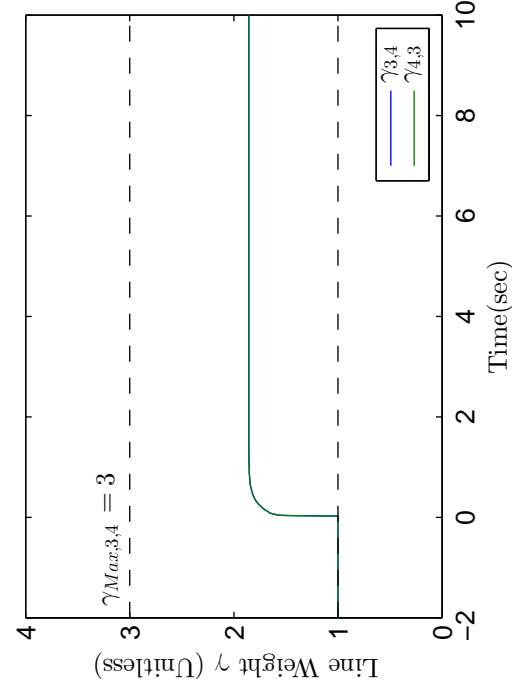
(d) Line Weight $\mathbf{\Gamma}$

Figure 6.1: Simulation 6.7: Six-Bus Radial Microgrid with Symmetric Sparse CED
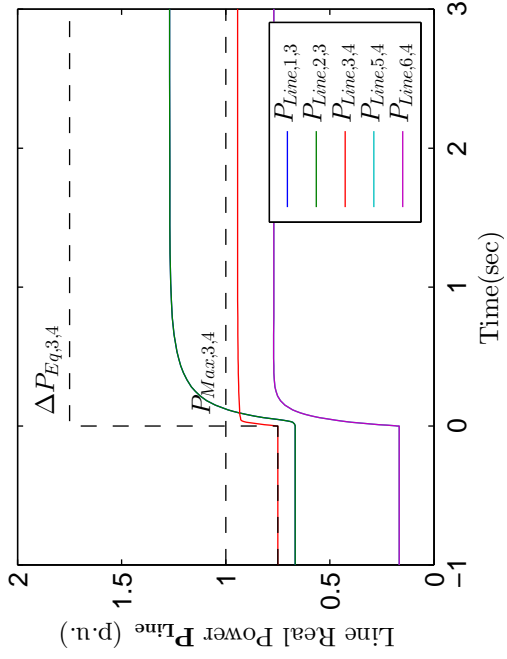
(a) Bus Frequency Error $\boldsymbol{\Delta\omega}$
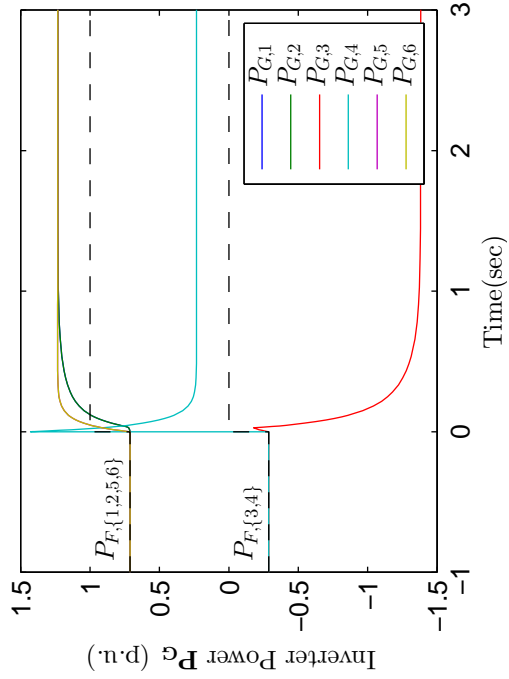
(b) Line Power Flows $\mathbf{P_{Line}}$

(c) Inverter Generated Power $\mathbf{P_G}$
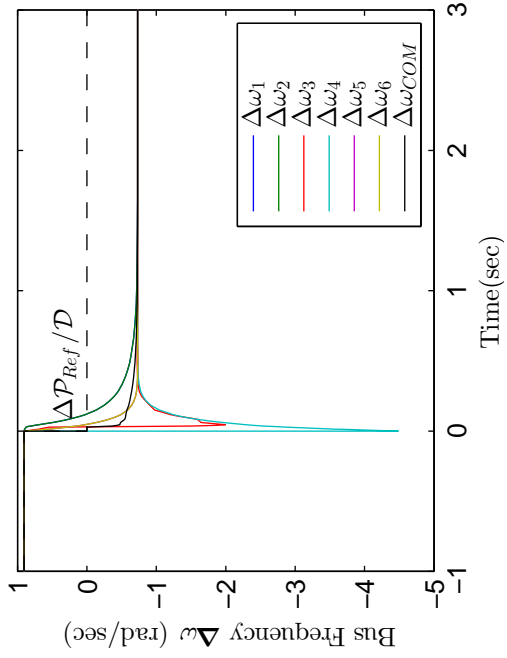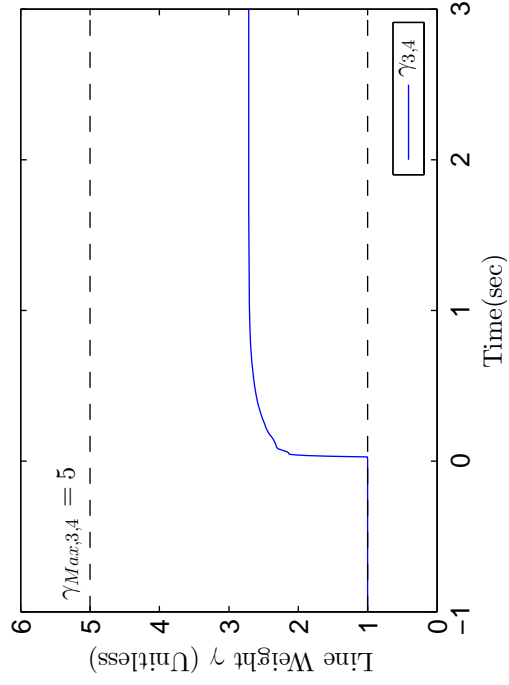
(d) Line Weight $\boldsymbol{\Gamma}$

Figure 6.8: Simulation 6.2: Six-Bus Radial Microgrid with Asymmetric Sparse CED

5. Inverters in symmetric CED configuration assigned to an active constraint provide complimentary power injections to enforce the constraint, while an inverter in asymmetric CED configuration assigned to an active constraint must provide a (generally larger) power injection to enforce the constraint.

6.7.2   Lossless Three-Bus Grid-Tied Microgrid

In the next series of simulations, we will consider a lossless three-bus microgrid with an external infinite bus source as in Figure 6.5. The purpose of this series of simulations is to show the behavior of both traditional droop and CED control while grid-tied under lossless conditions, and to show both the loss of synchronization under traditional droop and how this issue can be corrected using application of a constraint-satisficing droop control configuration. In Section 6.4.6.2, we showed that the key line set $\mathcal{E}_{Key} = \{(2,4)\}$ is the unique constraint-satisficing key line set for this network under the expected operating range in Table 6.2, and that a constraint-satisficing droop control configuration can be created by assigning inverter 2 to enforce the constraint on the tie line (line $(2,4)$) with $\gamma_{Max,2,4} = 5.5$.

In this series of simulations, we will force a set of reference and load changes to explore the behavior of this network under a variety of conditions and transients, representing the corners of the expected operating range. The network begins (at $t = 0$ sec) at zero state and inputs, that is, both inverters have zero reference ($P_{Ref,1} = P_{Ref,2} = 0.0$ p.u.), and there is no local load ($P_{L,1} = P_{L,2} = P_{L,3} = 0.0$ p.u.). At $t = 5.0$ sec, the reference power of inverter 1 is increased to $P_{G,Max,1} = 1.0$ p.u., and the network allowed to settle to a new equilibrium. Next, at $t = 15.0$ sec, a load of 1.0 p.u. is stepped onto bus 3, and the network again allowed to settle to a new equilibrium. Finally, at $t = 25.0$ sec, the maximum load of $P_{L,Max,3} = 6.0$ p.u. is stepped onto bus 3, which is sufficient to cause loss of synchronziation under traditional droop. These test conditions are summarized in Table 6.6 and illustrated

in Figure 6.9.

Table 6.6: Simulation Test Conditions for Lossless Three-Bus Grid-Tied Microgrid

| Parameter	$t < 5.0$sec	$5.0 \leq t < 15.0$sec	$15.0 \leq t < 25.0$sec	$t \geq 25.0$sec
$P_{Ref,1}$	0.0	1.0	1.0	1.0
$P_{Ref,2}$	0.0	0.0	0.0	0.0
$P_{L,3}$	0.0	0.0	1.0	6.0
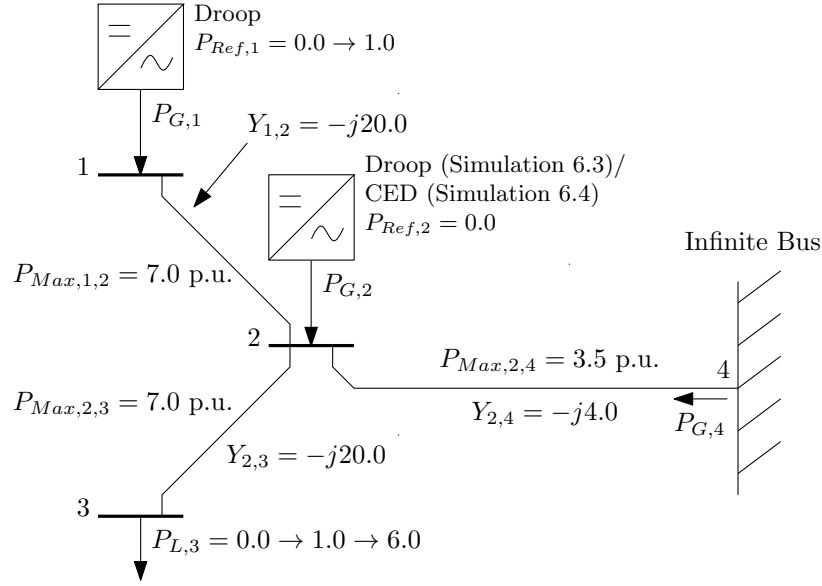
Figure 6.9: Single-Line Diagram of Lossless Three-Bus Grid-Tied Microgrid (Simulations 6.3 and 6.4)

We will apply the test conditions in Table 6.6 in simulation on this network under two different control settings. In Simulation 6.3, inverters 1 and 2 both implement traditional frequency-droop (results in Figure 6.10). In Simulation 6.4, we apply the constraint-satisficing droop control configuration developed in Section 6.4.6.2, where inverter 1 implements traditional droop while inverter 2 implements bounded, single-line CED to enforce a line power-flow constraint on line $(2, 4)$ (that is, the tie line between the microgrid and the external grid) (results in Figure 6.11).

Consider the results of Simulation 6.3 in Figure 6.10. In the first part of the test $(0 \leq t < 5.0$ sec), there is no load on the microgrid, and the inverters have zero power reference values. In this case, the network operates at the nominal frequency

205

($\Delta\omega_k = \Delta\omega_{COM} = 0$ rad/sec for all $k \in \mathcal{V}$), all the inverters source zero power ($P_{G,k} = 0$ for all $k \in \mathcal{V}$), and no power is drawn from the grid ($P_{Line,2,4} = 0$ p.u.). At $t = 5.0$ sec, the value of $P_{Ref,1}$ (the power reference value of inverter 1) is stepped to 1.0 p.u. This triggers a transient, but since no constraints are violated, the microgrid settles to a new equilibrium, with all inverters sourcing their reference power and a total of 1.0 p.u. being exported to the grid. Since bus 4 (modeling the grid) is an infinite bus, its frequency does not change ($\Delta\omega_4(t) = 0$ rad/sec for all t), and therefore the center-of-mass frequency $\Delta\omega_{COM}$ also has static value 0 rad/sec (and so the network settles to the nominal frequency).

At $t = 15.0$ sec, a load of 1.0 p.u. is stepped onto bus 3 (the passive bus), resulting in another transient. Since bus 3 is a passive bus, the power flow on line $(2,3)$ increases almost immediately to supply the load, and inverter 2 responds by decreasing its frequency. Inverter 1 responds by increasing its power generation and dropping its frequency briefly, but quickly returns to its reference power. Ultimately, the network again settles to a new equilibrium, again with all inverters sourcing their reference power and operating at nominal frequency, but now no power is exported to the grid, as inverter 1 sources all the power needed by the load.

Finally, at $t = 25.0$ sec, the maximum load of $P_{G,Max,3} = 6.0$ p.u. is stepped onto bus 3. While the network is physically capable of supplying this load (the total local generation on the microgrid is 3.0 p.u., plus the tie-line power limit of 3.5 p.u. should be able to source 6.5 p.u.), there does not exist a dynamic equilibrium for this network condition under traditional droop control (Theorem 3.1 applies across the cut $\mathcal{V}_C = \{(2,4)\}$). As a result, the traditional frequency-droop controlled inverters are not able to stabilize this case, and the microgrid loses synchronization with the external grid, resulting in continuous frequency and real power oscillations.

In Simulation 6.4 (Figure 6.11), the same test conditions are applied, but now inverter 2 implements bounded, single-line CED to enforce a line power-flow constraint

$|P_{Line,2,4}| \leq P_{Max,2,4} = 3.5$ p.u. Observe that for $t < 25.0$sec, Simulation 6.4 results are identical to those of Simulation 6.3, confirming that a constraint-satisficing droop inverter network behaves identically to traditional droop network under unconstrained conditions. However, after the large load step is applied at $t = 25.0$ sec, when $|P_{Line,2,4}|$ approaches $P_{Max,2,4}$, inverter 2 responds by increasing $\gamma_{2,4}$ to limit the power flow. This results in inverter 2 beginning to source power to make up for that that can't be drawn from the grid. As a result, the microgrid stabilizes and *does not lose synchronization with the grid*, instead settling to a (constrained) equilibrium, in which inverter 2 now supplies some of the power needed by the load. Because bus 4 is an infinite bus, the center-of-mass frequency is still $\Delta\omega_{COM} = 0$ rad/sec, resulting in network convergence to the nominal frequency.

Together, Simulation 6.3 and 6.4 demonstrate the following:

1. A constraint-satisficing droop inverter network (even one containing passive buses) is capable of enforcing line power-flow constraints to bound the network within the safe region of the voltage-angle space (Theorem 6.2) during grid-tied operation.

2. Such a network also synchronizes in frequency and shares power between both CED and traditional-droop inverters in a way that respects the network constraints (Theorems 6.1 and 6.2).

3. When no constraints are active, a constraint-satisficing droop inverter network behaves identically to the equivalent traditional droop inverter network.

4. When an infinite bus is present, then $\Delta\omega_{COM} = 0$, and so the network must converge to nominal-frequency operation. This can be compared to the concept of "leaders" in a consensus network (see [54]), where the infinite bus k acts as a leader with $\Delta\omega_k = 0$.
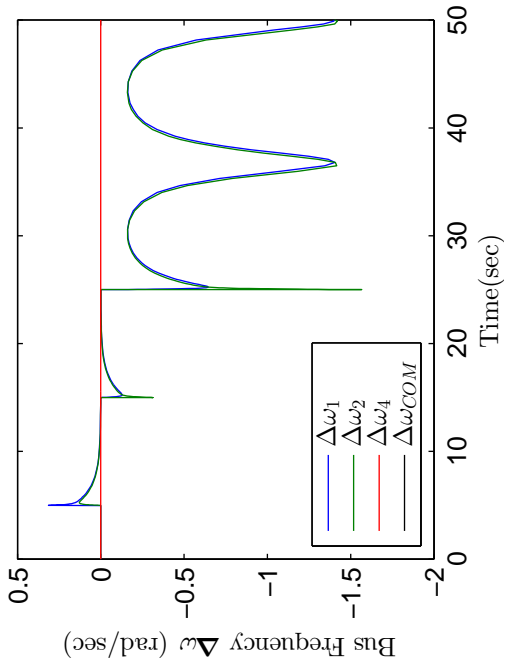
(a) Bus Frequency Error $\mathbf{\Delta\omega}$
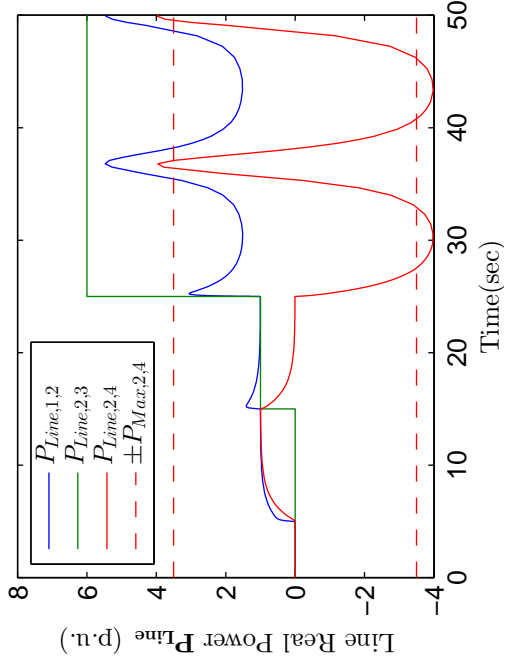
(b) Line Power Flows $\mathbf{P_{Line}}$
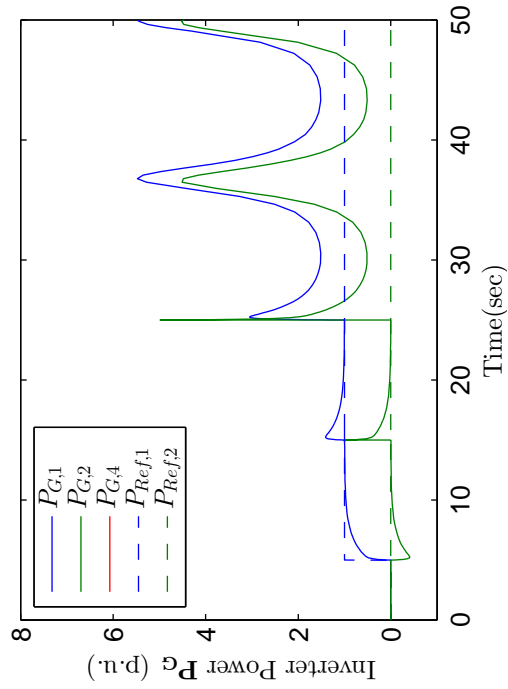
(c) Inverter Generated Power $\mathbf{P_G}$

Figure 6.10: Simulation 6.3: Lossless Three-Bus Grid-Tied Microgrid without CED

(a) Bus Frequency Error $\mathbf{\Delta\omega}$

(b) Line Power Flows $\mathbf{P_{Line}}$

(c) Inverter Generated Power $\mathbf{P_G}$

(d) Line Weight $\mathbf{\Gamma}$
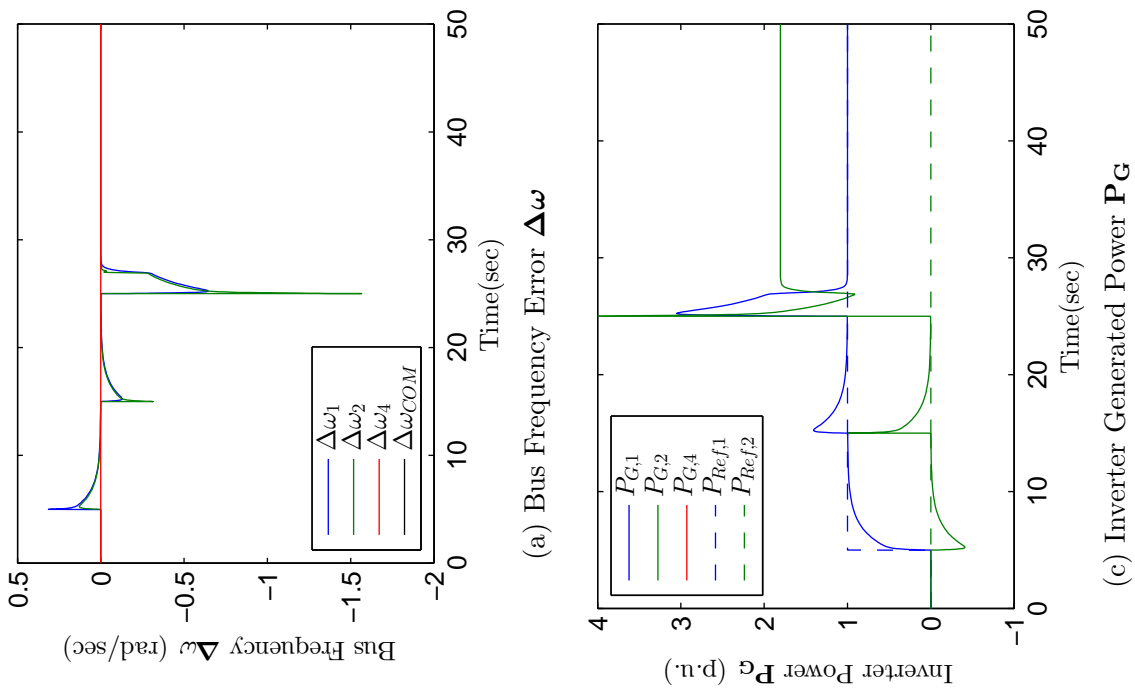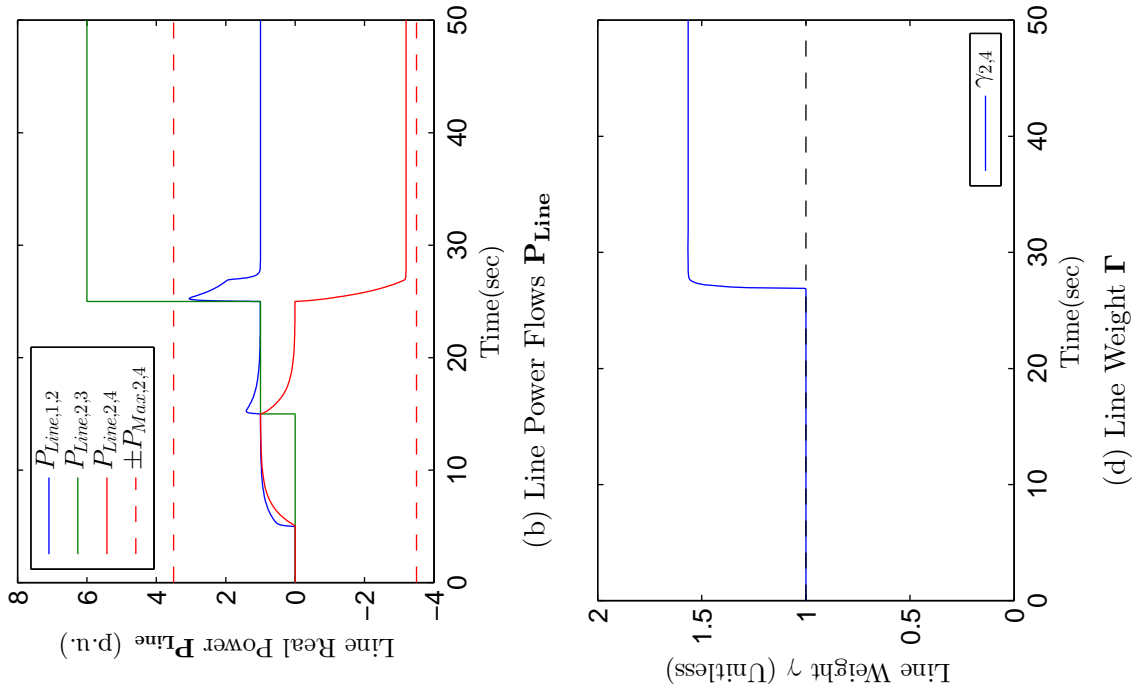
Figure 6.11: Simulation 6.4: Lossless Three-Bus Grid-Tied Microgrid with Assymetric CED Applied to Line (2, 4)

6.7.3 Lossy Three-Bus Grid-Tied Microgrid

The final series of simulations will consider a *lossy* three-bus, grid-tied microgrid. This network is identical to that considered in Simulations 6.3 and 6.4, but includes lines with non-negligible resistance, which has a significant effect on the behavior and synchronization behavior of the network. The single-line diagram of the lossy network is shown in Figure 6.12. Because our analytic results consider only lossless systems, they do not apply directly to this network. However, these results are included in order to demonstrate the ability of our methods to be extended to lossy systems.
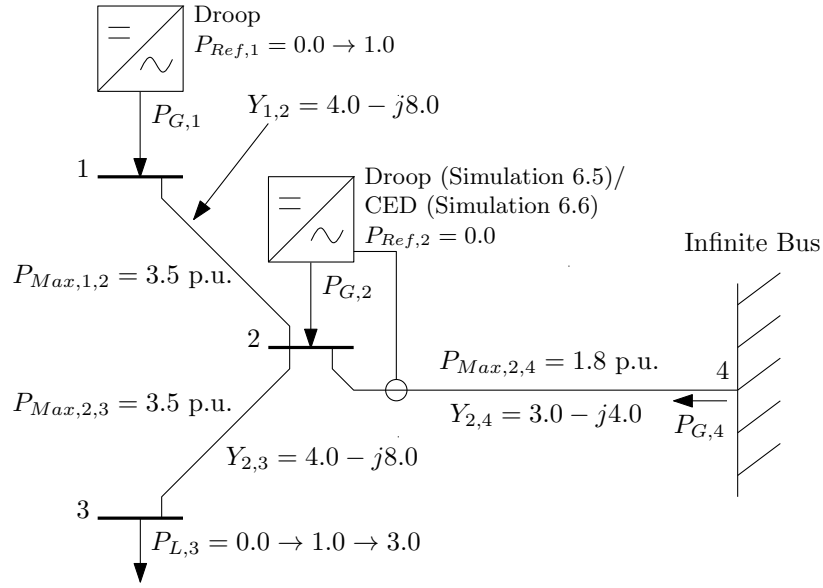
Figure 6.12: Single-Line Diagram of Lossy Three-Bus Grid-Tied Microgrid (Simulations 6.5 and 6.6)

We will apply a similar series of test conditions to the lossy network to those in Simulations 6.3 and 6.4, but with a few values altered due to the network losses (summarized in Table 6.7). Notice that in these tests, we apply a much more modest load of 3.0 p.u. to bus 3 at $t = 25.0$ sec. The goal of this series of tests is to demonstrate the behavior of traditional droop and bounded, single-line CED under losses, to show the effect of losses on synchronization of traditional droop inverters, and to show that CED control can similarly to be applied to guarantee synchronization

and power sharing in lossy networks.

Table 6.7: Simulation Test Conditions for Lossy Three-Bus Grid-Tied Microgrid

Parameter	$t < 5.0$ sec	$5.0 \leq t < 15.0$ sec	$15.0 \leq t < 25.0$ sec	$t \geq 25.0$ sec
$P_{Ref,1}$	0.0	1.0	1.0	1.0
$P_{Ref,2}$	0.0	0.0	0.0	0.0
$P_{L,3}$	0.0	0.0	1.0	3.0

Similarly to Simulations 6.3 and 6.4, we will apply the test conditions in Table 6.7 in simulation on the lossy network under two sets of control settings. In Simulation 6.5, inverters 1 and 2 both implement traditional frequency-droop (results in Figure 6.13). In Simulation 6.6, inverter 1 implements traditional droop, while inverter 2 implements bounded, single-line CED to enforce a line power-flow constraint of $P_{Max,2,4} = 1.8$ p.u. on line $(2,4)$ (results in Figure 6.14).

Similar to Simulations 6.3 and 6.4, in Simulation 6.5 (Figure 6.13) there is no power flow for $t < 5.0$ sec. At $t = 5.0$ sec, the power reference of inverter 1 ($P_{Ref,1}$) is stepped to 1.0 p.u, resulting in a transient which settles to a frequency synchronization equilibrium in which inverter 1 sources 1.0 p.u. (minus losses) to the grid. At $t = 15.0$ sec, a load of 1.0 p.u. is stepped onto bus 3, and again after a short transient inverter 1 sources 1.0 p.u. to the load, with the microgrid importing a small amount of power from the grid to cover losses. Finally, at $t = 25.0$ sec a moderate load of 3.0 p.u. is stepped onto bus 3. However, despite the fact that this load is within the physical capacity of the network (3.0 p.u. local capacity plus 1.8 p.u. maximum on the tie line $= 4.8$ p.u.), under traditional droop this additional load causes the loss of synchronization between the microgrid and the external grid.

Simulation 6.6 considers the same network, but now inverter 2 implements bounded gain, single-line CED to enforce the line power flow constraint $|P_{Line,2,4}| \leq P_{Max,2,4}$. The response in Figure 6.14 shows identical performance to Simulation 6.5 for $t < 25.0$ sec, again verifying that CED control behaves identically to traditional droop in the absence of active constraints. However, after $t = 25.0$ sec, inverter 2 responds to

the approach of $|P_{Line,2,4}|$ to $P_{Max,2,4} = 1.8$ p.u. by increasing $\gamma_{2,4}$ so as to limit the increase of power imported from the grid, enforcing the line power-flow constraint $|P_{Line,2,4}| \leq P_{Max,2,4}$. As a result, the network stabilizes to a frequency agreement equilibrium at which inverter 1 supplies its reference output power, the maximum power is imported from the grid on line $(2,4)$, and the CED inverter 2 makes up the difference, including losses.

Together, Simulations 6.5 and 6.6 demonstrate the following:

1. In *lossy* grid-tied operation, traditional frequency droop controlled inverters continue to be able to respond to transients, synchronize with each other and the grid, and settle to near reference power output *as long as the network stability constraints aren't violated.* The conditions under which desynchronization may occur are much more modest in the lossy network than in a lossless one.

2. A CED-controlled inverter is capable of synchronizing in frequency and sharing power (subject to constraints) with traditional frequency droop inverters in the presence of passive (load) buses and losses during grid-tied operation.

3. Again, when no constraints are active, a CED-controlled inverter behaves identically to a traditional droop controlled inverter with similar settings.

4. A CED-controlled inverter is capable (when applied in a mixed-bus, *lossy* grid-tied network with appropriate settings) of enforcing its assigned line power-flow constraint and thereby ensuring that the network synchronization conditions are not violated, resulting in significantly improved synchronization and power sharing behavior.

6.8   Chapter Conclusions

In this final technical chapter, we have introduced the concepts of *constraint-satisficing droop control configurations* and *constraint-satisficing droop inverter networks.* A

212
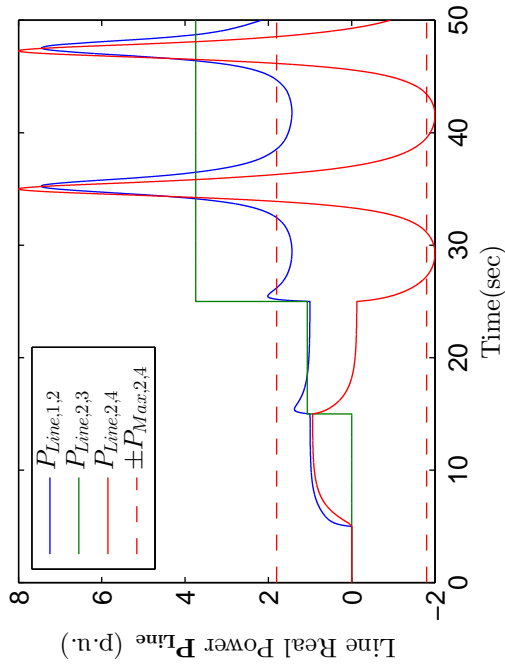
(a) Bus Frequency Error $\Delta\omega$
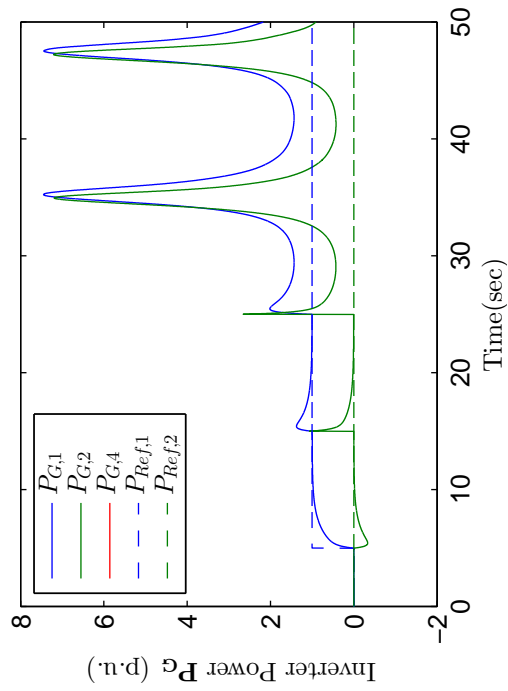
(b) Line Power Flows $\mathbf{P_{Line}}$
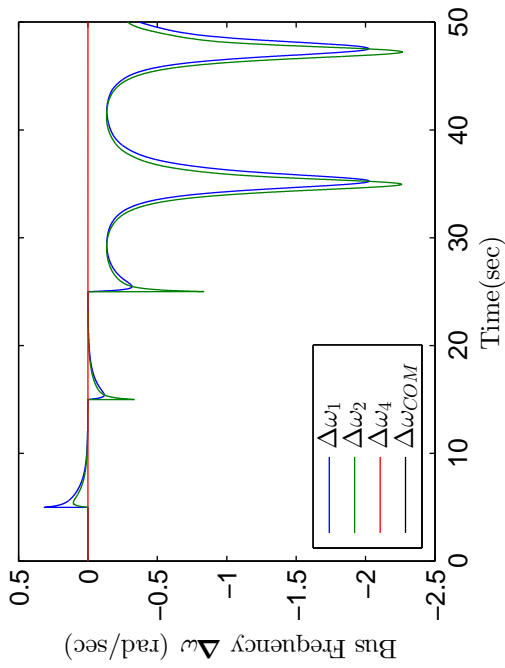
(c) Inverter Generated Power $\mathbf{P_G}$

Figure 6.13: Simulation 6.5: Lossy Three-Bus Grid-Tied Microgrid without CED
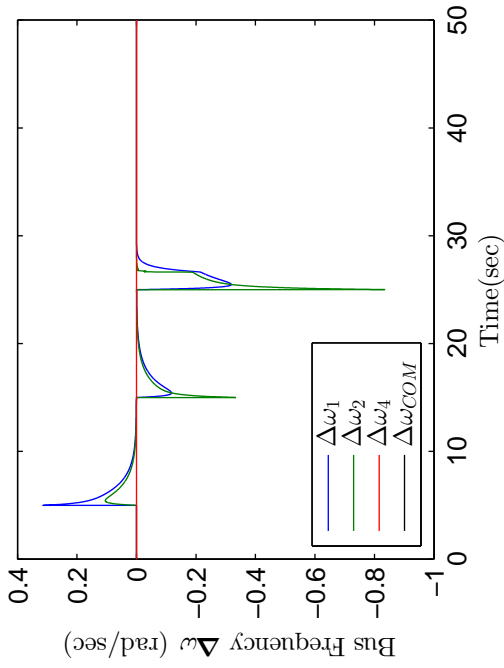
(a) Bus Frequency Error $\Delta\omega$
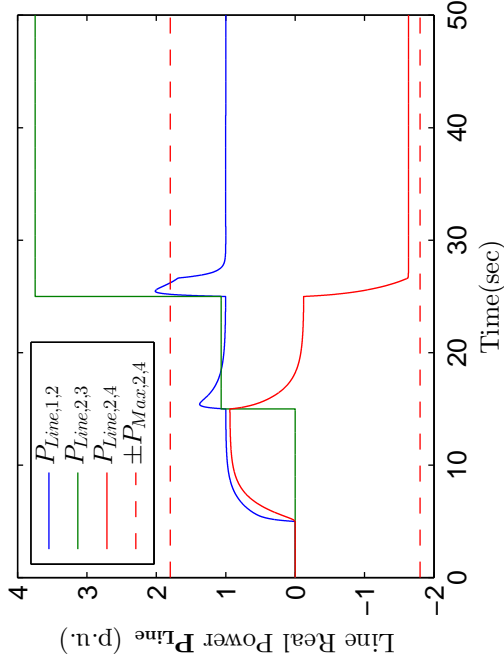
(b) Line Power Flows $\mathbf{P_{Line}}$
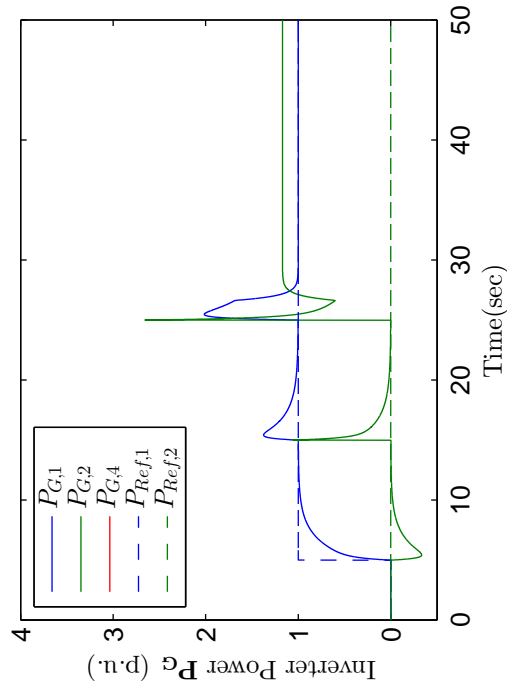
(c) Inverter Generated Power $\mathbf{P_G}$
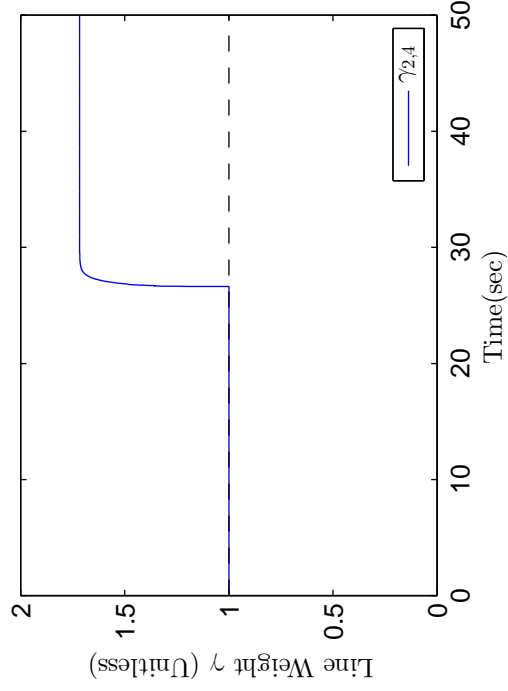
(d) Line Weight $\mathbf{\Gamma}$

Figure 6.14: Simulation 6.6: Lossy Three-Bus Grid-Tied Microgrid with Bus 2 CED

constraint-satisficing droop control configurations is a configuration of CED inverters in a mixed-bus inverter network, which are placed and configured so as to explicitly enforce the line power-flow constraints associated with the lines of a constraint-satisficing key line set, thus satisfing all of the network line power-flow constraints. Inverters operating the bounded, single-line form of the CED control law are placed incident to each key line constraint and configured so as the enforce the line power-flow constraints on the key lines as long as the network operates within the expected operating range, thus bounding the network state trajectory within the safe region. We further showed that bounding of the network state trajectory within the safe region ensures synchronization and constrained power sharing as long as both the network inputs (references and nominal-frequency loads) and the generation and load values are bounded within the expected operating range, and that the inputs converge to constant values.

While our results fall short of formal control-theoretic robustness due the assumption of generation and load bounds, in practice these assumptions are quite mild, and as a result a constraint-satisficing droop inverter network has significantly improved synchronziation behavior as compared with a simliar traditional frequency-droop network. Further, if symmetric CED configuration is used for the key lines, then the droop inverters and CED inverters not assigned to active constraints will converge to the same final power value as for the equivalent traditional droop network. Therefore, application of a constraint-satisficing droop control configuration to a network provides robust synchronization and power sharing behavior for inverter networks on a given expected operating range, which was the original goal of this dissertation.

CHAPTER VII

CONCLUSIONS AND CONTRIBUTIONS

7.1 Summary of Contributions

In this dissertation, we have considered the frequency synchronization and sharing of real power between sources in an inverter-based AC network. Our primary contributions are the following:

1. A *structure-preserving dynamic model for the frequency/voltage-angle/real-power dynamics of a droop inverter-based AC network*, which allows application of graph-theoretic control methods to analysis and control of synchronization and power sharing in inverter-based AC networks. These contributions were published in the IEEE Transactions on Power Systems paper [3].

2. A *dynamic sufficient condition for synchronization and power sharing* of droop inverter-based networks based on satisfaction of a set of line power-flow constraints. These contributions were published in the IEEE Transactions on Power Systems paper [3].

3. The *all-incident-line CED control law*, which was shown to enforce the above set of line power-flow constraints and provide robust synchronization and constrained power sharing of an all-active-bus, acyclic network for any bounded reference and load inputs. These results were first introduced in the conference paper [2] at the IEEE Power Engineering Society General Meeting 2013, and a more detailed journal paper has been prepared for submission to Automatica.

4. The concept of *constraint-satisfying key line sets*, which allow reduced-order enforcement of line power-flow constraints in a network as long as the network

generation and loads remain within a specified expected operating range. These results have not yet been published, but a journal paper based on Chapter 5 will be prepared targeted at the IEEE Transactions on Smart Grid.

5. *Constraint-satisficing droop control configurations* and *constraint-satisficing droop inverter networks*, which were shown to enforce the constraints associated with a constraint-satisficing key line set and thereby provide robust synchronization and constrained power sharing for all generation and loads within a specified expected operating range. These results have not yet been published, but a journal paper based on Chapter 6 will be prepared targeted at the IEEE Transactions on Smart Grid.

Tabel 7.1 summarizes the completed and planned publications associated with the contributions of this dissertation. Below, we discuss each of the above contributions, their capabilities, limitations, and application to solving real-world problems.

7.2 Structure-Preserving Model of an Inverter-Based AC Network

In Chapter 3, we introduced a novel dynamic model for the frequency, voltage-angle, and real-power dynamics for networks of arbitrary structure and scale with a mix of droop inverters buses and network buses. In Chapter 4, we extended the model to include all-active-bus, acyclic networks where each bus has an inverter operating the proposed all-incident-line CED control law, and in Chapter 6 it was further extended to include networks containing a mix of droop inverters, single-line CED inverters, and network buses.

The focus of the structure-preserving model is on allowing the application of graph-theoretic and multi-agent system control methods to the frequency, voltage-angle, and real-power dynamics of an inverter-based network for both analysis and control design in as simple a way as possible. As such, the model is based on a number of

Table 7.1: Completed and Planned Publications Associated with Dissertation Contributions

Title	Type
Venue	**Submission Date**
A Structure-Preserving Model and Sufficient Condition for Frequency Synchronization of Lossless Droop Inverter-Based AC Networks [3]	Journal Paper
IEEE Transactions on Power System	Nov 2012
A Line Weighted Frequency Droop Controller for Decentralized Enforcement of Transmission line power-flow constraints in Inverter-Based Networks [2]	Conference Paper
PES General Meeting 2013	Dec 2012
A Constraint-Enforcing Droop Controller for Improved Synchronization of All-Active-Bus Acyclic Inverter-Based AC Networks	Journal Paper
Automatica	June 2014
A Tool for Reduced-Order Enforcement of Line Power-Flow Constraints in AC Networks	Journal Paper
IEEE Transactions on Smart Grid	Sept 2014
A Constraint-Satisficing Sparse Application of Constraint-Enforcing Droop Controller for Improved Synchronization of Inverter-Based AC Networks	Journal Paper
IEEE Transactions on Smart Grid	Dec 2014

assumptions to allow this focus and simplicity, and to decouple other considerations in power network analysis and control. For example, the assumption of constant voltage-phasor magnitudes (which is also made by similar structure-preserving models such as [9]) decouples the problem of voltage stability (see [44] for a definition). The assumption of lossless lines renders the line power-flow values line-odd, thereby significantly simplifying much of the mathematics. Together, these two assumptions (constant voltage-phasor magnitudes and lossless lines) eliminate the need to consider the reactive power-flow equations, also significantly simplifying the mathematics. We do not include feedback time-delays in the model, nor do we include a detail model of the inverter power electronics, instead relying on a simple voltage-source or voltage-source-behind-reactance model for each inverter.

While these assumptions allow a straightforward derivation of our results, they also create limitations for both our model and the results based on it. Some results have shown that droop inverter-based networks may lose stability due to feedback time delays if the droop gains are too large [62, 8, 40, 51]; our model does not produce this result since we do not include feedback delays in the model. Since our model does not include the network reactive power-flow equations or variable voltage-phasor magnitudes, it does not necessarily protect against voltage collapse (see [44]), which could also cause network failure and/or loss of synchronization. Finally, we do not include synchronous machine dynamics in our model, and as such it and the results based on it are only applicable to networks that do not contain synchronous machines.

Despite these limitations, our novel structure-preserving model has proved extremely valuable for providing new understanding of synchronization and power sharing in inverter-based networks. Since it can be easily applied to networks of arbitrary size or structure, it allows a scale-invariant understanding of synchronization that is in keeping with the approach of the Prosumer-Based Power System Architecture. Its

graph-theoretic form allows analysis of how network structure is related to synchronization characteristics. Its relative simplicity allows for rapid simulation of large networks based on initial-value solution of the model dynamic equations, which was used to generate most of the simulation results in this dissertation. Finally, the rest of the contributions of this dissertation would not have been possible without the mathematical simplicity and graph-theoretic nature of the structure-preserving model.

It may be possible in future work to extend the structure-preserving model to mitigate its limitations and expand its applicability. If lossy lines were considered, then line power flows would be rendered line-asymmetric, necessitating that two line power-flow values be associated with each line (one in each direction). This would result in a complication of the mathematics and reduction of the size of the principal region, but most of our results should still apply with some modifications. It should also be possible to extend the model to include time-varying voltage-phasor magnitudes; most of our results should still apply if each voltage-phasor magnitude is bounded from below by given minimum value. Some multi-agent system methods have considered the possibility of convergence in networked systems with time delays (e.g. [63, 39, 56]), and it may also be possible to apply these methods to include the effects of time delays in our model.

Finally, it is possible that our structure-preserving model of an inverter-based network could be combined with similar models of synchronous-generator-based networks (e.g. [9]) to create a dynamic model for the frequency, voltage-angle, and real-power dynamics of a very general network containing a mix of synchronous generators, inverters (both traditional droop and CED-controlled), and network buses. The resulting model could be used to analyze the synchronization and power sharing behavior of almost any power network, including large-scale public utility networks with arbitrary penetration of inverter-interfaced sources. While most of the rest of

our contributions would not directly apply to such a network, it may form a basis of methods for real-time simulation or development of new methods of control for 21st-century power grids.

7.3   Dynamic Sufficient Condition for Synchronization and Power Sharing of Inverter-Based AC Networks

The second major contribution of this dissertation is a dynamic sufficient condition for synchronization and power sharing, which is stated in three forms: a bus voltage-angle form (Theorem 3.3), a line voltage-angle form (Theorem 3.4), and a line power-flow form (Theorem 3.5). The first two forms are equivalent, since both state that restriction of the voltage-angle trajectory to the (open) principal region is sufficient to ensure synchronization. The third (line power-flow form) is a stricter condition than the first two, since it requires the restriction of the network voltage-angle trajectory to a compact subset of the principal region defined by a set of line power-flow constraints (the "safe region" of the voltage-angle space).

The transitions from the sufficient conditions for stability based on voltage-angle trajectory (bus- and line-oriented) to the line power-flow form is based on the idea that line power-flow constraints are equivalent to line voltage-angle constraints on the principal region. This principal only holds when bus voltage-phasor magnitudes are constant. It could be generalized to the case when bus voltage-phasor magnitudes are time-varying and bounded from below, but not if they collapse to zero. Therefore, the sufficient conditions for synchronization do not protect against the possibility of bus voltage collapse (see [44]), which is beyond the scope of this dissertation.

The sufficient conditions for synchronization presented in this dissertation are dynamic conditions, meaning that they are conditions on the entire network voltage-angle trajectory (not just the intiial condition or parameters). Initially, this might seem to render them of little value, since they do not allow a-priori assessment of the synchronization properties of a given network condition. Their value lies in the

fact that they provide a set of measurable conditions, each of which can be enforced in real-time based on local feedback. In addition, they provide a valuable physical insight into the nature of synchronization in inverter-based networks: synchronization is created by the attractive coupling between bus frequency offsets across lines due to the monotonic relationship between line power flows and line voltage angles (increasing voltage angle results in increasing power flow). This coupling across lines must be larger enough to overcome the difference in reference power injections between different parts of the network. In general, greater line admittance creates more coupling, resulting in stronger network attraction to synchronization. As a result, the synchronization robustness of a network is limited by its weakest lines (those with least admittance) across which the greatest reference power injection difference occurs. These insights are the basis of the constraint-enforcing control method we develop later in the dissertation.

7.4 All-Incident-Line CED Control Law for All-Active-Bus, Acyclic CED Networks

The third major contribution of this dissertation is the all-incident-line constraint-enforcing droop (CED) control law, and its application to all-active-bus, acyclic networks (which we termed "all-active-bus acyclic CED networks"). The dynamic sufficient condition for synchronization showed that if an inverter-based network is constrained to a safe region of the voltage-angle space (equivalent to enforcement of a specified line power-flow constraint on each line in the network), then synchronization and power sharing will necessarily follow. However, because the traditional frequency-droop control law does not enforce any such line power-flow constraints, the network may lose synchronization as a result of a large reference power injection differential across a weak line. The all-incident-line CED control law solves this issue by applying an adaptive gain to each line power-flow measurement in the control law, detecting the approach of any line power flow to its constraint value, and increasing

its gain to "pull" the network away from the constraint. In an all-active-bus, acyclic CED network, since each bus has an inverter and each inverter applies a gain to each incident line, each line power-flow constraint will be explicitly enforced by both incident inverters. This bounds the network state trajectory in the safe region, and synchronization and constrained power sharing follow.

The all-incident-line CED control law and its application to all-active-bus, acyclic networksa are the most straightforward, conceptually simple way to enforce line power-flow constraints in a network so as to ensure that the dynamic sufficient condition for synchronization is met. While it is possible to construct a network of this type, in practice such networks rarely occur. Most power networks in practice contain a mix of source (active) and network (passive) buses. In addition, since the all-incident-line CED control law requires a measurement of the line power flow on each incident line, it has considerably higher measurement cost than traditional droop. Finally, many power networks are meshed (that is, contain cycles). Therefore, the all-active-bus acyclic application of all-incident-line CED control is not very applicable in practice.

Because we do not model inverter generation constraints and each bus has a local inverter, our results show that an all-active-bus acyclic CED network provides synchronization and constrained power sharing behavior that is robust to all reference and load inputs that are bounded and constant. While in practice many such inputs might be beyond the physical capacity of the network, our results show that the control approach will remain stable for all inputs that the network can physically handle.

We have shown that an all-active-bus, acyclic CED network provides power sharing behavior similar to that of a traditional droop network, but it enforces the network line power-flow constraints. If a constraint is active, then the inverters incident to it must adjust their output power to enforce the constraint, and as such will not converge

to the same final output power as in traditional droop. Because of its distributed nature, all-incident-line CED control does not propogate such constraint enforcement, and as such the two inverters incident to the constraint bear the complete resonsibility of its enforcement (and so must have the capacity to do so). In this dissertation, we have not provided a method for determining the maximum capacity necessary to enforce such constraints.

The primary value of the all-incident-line CED control law and its application to all-active-bus acyclic networks is as a proof-of-concept for the enforcement of line power-flow constraints and robust synchronization and power sharing in inverter-based networks. In this dissertation, it acts as a stepping stone to the more realistic results that follow based on sparse application of CED. The results that follow generalize the all-incident-line CED approach by showing that within a given expected operating range, it is possible to still provide robust synchronization and power sharing behavior by enforcement of a subset of the line power-flow constraints.

7.5 *Constraint-Satisficing Key Line Sets*

The next major contribution of this dissertation is the mathematical concept of constraint-satisficing key line sets. We first explicitly define the expected operating range of an AC network, based on a set of generation and load constraints. We then show that application of Kirchoff's law at each bus in the network, combined with the assumption of satisfaction of the line power-flow constraints associated with a selected set of lines (the candidate key line set), implies bounds on all of the other lines of the network. If these bounds on the non-key lines are sufficient to ensure that their constraints are met, then we say the candidate key line set is a constraint-satisficing key line set. The concept of constraint-satisficing key line sets allows the dynamic sufficient condition for synchronization of the network to be satisfied by the explicit enforcement of only a subset of the line constraints (those associated with

the key line set) as long as the network generation and loads are within the expected operating range.

Constraint-satisficing key line sets are the key to robust synchronization and power sharing in general inverter-based networks, since they allow control architectures using sparse constraint-enforcement to bound the network voltage-angle trajectory within the safe region. They are dependent on a specific network structure, a specific selection of the network expected operating range (defined by generation and load bound vectors), and a specific selection of key line flow constraints. We developed a method for determining the bounds implied on non-key lines by a given expected operating range and key line set, as well as a test for constraint-satisficing key line sets. This test is a sufficient condition only, and may return a false-negative result for some valid constraint-satisficing key line sets. In particular, our bounding procedure does not include a method for implicitly bounding cyclical power flows, and as such requires at least one key line per cycle in the network graph. Therefore, it may produce overly conservative results for meshed networks (those that contain may cycles).

We also introduced a search procedure to find constraint-satisficing key line sets for a given network structure, expected operating range, and power-flow constraints. This procedure starts from the set of all lines (which is always constraint-satisficiing), and tests each subset one by one, working down the tree of subsets until all irreducable constraint-satisficing key line sets are found. For a large network (with many lines), there are many such subsets, and our search procedure potentially might require running the bounding procedure on each one. As a result, our search procedure may require a very large computation time. Fortunately, this procedure need only be run during design time (not during network operation), and so a long computational time may be acceptable. In addition, it should be possible to significantly reduce the computational time by further study and application of high-performance computing techniques.

The greater limitation of our search procedure is due to its dependence on the bounding procedure and test. Since our test for constraint-satisficing key line sets is a sufficient condition only, and since the search procedure does not test any subsets of key line sets tested as non-constraint-satisficing, it may miss some valid constraint-satisficing key line sets, particularly in meshed networks. At present, this limitation of our approach results in unacceptably large constraint-satisficing key line sets when the search procedure is applied to utility transmission networks, which are typically heavily meshed. As a result, the example applications in this dissertation are limited to small networks with few cycles (similar to small distribution networks or micro-grids), rather than IEEE standard power-flow test cases.

However, by improvement of our existing test and search procedures (or development of alternative methods for generation of constraint-satisficing key line sets), it should be possible to generate constraint-satisficing key line sets for networks of arbitrary size and structure, including both distribution and transmission networks. Once a constraint-satisficing key line set of acceptable size for a given network and expected operating range, then the last major contribution of this dissertation shows that it is possible to develop a distributed control method to enforce the line power-flow constraints associated with only the lines of a constraint-satisficing key line set, thus satisfying all of the network line power-flow constraints and providing robust synchronization and power sharing for all operating conditions within the expected range.

7.6 Constraint-Satisficing Droop Inverter Networks

The final major technical contribution of this dissertation is constraint-satisficing droop control configurations and constraint-satisficing droop inverter networks. A constraint-satisficing droop control configuration is a configuration of CED inverters for a mixed-bus inverter-based network (one that contains a mix of CED inverter,

droop inverter, and network buses) and a given expected operating range. In a constraint-satisficing droop control configuration, a CED inverter is placed adjacent to each line in a constraint-satisficing key line set and configured so that it enforces the key line power-flow constraint. Since each key line constraint is enforced by a CED inverter, the line power-flow constraints associated with all lines will be satisfied, rendering it a constraint-satisficing droop inverter network. The network voltage-angle trajectory of such a network is bounded within the safe region, providing near-robust synchronization and power sharing for all operating conditions within the expected range, the ultimate goal of this dissertation.

A constraint-satisficing droop control configuration makes use of the bounded, single-line form of the CED control law. Because the maximum value in this form of the control law is bounded, it is more robust to faults and noise than the un-bounded form. In addition, application of a state-dependent gain to only a single incident line avoids conflicts between enforcement of multiple constraints. However, it means that each CED inverter can only enforce a single line power-flow constraint, necessitating at least one CED inverter per line in the constraint-satisficing key line set. Therefore, if the selected constraint-satisficing key line set is too large, it may be technically infeasible or uneconomical to implement a constraint-satisficing droop control configuration. Because of the limitations of our current procedure for generating constraint-satisficing key line sets, at present it is difficult to apply our method to utility transmission networks. Development of better methods for determination of constraint-satisficing key line sets will contribute directly to the practicality of constraint-satisficing droop inverter networks.

The determination of a constraint-satisficing droop control configuration for a given network is dependent on the network structure, the definition of the expected

operating range and line power-flow constraints, and the selection of a constraint-satisficing key line set. In this work, we have not proposed an optimal way to determine these quantities for a given network, only requirements for their validity. In addition, we have not proposed a strict design procedure for constraint-satisficing droop control configurations. The determination of such an optimal design procedure (which may be specific to a given application) is beyond the scope of this dissertation.

Despite its present limitations, constraint-satisficing droop control configurations provide a very important theoretical framework for improved synchronization and power sharing of inverter-based networks. In its present form, it allows development of control architectures for inverter-based microgrids that provide near-robust synchronization and power sharing behavior. With further development (particularly with better methods of generating constraint-satisficing key line sets), its results should also be applicable to larger-scale inverter-based networks. Therefore, in addition to its immediate applicability, it makes an important step towards enabling robust distributed power networks with high penetration of inverter-interfaced sources.

7.7 Future Work

In this dissertation, we have laid a theoretical groundwork for a distributed control method for robust synchronization and power sharing in inverter-based AC power networks, as well as provided methods for analyzing such synchronization using multi-agent control methods. These contributions open up a number of new research areas for future work, which we discuss below.

7.7.1 Structure-Preserving Models and Sufficient Condition for Synchornization of Inverter and Mixed Inverter/Machine Networks

The structure-preserving model for the frequency/voltage-angle/real-power dynamics developed in this dissertation considers a lossless, all-inverter network with ideal voltage regulation. While this captures the most significant dynamics for our purposes

in this dissertation, many of these assumptions could be relaxed to consider other effects.

First, relaxation of the assumption of all lossless lines in the network renders the line power flow function line-asymmetric. Therefore, it will be necessary to modify the dynamic sufficient condition for synchronization to include the effects of this asymmetry. The Lyanpunov-like method used for proof of synchronization in Theorems 3.3 and 3.5 will no longer be applicable (since it depends on the assumption of line-odd power flows), but the Contraction Property method used in the proof of Theorem 6.2 will still apply by modifying the auxiliary bounding system $\mathbf{v}(t)$ to include the line losses. The result will be synchronization on a "lossy principal region," where the range of line voltage angles for each line is reduced the the associated loss angle. This result is similar to that shown in [20].

The structure-preserving model can also be generalized by including time-varying voltage magnitudes and uncertain line admittances, both bounded from below. This results in a "minimum coupling coefficient" on each line, and synchronization can again be shown by the Contraction Property where the auxiliary bounding system $\mathbf{v}(t)$ evolves based on the minimum coupling. This result would prove the formal control-theoretic robustness of our proposed control methods to time-varying voltage magnitudes and uncertain line admittances.

The structure-preserving model in this dissertation avoids the problem of voltage stability by explicitly decoupling it from that of frequency synchronization. However, if time-varying voltage magnitudes are included in the model, then it may be possible to combine our dynamic sufficient conditions for synchronization with existing work in necessary conditions for voltage collapse (e.g. [33, 31, 25, 11]) to create a condition for combined voltage stability and synchronization of an inverter-based network. It is possible that our proposed control methods could then be modified to provide both robust synchronization and robust voltage stability.

Finally, our structure-preserving model for synchronization and power sharing in inverter-based networks can be combined with Bergen and Hill's famous structure-preserving model for synchronization in machine-based network to create a general model for analysis of synchronization in network with an arbitrary mix of inverter and machine sources. Such a model could be used to analyze the synchronization of almost any power network, including networks with arbitrary penetration of inverter sources, providing a very powerful new tool for analysis of next-generation power networks.

7.7.2 Constraint-Satisficing Key Line Sets

In this dissertation, we proposed the concept of constraint-satisficing key line sets, developed a method for testing for constraint-satisficing key line sets for a given network and expected operating range (Procedure 5.1 and Theorem 5.1), and developed a method for finding constraint-satisficing key line sets for a given network (Procedure 5.2). However, our method for testing for constraint-satisficing key line sets is limited in that it may miss some valid constraint-satisficing key line sets and does not include a method for explicitly bounding cyclical power flows. In addition, our search method is not very computationally efficient, and as such may be difficult to apply to large, highly meshed networks such as transmission networks. Since determination of an acceptable constraint-satisficing key line set for a given network is one of the greatest challenges in implementing our proposed control method, by improving both the test and search procedures, it should be possible to significantly expand the applicability of our methods.

First, our method for bounding power flows in a network (Procedure 5.1) terminates when it encounters a key line, simply using the assigned maximum power flow bounds. However, in many cases there may exist bounds on the power flow due to the network that are more strict than the assigned maximum power flows, and so our

230

method may be overly conservative. Instead of terminating when it encounters a key line, Procedure 5.1 could attempt to calculate the bounds for the key line, and use the stricter of the assigned maximum or the calculated bounds. This would result in tighter bounds on power flows, resulting in fewer false-negative results.

Second, Procedure 5.1 could be improved by including a method for explicitly bounding cyclical power flows in the network. This would relax the constraint that each cycle in the network contain at least one key line, potentially significantly improving its performance in highly meshed networks and resulting in much small constraint-satisficing key line sets.

Since the search procedure for constraint-satisficing key line sets (Procedure 5.2) is based on the bounding procedure (Procedure 5.1), improvements in Procedure 5.1 will directly improve the performance of Procedure 5.2. In addition, the computation time of Procedure 5.2 may be reduced directly by prioritization of key line set testing, by pruning the key line set tree that must be considered, or by eliminating redundancy of calculations. For example, by using the results of the Procedure 5.1 for a given key line set, it may be possible to a-priori eliminate many of its subsets such that they do not need to be tested, to prioritize some of its subsets for testing, or to eliminate some redundant calculations when testing its subsets.

Finally, rather than performing a top-down search of the solution space for a constraint-satisficing key line set for a given network and expected operating range, it may be possible to construct such a key line set directly (from the bottom up) by analyzing its power-flow bounds and determining where explicit constraint enforcement is needed. Such a method is more mathematically complex, but potentially computationally simpler than our proposed search method, and may produce more desirable constraint-satisficing key line sets for practical implementation of our control method.

7.7.3 Development of Constraint-Satisficing Droop Control Configurations for More General Networks

In this dissertation, we developed the concept of a constraint-satisficing droop control configuration, and we developed such configurations for several small example networks. However, while we determined the conditions defining such a configuration, we did not propose a method for selection of the expected operating range or design of a constraint-satisficing droop control configuration for an arbitrary network. In addition, due to limitations in the method of determation of a constraint-satisficing key line set for a given network and expected operating range, it is difficult to determine such a configuration for many types of networks, including large transmission networks. Our methods could be made much more practical by development of a design methodology to create a constraint-satisficing droop control configuration for an arbitrary network, along with an investigation of the design decisions involved and how they can be optimally made.

In addition, our method does not at present provide formally robust synchronization and power sharing, since our method of proof at present requires the assumption not only that the reference power injection inputs remain within the expected operating range, but that the generation and load (which are state-dependent quantities) do so as well. While we argued that this assumption is mild in practice, with further development it should be possible to refine our method to relax the need to assume that generation and load stay within the expected operating range, thus providing formal robustness. By explicitly integrating a power-limiting control transition for droop inverters, generation limits on droop inverter buses are enforced. It should also be possible to calculate the maximum power injection that a given CED inverter must provide on the expected operating range. Then, by requiring each CED inverter to have sufficient capacity to provide that power injection, it can be shown that generation limits on CED buses will be met. Finally, by combining the generation and load

limits into a single power injection limit, it should be possible to show that bounding of reference power injections within the expected operating range will ensure that actual power injections (generation minus load) are also so bounded, and formally robust synchronization and power sharing for all reference power injection inputs on the expected operating range will follow.

Further, improvements in the methods for testing and generation of constraint-satisficing key line sets, along with improved methods for design of expected operating range and an associated constraint-satisficing droop control configuration, should allow our control method to be applied to much more general networks, including large transmission networks. Therefore, with further development, it should be possible to extend our methods so that they provide formally robust synchronization and power sharing for inverter-based AC network of arbitrary size and structure.

7.7.4 Flexible, Robust 21st Century Power Network Control Architectures

In this dissertation, CED control was applied to provide robust synchronization and power sharing of all-inverter networks. However, CED also has application in mixed inverter/machine networks. Due to the mechanical interia of sychronous machines, it is probably not possible to formally bound the network within the safe region of the voltage-angle space for all expected operating conditions. However, CED inverters' ability to limit real power flows can still be used to improve synchronization in such networks. By placing CED inverters near synchronous machines, it should be possible to use the rapid response of the inverter to limit the real power differential experienced by the machines associated with faults in the network. This should allow significant improvement of the critical clearing time of such faults. This method could be combined with a weaker form of constraint-satisficing CED (possibly based on local constraint satisfaction) to provide a distributed control approach for robust synchronization and power sharing of AC networks with an arbitrary mix of inverter

and machine sources. This method could form a framework for a distributed control architecture meeting the needs of the Local Control Layer of the the Prosumer-based Power System Architecture [32]. Therefore, the methods introduced in this dissertation will contribute directly to the development of system-level control architectures to enable flexible, robust 21st-century power networks.

7.8 Closing Statements

Power network architectures are in a state of transition, moving from centralized power sources interfaced by synchronous generators to a more distributed system with a wide range of smaller sources, many or most of which are interfaced by power electronic inverters. As such, a new control architecture that allows more flexibility, technology independence, and consumer participation is needed. The Prosumer-Based Power System Architecture attempts to meet these needs, and it requires a distributed control method to provide robust synchronization and power sharing in networks with high penetration of inverter-interfaced sources.

The results of this dissertation form a theoretical framework for such a robust distributed control method for inverter-based networks. Therefore, our results are immediately applicable to inverter-based microgrids, capable of enabling robust network operation in the absence of communication or centralized control. However, they can also be combined with system-level control (through the power reference values) to perform optimization or market functions. In this application, our methods provide a robust basis on which the higher functions can be built. In addition, we have introduced a structure-preserving dynamic model that provides new mathematical tools for application of multi-agent system control analysis and design methods to inverter-based networks. Finally, by expanding our analysis into networks whose sources are a mix of inverters and synchronous generators, these methods will contribute to the development of a distributed control architecture for networks with

high penetration of inverter-interfaced sources (such as the Prosumer-Based Power System Architecture), allowing highly distributed, highly robust control and market structures for electric power to support the needs of 21st-century societies.

REFERENCES

[1] Aeyels, D. and Rogge, J. A., "Existence of partial entrainment and stability of phase locking behavior of coupled oscillators," *Progress of Theoretical Physics*, vol. 112, no. 6, pp. 921–942, 2004.

[2] Ainsworth, N. and Grijalva, S., "A line weighted frequency droop controller for decentralized enforcement of transmission line power flow constraints in inverter-based networks," in *Power and Energy Society General Meeting (PES), 2013 IEEE*, pp. 1–5.

[3] Ainsworth, N. and Grijalva, S., "A structure-preserving model and sufficient condition for frequency synchronization of lossless droop inverter-based AC networks," *Power Systems, IEEE Transactions on*, vol. 28, no. 4, pp. 4310–4319, 2013.

[4] Ajorlou, A., Momeni, A., and Aghdam, A. G., "A class of bounded distributed control strategies for connectivity preservation in multi-agent systems," *Automatic Control, IEEE Transactions on*, vol. 55, no. 12, pp. 2828–2833, 2010.

[5] Aloisio, G., Bochicchio, M. A., La Scala, M., and Sbrizzai, R., "A distributed computing approach for real-time transient stability analysis," *Power Systems, IEEE Transactions on*, vol. 12, no. 2, pp. 981–987, 1997.

[6] Ando, H., Oasa, Y., Suzuki, I., and Yamashita, M., "Distributed memoryless point convergence algorithm for mobile robots with limited visibility," *Robotics and Automation, IEEE Transactions on*, vol. 15, no. 5, pp. 818–828, 1999.

[7] Athay, T., Podmore, R., and Virmani, S., "A practical method for the direct analysis of transient stability," *Power Apparatus and Systems, IEEE Transactions on*, vol. PAS-98, no. 2, pp. 573–584, 1979.

[8] Barklund, E., Pogaku, N., Prodanovic, M., Hernandez-Aramburo, C., and Green, T. C., "Energy management in autonomous microgrid using stability-constrained droop control of inverters," *Power Electronics, IEEE Transactions on*, vol. 23, no. 5, pp. 2346–2352, 2008.

[9] Bergen, A. R. and Hill, D. J., "A structure preserving model for power system stability analysis," *Power Apparatus and Systems, IEEE Transactions on*, vol. PAS-100, no. 1, pp. 25–35, 1981.

[10] Bolton, C., "EGSA government relations session: Army R&D efforts," 2009. Available at http://www.egsa.org/Portals/7/Documents/CommitteeDocs/EGSA%20F09%20Gov%20Relations%20presentation.pdf.

[11] Byongjun, L. and Ajjarapu, V., "A piecewise global small-disturbance voltage-stability analysis of structure-preserving power system models," *Power Systems, IEEE Transactions on*, vol. 10, no. 4, pp. 1963–1971, 1995.

[12] Chandorkar, M. C., Divan, D. M., and Adapa, R., "Control of parallel connected inverters in standalone AC supply systems," *Industry Applications, IEEE Transactions on*, vol. 29, no. 1, pp. 136–143, 1993.

[13] Chopra, N. and Spong, M. W., "On exponential synchronization of kuramoto oscillators," *Automatic Control, IEEE Transactions on*, vol. 54, no. 2, pp. 353–357, 2009.

[14] Chung, F. R. K. and Langlands, R. P., "A combinatorial Laplacian with vertex weights," *Journal of Combinatorial Theory, Series A*, vol. 75, no. 2, pp. 316–327, 1996.

[15] Coelho, E. A. A., Cortizo, P. C., and Garcia, P. F. D., "Small-signal stability for parallel-connected inverters in stand-alone AC supply systems," *Industry Applications, IEEE Transactions on*, vol. 38, no. 2, pp. 533–542, 2002.

[16] David, H. and Chong Chi, N., "Energy functions for power systems based on structure preserving models," in *Decision and Control, 1986 25th IEEE Conference on*, vol. 25, pp. 1218–1223.

[17] De Brabandere, K., Bolsens, B., Van den Keybus, J., Woyte, A., Driesen, J., and Belmans, R., "A voltage and frequency droop control method for parallel inverters," *Power Electronics, IEEE Transactions on*, vol. 22, no. 4, pp. 1107–1115, 2007.

[18] Dib, W., Barabanov, A. E., Ortega, R., and Lamnabhi-Lagarrigue, F., "An explicit solution of the power balance equations of structure preserving power system models," *Power Systems, IEEE Transactions on*, vol. 24, no. 2, pp. 759–765, 2009.

[19] Dimarogonas, D. V. and Johansson, K. H., "Bounded control of network connectivity in multi-agent systems," *Control Theory & Applications, IET*, vol. 4, no. 8, pp. 1330–1338, 2010.

[20] Dörfler, F. and Bullo, F., "Synchronization and transient stability in power networks and non-uniform Kuramoto oscillators," in *American Control Conference (ACC), 2010*, pp. 930–937.

[21] Dörfler, F. and Bullo, F., "Topological equivalence of a structure-preserving power network model and a non-uniform Kuramoto model of coupled oscillators," in *Decision and Control and European Control Conference (CDC-ECC), 2011 50th IEEE Conference on*, pp. 7099–7104.

[22] DÖRFLER, F. and BULLO, F., "On the critical coupling for kuramoto oscillators," *SIAM Journal on Applied Dynamical Systems*, vol. 10, no. 3, pp. 1070–1099, 2011.

[23] DÖRFLER, F. and BULLO, F., "Synchronization and transient stability in power networks and nonuniform Kuramoto oscillators," *SIAM Journal on Control and Optimization*, vol. 50, no. 3, pp. 1616–1642, 2012.

[24] ETO, J., LASSETER, R., SCHENKMAN, B., STEVENS, J., KLAPP, D., VOLKOMMER, H., LINTON, E., HURTADO, H., and ROY, J., "Overview of the CERTS microgrid laboratory test bed," in *Integration of Wide-Scale Renewable Resources Into the Power Delivery System, 2009 CIGRE/IEEE PES Joint Symposium*, pp. 1–1.

[25] FEKIH-AHMED, L. and CHIANG, H. D., "Analysis of voltage collapse in structure preserving models of power systems," in *Circuits and Systems, 1992. ISCAS '92. Proceedings., 1992 IEEE International Symposium on*, vol. 5, pp. 2525–2528 vol.5.

[26] FILATRELLA, G., NIELSEN, A. H., and PEDERSEN, N. F., "Analysis of a power grid using a Kuramoto-like model," *The European Physical Journal B - Condensed Matter and Complex Systems*, vol. 61, no. 4, pp. 485–491, 2008.

[27] FILATRELLA, G., PEDERSEN, N. F., and WIESENFELD, K., "Generalized coupling in the Kuramoto model," *Physical Review E*, vol. 75, no. 1, p. 017201, 2007. PRE.

[28] FRANCI, A., CHAILLET, A., and PASILLAS-LÉPINE, W., "Existence and robustness of phase-locking in coupled kuramoto oscillators under mean-field feedback," *Automatica*, vol. 47, no. 6, pp. 1193–1202, 2011.

[29] GIUSTO, A., ORTEGA, R., and STANKOVIC, A., "On transient stabilization of power systems: A power-shaping solution for structure-preserving models," in *Decision and Control, 2006 45th IEEE Conference on*, pp. 4027–4031.

[30] GODSIL, C. and ROYLE, G., *Algebraic Graph Theory*. New York, N.Y.: Springer-Verlag, 2001.

[31] GRIJALVA, S., "Individual branch and path necessary conditions for saddle-node bifurcation voltage collapse," *Power Systems, IEEE Transactions on*, vol. 27, no. 1, pp. 12–19, 2012.

[32] GRIJALVA, S., COSTLEY, M., and AINSWORTH, N., "Prosumer-based control architecture for the future electricity grid," in *Control Applications (CCA), 2011 IEEE International Conference on*, pp. 43–48.

[33] GRIJALVA, S. and SAUER, P. W., "A necessary condition for power flow Jacobian singularity based on branch complex flows," *Circuits and Systems I: Regular Papers, IEEE Transactions on*, vol. 52, no. 7, pp. 1406–1413, 2005.

[34] GRIJALVA, S. and TARIQ, M. U., "Prosumer-based smart grid architecture enables a flat, sustainable electricity industry," in *Innovative Smart Grid Technologies (ISGT), 2011 IEEE PES*, pp. 1–6.

[35] GUERRERO, J. M., VASQUEZ, J. C., MATAS, J., CASTILLA, M., and DE VICUNA, L. G., "Control strategy for flexible microgrid based on parallel line-interactive UPS systems," *Industrial Electronics, IEEE Transactions on*, vol. 56, no. 3, pp. 726–736, 2009.

[36] HENDRICKX, J. M., ANDERSON, B. D. O., DELVENNE, J.-C., and BLONDEL, V. D., "Directed graphs for the analysis of rigidity and persistence in autonomous agent systems," *International Journal of Robust and Nonlinear Control*, vol. 17, no. 10-11, pp. 960–981, 2007.

[37] HILL, D. J., "On the equilibria of power systems with nonlinear loads," *Circuits and Systems, IEEE Transactions on*, vol. 36, no. 11, pp. 1458–1463, 1989.

[38] HILL, D. J. and GUANRONG, C., "Power systems as dynamic networks," in *Circuits and Systems, 2006. ISCAS 2006. Proceedings. 2006 IEEE International Symposium on*, pp. 4 pp.–725.

[39] HUIYANG, L., GUANGMING, X., and LONG, W., "Consensus of multi-agent systems with time-varying delay," in *Decision and Control (CDC), 2010 49th IEEE Conference on*, pp. 3078–3083.

[40] IYER, S. V., BELUR, M. N., and CHANDORKAR, M. C., "A generalized computational method to determine stability of a multi-inverter microgrid," *Power Electronics, IEEE Transactions on*, vol. 25, no. 9, pp. 2420–2432, 2010.

[41] JACOBS, D. J. and HENDRICKSON, B., "An algorithm for two-dimensional rigidity percolation: The pebble game," *Journal of Computational Physics*, vol. 137, no. 2, pp. 346–365, 1997.

[42] JAEHONG, K., GUERRERO, J. M., RODRIGUEZ, P., TEODORESCU, R., and KWANGHEE, N., "Mode adaptive droop control with virtual output impedances for an inverter-based flexible AC microgrid," *Power Electronics, IEEE Transactions on*, vol. 26, no. 3, pp. 689–701, 2011.

[43] KHALIL, H., *Nonlinear Systems.* Upper Saddle River, NJ 07458: Prentice-Hall, Inc., 2002.

[44] KUNDUR, P., PASERBA, J., AJJARAPU, V., ANDERSSON, G., BOSE, A., CANIZARES, C., HATZIARGYRIOU, N., HILL, D., STANKOVIC, A., TAYLOR, C., VAN CUTSEM, T., and VITTAL, V., "Definition and classification of power system stability: IEEE/CIGRE joint task force on stability terms and definitions," *Power Systems, IEEE Transactions on*, vol. 19, no. 3, pp. 1387–1401, 2004.

[45] Kuramoto, Y., *Chemical Oscillations, Waves, and Turbulence.* Mineloa, N.Y.: Dover Publications, Inc., 1984.

[46] Lasseter, R., Akhil, A., Marnay, C., Stephens, J., Dagle, J., Guttromson, R., Meliopoulous, A., Yinger, R., and Eto, J., "The CERTS microgrid concept," *White paper for Transmission Reliability Program, Office of Power Technologies, US Department of Energy*, 2002.

[47] Lasseter, R. and Piagi, P., "Providing premium power through distributed resources," in *System Sciences, 2000. Proceedings of the 33rd Annual Hawaii International Conference on*, p. 9 pp.

[48] Lei, W., "Techniques for high performance analysis of transient stability," in *Power and Energy Society General Meeting, 2012 IEEE*, pp. 1–6.

[49] Lin, Z., Francis, B., and Maggiore, M., "State agreement for continuous-time coupled nonlinear systems," *SIAM Journal on Control and Optimization*, vol. 46, no. 1, pp. 288–307, 2007.

[50] Marchei, E., Fioriti, V., Ruzzante, S., Castorini, E., and Rosato, V., "Stability of a model of power microgeneration network using the Kuramoto model," *International Journal of Systems of Systems Engineering*, vol. 2, no. 1, pp. 76–88, 2010.

[51] Marwali, M. N., Jin-Woo, J., and Keyhani, A., "Control of distributed generation systems - part II: Load sharing control," *Power Electronics, IEEE Transactions on*, vol. 19, no. 6, pp. 1551–1561, 2004.

[52] Marwali, M. N., Jin-Woo, J., and Keyhani, A., "Stability analysis of load sharing control for distributed generation systems," *Energy Conversion, IEEE Transactions on*, vol. 22, no. 3, pp. 737–745, 2007.

[53] Meng, J. and Egerstedt, M., "Distributed coordination control of multiagent systems while preserving connectedness," *Robotics, IEEE Transactions on*, vol. 23, no. 4, pp. 693–703, 2007.

[54] Mesbahi, M. and Egerstedt, M., *Graph Theoretic Methods in Multi-Agent Networks.* Princeton, N.J. 08540: Princeton University Press, 2010.

[55] Moreau, L., "Stability of continuous-time distributed consensus algorithms," in *Decision and Control, 2004. CDC. 43rd IEEE Conference on*, vol. 4, pp. 3998–4003 Vol.4.

[56] Moreau, L., "Stability of multiagent systems with time-dependent communication links," *Automatic Control, IEEE Transactions on*, vol. 50, no. 2, pp. 169–182, 2005.

[57] Nemirovski, A., "Lecture notes for ISYE6661 (optimization i): Introduction to linear optimization," 2013.

[58] Nikkhajoei, H. and Lasseter, R. H., "Distributed generation interface to the CERTS microgrid," *Power Delivery, IEEE Transactions on*, vol. 24, no. 3, pp. 1598–1608, 2009.

[59] Notarstefano, G., Savla, K., Bullo, F., and Jadbabaie, A., "Maintaining limited-range connectivity among second-order agents," in *American Control Conference, 2006*, p. 6 pp.

[60] Olfati-Saber, R., Fax, J. A., and Murray, R. M., "Consensus and co-operation in networked multi-agent systems," *Proceedings of the IEEE*, vol. 95, no. 1, pp. 215–233, 2007.

[61] Piagi, P. and Lasseter, R. H., "Autonomous control of microgrids," in *Power Engineering Society General Meeting, 2006. IEEE*, p. 8 pp.

[62] Pogaku, N., Prodanovic, M., and Green, T. C., "Modeling, analysis and testing of autonomous operation of an inverter-based microgrid," *Power Electronics, IEEE Transactions on*, vol. 22, no. 2, pp. 613–625, 2007.

[63] Saber, R. O. and Murray, R. M., "Consensus protocols for networks of dynamic agents," in *American Control Conference, 2003. Proceedings of the 2003*, vol. 2, pp. 951–956.

[64] Sauer, P. and Pai, M., *Power System Dynamics and Stability.* Upper Saddle River, N.J. 07458: Prentice-Hall, Inc., 1998.

[65] Simon, H. A., "Rational choice and the structure of the environment," *Psychological review*, vol. 63, no. 2, p. 129, 1956.

[66] Simpson-Porco, J., Dörfler, F., and Bullo, F., "Droop-controlled inverters are Kuramoto oscillators," in *Distributed Estimation and Control in Networked Systems, 2012 3rd IFAC Workshop on*, vol. 3, pp. 264–269.

[67] Smith, B., Egerstedt, M., and Howard, A., "Automatic generation of persistent formations for multi-agent networks under range constraints," *Mobile Networks and Applications*, vol. 14, no. 3, pp. 322–335, 2009.

[68] Sontag, E. D. and Yuan, W., "New characterizations of input-to-state stability," *Automatic Control, IEEE Transactions on*, vol. 41, no. 9, pp. 1283–1294, 1996.

[69] Sontag, E., *Input to State Stability: Basic Concepts and Results*, vol. 1932 of *Lecture Notes in Mathematics*, book section 3, pp. 163–220. Springer Berlin Heidelberg, 2008.

[70] Tavora, C. J. and Smith, O. J. M., "Equilibrium analysis of power systems," *Power Apparatus and Systems, IEEE Transactions on*, vol. PAS-91, no. 3, pp. 1131–1137, 1972.

[71] TAVORA, C. J. and SMITH, O. J. M., "Stability analysis of power systems," *Power Apparatus and Systems, IEEE Transactions on*, vol. PAS-91, no. 3, pp. 1138–1144, 1972.

[72] VARAIYA, P., WU, F. F., and RONG-LIANG, C., "Direct methods for transient stability analysis of power systems: Recent results," *Proceedings of the IEEE*, vol. 73, no. 12, pp. 1703–1715, 1985.

[73] VOROTNIKOV, V. I., "Partial stability and control: The state-of-the-art and development prospects," *Automation and Remote Control*, vol. 66, no. 4, pp. 511–561, 2005.

[74] VOROTNIKOV, V. I., *Partial stability and control*. Birkhuser Boston, 1997.

[75] WANG, L. and MORISON, K., "Implementation of online security assessment," *Power and Energy Magazine, IEEE*, vol. 4, no. 5, pp. 46–59, 2006.

[76] WENWU, Y., GUANRONG, C., and MING, C., "Consensus in directed networks of agents with nonlinear dynamics," *Automatic Control, IEEE Transactions on*, vol. 56, no. 6, pp. 1436–1441, 2011.

[77] XU, Z. K., "Generalization of nonhomogeneous farkas lemma and applications," *Journal of Mathematical Analysis and Applications*, vol. 186, no. 3, pp. 726–734, 1994.

[78] YU, C., HENDRICKX, J. M., FIDAN, B., ANDERSON, B. D. O., and BLON-DEL, V. D., "Three and higher dimensional autonomous formations: Rigidity, persistence and structural persistence," *Automatica*, vol. 43, no. 3, pp. 387–402, 2007.

[79] ZAVLANOS, M. M., EGERSTEDT, M. B., and PAPPAS, G. J., "Graph-theoretic connectivity control of mobile robot networks," *Proceedings of the IEEE*, vol. 99, no. 9, pp. 1525–1540, 2011.

[80] ZELAZO, D. and MESBAHI, M., "Edge agreement: Graph-theoretic performance bounds and passivity analysis," *Automatic Control, IEEE Transactions on*, vol. 56, no. 3, pp. 544–555, 2011.

[81] ZHIYUN, L., FRANCIS, B., and MAGGIORE, M., "Coupled dynamic systems: From structure towards state agreement," in *Decision and Control, 2005 and 2005 European Control Conference. CDC-ECC '05. 44th IEEE Conference on*, pp. 3303–3308.

VITA

Nathan Ainsworth (BsCmpE 2005, MSEE 2010) is a PhD Candidate at Georgia Institute of Technology and a Grid Innovation Leaders (GIL) Fellow at Oak Ridge National Laboratory. He received his BS in Computer Engineering from Purdue University in West Lafayette, IN, in 2005. From 2006-2008 he designed control and developed embedded software for military power system products at DRS Test and Energy Management, Inc. in Huntsville, AL. In 2008 he returned to academia as a graduate student at Georgia Institute of Technology, where he recieved the MSEE in 2010. In 2012 he was selected as the pilot student for the Grid Innovation Leaders fellowship, a joint graduate fellowship between Oak Ridge National Laboratory at Georgia Tech. His research interests include power system dynamics and stability, multi-agent control, computational intelligence, distributed and renewable generation, SmartGrid technologies, and energy policy.